Tracing the Echoes of Childhood Adversity

Maladaptive Schemas in Memory Bias and Brain Functional Organization

Xiangshen Liu

DONDERS SERIES

RADBOUD UNIVERSITY PRESS

Radboud Dissertation Series

Tracing the Echoes of Childhood Adversity

Maladaptive Schemas in Memory Bias and Brain Functional Organization

Xiangshen Liu

The work described in this thesis was carried out at the Donders Institute for Brain, Cognition and Behaviour, Radboud University Medical Center, Nijmegen, The Netherlands, financially supported by a Ph.D. fellowship from Chinese Scholarship Council (NO.202106010068) awarded to Xiangshen Liu and Prof. dr. Guillén Fernández.

Tracing the Echoes of Childhood Adversity: Maladaptive Schemas in Memory Bias and Brain Functional Organization
Xiangshen Liu

Radboud Dissertation Series
ISSN: 2950-2772 (Online); 2950-2780 (Print)

Published by RADBOUD UNIVERSITY PRESS
Postbus 9100, 6500 HA Nijmegen, The Netherlands
www.radbouduniversitypress.nl

Design: Proefschrift AIO | Annelies Lips
Cover: Proefschrift AIO | Guntra Laivacuma
Printing: DPN Rikken/Pumbo

ISBN: 9789465152219
DOI: 10.54195/9789465152219
Free download at: https://doi.org/10.54195/9789465152219

RADBOUD
UNIVERSITY
PRESS

Tracing the Echoes of Childhood Adversity

Maladaptive Schemas in Memory Bias and Brain Functional Organization

Proefschrift ter verkrijging van de graad van doctor
aan de Radboud Universiteit Nijmegen
op gezag van de rector magnificus prof. dr. J.M. Sanders,
volgens besluit van het college voor promoties
in het openbaar te verdedigen op

woensdag 11 februari 2026
om 14.30 uur precies

door

Xiangshen Liu
geboren op 15 november 1996
te Shandong, China

Promotoren:
Prof. dr. G. Fernández
Prof. dr. I. Tendolkar
Prof. dr. J.N. Vrijsen

Copromotor:
Dr. N. Kohn

Manuscriptcommissie:
Prof. dr. K. Roelofs
Prof. dr. A.F. Marquand
Prof. dr. U. Dannlowski (Universität Münster, Duitsland)

Tracing the Echoes of Childhood Adversity

Maladaptive Schemas in Memory Bias and Brain Functional Organization

Dissertation to obtain the degree of doctor
from Radboud University Nijmegen
on the authority of the Rector Magnificus prof. dr. J.M. Sanders,
according to the decision of the Doctorate Board
to be defended in public on

Wednesday, February 11, 2026
at 2.30 pm

by

Xiangshen Liu
born on November 15, 1996
in Shandong, China

Supervisors:
Prof. dr. G. Fernández
Prof. dr. I. Tendolkar
Prof. dr. J.N. Vrijsen

Co-supervisor:
Dr. N. Kohn

Manuscript Committee:
Prof. dr. K. Roelofs
Prof. dr. A.F. Marquand
Prof. dr. U. Dannlowski (University of Münster, Germany)

Table of Contents

Chapter 1.
General introduction

"The past is never dead. It's not even past." — William Faulkner

Childhood is a season of hope—the time filled with endless possibilities; yet it is also a period that is fragile, as many internal or external factors may deviate the course of a child's development. In today's world, childhood adversity remains a global issue that profoundly impacts the healthy growth of millions of children. According to 2024 statistics from the World Health Organization (WHO) and the United Nations International Children's Emergency Fund (UNICEF), six in ten children under the age of five regularly experience physical or psychological maltreatment at home (WHO, 2024; UNICEF, 2024). An estimated US $1.3 trillion has been spent per year on managing the consequences of childhood adversity across North America and Europe (Bellis et al., 2019). Along with the tremendous burden it places on society, childhood adversity leads to life-long impacts on individuals' mental health. A growing body of evidence has identified childhood adversity as a robust environmental risk factor for psychopathology, increasing vulnerability to a range of mental disorders, including stress-related disorders (e.g., depression, anxiety, post-traumatic stress disorder (PTSD); McLaughlin et al., 2010; Sahle et al., 2021; Abate et al., 2025), schizophrenia (Matheson et al., 2013; Woolway et al., 2022), and substance use disorders (Brown & Shillington, 2017; SooHoo et al., 2025). It is also increasingly recognized as a transdiagnostic factor across psychiatric conditions (Vrijsen et al., 2017; McKay et al., 2022; Chen et al., 2025). Gaining a clear understanding of how childhood adversity alters brain and behavior across the psychopathological continuum—and how such changes translate into psychiatric symptoms—is an essential and urgent step toward developing effective interventions for affected populations.

Childhood adversity: definition and category

Although research on childhood adversity has made notable progress in recent years, its definition remains inconsistent across studies (Humphreys & Zeanah, 2015; Smith & Pollak, 2021). Childhood adversity is something "you know it when you see it," but a unified definition is important for facilitating comparisons and communication between studies. Based on empirical evidence and theoretical models of stress, adversity, and brain development, McLaughlin (2018) proposed a comprehensive definition of childhood adversity as "*experiences that are likely to require significant adaptation by an average child and that represent a deviation from the expectable environment*." This definition has greatly contributed to the field by offering clearer boundaries on what should and should not be classified as childhood adversity. The first key element of the definition is "significant adaptation", which indicates that experiences causing only minor but not substantial distress,

do not qualify. For instance, a quarrel with a classmate may be unpleasant, but most children recover quickly and are unlikely to suffer substantial harm. In contrast, if such conflict escalates into long-term isolation or even violence, it may disrupt daily life and well-being, and thus constitutes a form of childhood adversity. The second key element is "deviation from the expectations," meaning that not all stressors encountered during childhood count as adversity—especially if they are part of a typical life trajectory. For example, moving to a new neighborhood may be stressful, but when planned and supported, it usually does not pose a serious threat to a child's development. By comparison, the sudden loss of stable housing due to an accident is highly unexpected and likely to demand significant psychological resources to cope with, thus qualifying as adversity. Importantly, this definition evaluates adversity based on what would affect an average child, corresponding to population-normative measures (e.g., standardized questionnaires that quantify childhood adversity on the basis of frequency and severity) commonly used in research (Fisher et al., 2010; Sætren et al., 2024).

Childhood adversity can happen in various forms, both physical and psychological, and may originate from adults as well as peers. One widely adopted classification approach is based on the nature of the deviation from expected environments (Humphreys & Zeanah, 2015; McLaughlin, 2018). Deviation can occur in two directions: on the one hand, it may involve the lack of necessary factors that support normal development. For example, an insensitive caregiver may fail to provide adequate physical and emotional input, leading to physical and emotional neglect; on the other hand, deviation can arise from the presence of harmful factors that interfere with development. For instance, verbal or physical violence from a caregiver constitutes adversity categorized as emotional or physical abuse. This classification approach inspired McLaughlin and colleagues (2014; see also McLaughlin & Sheridan, 2016) to further propose a dimensional model, where the lack of expected inputs is conceptualized as deprivation, and the presence of harmful inputs as threat. Common types of childhood adversity can thus be situated within this two-dimensional space, based on the levels of deprivation and threat they entail (see Figure 1.1). Notably, evidence from neurobiological studies have shown supports to this two-dimensional distinction: threat-related experiences have been associated with heightened reactivity in fear learning and salience processing circuits (McCrory et al., 2011; Herringa et al., 2013; McLaughlin et al., 2015), while deprivation tends to be linked with reduced cortical thickness and impaired functioning in higher-order emotional and cognitive systems (Monteleone et al., 2019; Cheng, Mills, Dominguez, et al., 2021; Luo et al., 2023).

In real-life contexts, childhood adversity often appears in more complex and combined forms. The dimensional model offers a potentially effective quantitative framework. Compared to cumulative exposure models (Evans et al., 2013; Sheridan et al., 2017), it facilitates a more nuanced and systematic evaluation of adversity—something that future research critically needs.

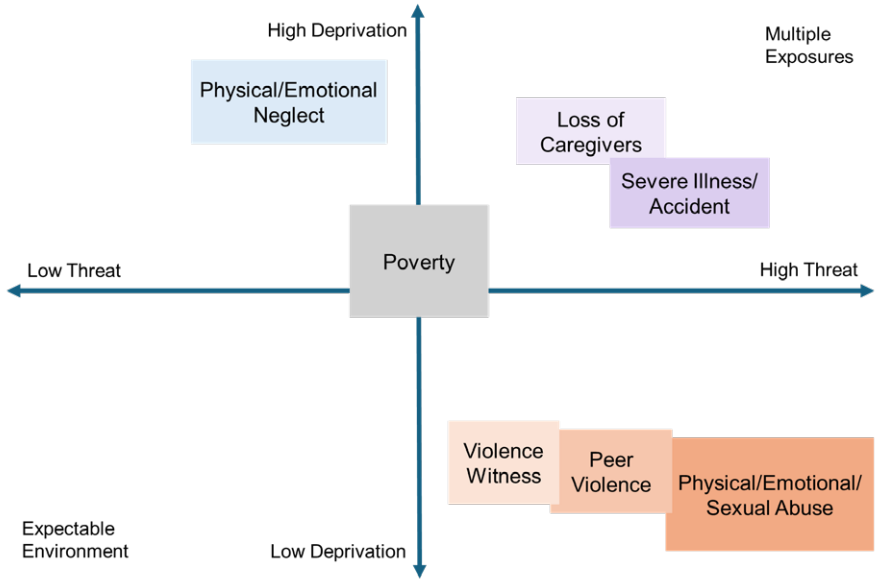

Figure 1.1 Illustrative positioning of common forms of childhood adversity within the deprivation–threat space. Adapted from McLaughlin et al (2014) and McLaughlin & Sheridan (2016)

From childhood adversity to psychopathology: Beck's cognitive model and the role of schemas

Psychiatric disorders are widely recognized to develop through the interplay of genetic and environmental factors (Klengel & Binder, 2015; Tsuang et al., 2004). As defined above, childhood adversity is a detrimental environmental factor that acts on the organism and leads to adaptive changes in its structure and function. To describe what childhood adversity specifically alters, and how these alterations ultimately increase the risk of psychiatric disorders, decades of research have focused on examining behavioral outcomes as well as changes in brain morphology and function related to childhood adversity (Blair & Raver, 2012; Gur et al., 2019; Nelson et al., 2025). In terms of theoretical models, one that integrates both behavioral and neural studies and has a significant impact on clinical practice

is Aaron T. Beck's cognitive model of depression (Beck, 1967, 2008; Beck & Haigh, 2014). Focusing on the psychopathology of depression, this model clearly defines the concept of a "depressive schema", which is understood as a pessimistic internal knowledge structure concerning the self and the world. The initial formation of this latent schema is shaped by adverse experiences during childhood, in interaction with vulnerable genetic and personality traits. As children grow into adults, the schema develops alongside them and can be activated by environmental triggers (e.g., stressful life events). Once activated, it imposes a depressive filter on ongoing cognitive processes, leading to negative biases in attention, information processing, and memory. These cognitive biases accelerate the onset of depressive episodes, which in turn further reinforce cognitive biases and strengthen the depressive schema, forming a vicious cycle (Beck, 1967; Disner et al., 2011).

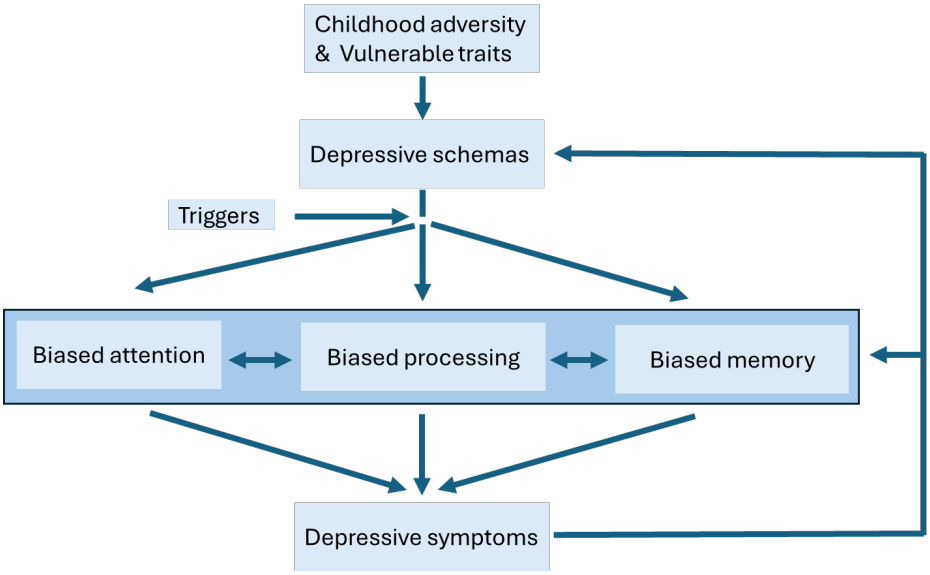

Figure 1.2 Conceptual illustration of Beck's cognitive model of depression. Adapted from Disner et al (2011).

The construct of schema and its essential role in human cognition have a long-standing history in psychological research. As early as 1933, Bartlett illustrated how prior experiences and cultural backgrounds influence memory through his renowned "War of the Ghosts" experiment (Bartlett & Burt, 1933). He suggested that memory is not a passive recording of sensory information but is actively reconstructed through individuals' cognitive frameworks based on preexisting knowledge—namely schemas. Schema also occupies a central place in Piaget's

influential theory of cognitive development (Piaget, 1953). In this framework, a schema is a single unit of how information is organized and processed—a fundamental internal representation of the external world. Children form new schemas, acquire knowledge and skills by assimilating them into existing schemas, and adjust their schemas through accommodation in response to novel experiences. Thus, the development of schemas emerges from continuous interaction with, and learning from, the environment. Another theoretical model closely related to research on childhood adversity is Bowlby's attachment theory (Bowlby, 1969), in which the concept of the "internal working model" aligns with that of schema. Based on years of observation of child–caregiver behaviors, Bowlby proposed that early interactions with caregivers shape children's beliefs about the self and others—forming internal working models that influence attachment behavior across the lifespan. This perspective resonates with Beck's cognitive model, while the latter further describes the related cognitive alterations from a more psychopathological perspective. Building on Beck's theory, Young developed the schema theory and schema therapy (Young, 1999; Young et al., 2006), offering a more explicit conceptualization of "maladaptive schemas". He also believed that toxic childhood experiences were the primary origins of these schemas, and identified 18 typical maladaptive schemas in five domains. The schema therapy therefore aims to help individuals recognize the maladaptive schemas and their origins, and then modify these schemas along with the associated emotional and behavioral patterns.

Among the theories involving schemas, Beck's cognitive model offers a clear explanation of the pathway from childhood adversity to the formation of maladaptive schemas, and subsequently to alterations in cognitive domains. In recent years, this model has gained substantial support from both behavioral and neuroscience research. In the following sections, we will present relevant empirical evidence for the three types of cognitive biases proposed by Beck, with a specific focus on biased memory.

Biased attention

Flexibly allocating attention based on task demands is an important cognitive functioning, and the attentional bias reflects impairments in this ability. Consistent with Beck's model, individuals with depression exhibit a sustained attentional bias toward sad stimuli (Gotlib, Krasnoperova, et al., 2004). They also show greater difficulty disengaging from dysphoric information (Kellough et al., 2008). This reduced attentional flexibility has been linked to impairments in executive control and inhibition, involving regions such as the ventrolateral and dorsolateral

prefrontal cortex (VLPFC, DLPFC), as well as the anterior cingulate cortex (ACC) (Disner et al., 2011). Compared to research on clinical depression, findings on the relationship between childhood adversity and attentional bias are more inconsistent. While some studies report that experiences such as maltreatment or family violence are associated with biased attention toward negative stimuli (Briggs-Gowan et al., 2015; Günther et al., 2015), others have found the opposite—avoidance of threatening or bias towards positive (e.g., happy) stimuli (Pine et al., 2005; Fani et al., 2011; Letkiewicz et al., 2020). These discrepancies may stem from variations in how childhood adversity is assessed (e.g., type, severity), differences in sample characteristics (e.g., psychiatric profiles), and task manipulations such as stimulus presentation duration.

Biased information processing and interpretation

Depression patients generally exhibit enhanced processing of the negative aspects of stimuli and reduced processing of positive information (Kube et al., 2020; Surguladze et al., 2004; Yoon et al., 2009). The alteration in information processing is also reflected in negatively biased interpretation: when presented with ambiguous situations individuals with depression tend to interpret them in a more negative manner (Mathews & MacLeod, 2005). Such biased processing may be driven by heightened amygdala reactivity (Siegle et al., 2002; Dannlowski et al., 2007), its reduced top-down control from DLPFC and dorsal ACC (Disner et al., 2011), as well as hypoactivity in reward-processing regions (e.g., the striatum and mPFC) (Heller et al., 2009; Cléry-Melin et al., 2019; Ng et al., 2019).

Regarding childhood adversity, individuals with exposure to childhood traumatic events, in combination with risk-related genotypes, demonstrate reduced positive processing biases compared to those without such exposure (Vrijsen et al., 2014). Childhood adversity has also been linked to increased perceptual sensitivity to threat-related stimuli (McLaughlin et al., 2020), and sustained hyperactivity in the amygdala in response to negative information (Grant et al., 2011; McCrory et al., 2011; Dannlowski et al., 2012). In contrast, responsiveness to reward and positive stimuli appears blunted in individuals with histories of childhood adversity (Dillon et al., 2009; Oltean et al., 2023).

Biased memory

Preferential remembering and recalling negative information versus positive information is one of the most robust cognitive observations in patients with depression (Gotlib & Joormann, 2010). This negative memory bias can manifest in both explicit and implicit forms. Explicit, or declarative memory, refers to the

memory retrieval process that requires conscious control (Cohen & Squire, 1980). Explicit memory bias is typically investigated using the Self-Referent Encoding Task (SRET; Hammen & Zupan, 1984; Vrijsen et al., 2015). In the SRET, participants are asked to remember a list of positive and negative trait adjectives and judge whether each word is self-referential. Subsequently, their memory is tested via a free recall task. The memory bias index is calculated as the proportion of correctly recalled self-referential words of each valence among all self-referential words. Numerous studies have consistently shown that the self-referent negative memory bias is a strong marker of depressive symptom severity (Gotlib, Kasch, et al., 2004; Duyser et al., 2020; Duyser et al., 2025). Explicit memory bias can also be captured through the Autobiographical Memory Test (AMT; Williams & Broadbent, 1986; Dillon & Pizzagalli, 2018). In the AMT, participants are provided with positive and negative cue words and instructed to retrieve a specific autobiographical memory related to each cue. Depressed individuals tend to access negative autobiographical memories more easily, with these memories being more vivid and emotionally intense than positive ones (Dalgleish & Hitchcock, 2023). In contrast, positive autobiographical memories are often overgeneralized and lack details (Dillon & Pizzagalli, 2018).

The implicit (nondeclarative) memory refers to memory retrieval that occurs without conscious awareness (Squire, 1987). This form of memory bias has been examined through the work-stem completion task (WSC; Gotlib & Krasnoperova, 1998). Similar to the SRET, participants are presented with valenced words and rate their self-descriptiveness. In the memory test, instead of a free recall, participants are instructed to complete a word-stem (e.g., "so _ _ _ _") with the first word that they can think of. For example, participants may complete the word with "sorrow" through automatic memory retrieval if it was previously included in the word list. Depressed populations have demonstrated a higher implicit memory for negative words compared to positive ones, whereas nondepressed controls show the opposite pattern (Ruiz-Caballero & Gonzilez, 1994).

Neuroimaging studies have identified the central role of the amygdala underlying negative memory biases observed in depression patients. Compared to healthy individuals, people with depression show heightened amygdala activity and increased amygdala-hippocampus connectivity during the encoding of negative stimuli (Ramel et al., 2007; Hamilton & Gotlib, 2008; van Eijndhoven et al., 2011). Amygdala hyperactivity is associated with higher depressive symptom levels and predicts stronger negative memory biases (Hamilton & Gotlib, 2008; Ramel et al., 2007). Conversely, a blunted amygdala response has been observed during the recall of positive autobiographical memories in depressed individuals (Young et

al., 2016), possibly contributing to impaired retrieval of positive memory engrams. Thus, functional alterations in the amygdala appear to underlie both the enhanced negative memory and impaired positive memory, affecting both encoding and retrieval processes. Moreover, as a structure anatomically adjacent to the amygdala, the hippocampus may also be involved: negative memory bias has been associated with reduced hippocampal volume (Gerritsen et al., 2012).

As the origin of depressive schemas in Beck's model, childhood adversity has also been linked to negative memory bias. For instance, in a naturalistic psychiatric sample, Vrijsen et al. (2017) found that the frequency of childhood trauma was positively correlated with negative memory bias, and this memory bias mediated the relationship between childhood trauma frequency and the severity of psychiatric comorbidities. Similarly, individuals exposed to early-life stress exhibited a reduced positive memory bias for socially relevant stimuli, which was also correlated with the number of past depressive episodes (Gethin et al., 2017).

The above evidence demonstrates that both childhood adversity and depression are associated with negative memory bias. However, several open questions remain regarding the relationship among childhood adversity, depression, and memory bias. First, most previous studies have examined the link between childhood adversity and memory bias in psychiatric patient samples, where childhood adversity and levels of depression symptoms are often closely entangled (Korkeila et al., 2010; Norman et al., 2012; Vrijsen et al., 2017). It raises the possibility that the observed association between childhood adversity and memory bias may be driven primarily by elevated levels of depression commonly seen in individuals with adverse childhood experiences. Therefore, the distinct and interactive contributions of childhood adversity and depressive symptoms to negative memory bias require further clarification. Second, another important element in Beck's model — the role of external schema activation — has yet to be systematically investigated, as most studies have not directly manipulated schema activation when examining the impact of childhood adversity. External schema activation may modulate the relationship between childhood adversity or depressive symptoms and memory bias. For instance, among individuals exposed to childhood adversity but with low current depression, the manifestation of negative memory bias may depend on whether depressive schemas are externally activated by stressors. In short, childhood adversity, depressive symptoms, and schema activation are all important components of Beck's cognitive model, and clarifying their intertwined roles is essential to deepen our understanding of the mechanisms underlying negative memory bias and to refine the model's application in clinical fields.

Box 1 The influence of schemas on memory and its neural substrates

How childhood adversity contributes to the formation of the depressive schema, and how this schema subsequently leads to negatively biased memory, may parallel the well-established "schema effect" on memory. Here, schema refers to an associative network embedded with structured knowledge and experience, which alters the way new information is processed and remembered (Fernández & Morris, 2018; Gilboa & Marlatte, 2017). Information congruent with existing schemas tends to be encoded more efficiently, consolidated with higher priority, and accessed more easily during retrieval (van Kesteren et al., 2012). At the neural level, the medial prefrontal cortex (mPFC) has been implicated as playing key roles throughout the life cycle of schema-modulated memory, functioning in close interaction with medial temporal lobe structures (e.g., the hippocampus). During initial encoding, the mPFC may act as a schema coordinator, detecting whether incoming information aligns with existing schemas and facilitating the formation of schema-congruent memory traces (Frühholz et al., 2011; Gilboa & Marlatte, 2017; van Kesteren et al., 2010, 2013). During consolidation, the mPFC is proposed to enhance synchronized activity across neocortical areas (e.g., posterior cortical regions), thereby accelerating the integration of new information into cortical memory networks (Tompary & Davachi, 2017; Tse et al., 2007; van Kesteren et al., 2010). The mPFC has also been shown to support schema-modulated retrieval, by guiding the retrieval process through the use of schematic information as a scaffold (Guo & Yang, 2020; van Buuren et al., 2014).

In addition to the mPFC, regions such as the angular gyrus (AG) and temporo-parietal junction (TPJ) involved in multimodal integration, as well as the lateral temporal cortex associated with conceptual and semantic processing, also play roles in the encoding and retrieval of schema-modulated memories (Wagner et al., 2015; Webb et al., 2016; Gilboa & Moscovitch, 2017). These findings may indicate that, beyond the role of the amygdala emphasized in previous studies (see sections below), the depressive schema formed through childhood adversity may influence emotional memory processing through a broader cortical network centered around the mPFC. This perspective remains to be systematically tested in future research.

A generalized childhood adversity - maladaptive schema framework

In above sections, we introduced the theoretical framework and empirical evidence for Beck's cognitive model, in which childhood adversity contributes to the formation of depressive schemas and affects individuals' performance on cognitive tasks. These negatively biased cognitions in the domains of attention, information processing/interpretation and memory are associated with corresponding structural and functional changes in the brain. The alterations are primarily observed in the prefrontal cortex, which supports higher-order cognitive regulation (with the mPFC playing an important role in schema coordination), as well as in its connected regions involved in reward and motivation processing (e.g., the striatum) and threat processing (e.g., the amygdala and hippocampus). Such neural changes may underlie the mechanisms by which maladaptive schemas influence cognitive processing. However, the impact of childhood adversity often extends beyond specific cognitive tasks. As a detrimental environmental factor that requires substantial adaptation by children, childhood adversity alters brain developmental trajectories and leaves lasting neural imprints (Teicher et al., 2003, 2016; McLaughlin et al., 2019). Even prior to engaging in cognitive

tasks, alterations in aforementioned regions (mPFC, the striatum, amygdala and hippocampus) may place the brain in a distinct state that serves as the foundation for a subsequent biased cognitive processing mode. Therefore, as an associative network built upon structured knowledge and experience (Fernández & Morris, 2018), maladaptive schemas shaped by childhood adversity may also be reflected in the regional functional communication during resting-states, in a covert, generalized form.

In recent years, an increasing number of resting-state functional Magnetic Resonance Imaging (rs-fMRI) studies have offered opportunities to capture the impact of childhood adversity on functional communication in the brain. In this section, we will introduce several findings on resting-state functional connectivity (rs-FC) related to childhood adversity, and explore the potential of a relatively new data-driven approach —"connectopic mapping"— as a promising method for characterizing maladaptive schemas embedded in the brain's functional architecture.

Previous findings on childhood adversity and resting-state functional connectivity

Similar to task-state neuroimaging studies, research on rs-FC has also focused on how threat-processing circuits, centered on the amygdala, are altered by childhood adversity. rs-FC between the amygdala and frontal regions, such as the mPFC, orbitofrontal cortex, and AC, is often changed following childhood adversity, typically showing reduced coupling, which may reflect diminished top-down regulatory control (Thomason et al., 2015; Cheng, Mills, Miranda Dominguez, et al., 2021; Teicher et al., 2016; Hanson et al., 2019). The hippocampus, a neighboring region also involved in threat-related processing, exhibits similar reduced rs-FC with the ventromedial prefrontal cortex (vmPFC) in individuals with a history of childhood adversity (Birn et al., 2014). The hippocampus has also shown decreased rs-FC with the amygdala (van der Werff et al., 2013) and increased rs-FC with the insula (Saxbe et al., 2018). These findings collectively point to the altered functional dynamic among threat-related sub(neo)cortical structures as a neural signature of childhood adverse experiences. Beyond threat-processing regions, alterations in functional connectivity between reward-related brain regions have also been observed, corresponding to the impact of childhood adversity on the processing of reward and other positive stimuli. For instance, socioeconomic disadvantage has been associated with reduced rs-FC between the ventral striatum and mPFC in children and adolescents (Marshall et al., 2018). Another study has reported increased ventral striatum–mPFC coupling in youth with histories of early institutional care, and this increase was positively associated with social problems (Fareri et al., 2017). These results suggest that altered reward circuitry connectivity

may form part of the neural basis for maladaptive behavioral outcomes linked to childhood adversity (Herzberg & Gunnar, 2020).

Studies have also examined rs-FC alterations at the level of brain networks, with the most consistent findings involving the default mode network (DMN; Teicher et al., 2016). Several studies have reported decreased intra-network synchrony within the DMN (Sripada et al., 2014; Dauvermann et al., 2021; Wei et al., 2024), as well as altered inter-network connectivity, such as increased DMN–sensorimotor network connectivity and reduced DMN–salience network connectivity (Marusak et al., 2015; Luo et al., 2022; Gálber et al., 2024). Given the DMN's central role in self-referential processing (Sheline et al., 2009; Qin & Northoff, 2011), these alterations may reflect how childhood adversity shapes the development of internal self-related schemas.

Exploring functional topography: the "connectopic mapping"

Existing rs-FC studies, to some extent, have provided evidence on how childhood adversity affects brain functional connectivity. However, the complexity of brain function often goes beyond what can be explained by specific connectivity pathways or networks. The impact of childhood adversity on brain function tends to be systemic (McLaughlin, Sheridan, Winter, et al., 2014; Tooley et al., 2021), influencing functional communication at a large scale. Thus, it may be speculated that the resulting maladaptive schema is embedded within the broader functional organization of the brain, centered around but not limited to specific hub regions. The widespread alterations are difficult to fully capture through analyses focused solely on discrete pathways or networks.

As a novel rs-fMRI analysis method developed by Beckmann and his group (Marquand et al., 2017; Haak et al., 2018), "connectopic mapping" may offer a new perspective in this context. Unlike approaches restricted to specific pathways, "connectopic mapping" aims to estimate the whole-brain functional connectivity organization within a predefined region of interest (ROI). It decomposes functional connectivity between the ROI and the entire grey matter into several biologically valid components. Each component captures a topographic pattern of connectivity variation across ROI voxels—referred to as a gradient map.

Compared to traditional methods, "connectopic mapping" represents a significant advancement in rs-fMRI analysis through following aspects. First, whereas classical neuroimaging research has aimed to establish point-to-point mappings between brain regions and functions, an increasing number of studies suggest that brain functionality is not organized along sharp borders, but rather exhibits gradual

transitions across space or structure (Ralph et al., 2017; Przeździk et al., 2019). A clear example is from the mPFC, where a dorsal-anterior to ventral-posterior gradient has been linked to a shift from abstract to concrete representations (Bein & Niv, 2025). Similarly, the gradual functional changes along the hippocampal long axis have also been an important topic in memory research (Strange et al., 2014). By generating continuous gradient maps, "connectopic mapping" enables direct testing of whether a given brain region exhibits sharp boundaries or gradual transitions in its functional organization. Second, another feature of brain functional organization is its multiplicity—the coexistence of multiple, overlapping functional patterns within a single brain region. Taking the hippocampus again as an example: in addition to the widely studied long-axis gradient, the hippocampus also exhibits functional organization across its subfields (e.g., dentate gyrus, CA3, CA1), which plays essential roles in memory formation and consolidation (Ko et al., 2025). Traditional rs-fMRI methods, typically treating brain regions as homogeneous units, may miss this multiplicity. In contrast, "connectopic mapping" is specifically suited to uncover such overlapping functional architectures by decomposing a region's functional connectivity profile into multiple components (i.e., gradient maps). Each gradient mode captures a unique topographic dimension of rs-FC variation, enabling multi-layered mapping of brain functionality. Attention to functional multiplicity may also benefit how we understand the neural representation of maladaptive schemas. Schemas themselves are abstract associative networks derived from multiple experiences (in this case, various childhood adverse events), and are characterized by hierarchical organization and cross-connectivity (Ghosh & Gilboa, 2014; Rumelhart & Ortony, 2017). Overlapping units often exist across schemas, where sub-schemas can contribute to multiple higher-order schemas, effectively linking them. This helps explain why a minor negative trigger can lead to broad activation of the depressive working mode. The decomposed gradient maps, in this context, may offer greater sensitivity in capturing these subtle, distributed patterns of schema-related functional organization represented in the brain's connectivity architecture.

The utility of "connectopic mapping" has been demonstrated in several studies, indicating both its biological and psychological relevance. One particularly compelling finding is about the brain topography—a fundamental organizational principle whereby adjacent neurons in a sender region project to adjacent neurons in a target region, thereby supporting efficient information transmission (Haber et al., 2000; Thivierge & Marcus, 2007). Applied to regions such as the primary motor cortex, striatum, and hippocampus, "connectopic mapping" has successfully recovered topographic patterns of connectivity that align with those previously identified in animal and anatomical studies (Marquand et al., 2017; Haak et al., 2018; Nordin et

al., 2025), using rs-fMRI data from living humans. Importantly, these topographic gradients have shown functional significance beyond anatomy. For example, individual variation in one striatal gradient map predicts individual differences in goal-directed behavior (Marquand et al., 2017), while another gradient map corresponds closely to the distribution of striatal dopamine transporters (Oldehinkel et al., 2022). Similarly, inter-individual variation in the hippocampal long-axis gradient has been shown to correlate with memory recollection performance (Przeździk et al., 2019). Moreover, when applied to clinical and aging populations, "connectopic mapping" has proven sensitive to functional connectivity alterations associated with psychiatric comorbidities (Mulders et al., 2022), aging (Nordin et al., 2025), cocaine use disorder as well as its intervention-related changes (Zhang et al., 2025). Collectively, these findings underscore the potential of "connectopic mapping" as a powerful tool for capturing the large-scale organization of resting-state functional connectivity, and for revealing multi-layered, gradual mappings of brain function.

Box 2 The pipeline of "connectopic mapping"

The general workflow of "connectopic mapping" involves the following steps:

1. For each voxel within the ROI, its time series is correlated (using Pearson's correlation) with dimension-reduced time-series data from all other grey-matter voxels outside the ROI.
2. Based on these correlation coefficients, a similarity matrix is created to represent the similarity of connection patterns among all ROI voxels.
3. A manifold learning algorithm using Laplacian Eigenmaps is then applied to this similarity matrix, resulting in a set of topographic gradient maps. Each gradient map reveals a distinct mode of variation across ROI voxels, reflecting how functional connectivity between the ROI voxel and the rest of the cortex changes.
4. To validate the statistical representation and analysis, a trend surface model (TSM) is fitted to each gradient map, producing a set of TSM coefficients that describe its spatial features.
5. The ROI topographic modes can be projected back onto the cortex, by labeling each cortical vertex according to the ROI voxel with which it has the highest correlation, thereby producing corresponding projection maps.

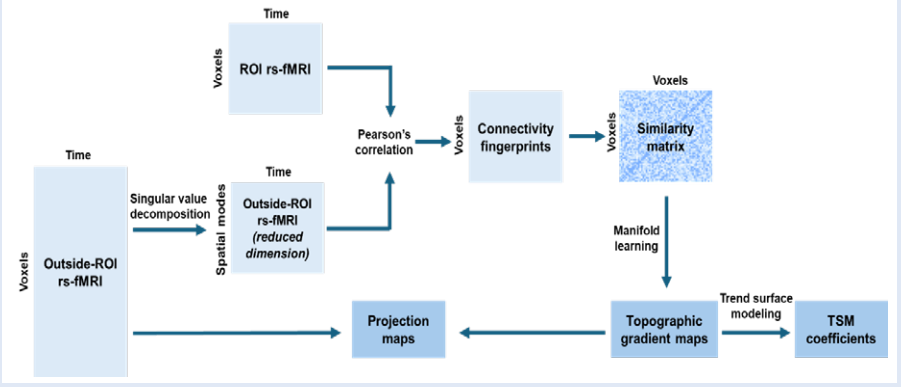

Figure 1.3 The "connectopic mapping" workflow. Adapted from Haak et al., 2018 and Marquand et al., 2017

Utilizing "connectopic mapping" in reward- and threat-processing regions

As reviewed above, functional alterations in brain regions involved in reward and threat processing play crucial roles in negatively biased cognition, and may underlie how maladaptive schemas shaped by childhood adversity are represented in the brain. As an important complement to traditional rs-fMRI analysis methods that focus on specific connectivity pathways, applying "connectopic mapping" to these reward- and threat-related regions can provide a detailed readout of their functional architecture under the influence of childhood adversity, offer a multi-layered approach to capturing the neural representation of maladaptive schemas, and help elucidate open questions related to the functions of these regions.

In the context of reward processing, functional alterations have been proposed to underlie the blunted stress response often observed in individuals with childhood adversity (Carroll et al., 2012, 2017). However, most of the existing evidence focuses on specific connectivity pathways (Fareri et al., 2017; Marshall et al., 2018), leaving a gap in our understanding of how childhood adversity may shape broader, large-scale functional organization of the reward system. Approaches that capture its topographic architecture, such as "connectopic mapping", could therefore offer complementary perspectives. The method's application to the striatum, an important hub of the reward-processing circuit, has been well-established (Marquand et al., 2017; Mulders et al., 2022; Oldehinkel et al., 2022). Applying "connectopic mapping" to examine how childhood adversity relates to variation in striatal connectivity gradients, both at baseline and following acute stress induction (as a form of external schema activation), could offer new insights into existing theories linking childhood adversity, stress responsivity, and reward circuitry. More broadly, this approach may further help with exploring how maladaptive schemas shaped by childhood adversity are embedded in the functional architecture of the reward system.

Beyond reward processing, the amygdala and hippocampus, as brain regions central to the detection and processing of threat, are also known to be vulnerable to the impacts of childhood adversity. In addition to their essential roles in negative memory bias, it is worth investigating whether their resting-state functional connectivity might reflect an inherent maladaptive schema associated with childhood adverse experiences. While previous research has explored hippocampal connectivity gradients, the functional topography of the amygdala has remained understudied in human fMRI studies due to its small size and deep location, which pose challenges related to imaging resolution. Given the amygdala's close

interaction with the hippocampus in the threat processing circuit, treating these two structures as a unified complex, and examining their combined connectivity gradients may offer a more comprehensive approach to capturing how maladaptive schemas are embedded in their intrinsic functional architecture. As there is currently no established reference for gradient mapping of the hippocampus-amygdala complex, a necessary first step is to characterize their spatial layouts and explore the potential biological and psychological significance.

Research questions and thesis outline

Echoes of childhood adversity extend far beyond the childhood. Beck's cognitive model of depression, as the theoretical foundation of cognitive-based therapies, proposes that childhood adversity impacts cognitive behaviors through the formation of maladaptive schemas. After reviewing research examining the cognitive and neural consequences of childhood adversity, we put forward the view that these maladaptive schemas may be traced in two potential ways: first, as predicted by Beck's model, through associations between childhood adversity and biased cognition; and second, in a form of neural representation—through alterations in resting-state functional communication between brain regions. These two aspects constitute the core focus of this thesis, which aims to trace the imprint of maladaptive schemas shaped by childhood adversity using a task-based fMRI study and "connectopic mapping" analysis in resting-state fMRI data from both healthy and psychiatric cohorts. As childhood adversity is a well-recognized risk factor for psychopathology, this series of work is intended to contribute to a deeper understanding of how childhood adversity relates to brain and behavioral changes across the psychopathological continuum, and may support the development of transdiagnostic mechanisms.

Beck's cognitive model of depression delineates how childhood adversity, schema activation, and depressive symptoms are interconnected through the manifestation of negative cognitive bias. However, in the domain of biased memory, the distinct roles and interactions of childhood adversity, depressive symptoms and depressive schema activation in relation to negative memory bias still need further empirical evidence for clear elucidation. **In Chapter 2,** we present a multi-session fMRI study designed to help clarify this issue. We employed a sample encompassing a broad range of childhood adversity and depressive symptom levels. Schema activation was directly manipulated within subjects prior to participants completing an emotional memory encoding task. The negative memory bias index was derived

from participants' memory performance on the second day of encoding sessions. Its associations with childhood adversity, depressive symptoms, and schema activation were examined within a unified analytical model. To trace the imprint of childhood adversity and maladaptive schemas at the neural level, the encoding activity in the amygdala and hippocampus was also extracted. We tested how these neural responses varied as a function of childhood adversity, levels of depressive symptom, and external schema activation.

Childhood adversity has been associated with alterations in functional connectivity within reward-processing circuits. These alterations may play a role in the diminished stress response among populations with childhood adversity. As previous studies have primarily focused on specific connectivity pathways within the reward system, evidence from large-scale connectivity is needed to reveal brain functional architecture changes at the system level—a potential reflection of maladaptive schemas shaped by childhood adversity and activated by acute stress. **In Chapter 3,** we applied "connectopic mapping" to a combined sample of psychiatric patients and healthy controls, to investigate how striatal connectivity gradients vary as a function of childhood adversity, and how these patterns are modulated by acute stress induction. Both the type and frequency of adversity were taken into account. To explore the transdiagnostic relevance, we also assessed psychiatric comorbidity and examined its associations with the observed connectivity variations.

Childhood adversity also induces functional changes in the threat processing regions, such as the amygdala and hippocampus. In Chapter 2, we examined how activation in these two regions varies as a function of childhood adversity during an emotional memory task. As a complementary aspect of it, the resting-state functional architecture of the amygdala and hippocampus might also reflect the enduring impact of childhood adversity—representing the embedded neural trace of maladaptive schemas. **In Chapter 4**, we applied "connectopic mapping" to the hippocampus-amygdala complex in both healthy and psychiatric cohorts. Given the absence of a prior reference for functional gradients in this complex, we first characterized the spatial organization of these gradients, and explored their biological relevance by comparing the resulting gradient maps with positron emission tomography (PET) or single photon emission computed tomography (SPECT) data indexing different neurotransmitter systems. To assess the psychological relevance and whether maladaptive schemas are reflected in the hippocampus-amygdala functional architectures, we further examined the associations with childhood adversity, depressive symptom severity, and anxiety sensitivity.

Chapter 2.

The lasting imprint—negative memory bias in adults with childhood adversity: behavioral and neural evidence

This chapter is based on: Liu, X. S., Vrijsen, J. N., Fröhling, J., Duan, H., Tendolkar, I., Fernández, G., & Kohn, N. (In Preparation). The lasting imprint—negative memory bias in adults with childhood adversity: behavioral and neural evidence.

Abstract

Background

Negative memory bias is a common cognitive feature among patients with depression. According to Beck's cognitive model of depression, adverse experiences during one's childhood can lead to the development of depressive schemas and further promote negative memory bias. However, the distinct roles and interactions of childhood adversity, depressive symptoms and depressive schema activation in relation to negative memory bias have not been clearly elucidated.

Methods

A sample of volunteers encompassing diverse levels of childhood adversity and depressive symptoms was recruited (N = 82). Participants completed a two-phase study consisting of four sessions—one phase with the depressive schema activation and the other with a control task. Following the schema activation/control task, they encoded 180 pictures with negative, neutral or positive valence during functional magnetic resonance imaging (fMRI). Their memory performance was assessed through a recognition memory test on the second day of each encoding session.

Results

Higher levels of depressive symptoms were associated with stronger negatively biased stimuli processing, whereas more severe childhood adversity was linked to greater negatively biased memory. Individuals with higher levels of childhood adversity also exhibited a negative (vs. positive) advantage in amygdala and hippocampal encoding activity, paralleling the behavioral memory bias. External activation of the depressive schema, as done here, did not show additional effects on negative memory bias.

Conclusions

Our study characterized the relationship between childhood adversity and negative memory bias using a classical emotional memory task. Childhood adversity was associated with negative memory bias independent of depressive symptom levels, supporting a potential influence of the inherent depressive schema, as proposed in Beck's model.

Keywords: Negative memory bias; Childhood adversity; Depression; Depressive schema; Amygdala; Hippocampus

Introduction

For individuals with depression, negative information tends to be remembered better and retrieved more frequently than positive information (Gaddy & Ingram, 2014; Gotlib & Joormann, 2010). This negative memory bias is one of the most well-established cognitive findings in depression research, observed not only in clinical patients, but also in populations with remitted depression (Leppänen, 2006). It is intertwined with a ruminative response style (Hertel et al., 2014; Kuo et al., 2012), and significantly contributes to the onset, maintenance and recurrence of depressive episodes (Graaf et al., 2010; Sarason et al., 2014). Beyond this close connection to depression, substantial evidence has suggested that negative memory bias is also related to the adverse events experienced during an individual's childhood (Gethin et al., 2017; Vrijsen et al., 2015, 2017), which are recognized as impactful risk factors for depression and other psychiatric disorders (Tunnard et al., 2014). Childhood adversity (CA), including various forms of threat and deprivation (McLaughlin & Sheridan, 2016), can result in maladaptive cognitive alterations. Higher levels of negative memory bias have been associated with more frequent CA, and mediated the relationship between CA and psychiatric comorbidities (Vrijsen et al., 2017).

In addition to empirical evidence, associations between negative memory bias, CA and depression have been well interpreted by a theoretical model—Beck's cognitive model of depression (Beck, 1967, 2008; Beck & Bredemeier, 2016; Disner et al., 2011). Within this framework, CA plays a critical role in the formation of a negative internal world knowledge system—the "depressive schema". This schema can be activated later in life (e.g., by stressful events, or a negative affective state) and subsequently guide the cognitive function toward a negative mode, which triggers biased automatic information processing including negatively biased memory. Negative memory bias, in turn, strengthens the depressive schema and again reinforces negatively biased cognition (Disner et al., 2011). Beck's cognitive model of depression has served as theoretical underpinning for cognitive-based therapy (Beck, 2005; Beck & Haigh, 2014), and several of its elements have been supported by behavioral and neuroimaging findings (Gotlib, Krasnoperova, et al., 2004; Groenewold et al., 2013; Hamilton & Gotlib, 2008; Heller et al., 2009; Siegle et al., 2002).

In previous studies, the relationship between CA and negative memory bias was primarily investigated in psychiatric patient samples (Vrijsen et al., 2017), where CA and levels of depressive symptom (DS) were highly correlated (Comijs et al., 2007; Korkeila et al., 2010; Norman et al., 2012). The roles of CA and DS levels were not clearly disentangled as they were often not analyzed within a single

integrated model. It's possible that negative memory bias simply reflects a symptom accompanying depressive states, and thus the observed association between CA and negative memory bias may be attributable to elevated DS levels commonly seen in individuals with adverse childhood experiences. To clarify this issue, it's essential to examine a sample that encompasses a broader range of CA and DS levels, while also ensuring greater independence between the two factors (e.g., including individuals with high CA but low DS, and vice versa). In an insightful study, Abercrombie and colleagues utilized a sample that varied in both DS and childhood emotional abuse (a specific type of CA), with the two variables not fully overlapping (Abercrombie et al., 2018). This study found that negative memory bias was related to DS, but they did not report an association between childhood emotional abuse and memory bias. In translating the findings into Beck's model, the study did not include the factor of depressive schema activation. This raises the possibility that the latent relationship between CA and negative memory bias may only present itself after schema activation (e.g., for individuals with high CA but low current depression). Therefore, it is also important to examine the role of depressive schema activation and how it interacts with both CA and DS in shaping negative memory bias.

In this study, we aimed to investigate the roles of CA, DS levels and depressive schema activation, as well as their interactions, in relation to negative memory bias. Within a sample covering diverse but non-collinear levels of CA and DS, participants encoded pictures of negative, neutral or positive valence following both a depressive schema activation task (Vrijsen et al., 2019) and a control task (within-subject design). Memory performance was assessed the next day through recognition memory tests. We hypothesized that CA and DS would each show a general positive association with negative memory bias strength, and that schema activation would amplify the association between CA and negative memory bias—particularly among participants with high CA but low DS.

The development of negative memory bias is related to functional changes in brain regions involved in emotional memory processing. In healthy individuals, the amygdala plays an important role in the encoding, consolidation, and retrieval of emotional memories, particularly for high-arousal negative stimuli (Bisby et al., 2016; Dolcos et al., 2004; Kark & Kensinger, 2019; LaBar & Cabeza, 2006). Studies with depressed patients and individuals in remission from depression have consistently shown greater amygdala engagement during the encoding of negative stimuli compared to healthy controls (Hamilton & Gotlib, 2008; Ramel et al., 2007; van Eijndhoven et al., 2011). Moreover, this heightened amygdala responsivity has been associated with depression severity and, in some cases, directly with negative

memory bias (Duyser et al., 2022; Hamilton & Gotlib, 2008; Ramel et al., 2007; Young et al., 2016). These findings identify the amygdala's central role in negative memory bias. Besides the amygdala, the hippocampus is another essential region for emotional memory processing. It is the hub for episodic memory (Moscovitch et al., 2016; Tulving & Markowitsch, 1998), and studies have shown that remembering emotional information does not rely on a separate neural mechanism, but instead modulates memory by influencing hippocampal activity (Kensinger, 2007; Qasim et al., 2023; Richardson et al., 2004). The amygdala mainly functions as an emotional responder, whereas the hippocampus acts more directly as a memory processor. Compared to the amygdala, the hippocampus has been relatively understudied in relation to negative memory bias, and findings remain inconclusive. In healthy individuals, reduced hippocampal volume has been associated with greater negative memory bias (Gerritsen et al., 2012); while depressed patients have shown greater negative memory bias and heightened hippocampus-amygdala functional connectivity during the negative encoding, compared to healthy controls (Hamilton & Gotlib, 2008). This inconsistency may be partially explained by individual differences in CA and DS. Both the amygdala and hippocampus are known to be vulnerable to CA (McLaughlin et al., 2019; Teicher et al., 2016). Substantial evidence has demonstrated sensitized amygdala responsivity to negative stimuli and reduced hippocampal volume following CA exposure (Grant et al., 2011; McCrory et al., 2011; Riem et al., 2015; Teicher et al., 2016). These alterations may further contribute to a neural substrate for altered emotional memory processing in individuals with CA. Thus, to examine how the well-established role of the amygdala in memory bias is linked to CA, and to provide more evidence on how hippocampal activity varies with CA and contributes to negative memory bias, we chose the amygdala and hippocampus as our regions of interest (ROIs). Functional magnetic resonance imaging (fMRI) data were collected to examine how encoding activity in these regions relates to the interaction among CA, DS, and depressive schema activation.

Materials and Methods

Participants

To recruit participants with varying levels of CA and DS, we utilized a two-step screening procedure, including online and onsite screenings (see Supplement for details). A total of 87 adults completed the study. Of these, data of four participants were excluded due to falling asleep during an fMRI scan and of one participant due to taking psychotropic medication during participation. The final sample comprised 82 participants (51 female, 29 male, 2 diverse), covering, as intended, a large range of CA

and DS levels (see Table 2.1 and Figure 2.1 for sample characteristics). For MRI analyses involving the memory encoding stage, data of two participants were excluded due to a technical failure of scanning (n = 1) and excessive head motion (n = 1; Table S2.1).

This study was approved by the regional ethics committee (METC Oost-Nederland; Dossiernummer: 2022-13885). All participants provided written informed consent and were compensated for participation.

Table 2.1 Sample characteristics

	Min	Max	Mean	SD	Median
CA_severity [a]	0.00	71.00	24.88	18.54	20.59
CA_multiplicity [a]	0.00	10.00	2.65	2.68	2.00
DS level[a]	0.00	40.00	13.33	8.94	11.00
Age	18.06	48.66	25.00	7.32	22.15
Education[b]	1.00	7.00	4.10	1.55	3.00
Social Status[c]	2.00	8.00	6.15	1.38	6.00
Community Status[c]	2.00	9.00	5.91	1.55	6.00

[a] CA_severity: the overall severity score, range 0-100; CA_multiplicity: number of types of CA experienced range 0-10; DS level: levels of depressive symptoms, range 0-63; see Questionnaires section.

[b] Education categories: 1 = Elementary education; 2 = Pre-vocational education; 3 = General secondary education, or pre-university education; 4 = Secondary vocational education; 5 = University of applied sciences; 6 = Research university; 7 = Master, PhD or higher.

[c] The subjective impression of social status and status in their community (range 1-10) was measured through MacArthur Scale of Subjective Social Status (Adler et al., 2000).

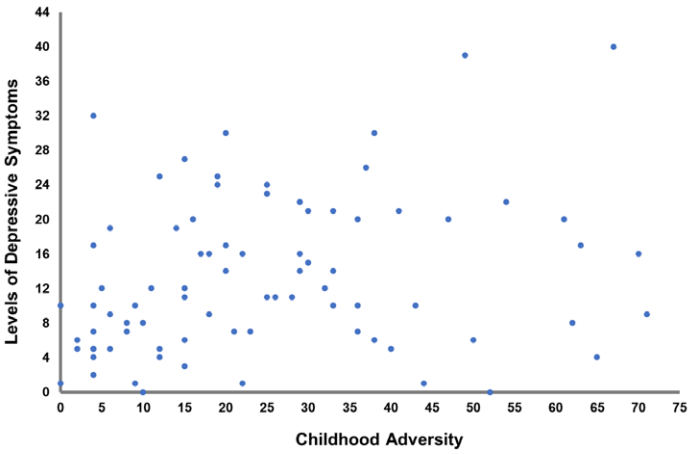

Figure 2.1 Distributions of childhood adversity (MACE overall severity scores) and levels of depressive symptoms (BDI-II sum scores) in the sample (N = 82). The two variables are correlated but not collinear (r = .256, p = .020).

Procedure

The complete procedure consisted of five sessions: one preparational visit followed by four MRI sessions (Figure 2.2A). During the preparational visit, participants were informed about the study procedure, screened for MRI compatibility, and gave their written consent. They then filled out questionnaires including demographic information, and measurements for CA and DS.

The four MRI sessions were divided into two phases, one involving depressive schema activation condition and the other a control condition, separated by at least a one-week interval. The order of these two conditions was counterbalanced across participants. Each phase spanned sessions on two consecutive days, with the memory encoding session conducted on the first day and the recognition memory test on the second — both in the scanner (Figure 2.2B).

Memory encoding sessions included an anatomical scan, functional scans during both the depressive schema activation/control task and the encoding task, as well as an 8-minute post-encoding resting-state scan. Affective states were assessed using the Positive and Negative Affect Schedule (PANAS, Watson et al., 1988) before and after the depressive schema activation/control task, and again after the encoding task. On the following day, participants completed corresponding recognition memory tests in the scanner, scheduled at similar time of the day to respective encoding sessions.

Measurements

Questionnaires

Childhood Adversity: Participants' detailed CA history was assessed by the Maltreatment and Abuse Chronology of Exposure scale (MACE, Dutch-translated version with 75 items) (Teicher & Parigger, 2015) during preparational visits. MACE measures the severity of ten types of childhood maltreatment (e.g., emotional neglect, non-verbal emotional abuse, parental physical maltreatment; see Teicher & Parigger, 2015 for the full list) experienced during the first 18 years of life, providing both an overall severity score (range 0-100) and a multiplicity score (range 0-10). The scale not only captures a comprehensive range of adverse exposures, but also offers a fundamental measurement of each exposure with items assessed on a uniform interval scale, which are its remarkable advantages (Teicher et al., 2018). MACE has demonstrated high reliability and strong correlations with scores from the Childhood Trauma Questionnaire (CTQ) and the Adverse Childhood Experiences (ACE) scale (Teicher et al., 2018; Zhu et al., 2023). In our study, the overall CA severity score was calculated following the scoring guidelines provided by Teicher and Parigger (2015) and used in subsequent analyses.

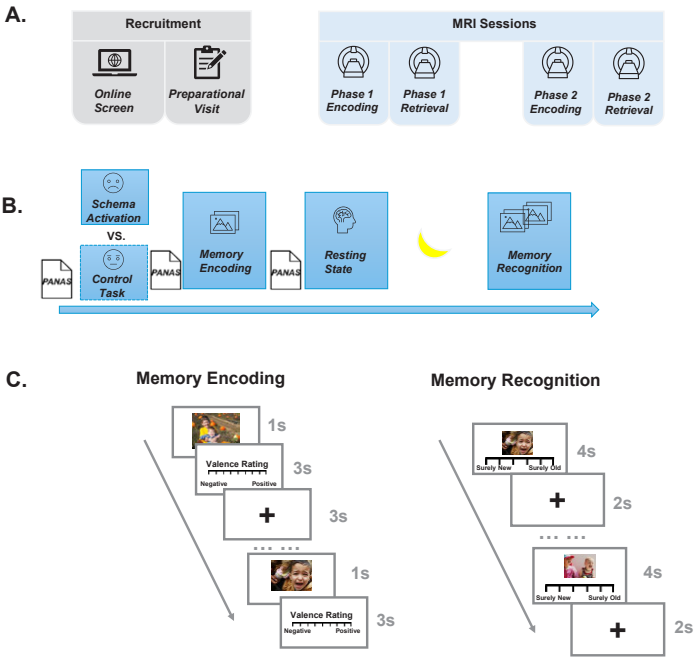

Figure 2.2 Experimental procedure and paradigm: (A) Following an online screening and a preparational visit, participants completed four MRI sessions, with an interval of at least one week between phase 1 and phase 2. (B) During encoding sessions (phase 1 and 2), participants first completed either the depressive schema activation or a control task (the assignment of the two conditions to phase 1 or 2 was counterbalanced); then they did the memory encoding and a resting-state scan. Their affective states were assessed by PANAS before and after the schema activation/control task, and again after the encoding. After about 24 hours, participants did the retrieval sessions. (C) During memory encoding tasks, participants viewed 180 pictures across two runs and rated the picture valence. In recognition memory tests, for 180 old and 180 new pictures, they made old/new judgments along with the confidence rating across three runs.

Levels of depressive symptoms: Beck Depression Inventory-II (BDI-II; Beck et al., 1996) was used to assess DS levels. As one of the most widely used self-report measures for depressive symptoms, BDI-II evaluates the severity of 21 depressive statements and yields an overall severity score (ranging from 0 to 63) by summing the 21 items.

Affective states: Prior to each memory encoding session, we utilized the Hospitality Anxiety and Depression Scale (HADS; Snaith, 2003) to measure participants' levels of anxiety and depression on the experimental day. Additionally, during each encoding session, the PANAS was administrated to record their affective states at three timepoints (see Procedure section).

Participants also completed Young Schema Questionnaire (YSQ; Young, 1999), for the assessment of early maladaptive schemas. Data and analyses related to this measure will be reported elsewhere.

Depressive schema activation

Depressive schemas were activated using a standardized music-based mood induction procedure. In the schema activation condition, participants listened to a 6-minute clip from the classical piece "Russia Under the Mongolian Yoke" played at half speed, which was used earlier to effectively induce a sad mood state (Vrijsen et al., 2019). Participants were instructed to allow the sadness conveyed by the music to influence their mood and to maintain that emotional state. In the control condition, participants listened to a 6-minute clip from the neutral piece "Adagio of Mozart's Clarinet Concerto", which also has been used for this purpose before (Berthold-Losleben et al., 2021). The instruction was "listen to the music without engaging in any emotions." A debriefing was employed at the end of sessions to ensure no sustained negative mood was induced.

Emotional memory encoding and recognition memory test

A total of 720 emotionally normed photographs were selected for our memory tasks from the International Affective Picture System (IAPS; Lang et al., 1997), the Emotional Picture Set (EmoPicS; Wessa et al., 2010), and the Geneva Affective Picture Database (GAPED; Dan-Glauser & Scherer, 2011). To align with the internal schemas depicted in Beck's model, the majority of the selected images depicted human activities. Pictures for different valence categories (negative, neutral, and positive) significantly differed in normative valence and arousal ratings, while contrast, luminance, and content were matched across categories (all *p*s > .400). See Supplement and Table S2.2 for statistics.

240 pictures for each valence type were divided into four sets of 60 images, balanced for valence and arousal ratings within each valence type, and for contrast and luminance across valence types. The assignment of picture sets to experimental conditions (old/new × schema activation/control × first/second phase) was counterbalanced across participants, ensuring that each picture had an equal probability of being used in each condition.

During memory encoding for each condition (schema activation or control), participants viewed 180 distinct pictures across 2 runs (30 per valence per run). Each image was presented centrally on the screen for 1s. Participants were instructed to view the pictures attentively and rate their emotional valence on a nine-point

scale (1 = "very negative" to 9 = "very positive") within 3s. The inter-trial interval (ITI) varied with the average of 3s.

In recognition memory tests on the following day, participants were presented with 360 pictures across 3 runs, comprising 180 old images encoded on the previous day and 180 new images (60 per valence). Each picture was displayed for 4s, during which participants made an old/new judgment along with a confidence rating on a 1–6 scale (1 = "surely new" to 6 = "surely old"). The ITI varied with the average of 2s. For both encoding and recognition tasks, picture presentation was pseudorandomized, ensuring that no identical condition (valence, old/new) was repeated more than twice consecutively. Participants were given detailed instructions and completed practice trials using additional images outside the scanner. See Figure 2.2C for illustration of the memory paradigms.

Statistical analyses

Behavioral data analyses

We first tested the effectiveness of depressive schema activation. A repeated measures analysis of variance (ANOVA) was performed on affective states measured by PANAS, taking schema activation (activation, control), timepoint (before activation/control, after activation/control, after encoding) and affect type (negative, positive) as within-subject factors ($p < .05$, two tailed, Bonferroni correction). Successful depressive schema activation was operationally defined as higher negative affect following the schema activation condition compared to the control condition.

Valence rating data obtained during encoding periods provided an opportunity to examine the "biased processing" aspect of Beck's model. To test how CA, DS levels and schema activation interact to influence participants' valence rating across different pictures categories (negative, neutral and positive), linear mixed-effects modelling (LMM) was performed with valence rating as the dependent variable, CA (overall severity score on the MACE), DS levels (BDI-II), picture category, and schema activation as fixed effects, and participant identity as the random effect.

To evaluate participants' memory performance, a recognition memory index was calculated by subtracting the false alarm rate (i.e., the proportion of new pictures incorrectly identified as old) from the hit rate (i.e., the proportion of old pictures correctly identified as old) for each participant and condition. A LMM with CA, DS levels, picture category, and schema activation as fixed effects, and participant identity as the random effect, was performed on the recognition memory index. Additionally, to further capture the difference between negative and positive

memory, a memory bias index was derived as ($recognition_{negative}$ – $recognition_{positive}$)/ $recognition_{neutral}$, adapted from Hamilton & Gotlib (2008). Another LMM was conducted on this memory bias index, with CA, DS levels, and schema activation included as fixed effects, and participant as a random effect.

All LMMs (including those for MRI data shown below) were conducted using the lmerTest package (https://CRAN.R-project.org/package=lmerTest) in R (v4.3.3) (R Core Team, 2024) via RStudio (v2024.04.1) (RStudio Team, 2024). Data was standardized to z-scores before entering LMM. We additionally compared models incorporating schema activation as a random slope to account for individual variability in schema activation effects, as well as models that further included age and gender as covariates. Model selection was guided by likelihood ratio tests, along with comparisons of the Akaike Information Criterion (AIC) and Bayesian Information Criterion (BIC). See Supplement for details on all model statistics.

MRI data analyses

To capture the brain activity during successful encoding of pictures in different valence categories (negative, neutral, positive), a univariate general linear model (GLM) was conducted on the encoding period. Temporal autocorrelation was corrected using FILM(Woolrich et al., 2001). Each picture trial was modeled as a 1-second event from stimulus onset, convolved with the canonical hemodynamic response function (HRF). Picture presentations were categorized into four regressors based on valence and subsequent memory performance: Negative_ Remember, Neutral_Remember, Positive_Remember, and Forget. The presentation of the valence rating scale (duration = 3 s) was modeled as an additional regressor. Volumes with relative head displacement exceeding 1 mm were included as nuisance regressors to control for motion artifacts. Four contrasts of interest (i.e., Negative_remember vs. Neutral_remember; Positive_remember vs. Neutral_ remember; Negative_remember vs. Positive_remember; Remember vs. Forget) were performed first at the individual space. Due to high memory performance (see Table S2.5), there were insufficient trials in the Forget condition for meaningful contrasts involving valence category × memory interactions (e.g, Negative_ remember vs. Negative_Forget). The resulting statistical maps were normalized to MNI standard space, averaged across the two runs within each encoding session, and then across the two encoding sessions (schema activation, control). The contrast of schema activation vs. control was generated per participant. These resulting images were analyzed at the group level, including CA and DS levels as factors of interest, with age and gender as covariates. Multiple comparison correction was applied using cluster-mass thresholding in FEAT (voxel-wise $z > 3.1$,

cluster-level $p < 0.05$ FWER corrected). Results for this whole-brain univariate GLM are reported in Supplement.

Based on our hypotheses regarding the vulnerability of the amygdala and hippocampus to CA and their potential roles in negative memory bias, we took these two regions as our prior ROIs. Anatomical masks for the bilateral amygdala and hippocampus were derived from the Harvard-Oxford subcortical atlas, using a 50% probability threshold (Krenz et al., 2021). For each participant, Zstat maps corresponding to each condition (i.e., Negative_Remember under schema activation, Negative_Remember under control, Neutral_Remember under schema activation, Neutral_Remember under control, Positive_Remember under schema activation, and Positive_Remember under control) were extracted. The median z-value across all voxels within each ROI was used to represent the blood oxygenation level-dependent (BOLD) response of the amygdala and hippocampus. To examine how CA, DS levels, and schema activation interactively influence amygdala and hippocampus activity during emotional memory encoding, similar to the behavioral analyses, we conducted LMMs including BOLD response of the two ROIs as dependent variables, with CA, DS levels, picture category, and schema activation as fixed effects, and participant identity as a random effect. To further investigate the brain-behavior association, we then examined the relationship between biased encoding activity in amygdala and hippocampus and the biased memory. For each participant and ROI, the biased activity score was computed by subtracting BOLD response to later-remembered positive pictures from negative ones. LMMs were built with memory bias index as the dependent variable, schema activation condition and the biased activity score of two ROIs as fixed effects, and participant identity as a random effect.

Moreover, to verify that the results we found were not unduly influenced by outliers, we conducted sensitivity analyses guided by the Mahalanobis distance (Mahalanobis, 1930). See Supplement for full details.

Results

Manipulation check: depressive schema activation

The repeated measures ANOVA on affect ratings showed a significant interaction between schema activation, timepoint and affect type ($F(2, 162) = 19.577$, $p < .001$). For negative affect, while participants showed same baseline under the schema activation and control condition ($p = .181$), they had significantly higher negative affect after the schema activation than the control condition ($p < .001$; Figure S2.3);

after the memory encoding, negative affect returned to similar values across the two conditions (p = .340). For positive affect, no significant differences were found between the two conditions across all three timepoints (ps > .070), and a general decline over time was observed. Notably, positive affect did not differ significantly before and after the control task (p = .500), whereas it was significantly reduced following the depressive schema activation (p < .001). These results indicate our depressive schema activation successfully induced participants' negative mood.

Biased processing: depressive symptoms and picture valence rating

LMM with valence rating as the dependent variable identified an interaction between DS levels and picture categories (positive vs. negative; *Beta* = -.130, $t(390)$ = -2.587, p = .010, 95% CI = [-.226; -.034]): participants with higher levels of depressive symptoms rated positive pictures more negatively compared to those with lower depressive symptoms (Figure 2.3A). CA and schema activation didn't show significant main effects or interactions (ps > .070).

Biased memory: higher CA, more negative memory bias

For the recognition memory, there was an interaction between CA and picture categories (positive vs. negative; *Beta* = -.178, $t(312)$ = -2.157, p = .032, 95% CI = [-.336; -.020]). Compared to negative pictures, CA was more negatively associated with recognition memory for positive pictures, indicating a relative advantage for negative over positive memory among participants with higher severity of CA (Figure 2.3C).

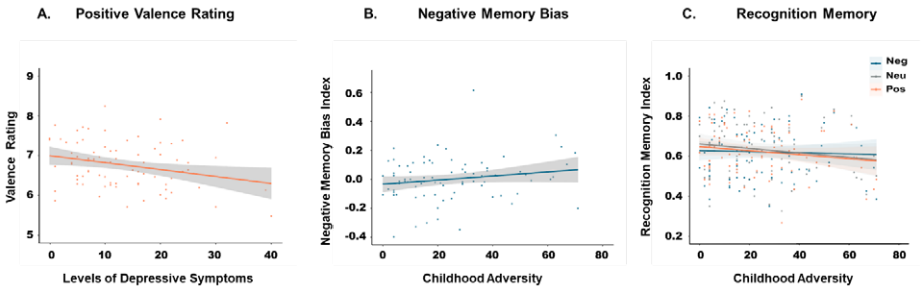

Figure 2.3 (A) During encoding, participants rated the emotional valence of each picture on a nine-point scale. Higher levels of DS (BDI-II sum scores) were associated with lower valence ratings for positive pictures. (B) Negative memory bias was calculated as the difference between recognition memory for negative versus positive pictures, divided by memory for neutral pictures. Participants with higher levels of CA (MACE overall severity scores) showed more negative memory bias. (C) The recognition memory index was quantified using the hit rate minus false alarm rate. Compared to memory for negative pictures, CA was more negatively associated with memory for positive pictures. Neg, negative pictures; Neu, neutral pictures; Pos, positive pictures.

Same pattern was found for the memory bias index, where CA was positively associated with negative memory bias (*Beta* = .253, *t*(155) = 2.212, *p* = .028, 95% CI = [.033; 0.473]; Figure 2.3B). DS levels and schema activation didn't show significant main effects or interactions (*p*s > .090).

Biased BOLD-fMRI response in the amygdala and hippocampus during memory encoding

For our ROIs of bilateral amygdala and hippocampus, the encoding activity for subsequently remembered pictures also indicated a negative bias related to CA (amygdala: *Beta* = -.097, *t*(312) = -3.630, *p* < .001, 95% CI = [-.149; -.045]; hippocampus: *Beta* = -.058, *t*(312) = -2.031, *p* = .043, 95% CI = [-.114; -.003]). Consistent with the recognition memory performance, CA was more negatively associated with amygdala and hippocampus BOLD response to later-remembered positive pictures, compared to negative ones, indicating a greater negative–positive imbalance in encoding activity among individuals with more severe CA (Figure 2.4). No main effects or interactions related to DS levels and schema activation were observed (*p*s > .050). See Supplementary for full model statistics.

Association between biased memory and biased hippocampal activity

We further examined whether the observed imbalanced encoding activity in amygdala and hippocampus played a role in negative memory bias. LMMs were built to test associations between memory bias index and the biased activity score of two ROIs. The LMM for amygdala did not find any main effects or interactions, while the model with the hippocampus revealed a relationship between the biased activity score and memory bias index (*Beta* = .273, *t*(155) = 2.000, *p* = .047, 95% CI = [.007; .539]), showing more biased hippocampal activity was related to stronger negative memory bias.

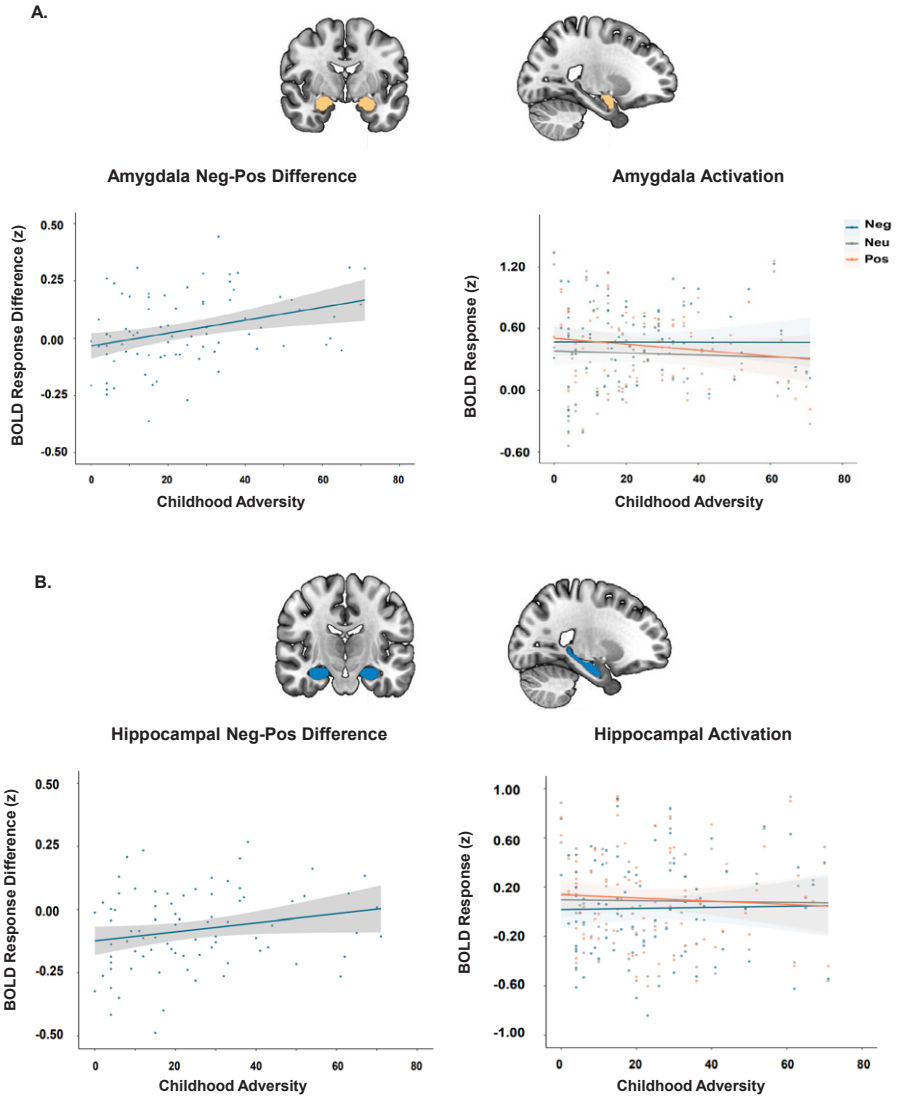

Figure 2.4 For the subsequently remembered pictures, participants with higher levels of CA (MACE overall severity scores) showed more negative-positive imbalanced encoding BOLD-fMRI response in the (A) amygdala and (B) hippocampus. For both regions, there was a trend for decreased activation in response to positive pictures related to higher levels of CA. Neg, negative pictures; Neu, neutral pictures; Pos, positive pictures.

Discussion

Negative memory bias has been related to both depression and CA, yet their distinct contributions and interactions with the depressive schema activation remain to be elaborated. In a sample covering diverse but non-collinear levels of DS and CA, we found that while DS was related to negatively biased processing of emotional stimuli, it was CA that was associated with negatively biased memory performance in a classical emotional memory task. CA was also linked to a negative-positive imbalanced encoding activity in the amygdala and hippocampus, mirroring the negatively biased behavioral pattern. External activation of the depressive schema did not further modulate the relationship between CA and either negative memory or neural activity bias.

Our findings draw focused attention to the role of CA in negative memory bias. Given the high correlation between CA and DS levels (Hovens et al., 2010; Tunnard et al., 2014), previous studies have rarely evaluated roles of CA and DS within the same analytical model. Our sample design included individuals with high CA but low DS levels, and vice versa, allowing us to examine the contributions of each factor while controlling for the other, as well as their interaction. We found that higher CA was associated with greater negative memory bias after controlling for levels of DS. This result contrasts with findings from Abercrombie et al. (2018), who also used a sample with varying levels of DS and childhood emotional abuse, but did not report a direct association between childhood emotional abuse and negative memory bias. One difference lies in the measurement of CA: while Abercrombie et al. focused on a single type of adversity, our study used a composite severity score based on multiple types of adverse childhood experiences. Another possible explanation for the discrepancy involves sample composition. In Abercrombie et al.'s study, the majority of participants were psychiatric patients (including 47 with depression), whereas in our sample, only 6 participants reported psychiatric diagnoses (including 1 with depression and 1 with PTSD). The robust association between negative memory bias and depression in clinical populations may overshadow any additional effects of CA (Gotlib & Joormann, 2010; Mathews & MacLeod, 2005; Matt et al., 1992), potentially also explaining why they observed a stable link between DS and negative memory bias while we did not. Our results suggest that, within this sample of minimal clinical diagnoses, individuals with high CA but low DS already exhibit negatively biased memory processes—possibly a lasting imprint left by adverse experience. This early-stage cognitive maladaptation may lead individuals to adopt negative coping strategies, and interact with other cognitive processes to facilitate the eventual onset of depression (Connolly & Alloy, 2018; Nolen-Hoeksema et al., 2008).

Looking back at Beck's model, this study supports several components of the framework. We found that DS was negatively associated with valence ratings for positive pictures, indicating a potential loss of healthy positive processing styles (Arnold et al., 2011). Individuals with higher DS reported less pleasure in response to being presented with positive stimuli, consistent with prior findings of diminished reactivity to pleasant stimuli in depression (Duyser et al., 2025; Schaefer et al., 2006; Shestyuk et al., 2005; Sloan et al., 2001). Loss of pleasure is a feature of depressive episodes (Rizvi et al., 2016). Our results might suggest that biased processing of positive stimuli is more directly tied to current affective states, sensitively fluctuating with DS levels; in contrast, emotional memory processes appear to be heavily biased by individuals' past life experiences. This phenomenon, to some extent, reflects the influence of prior knowledge on new learning and memory formation, extensively studied in memory research (Fernández & Morris, 2018; Ghosh & Gilboa, 2014; Gilboa & Marlatte, 2017), and also supports Beck's conceptualization of the "depressive schema".

Our schema activation manipulation via negative mood induction did not alter the relationship between CA and negative memory bias. Therefore, the inherent schema shaped by CA may not require extra activation to exert its effects. Rather, it may be automatically activated by new emotional stimuli, thereby biasing how they are processed and remembered. Notably, previous studies have mostly characterized this depressive schema effect through the Self-Referent Encoding Task (Hammen & Zupan, 1984; Vrijsen et al., 2015, 2017), which evaluates memory for self-relevant adjectives. Our study extended it through a classical emotional memory task with commonly-used picture viewing and recognition paradigms. Although images in our tasks primarily depicted human activities, they were not directly self-referential. This extension suggests that the relationship between CA and negative memory bias could generalize beyond explicitly self-referential material, and depressive schemas may influence a broader emotional memory process.

CA-related negative bias was also observed at the neural level. In both the amygdala and hippocampus—key regions for emotional memory processing, encoding activity showed more advantages for negative compared to positive pictures among individuals with higher CA severity. A negatively biased amygdala response has been consistently found in CA victims (McCrory et al., 2011; Teicher et al., 2016) and depression patients (Hamilton & Gotlib, 2008; van Eijndhoven et al., 2011). Our findings add to prior studies by providing direct evidence of CA-related amygdala response bias from the memory encoding phase. In addition, we noticed that the negative (vs. positive) advantage pattern in amygdala activity was primarily driven

by a trend toward reduced activation in response to positive stimuli, consistent with the impaired processing of positive stimuli described above. The blunted amygdala reactivity has also been reported in depression patients during the retrieval of positive autobiographical memories (Dillon & Pizzagalli, 2018; Young et al., 2016), which may indicate insufficient recovery of positive memory engrams and lead to overgeneralized positive retrieval. Given that amygdala engagement at encoding is known to support the vividness of emotional memory recall (Kensinger et al., 2011), reduced amygdala activation in individuals with CA may result in less vivid formation of positive engrams, thereby hindering their later recall.

Similar to the amygdala, our results also showed that higher CA was associated with a more negatively biased pattern of hippocampal encoding activity. CA can disrupt hippocampal development, reduce hippocampal volume and plasticity (Raymond et al., 2018; Riem et al., 2015), and lead to long-term memory impairments (Bolton et al., 2020; Lambert et al., 2017, 2019). Our findings indicate that, in individuals with high CA severity, hippocampal responses to negative stimuli may be relatively preserved compared to those for positive stimuli, contributing to a valence-specific imbalance in hippocampal activity. Furthermore, this imbalance was associated with greater negative memory bias at the behavioral level. The correspondence between hippocampal activity and memory performance supports the hippocampus's critical and direct involvement in emotional memory processing (Kensinger, 2007; Pronier et al., 2023; Qasim et al., 2023; Richardson et al., 2004), although this interpretation should be made with caution due to the small effect size. Future research is needed to deeply explore the hippocampal mechanisms underlying negative memory bias, such as its representational patterns and interactions with other brain regions.

Besides the findings, several limitations in our study should also be considered. First, although the music induction is a well-validated mood induction method (Vrijsen et al., 2019), it may not able to fully capture the complexity of depressive schemas shaped by CA, and therefore did not show additive effects on biased processing and memory. This method was chosen to find a balance between experimental efficacy and the necessity of avoiding prolonged psychological distress in participants. Future studies are needed to explore more personalized and ecologically valid schema activation approach that also minimizes psychological burden. Second, while we observed a negatively biased pattern in amygdala and hippocampus encoding activity, the neural mechanisms underlying CA-related negative memory bias may be more complex. In this regard, substantial research on schema effects in the memory domain may provide new perspectives for future investigations.

In conclusion, our study demonstrated that individuals with a history of CA showed negative biases in both memory performance and neural activity, even in the absence of elevate depressive symptoms. These findings provide more empirical evidence for Beck's cognitive model of depression, and highlight the necessity of considering CA as an important individual factor when designing psychiatric research and clinical interventions targeting maladaptive cognition.

Supplementary Material

Materials and Methods

Participants

The basic inclusion and exclusion criteria were as follows:

Inclusion criteria

- Legally competent adults with the ages between 18-50
- Normal or corrected-to-normal vision
- Normal uncorrected hearing
- Willingness and ability to understand nature and content of the study
- Ability to participate and comply with study requirements
- Fluent in Dutch (>= B1 level)

Exclusion criteria

- History of or current cognitive impairments or other relevant medical condition
- Currently under psychotropic or other relevant medication
- History of or current brain surgery or epilepsy
- Pregnancy
- MRI incompatibility (unremovable metal parts in upper body [plates, screws, serrefines, dental plates (pontics), metal splinters, piercings or medicinal plasters], active implant [e.g. Pacemaker, neuro stimulator, insulin pump and/or hearing aid], head operation, epilepsy, claustrophobia).

Our recruitment consisted of two steps. The initial screening was conducted via an anonymous online survey (www.soscisurvey.com), which included eight items assessing CA and two items assessing DS. The CA questions assessed the frequency (rated from 1 = "Never" to 5 = "Very often") of eight different types of adversity. Two DS questions were adapted from BDI-II (pessimism and loss of pleasure). Psychotropic medication use and general MRI incompatibility were also screened in the online survey. To recruit individuals with diverse levels of CA and DS, we oversampled for high CA and DS by inviting all participants with elevated CA (>=12) or DS scores (>=2) to the onsite screening, while individuals with both CA < 12 and DS < 2 were randomly selected for participation based on a 10% inclusion probability. CA and DS scores were screened in the algorithm independently, thereby reducing potential overlap between the two variables. Eligible participants at this step were notified by the survey platform, and contacted researchers to schedule a preparational visit. During preparational visits, informed consent was

obtained, then participants completed detailed assessments of CA and DS using MACE and BDI-II. MRI incompatibility was further screened with the standardized screening form at the Donders Institute. We consistently monitored the distribution of CA and DS within the sample, and at the late stage of recruitment, to include more people with elevated CA and DS scores, we ceased including participants with an online CA < 12 and DS scores < 4, as well as those with both MACE < 15 and BDI-II < 13 at the onsite screening.

Based on participants' self-reported medical conditions, among 82 individuals included in the analyses, 6 reported ongoing psychiatric conditions at the time of participation (1 with depression, 1 with post-traumatic stress disorder (PTSD), and 4 with attention-deficit/hyperactivity disorder (ADHD)).

Considering the possible influence of cultural background on CA experiences (Alcaraz et al., 2024; Basto-Pereira et al., 2022), and the recruitment feasibility as well, all participants were recruited from western European countries. 79 participants held Dutch nationality, including 4 with dual nationality (2 American, 1 Moroccan, and 1 Spanish), and 3 participants held the German nationality. All participants were fluent in Dutch (>= B1 level).

Table S2.1 Sample characteristics (for MRI analyses, N=80)

	Min	Max	Mean	SD	Median
CA_severity [a]	0.00	71.00	24.44	18.55	20.00
CA_multiplicity [a]	0.00	10.00	2.58	2.68	2.00
DS level [a]	0.00	40.00	13.34	8.98	11.00
Age	18.06	48.66	24.90	7.42	22.06
Education [b]	1.00	7.00	4.08	1.53	3.00
Social Status [c]	2.00	8.00	6.15	1.36	6.00
Community [c] **Status**	2.00	9.00	5.91	1.57	6.00

[a] CA_severity: the overall severity score, range 0-100; CA_multiplicity: number of types of CA experienced range 0-10; DS level: levels of depressive symptoms, range 0-63; see Questionnaires section.

[b] Education categories : 1 = Elementary education; 2 = Pre-vocational education; 3 = General secondary education, or pre-university education; 4 = Secondary vocational education; 5 = University of applied sciences; 6 = Research university; 7 = Master, PhD or higher.

[c] The subjective impression of social status and status in their community (range 1-10) was measured through MacArthur Scale of Subjective Social Status (Adler et al., 2000).

Stimuli

Pictures from different valence categories differed significantly in valence and arousal ratings (valence: $F(2, 717) = 4966.15$, $p < .001$; arousal: $F(2, 717) = 356.33$,

$p < .001$). Negative images exhibited the lowest valence scores, while positive images showed the highest ($ps < .001$). Negative images were more arousing than both positive and neutral images, and positive images were more arousing than neutral images ($ps < .001$). There were no significant differences among the three categories in terms of contrast or luminance ($ps > .400$). Additionally, the proportions of content types (e.g., human activity, animal, scene, object) were comparable across categories ($p = .158$).

Table S2.2 Stimuli characteristics

	Negative	**Neutral**	**Positive**	**All**
Valence [a]	2.60 ± 0.64	5.06 ± 0.37	7.25 ± 0.49	4.97 ± 1.96
Arousal [b]	5.74 ± 0.87	3.53 ± 0.79	4.69 ± 1.04	4.65 ± 1.28
Contrast [c]	6.76 ± 1.77	6.61 ± 1.68	6.56 ± 1.98	6.65 ± 1.82
Luminance [d]	105.38 ± 29.40	103.60 ± 33.14	106.41 ± 34.31	105.13 ± 32.37
Contents:				
Human activity	208	192	191	591
Animal	18	20	28	66
Scene	11	17	13	41
Object	3	11	8	22

[a] Valence: the pleasantness of the image, from unpleasant to pleasant, range 1-9.
[b] Arousal: the emotional intensity, from calm to excited, range 1-9.
[c] Contrast: the difference in brightness between regions of the image, calculated by the global contrast factor.
[d] Luminance: the mean brightness of the image, range 0-255.

MRI data acquisition and preprocessing

MRI scans were collected using the 3.0 T Siemens Magnetom Prisma (Alcaraz et al., 2024; Basto-Pereira et al., 2022)(Erlangen, Germany) system with a 32-channel head coil. During depressive schema activation/control tasks, memory encoding and recognition tasks, as well as post-encoding resting-state scans, T2*-weighted BOLD images were recorded using a multi-echo, multi-band EPI sequence with interleaved slice acquisition (51 slices; TR = 1.5 s; TEs = 13.4 ms, 34.8ms and 56.2 ms; flip angle = 75°; multi-band accel. factor = 3; slice thickness = 2.5 mm; voxel size = 2.5 × 2.5 × 2.5 mm; FOV = 210 x 210 x 128 mm). Fieldmap images were acquired (51 slices; TR = 380 ms; TEs = 2.60 ms and 5.06 ms; multi-slice mode, interleaved; slice thickness = 2.5 mm; flip angle = 60°; voxel size = 2.5 × 2.5 × 2.5 mm; FOV = 210 x 210 x 128 mm) for spatial distortion correction. High-resolution structural images (1 mm isotropic) were collected using a T1-weighted MP-RAGE sequence (TR = 2.3 s; TE = 3.03 ms; flip angle = 8°; FOV = 256 × 256 × 192 mm).

Before preprocessing, MRI data were converted into standardized datasets using BIDScoin (Zwiers et al., 2022). Multi-echo images were combined through the echocombine tool embedded in BIDScoin (algorithm: average). Preprocessing and analyses were conducted with the FMRI Expert Analysis Tool (FEAT; v6.00) from the FMRIB Software Library (FSL; v6.0.5)(Jenkinson et al., 2012). The first two volumes of each functional run were discarded to allow for T2 equilibration. Brain extraction was performed using BET (S. M. Smith, 2002). Field inhomogeneities were corrected with fieldmaps, and head motion correction was conducted with MCFLIRT (Jenkinson et al., 2002). Spatial smoothing was applied with a Gaussian kernel of FWHM 4.0 mm. Functional images were registered to each participant's high-resolution T1 image using boundary-based registration (BBR) via FLIRT (Jenkinson and Smith, 2001; Jenkinson et al., 2002), and normalized to Montreal Neurological Institute (MNI) 152 standard space (2 mm) for group analysis, using nonlinear registration (Andersson et al., 2007a, 2007b). Additionally, we carried out the Advanced Removal of Motion Artefacts based on independent component analysis (ICA-AROMA) (Pruim et al., 2015) to further mitigate motion-related noise, and applied high-pass temporal filtering with a cut-off of 100s.

Results

Linear mixed-effects model comparison and selection

Our primary hypothesis held that CA, levels of DS and schema activation interacted to influence participants' valence rating, recognition memory and brain activity for different categories, therefore, LMM started from the model with a full 4-way interaction (M1). Considering individual variability in schema activation effects on the dependent variables, we compared models incorporating schema activation as a random slope (M2); and models including age and gender as covariates to account for their influence (M3). For LMMs involving amygdala and hippocampal activity, we additionally tested the model of 3-way interaction (CA × DS × picture category; M4) with the influence of schema activation controlled, given that we didn't find significant effects of schema activation in any behavioral outcomes (valence rating, recognition memory). The 3-way interaction model might offer a more targeted structure for interpreting the observed behavioral results. Models with age and gender as covariates were also tested (M5).

All the model structure and statistics are listed in Tables S2.6–S2.12.

Whole-brain univariate BOLD-fMRI response

Memory effects

We identified brain regions involved in the general subsequent memory effect (i.e., Remember vs. Forget) in the whole-brain analysis, across all picture categories and schema activation conditions. Increased activation was observed in regions typically implicated in memory–emotion interactions, including bilateral amygdala extending into the anterior hippocampus, the left inferior frontal gyrus, and the ventral and dorsal medial prefrontal cortex. Additionally, regions involved in visual processing including the lateral occipital cortex, inferior temporal gyrus, and temporal fusiform cortex also showed heightened BOLD responses for subsequently remembered pictures (voxel-wise $z > 3.1$, cluster-level $p < 0.05$ FWER corrected; Figure S2.1, Table S2.3).

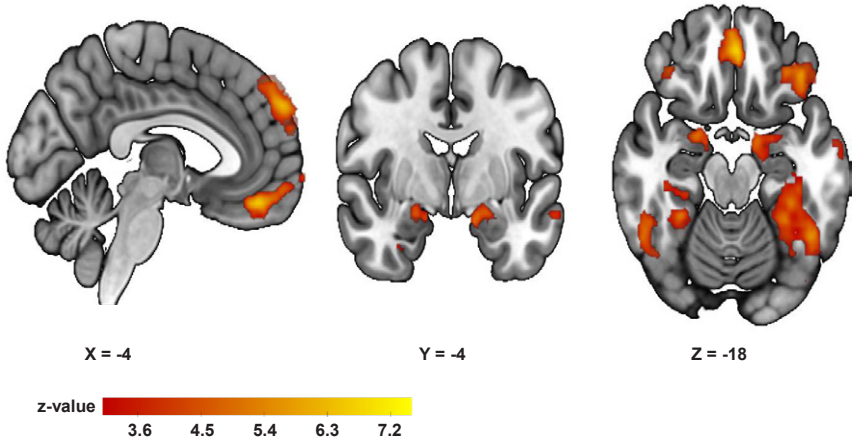

Figure S2.1 Encoding BOLD-fMRI response patterns for the contrast subsequent Remember vs. Forget. p < 0.05, corrected at the cluster level.

Interaction between CA, picture category and schema activation

Across schema conditions, higher CA scores were associated with greater activation in the dorsal medial prefrontal cortex and anterior cingulate cortex during the encoding of subsequently remembered negative pictures compared to positive ones (Negative_remember vs. Positive_remember; voxel-wise z > 3.1, cluster-level p < 0.05, FWER corrected; Figure S2.2, Table S2.4)., To further understand these interactions, we extracted median z-values from the significant clusters for each participant and visualized them in Figure S2.2 (same for other significant clusters reported below).

When accounting for the schema activation condition, we found that for schema (activation vs. control) × picture category (Negative_remember vs. Positive_remember) interaction, increased activities in the left frontal operculum cortex (extending into insula) were associated with higher CA scores. A similar interaction effect was observed in the precuneus for Negative_remember vs. Neutral_remember contrast (voxel-wise $z > 3.1$, cluster-level $p < 0.05$ FWER corrected; Figure S2.2, Table S2.4).

Analyses of other interaction effects related to CA, DS and schema activation, on the contrasts of subsequent memory and picture categories did not reveal any significant clusters.

Table S2.3 Significant activated clusters for subsequent Remember vs. Forget

Region	Hemisphere	MNI Coordinates	Cluster Size (voxels)	Peak Voxel Value (z)
Inferior Temporal Gyrus/ Temporal Fusiform Cortex/ Parahippocampal Gyrus	L	-48 -54 -18	1683	5.65
Frontal Orbital Cortex/ Inferior Frontal Gyrus	L	-40 32 -14	1430	7.22
Inferior Temporal Gyrus/ Temporal Fusiform Cortex/ Parahippocampal Gyrus	R	46 -60 -10	1260	6.34
Dorsal medial prefrontal cortex/ Superior Frontal Gyrus	L	-8 54 48	887	6.79
Ventral medial prefrontal cortex	L/R	-2 44 -20	476	6.76
Amygdala/Hippocampus	L	-16 -4 -16	250	4.95
Amygdala/Hippocampus	R	22 -2 -16	153	5.64
Lateral Occipital Cortex	R	34 -90 -6	141	4.36
Frontal pole/ Frontal Orbital Cortex	R	38 34 -12	133	5.38
Cerebellum	R	34 -80 -36	99	4.97
Middle Temporal Gyrus	L	-66 -12 -20	73	4.05

Clusters significant at $p < 0.05$, corrected at the cluster level, are reported. L: Left; R: Right.

Table S2.4 Significant activated clusters for interaction between CA, picture category and schema activation

Region	Hemisphere	MNI Coordinates	Cluster Size(voxels)	Peak VoxelValue (z)
CA* × *picture category (Negative_remember vs. Positive_remember)				
Dorsal medial prefrontal cortex	L/R	-6 66 26	98	4.37
Anterior cingulate gyrus	L/R	-6 28 24	79	3.82
CA* × *picture category (Negative_remember vs. Positive_remember)* ×*schema (activation vs. control)				
Frontal operculum cortex/Insula	L	-40 16 0	83	4.46
CA* × *picture category (Negative_remember vs. Neutral_remember)* ×*schema (activation vs. control)				
Precuneus Cortex	L/R	2 -74 38	77	3.95

Clusters significant at $p < 0.05$, corrected at the cluster level, are reported. L: Left; R: Right.

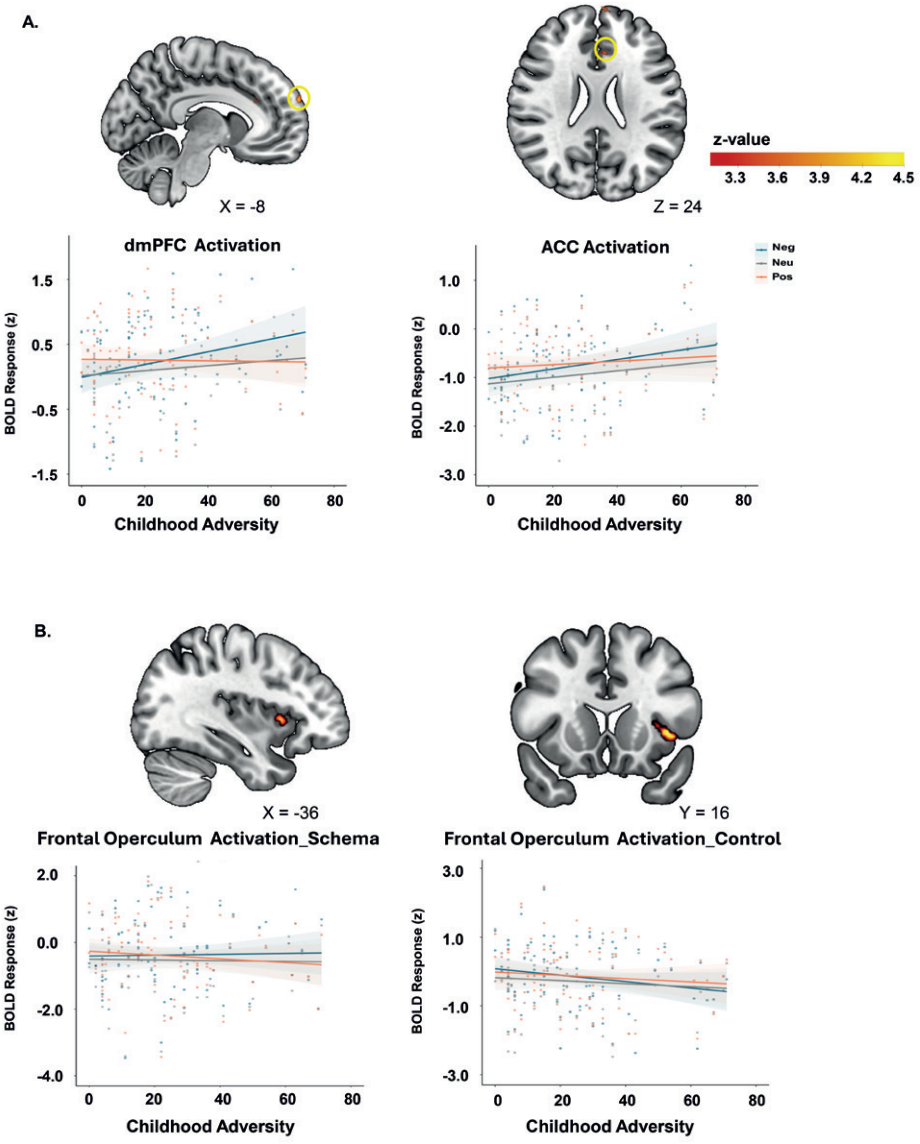
A.
X = -8
Z = 24
z-value
3.3 3.6 3.9 4.2 4.5
dmPFC Activation
ACC Activation
Neg
Neu
Pos
BOLD Response (z)
Childhood Adversity
B.
X = -36
Y = 16
Frontal Operculum Activation_Schema
Frontal Operculum Activation_Control

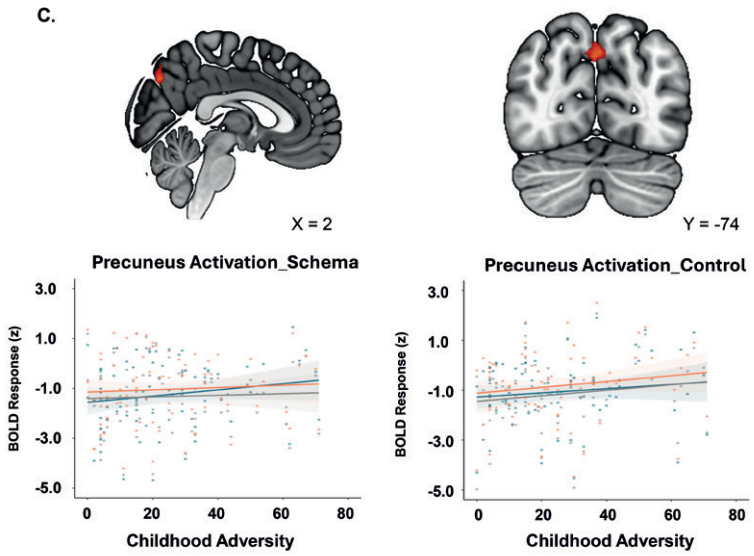

Figure S2.2 To interpret the brain activity pattens under interactions between CA, picture category and schema activation, median z-values from significantly activated clusters were extracted per participant, and used for visualization. (A) Higher levels of CA (MACE overall severity scores) were associated with greater activation in the dorsal medial prefrontal cortex (dmPFC) and anterior cingulate cortex (ACC) during the encoding of subsequently remembered negative pictures, compared to positive ones. (B) Under schema activation condition (vs. control condition), participants with higher levels of CA showed larger activation in the frontal operculum cortex when encoding subsequently remembered negative versus positive pictures. (C) Similarly, under schema activation condition (vs. control condition), higher levels of CA were linked to greater activation in the precuneus during encoding of subsequently remembered negative compared to neutral pictures.

Sensitivity analyses by excluding outliers

To ensure our main findings regarding CA, DS and memory bias were not heavily influenced by outliers, we computed the Mahalanobis distance of each subject's data point from the overall sample distribution, based on a covariate matrix comprising the three variables. A data point was classified as an outlier if its Mahalanobis distance exceeded the 99th percentile of the chi-squared distribution ($\alpha = 0.01$, one-tailed). This analysis detected three outliers, each corresponding to the highest value in CA, DS, and memory bias, respectively. We then repeated the main analyses after excluding these outliers. The results remained largely consistent, with all previously significant effects still present, except for two that became marginally significant: the relationship between CA, picture category and hippocampus activity (*Beta* = -.056, $t(300) = -1.934$, $p = .054$, 95% CI = [-.113; .000]); the relationship between biased hippocampal activity and memory bias (*Beta* = -.265, $t(150) = -1.793$, $p = .075$, 95% CI = [-.022; .527]). See Table S2.13 for full statistics.

Supplementary figure and tables

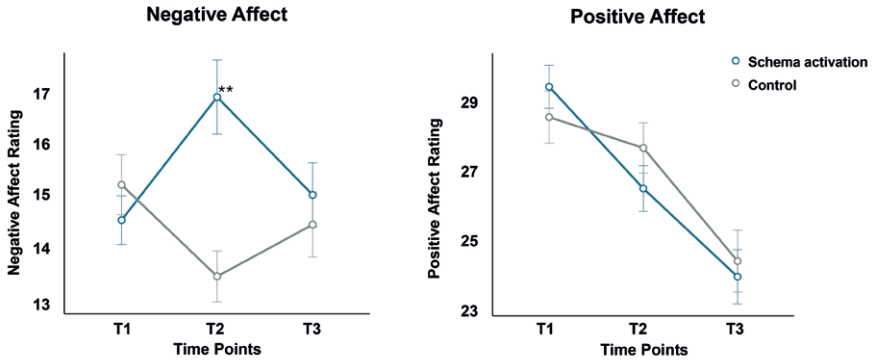

Figure S2.3 Negative and positive affect were measured using the PANAS at three time points: before the depressive schema activation/control task (T1), after the activation/control task (T2), and after memory encoding (T3). The depressive schema activation significantly increased participants' negative affect. **$p < 0.01$.

Table S2.5 Behavioral statistics

	A_Neg	A_Neu	A_Pos	C_Neg	C_Neu	C_Pos	Neg_all	Neu_all	Pos_all
Valence Rating [a]	2.76 ± 0.60	5.06 ± 0.32	6.75 ± 0.60	2.75 ± 0.68	5.09 ± 0.35	6.78 ± 0.63	2.75 ± 0.60	5.07 ± 0.31	6.77 ± 0.58
Hit Rate [b]	0.79 ± 0.12	0.78 ± 0.13	0.80 ± 0.11	0.80 ± 0.11	0.79 ± 0.12	0.81 ± 0.11	0.79 ± 0.11	0.78 ± 0.12	0.80 ± 0.10
False AlarmRate [b]	0.18 ± 0.12	0.15 ± 0.12	0.18 ± 0.13	0.17 ± 0.12	0.15 ± 0.11	0.18 ± 0.11	0.17 ± 0.11	0.15± 0.10	0.18 ± 0.10
RecognitionMemory Index [c]	0.61 ± 0.15	0.62 ± 0.16	0.62 ± 0.14	0.63 ± 0.15	0.64 ± 0.15	0.63 ± 0.14	0.62 ± 0.13	0.63 ± 0.14	0.62 ± 0.12

[a] The emotional valence of each picture was rated on a nine-point scale during encoding.

[b] The hit rate was defined as the proportion of previously seen pictures correctly identified as old in the recognition memory test, and the false alarm rate was the proportion of new pictures incorrectly judged as old.

[c] The recognition memory index was calculated by subtracting the false alarm rate from the hit rate. Neg: negative picture; Neu: neutral picture. Pos: positive picture. A_: schema activation condition, C_: control condition.

Table S2.6 Linear mixed models for valence rating

	Estimate	Std. Error	DF	t value	Pr(>|t|)
M1: Fixed effects: Schema Activation (SA)*Picture Category (PC)*Childhood Adversity (CA) * Levels of Depressive Symptoms (DS) + Random effect: participant *(chosen model)*					
SA (control vs. activation)	0.002	0.048	390	0.033	0.974
PC_neu (vs. neg)	1.331	0.048	390	27.636	< 0.001 ***
PC_pos (vs. neg)	2.321	0.048	390	48.189	< 0.001 ***
CA	-0.047	0.035	464	-1.339	0.181
DS	0.047	0.036	464	1.301	0.194
SA × PC_neu	0.027	0.068	390	0.394	0.694
SA × PC_pos	0.019	0.068	390	0.277	0.782
SA × CA	-0.057	0.049	390	-1.175	0.241
PC_neu × CA	0.049	0.049	390	0.998	0.319
PC_pos × CA	0.059	0.049	390	1.219	0.224
SA × DS	-0.012	0.050	390	-0.249	0.804
PC_neu × DS	-0.076	0.050	390	-1.514	0.131
PC_pos × DS	-0.130	0.050	390	-2.587	0.010 *
CA × DS	0.006	0.030	464	0.189	0.850
SA × PC_neu × CA	0.062	0.069	390	0.894	0.372
SA × PC_pos × CA	0.027	0.069	390	0.388	0.698
SA × PC_neu × DS	0.022	0.071	390	0.314	0.754
SA × PC_pos × DS	0.041	0.071	390	0.572	0.568
SA × CA × DS	-0.033	0.041	390	-0.792	0.429
PC_neu × CA × DS	-0.026	0.041	390	-0.634	0.527
PC_pos × CA × DS	-0.074	0.041	390	-1.777	0.076
SA × PC_neu × CA × DS	-0.001	0.059	390	-0.014	0.989
SA × PC_pos × CA × DS	0.025	0.059	390	0.429	0.668
M2: Fixed effects: SA* PC*CA*DS + Random effect: participant + Random slope:SA *(boundary (singular) fit, not chosen)*					
SA (control vs. activation)	0.002	0.048	391	0.033	0.974
PC_neu (vs. neg)	1.331	0.048	390	27.646	< 0.001 ***
PC_pos (vs. neg)	2.321	0.048	390	48.207	< 0.001 ***
CA	-0.047	0.035	429	-1.342	0.180
DS	0.047	0.036	429	1.304	0.193
SA × PC_neu	0.027	0.068	390	0.394	0.694
SA × PC_pos	0.019	0.068	390	0.278	0.782
SA × CA	-0.057	0.049	391	-1.175	0.241
PC_neu × CA	0.049	0.049	390	0.998	0.319

Table S2.6 Continued

	Estimate	Std. Error	DF	t value	Pr(>|t|)
PC_pos × CA	0.059	0.049	390	1.219	0.224
SA × DS	-0.012	0.050	391	-0.249	0.804
PC_neu × DS	-0.076	0.050	390	-1.515	0.131
PC_pos × DS	-0.130	0.050	390	-2.588	0.010 *
CA × DS	0.006	0.030	429	0.189	0.850
SA × PC_neu × CA	0.062	0.069	390	0.894	0.372
SA × PC_pos × CA	0.027	0.069	390	0.388	0.698
SA × PC_neu × DS	0.022	0.071	390	0.314	0.754
SA × PC_pos × DS	0.041	0.071	390	0.572	0.568
SA × CA × DS	-0.033	0.041	391	-0.792	0.429
PC_neu × CA × DS	-0.026	0.041	390	-0.634	0.526
PC_pos × CA × DS	-0.074	0.041	390	-1.778	0.076
SA × PC_neu × CA × DS	-0.001	0.059	390	-0.014	0.989
SA × PC_pos × CA × DS	0.025	0.059	390	0.430	0.668
M3: Fixed effects: SA* PC*CA*DS, Age, Gender + Random effect: participant + Random slope:SA ***(boundary (singular) fit, not chosen)***					
SA (control vs. activation)	0.002	0.048	391	0.033	0.974
PC_neu (vs. neg)	1.331	0.048	390	27.643	< 0.001 ***
PC_pos (vs. neg)	2.321	0.048	390	48.201	< 0.001 ***
CA	-0.046	0.036	421	-1.288	0.199
DS	0.047	0.036	422	1.288	0.199
Age	-0.001	0.016	75	-0.032	0.975
Gender_male (vs. female)	0.029	0.032	75	0.879	0.382
Gender_trans (vs. female)	0.106	0.101	75	1.055	0.295
SA × PC_neu	0.027	0.068	390	0.394	0.694
SA × PC_pos	0.019	0.068	390	0.277	0.782
SA × CA	-0.057	0.049	391	-1.175	0.241
PC_neu × CA	0.049	0.049	390	0.998	0.319
PC_pos × CA	0.059	0.049	390	1.219	0.224
SA × DS	-0.012	0.050	391	-0.249	0.804
PC_neu × DS	-0.076	0.050	390	-1.515	0.131
PC_pos × DS	-0.130	0.050	390	-2.588	0.010 *
CA × DS	0.006	0.030	422	0.205	0.838
SA × PC_neu × CA	0.062	0.069	390	0.894	0.372
SA × PC_pos × CA	0.027	0.069	390	0.388	0.698
SA × PC_neu × DS	0.022	0.071	390	0.314	0.754

Table S2.6 Continued

	Estimate	Std. Error	DF	t value	Pr(>|t|)
SA × PC_pos × DS	0.041	0.071	390	0.572	0.568
SA × CA × DS	-0.033	0.041	391	-0.792	0.429
PC_neu × CA × DS	-0.026	0.041	390	-0.634	0.526
PC_pos × CA × DS	-0.074	0.041	390	-1.778	0.076
SA × PC_neu × CA × DS	-0.001	0.059	390	-0.014	0.989
SA × PC_pos × CA × DS	0.025	0.059	390	0.430	0.668
Comparison: M1 vs. M2					
	AIC	**BIC**	**logLik**	**Chisq**	**Pr(>Chisq)**
M1	259.37	368.53	-103.68		
M2	263.31	380.86	-103.65	0.0602	0.9703
Comparison: M2 vs. M3					
M2	263.31	380.86	-103.65		
M3	267.45	397.6	-102.72	1.8597	0.602

In LMMs, categorical variables are coded with one condition as reference level for comparison. The reference level for Schema Activation (SA: activation/control) is activation, for Picture Category (PC: negative[neg], neutral[neu], positive[pos]) is negative, and for Gender (female, male, transgender[trans]) is female. Childhood adversity (CA) was indexed by the MACE overall severity score, and the level of depressive symptoms (DS) was the total score on BDI-II. *p<0.05, ***p<0.001.

Table S2.7 Linear mixed models for recognition memory

	Estimate	Std. Error	DF	t value	Pr(>|t|)
M1: Fixed effects: Schema Activation (SA)*Picture Category (PC) * Childhood Adversity (CA) * Levels of Depressive Symptoms (DS) + Random effect: participant					
SA (control vs. activation)	0.074	0.097	390	0.764	0.446
PC_neu (vs. neg)	0.070	0.097	390	0.722	0.471
PC_pos (vs. neg)	0.048	0.097	390	0.493	0.622
CA	-0.002	0.115	155	-0.015	0.988
DS	-0.178	0.119	155	-1.497	0.136
SA × PC_neu	0.035	0.138	390	0.254	0.799
SA × PC_pos	-0.055	0.138	390	-0.399	0.690
SA × CA	-0.027	0.098	390	-0.270	0.788
PC_neu × CA	-0.125	0.098	390	-1.268	0.206
PC_pos × CA	-0.178	0.098	390	-1.804	0.072
SA × DS	0.196	0.101	390	1.937	0.054
PC_neu × DS	0.155	0.101	390	1.525	0.128
PC_pos × DS	0.134	0.101	390	1.325	0.186
CA × DS	0.014	0.098	155	0.143	0.886
SA × PC_neu × CA	-0.014	0.139	390	-0.103	0.918
SA × PC_pos × CA	0.108	0.139	390	0.774	0.439
SA × PC_neu × DS	-0.104	0.143	390	-0.726	0.468
SA × PC_pos × DS	-0.020	0.143	390	-0.142	0.887
SA × CA × DS	0.092	0.084	390	1.097	0.273
PC_neu × CA × DS	-0.038	0.084	390	-0.451	0.652
PC_pos × CA × DS	-0.048	0.084	390	-0.568	0.571
SA × PC_neu × CA × DS	0.046	0.118	390	0.391	0.696
SA × PC_pos × CA × DS	0.026	0.118	390	0.219	0.826
M2: Fixed effects: SA* PC*CA*DS + Random effect: participant + Random slope:SA *(chosen model)*					
SA (control vs. activation)	0.074	0.107	189	0.697	0.487
PC_neu (vs. neg)	0.070	0.081	312	0.864	0.388
PC_pos (vs. neg)	0.048	0.081	312	0.590	0.556
CA	-0.002	0.119	110	-0.014	0.989
DS	-0.178	0.122	110	-1.454	0.149
SA × PC_neu	0.035	0.115	312	0.304	0.761
SA × PC_pos	-0.055	0.115	312	-0.477	0.634
SA × CA	-0.027	0.108	189	-0.246	0.806
PC_neu × CA	-0.125	0.082	312	-1.516	0.131

Table S2.7 Continued

	Estimate	Std. Error	DF	t value	Pr(>|t|)
PC_pos × CA	-0.178	0.082	312	-2.157	0.032 *
SA × DS	0.196	0.111	189	1.768	0.079
PC_neu × DS	0.155	0.085	312	1.824	0.069
PC_pos × DS	0.134	0.085	312	1.585	0.114
CA × DS	0.014	0.101	110	0.139	0.890
SA × PC_neu × CA	-0.014	0.116	312	-0.123	0.902
SA × PC_pos × CA	0.108	0.116	312	0.926	0.355
SA × PC_neu × DS	-0.104	0.120	312	-0.869	0.386
SA × PC_pos × DS	-0.020	0.120	312	-0.170	0.865
SA × CA × DS	0.092	0.092	189	1.001	0.318
PC_neu × CA × DS	-0.038	0.070	312	-0.540	0.590
PC_pos × CA × DS	-0.048	0.070	312	-0.679	0.498
SA × PC_neu × CA × DS	0.046	0.099	312	0.468	0.640
SA × PC_pos × CA × DS	0.026	0.099	312	0.262	0.793
M3: Fixed effects: SA* PC*CA*DS, Age, Gender + Random effect: participant + Random slope:SA					
SA (control vs. activation)	0.074	0.107	189	0.697	0.487
PC_neu (vs. neg)	0.070	0.081	312	0.864	0.388
PC_pos (vs. neg)	0.048	0.081	312	0.590	0.556
CA	0.012	0.124	106	0.095	0.925
DS	-0.173	0.125	106	-1.382	0.170
Age	-0.030	0.099	75	-0.300	0.765
Gender_male (vs. female)	0.143	0.199	75	0.718	0.475
Gender_trans (vs. female)	0.193	0.616	75	0.313	0.755
SA × PC_neu	0.035	0.115	312	0.304	0.761
SA × PC_pos	-0.055	0.115	312	-0.477	0.634
SA × CA	-0.027	0.108	189	-0.246	0.806
PC_neu × CA	-0.125	0.082	312	-1.516	0.131
PC_pos × CA	-0.178	0.082	312	-2.157	0.032 *
SA × DS	0.196	0.111	189	1.768	0.079
PC_neu × DS	0.155	0.085	312	1.824	0.069
PC_pos × DS	0.134	0.085	312	1.585	0.114
CA × DS	0.015	0.103	105	0.148	0.882
SA × PC_neu × CA	-0.014	0.116	312	-0.123	0.902
SA × PC_pos × CA	0.108	0.116	312	0.926	0.355
SA × PC_neu × DS	-0.104	0.120	312	-0.869	0.386
SA × PC_pos × DS	-0.020	0.120	312	-0.170	0.865

Table S2.7 Continued

	Estimate	Std. Error	DF	t value	Pr(>|t|)
SA × CA × DS	0.092	0.092	189	1.001	0.318
PC_neu × CA × DS	-0.038	0.070	312	-0.540	0.590
PC_pos × CA × DS	-0.048	0.070	312	-0.679	0.498
SA × PC_neu × CA × DS	0.046	0.099	312	0.468	0.640
SA × PC_pos × CA × DS	0.026	0.099	312	0.262	0.793
Comparison: M1 vs. M2					
	AIC	**BIC**	**logLik**	**Chisq**	**Pr(>Chisq)**
M1	1133.4	1242.6	-540.71		
M2	1084.1	1201.6	-514.03	53.371	2.57E-12***
Comparison: M2 vs. M3					
M2	263.31	380.86	-103.65		
M3	267.45	397.6	-102.72	1.8597	0.602

Categorical variables are coded with one condition as reference level for comparison. The reference level for Schema Activation (SA: activation/control) is activation, for Picture Category (PC: negative[neg], neutral[neu], positive[pos]) is negative, and for Gender (female, male, transgender[trans]) is female. Childhood adversity (CA) was indexed by the MACE overall severity score, and the level of depressive symptoms (DS) was the total score on BDI-II. *p<0.05, ***p<0.001.

Table S2.8 Linear mixed models for memory bias

	Estimate	Std. Error	DF	t value	Pr(>|t|)
M1: Fixed effects: Schema Activation (SA)* Childhood Adversity (CA) * Levels of Depressive Symptoms (DS) + Random effect: participant *(chosen model)*					
SA (control vs. activation)	0.109	0.155	78	0.699	0.487
CA	0.253	0.114	156	2.212	0.028 *
DS	-0.197	0.118	156	-1.676	0.096
SA × CA	-0.156	0.157	78	-0.989	0.326
SA × DS	0.071	0.162	78	0.435	0.665
CA × DS	0.058	0.097	156	0.597	0.551
SA × CA × DS	-0.060	0.134	78	-0.447	0.656
M2: Fixed effects: SA* CA*DS, Age, Gender + Random effect: participant					
SA (control vs. activation)	0.109	0.155	78	0.699	0.487
CA	0.248	0.118	151	2.111	0.037 *
DS	-0.173	0.119	152	-1.458	0.147
Age	0.017	0.085	75	0.206	0.837
Gender_male (vs. female)	0.196	0.170	75	1.152	0.253
Gender_trans (vs. female)	-0.568	0.526	75	-1.080	0.284
SA × CA	-0.156	0.157	78	-0.989	0.326
SA × DS	0.071	0.162	78	0.435	0.665
CA × DS	0.050	0.098	152	0.515	0.607
SA × CA × DS	-0.060	0.134	78	-0.447	0.656
Comparison: M1 vs. M2					
	AIC	**BIC**	**logLik**	**Chisq**	**Pr(>Chisq)**
M1	475.81	506.81	-227.9		
M2	478.75	519.05	-226.38	3.0558	0.3831

The reference level for Schema Activation (SA: activation/control) is activation, for Picture Category (PC: negative[neg], neutral[neu], positive[pos]) is negative, and for Gender (female, male, transgender[trans]) is female. Childhood adversity (CA) was indexed by the MACE overall severity score, and the level of depressive symptoms (DS) was the total score on BDI-II.*$p<0.05$.

Table S2.9 Linear mixed models for amygdala BOLD-fMRI response

	Estimate	Std. Error	DF	t value	Pr(>|t|)
M1: Fixed effects: Schema Activation (SA)*Picture Category (PC)* Childhood Adversity (CA) * Levels of Depressive Symptoms (DS) + Random effect: participant					
SA (control vs. activation)	0.083	0.125	380	0.668	0.505
PC_neu (vs. neg)	-0.206	0.125	380	-1.657	0.098
PC_pos (vs. neg)	-0.043	0.125	380	-0.341	0.733
CA	0.123	0.116	249	1.057	0.292
DS	-0.126	0.120	249	-1.049	0.295
SA × PC_neu	-0.010	0.176	380	-0.056	0.955
SA × PC_pos	-0.028	0.176	380	-0.159	0.874
SA × CA	-0.208	0.126	380	-1.647	0.100
PC_neu × CA	-0.061	0.126	380	-0.480	0.632
PC_pos × CA	-0.095	0.126	380	-0.751	0.453
SA × DS	0.075	0.130	380	0.575	0.566
PC_neu × DS	0.036	0.130	380	0.276	0.783
PC_pos × DS	0.020	0.130	380	0.151	0.880
CA × DS	0.057	0.098	249	0.577	0.564
SA × PC_neu × CA	0.056	0.178	380	0.312	0.755
SA × PC_pos × CA	-0.005	0.178	380	-0.027	0.979
SA × PC_neu × DS	-0.058	0.184	380	-0.314	0.754
SA × PC_pos × DS	-0.051	0.184	380	-0.278	0.781
SA × CA × DS	0.160	0.107	380	1.495	0.136
PC_neu × CA × DS	0.033	0.107	380	0.307	0.759
PC_pos × CA × DS	-0.001	0.107	380	-0.009	0.993
SA × PC_neu × CA × DS	-0.074	0.151	380	-0.492	0.623
SA × PC_pos × CA × DS	0.083	0.125	380	0.668	0.505
M2: Fixed effects: SA* PC*CA*DS + Random effect: participant + Random slope:SA					
SA (control vs. activation)	0.083	0.158	82	0.527	0.600
PC_neu (vs. neg)	-0.206	0.037	304	-5.531	< 0.001 ***
PC_pos (vs. neg)	-0.043	0.037	304	-1.140	0.255
CA	0.123	0.118	81	1.037	0.303
DS	-0.126	0.122	81	-1.029	0.306
SA × PC_neu	-0.010	0.053	304	-0.187	0.852
SA × PC_pos	-0.028	0.053	304	-0.530	0.597
SA × CA	-0.208	0.160	82	-1.299	0.198
PC_neu × CA	-0.061	0.038	304	-1.602	0.110
PC_pos × CA	-0.095	0.038	304	-2.506	0.013 *

Table S2.9 Continued

	Estimate	Std. Error	DF	t value	Pr(>|t|)
SA × DS	0.075	0.165	82	0.453	0.652
PC_neu × DS	0.036	0.039	304	0.922	0.357
PC_pos × DS	0.020	0.039	304	0.503	0.616
CA × DS	0.057	0.100	81	0.567	0.573
SA × PC_neu × CA	0.056	0.053	304	1.043	0.298
SA × PC_pos × CA	-0.005	0.053	304	-0.090	0.929
SA × PC_neu × DS	-0.058	0.055	304	-1.049	0.295
SA × PC_pos × DS	-0.051	0.055	304	-0.928	0.354
SA × CA × DS	0.160	0.135	82	1.179	0.242
PC_neu × CA × DS	0.033	0.032	304	1.025	0.306
PC_pos × CA × DS	-0.001	0.032	304	-0.028	0.977
SA × PC_neu × CA × DS	-0.074	0.045	304	-1.641	0.102
SA × PC_pos × CA × DS	-0.074	0.045	304	-1.646	0.101
M3: Fixed effects: SA* PC*CA*DS, Age, Gender + Random effect: participant + Random slope:SA					
SA (control vs. activation)	0.083	0.158	82	0.527	0.600
PC_neu (vs. neg)	-0.206	0.037	304	-5.531	< 0.001 ***
PC_pos (vs. neg)	-0.043	0.037	304	-1.140	0.255
CA	0.141	0.120	84	1.178	0.242
DS	-0.149	0.122	82	-1.227	0.224
Age	-0.070	0.084	73	-0.839	0.404
Gender_male (vs. female)	-0.203	0.169	73	-1.195	0.236
Gender_trans (vs. female)	0.487	0.515	73	0.946	0.347
SA × PC_neu	-0.010	0.053	304	-0.187	0.852
SA × PC_pos	-0.028	0.053	304	-0.530	0.597
SA × CA	-0.208	0.160	82	-1.299	0.198
PC_neu × CA	-0.061	0.038	304	-1.602	0.110
PC_pos × CA	-0.095	0.038	304	-2.506	0.013 *
SA × DS	0.075	0.165	82	0.453	0.652
PC_neu × DS	0.036	0.039	304	0.922	0.357
PC_pos × DS	0.020	0.039	304	0.503	0.616
CA × DS	0.066	0.099	81	0.666	0.507
SA × PC_neu × CA	0.056	0.053	304	1.043	0.298
SA × PC_pos × CA	-0.005	0.053	304	-0.090	0.929
SA × PC_neu × DS	-0.058	0.055	304	-1.049	0.295
SA × PC_pos × DS	-0.051	0.055	304	-0.928	0.354
SA × CA × DS	0.160	0.135	82	1.179	0.242

Table S2.9 Continued

	Estimate	Std. Error	DF	t value	Pr(>|t|)
PC_neu × CA × DS	0.033	0.032	304	1.025	0.306
PC_pos × CA × DS	-0.001	0.032	304	-0.028	0.977
SA × PC_neu × CA × DS	-0.074	0.045	304	-1.641	0.102
SA × PC_pos × CA × DS	-0.074	0.045	304	-1.646	0.101
M4: Fixed effects: PC*CA*DS, SA + Random effect: participant + Random slope:SA (chosen model)					
SA (control vs. activation)	0.099	0.150	79	0.657	0.513
PC_neu (vs. neg)	-0.211	0.026	312	-8.001	< 0.001 ***
PC_pos (vs. neg)	-0.057	0.026	312	-2.139	0.033 *
CA	0.015	0.084	81	0.175	0.862
DS	-0.087	0.087	81	-1.008	0.316
PC_neu × CA	-0.033	0.027	312	-1.221	0.223
PC_pos × CA	-0.097	0.027	312	-3.630	< 0.001 ***
PC_neu × DS	0.007	0.028	312	0.255	0.799
PC_pos × DS	-0.006	0.028	312	-0.217	0.828
CA × DS	0.139	0.071	81	1.954	0.054
PC_neu × CA × DS	-0.004	0.023	312	-0.191	0.848
PC_pos × CA × DS	-0.038	0.023	312	-1.685	0.093
M5: Fixed effects: PC*CA*DS, SA, Age, Gender + Random effect: participant + Random slope:SA					
SA (control vs. activation)	0.099	0.150	79	0.657	0.513
PC_neu (vs. neg)	-0.211	0.026	312	-8.001	< 0.001 ***
PC_pos (vs. neg)	-0.057	0.026	312	-2.139	0.033 *
CA	0.035	0.088	78	0.399	0.691
DS	-0.112	0.088	78	-1.272	0.207
Age	-0.070	0.084	73	-0.839	0.404
Gender_male (vs. female)	-0.202	0.169	73	-1.195	0.236
Gender_trans (vs. female)	0.487	0.515	73	0.946	0.347
PC_neu × CA	-0.033	0.027	312	-1.221	0.223
PC_pos × CA	-0.097	0.027	312	-3.630	< 0.001 ***
PC_neu × DS	0.007	0.028	312	0.255	0.799
PC_pos × DS	-0.006	0.028	312	-0.217	0.828
CA × DS	0.147	0.071	78	2.072	0.042
PC_neu × CA × DS	-0.004	0.023	312	-0.191	0.848
PC_pos × CA × DS	-0.038	0.023	312	-1.685	0.093

Table S2.9 Continued

	Estimate	Std. Error	DF	t value	Pr(>|t|)
Comparison: M1 vs. M2					
	AIC	**BIC**	**logLik**	**Chisq**	**Pr(>Chisq)**
M1	1267.45	1375.97	-607.72		
M2	622.77	739.63	-283.38	648.68	< 0.001 ***
Comparison: M2 vs. M3					
M2	622.77	739.63	-283.38		
M3	625.14	754.53	-281.57	3.6212	0.3054
Comparison: M2 vs. M4					
M4	612.13	683.08	-289.06		
M2	622.77	739.63	-283.38	11.362	0.4135
Comparison: M4 vs. M5					
M4	612.13	683.08	-289.06		
M5	614.51	697.98	-287.25	3.6212	0.3054

Categorical variables are coded with one condition as reference level for comparison. The reference level for Schema Activation (SA: activation/control) is activation, for Picture Category (PC: negative[neg], neutral[neu], positive[pos]) is negative, and for Gender (female, male, transgender[trans]) is female. Childhood adversity (CA) was indexed by the MACE overall severity score, and the level of depressive symptoms (DS) was the total score on BDI-II. *p<0.05, ***p<0.001.

Table S2.10 Linear mixed models for hippocampus BOLD-fMRI response

	Estimate	Std. Error	DF	t value	Pr(>|t|)
M1: Fixed effects: Schema Activation (SA)*Picture Category (PC) * Childhood Adversity (CA) * Levels of Depressive Symptoms (DS) + Random effect: participant					
SA (control vs. activation)	0.090	0.115	380	0.783	0.434
PC_neu (vs. neg)	0.130	0.115	380	1.129	0.260
PC_pos (vs. neg)	0.166	0.115	380	1.442	0.150
CA	0.135	0.116	202	1.164	0.246
DS	-0.039	0.120	202	-0.329	0.743
SA × PC_neu	-0.009	0.162	380	-0.055	0.956
SA × PC_pos	0.001	0.162	380	0.004	0.996
SA × CA	-0.255	0.116	380	-2.196	0.029 *
PC_neu × CA	-0.081	0.116	380	-0.693	0.489
PC_pos × CA	-0.061	0.116	380	-0.523	0.602
SA × DS	0.139	0.120	380	1.157	0.248
PC_neu × DS	0.021	0.120	380	0.179	0.858
PC_pos × DS	-0.005	0.120	380	-0.042	0.967
CA × DS	0.013	0.098	202	0.133	0.894
SA × PC_neu × CA	0.100	0.164	380	0.605	0.545
SA × PC_pos × CA	0.005	0.164	380	0.032	0.974
SA × PC_neu × DS	-0.032	0.170	380	-0.190	0.849
SA × PC_pos × DS	-0.040	0.170	380	-0.234	0.815
SA × CA × DS	0.174	0.098	380	1.772	0.077
PC_neu × CA × DS	0.019	0.098	380	0.196	0.845
PC_pos × CA × DS	-0.013	0.098	380	-0.134	0.894
SA × PC_neu × CA × DS	-0.070	0.139	380	-0.502	0.616
SA × PC_pos × CA × DS	-0.048	0.139	380	-0.346	0.729
M2: Fixed effects: SA* PC*CA*DS + Random effect: participant + Random slope:SA					
SA (control vs. activation)	0.090	0.145	84	0.622	0.536
PC_neu (vs. neg)	0.130	0.040	304	3.241	0.001**
PC_pos (vs. neg)	0.166	0.040	304	4.142	< 0.001 ***
CA	0.135	0.111	83	1.216	0.227
DS	-0.039	0.115	83	-0.343	0.732
SA × PC_neu	-0.009	0.057	304	-0.159	0.874
SA × PC_pos	0.001	0.057	304	0.013	0.990
SA × CA	-0.255	0.146	84	-1.744	0.085
PC_neu × CA	-0.081	0.040	304	-1.990	0.048 *
PC_pos × CA	-0.061	0.040	304	-1.501	0.134

Table S2.10 Continued

	Estimate	Std. Error	DF	t value	Pr(>|t|)
SA × DS	0.139	0.151	84	0.918	0.361
PC_neu × DS	0.021	0.042	304	0.514	0.608
PC_pos × DS	-0.005	0.042	304	-0.121	0.904
CA × DS	0.013	0.094	83	0.139	0.890
SA × PC_neu × CA	0.100	0.057	304	1.738	0.083
SA × PC_pos × CA	0.005	0.057	304	0.093	0.926
SA × PC_neu × DS	-0.032	0.059	304	-0.545	0.586
SA × PC_pos × DS	-0.040	0.059	304	-0.673	0.501
SA × CA × DS	0.174	0.124	84	1.407	0.163
PC_neu × CA × DS	0.019	0.034	304	0.562	0.575
PC_pos × CA × DS	-0.013	0.034	304	-0.385	0.701
SA × PC_neu × CA × DS	-0.070	0.048	304	-1.441	0.151
SA × PC_pos × CA × DS	-0.048	0.048	304	-0.994	0.321
M3: Fixed effects: SA* PC*CA*DS, Age, Gender + Random effect: participant + Random slope:SA					
SA (control vs. activation)	0.090	0.145	84	0.622	0.536
PC_neu (vs. neg)	0.130	0.040	304	3.241	0.001**
PC_pos (vs. neg)	0.166	0.040	304	4.142	< 0.001 ***
CA	0.096	0.117	83	0.826	0.411
DS	-0.054	0.118	81	-0.457	0.649
Age	0.121	0.091	73	1.339	0.185
Gender_male (vs. female)	-0.121	0.183	73	-0.659	0.512
Gender_trans (vs. female)	0.215	0.558	73	0.386	0.701
SA × PC_neu	-0.009	0.057	304	-0.159	0.874
SA × PC_pos	0.001	0.057	304	0.013	0.990
SA × CA	-0.255	0.146	84	-1.744	0.085
PC_neu × CA	-0.081	0.040	304	-1.990	0.048 *
PC_pos × CA	-0.061	0.040	304	-1.501	0.134
SA × DS	0.139	0.151	84	0.918	0.361
PC_neu × DS	0.021	0.042	304	0.514	0.608
PC_pos × DS	-0.005	0.042	304	-0.121	0.904
CA × DS	0.008	0.096	81	0.086	0.932
SA × PC_neu × CA	0.100	0.057	304	1.738	0.083
SA × PC_pos × CA	0.005	0.057	304	0.093	0.926
SA × PC_neu × DS	-0.032	0.059	304	-0.545	0.586
SA × PC_pos × DS	-0.040	0.059	304	-0.673	0.501
SA × CA × DS	0.174	0.124	84	1.407	0.163

Table S2.10 Continued

	Estimate	Std. Error	DF	t value	Pr(>|t|)
PC_neu × CA × DS	0.019	0.034	304	0.562	0.575
PC_pos × CA × DS	-0.013	0.034	304	-0.385	0.701
SA × PC_neu × CA × DS	-0.070	0.048	304	-1.441	0.151
SA × PC_pos × CA × DS	-0.048	0.048	304	-0.994	0.321
M4: Fixed effects: PC*CA*DS, SA + Random effect: participant + Random slope:SA (chosen model)					
SA (control vs. activation)	0.122	0.139	79	0.879	0.382
PC_neu (vs. neg)	0.125	0.028	312	4.429	< 0.001 ***
PC_pos (vs. neg)	0.166	0.028	312	5.875	< 0.001 ***
CA	0.020	0.090	81	0.223	0.824
DS	0.024	0.093	81	0.253	0.801
PC_neu × CA	-0.031	0.029	312	-1.077	0.282
PC_pos × CA	-0.058	0.029	312	-2.031	0.043 *
PC_neu × DS	0.005	0.030	312	0.181	0.856
PC_pos × DS	-0.025	0.030	312	-0.844	0.399
CA × DS	0.093	0.076	81	1.217	0.227
PC_neu × CA × DS	-0.016	0.024	312	-0.647	0.518
PC_pos × CA × DS	-0.037	0.024	312	-1.540	0.125
M5: Fixed effects: PC*CA*DS, SA, Age, Gender + Random effect: participant + Random slope:SA					
SA (control vs. activation)	0.122	0.139	79	0.879	0.382
PC_neu (vs. neg)	0.125	0.028	312	4.429	< 0.001 ***
PC_pos (vs. neg)	0.166	0.028	312	5.875	< 0.001 ***
CA	-0.023	0.095	78	-0.245	0.807
DS	0.011	0.095	78	0.119	0.906
Age	0.121	0.091	73	1.339	0.185
Gender_male (vs. female)	-0.121	0.183	73	-0.659	0.512
Gender_trans (vs. female)	0.215	0.558	73	0.386	0.701
PC_neu × CA	-0.031	0.029	312	-1.077	0.282
PC_pos × CA	-0.058	0.029	312	-2.031	0.043 *
PC_neu × DS	0.005	0.030	312	0.181	0.856
PC_pos × DS	-0.025	0.030	312	-0.844	0.399
CA × DS	0.091	0.077	78	1.178	0.242
PC_neu × CA × DS	-0.016	0.024	312	-0.647	0.518
PC_pos × CA × DS	-0.037	0.024	312	-1.540	0.125

Table S2.10 Continued

Comparison: M1 vs. M2					
	AIC	**BIC**	**logLik**	**Chisq**	**Pr(>Chisq)**
M1	1214.73	1323.2	-581.37		
M2	663.63	780.5	-303.82	555.1	< 0.001 ***
Comparison: M2 vs. M3					
M2	663.63	780.5	-303.81		
M3	667.16	796.54	-302.58	2.4735	0.4801
Comparison: M2 vs. M4					
M4	653.8	724.75	-309.9		
M2	663.63	780.5	-303.81	12.169	0.3511
Comparison: M4 vs. M5					
M4	653.8	724.75	-309.9		
M5	657.33	740.8	-308.66	2.4735	0.4801

Categorical variables are coded with one condition as reference level for comparison. The reference level for Schema Activation (SA: activation/control) is activation, for Picture Category (PC: negative[neg], neutral[neu], positive[pos]) is negative, and for Gender (female, male, transgender[trans]) is female. Childhood adversity (CA) was indexed by the MACE overall severity score, and the level of depressive symptoms (DS) was the total score on BDI-II. *p<0.05, **p<0.01, ***p<0.001.

Table S2.11 Exploratory analysis: amygdala biased activity and memory bias

Dependent variable: memory bias; Fixed effects: Schema Activation (SA)* Amygdala biased activity + Random effect: participant					
	Estimate	**Std. Error**	**DF**	**t value**	**Pr(>|t|)**
SA (control vs. activation)	0.133	0.149	78	0.892	0.375
Amygdala biased activity	0.258	0.144	155	1.787	0.076
SA × Amygdala biased activity	-0.118	0.170	139	-0.695	0.488

The reference level for Schema Activation (SA: activation/control) is activation.

Table S2.12 Exploratory analysis: hippocampus biased activity and memory bias

Dependent variable: memory bias; Fixed effects: Schema Activation (SA)* Hippocampus biased activity + Random effect: participant					
	Estimate	**Std. Error**	**DF**	**t value**	**Pr(>|t|)**
SA (control vs. activation)	0.153	0.148	78	1.034	0.304
Hippocampus biased activity	0.273	0.136	155	2.000	0.047 *
SA × Hippocampus biased activity	-0.236	0.164	137	-1.439	0.152

The reference level for Schema Activation (SA: activation/control) is activation.*$p<0.05$.

Table S2.13 Linear mixed models without outliers (N=79)

	Estimate	Std. Error	DF	t value	Pr(>|t|)
Dependent variable: valence rating. Fixed effects: Schema Activation (SA)*Picture Category (PC)*Childhood Adversity (CA) * Levels of Depressive Symptoms (DS) + Random effect: participant					
SA (control vs. activation)	-0.001	0.049	375	-0.023	0.981
PC_neu (vs. neg)	1.324	0.049	375	26.923	< 0.001 ***
PC_pos (vs. neg)	2.319	0.049	375	47.169	< 0.001 ***
CA	-0.018	0.036	447	-0.505	0.614
DS	0.043	0.036	447	1.213	0.226
SA × PC_neu	0.029	0.070	375	0.418	0.676
SA × PC_pos	0.029	0.070	375	0.421	0.674
SA × CA	-0.058	0.050	375	-1.158	0.248
PC_neu × CA	0.022	0.050	375	0.441	0.659
PC_pos × CA	0.036	0.050	375	0.716	0.475
SA × DS	-0.008	0.050	375	-0.161	0.872
PC_neu × DS	-0.065	0.050	375	-1.317	0.189
PC_pos × DS	-0.119	0.050	375	-2.385	0.018 *
CA × DS	0.021	0.035	447	0.600	0.549
SA × PC_neu × CA	0.061	0.070	375	0.866	0.387
SA × PC_pos × CA	0.032	0.070	375	0.454	0.650
SA × PC_neu × DS	0.019	0.070	375	0.268	0.789
SA × PC_pos × DS	0.033	0.070	375	0.468	0.640
SA × CA × DS	-0.033	0.048	375	-0.676	0.499
PC_neu × CA × DS	-0.023	0.048	375	-0.469	0.639
PC_pos × CA × DS	-0.078	0.048	375	-1.622	0.106
SA × PC_neu × CA × DS	-0.001	0.068	375	-0.021	0.984
SA × PC_pos × CA × DS	0.024	0.068	375	0.359	0.720
Dependent variable: recognition memory. Fixed effects: SA* PC*CA*DS + Random effect: participant + Random slope:SA					
SA (control vs. activation)	0.054	0.112	181	0.482	0.630
PC_neu (vs. neg)	0.067	0.085	300	0.787	0.432
PC_pos (vs. neg)	0.047	0.085	300	0.553	0.581
CA	0.175	0.117	110	1.491	0.139
DS	-0.167	0.117	110	-1.425	0.157
SA × PC_neu	0.051	0.121	300	0.422	0.673
SA × PC_pos	-0.041	0.121	300	-0.336	0.737
SA × CA	-0.138	0.114	181	-1.215	0.226
PC_neu × CA	-0.177	0.086	300	-2.043	0.042 *

Table S2.13 Continued

	Estimate	Std. Error	DF	t value	Pr(>|t|)
PC_pos × CA	-0.237	0.086	300	-2.747	0.006 **
SA × DS	0.181	0.113	181	1.592	0.113
PC_neu × DS	0.165	0.086	300	1.908	0.057
PC_pos × DS	0.146	0.086	300	1.694	0.091
CA × DS	0.191	0.114	110	1.686	0.095
SA × PC_neu × CA	0.040	0.122	300	0.329	0.742
SA × PC_pos × CA	0.194	0.122	300	1.589	0.113
SA × PC_neu × DS	-0.103	0.122	300	-0.841	0.401
SA × PC_pos × DS	-0.024	0.122	300	-0.194	0.847
SA × CA × DS	-0.030	0.110	181	-0.273	0.785
PC_neu × CA × DS	-0.042	0.084	300	-0.507	0.612
PC_pos × CA × DS	-0.053	0.084	300	-0.637	0.524
SA × PC_neu × CA × DS	0.101	0.118	300	0.858	0.392
SA × PC_pos × CA × DS	0.091	0.118	300	0.771	0.441
Dependent variable: memory bias. Fixed effects: SA* CA* DS + Random effect: participant					
SA (control vs. activation)	0.086	0.160	150	0.538	0.591
CA	0.340	0.115	150	2.964	0.004 **
DS	-0.215	0.115	150	-1.879	0.062
SA × CA	-0.286	0.162	150	-1.765	0.080
SA × DS	0.081	0.162	150	0.502	0.616
CA × DS	0.062	0.111	150	0.554	0.580
Dependent variable: amygdala BOLD-fMRI response. Fixed effects: PC*CA*DS, SA + Random effect: participant + Random slope:SA					
SA (control vs. activation)	0.138	0.154	76	0.893	0.375
PC_neu (vs. neg)	-0.191	0.026	300	-7.265	< 0.001 ***
PC_pos (vs. neg)	-0.034	0.026	300	-1.307	0.192
CA	0.068	0.083	78	0.818	0.416
DS	-0.069	0.083	78	-0.829	0.410
PC_neu × CA	-0.015	0.027	300	-0.559	0.576
PC_pos × CA	-0.071	0.027	300	-2.643	0.009 **
PC_neu × DS	-0.008	0.027	300	-0.299	0.765
PC_pos × DS	-0.011	0.027	300	-0.427	0.669
CA × DS	0.239	0.080	78	2.992	0.004 **
PC_neu × CA × DS	-0.036	0.026	300	-1.413	0.159
PC_pos × CA × DS	-0.039	0.026	300	-1.503	0.134

Table S2.13 Continued

	Estimate	Std. Error	DF	t value	Pr(>|t|)
Dependent variable: hippocampus BOLD-fMRI response. Fixed effects: PC*CA*DS, SA + Random effect: participant + Random slope:SA					
SA (control vs. activation)	0.148	0.141	76	1.045	0.299
PC_neu (vs. neg)	0.126	0.029	300	4.366	< 0.001 ***
PC_pos (vs. neg)	0.174	0.029	300	6.028	< 0.001 ***
CA	0.064	0.092	78	0.697	0.488
DS	0.015	0.092	78	0.163	0.871
PC_neu × CA	-0.032	0.029	300	-1.082	0.280
PC_pos × CA	-0.056	0.029	300	-1.934	0.054
PC_neu × DS	0.004	0.029	300	0.144	0.886
PC_pos × DS	-0.023	0.029	300	-0.778	0.437
CA × DS	0.109	0.088	78	1.231	0.222
PC_neu × CA × DS	-0.025	0.028	300	-0.905	0.366
PC_pos × CA × DS	-0.036	0.028	300	-1.292	0.197
Dependent variable: memory bias. Fixed effects: Schema Activation (SA)* Amygdala biased activity + Random effect: participant					
SA (control vs. activation)	0.108	0.161	150	0.673	0.502
Amygdala biased activity	0.247	0.150	150	1.652	0.101
SA × Amygdala biased activity	-0.181	0.178	150	-1.018	0.310
Dependent variable: memory bias. Fixed effects: Schema Activation (SA)* Hippocampus biased activity + Random effect: participant					
SA (control vs. activation)	0.122	0.161	150	0.762	0.447
Hippocampus biased activity	0.253	0.141	150	1.793	0.075
SA × Hippocampus biased activity	-0.265	0.172	150	-1.545	0.125

Categorical variables are coded with one condition as reference level for comparison. The reference level for Schema Activation (SA: activation/control) is activation, for Picture Category (PC: negative[neg], neutral[neu], positive[pos]) is negative. Childhood adversity (CA) was indexed by the MACE overall severity score, and the level of depressive symptoms (DS) was the total score on BDI-II. *p<0.05, ** p<0.01, ***p<0.001.

Chapter 3.

Childhood adversity predicts striatal functional connectivity gradient changes after acute stress

This chapter is based on: Liu, X. S., Haak, K. V., Figa, K., Vrijsen, J. N., Oldehinkel, M., Mulders, P. C. R., Collard, R. M., van Eijndhoven, P. F. P., Beckmann, C. F., Fernández, G., Tendolkar, I., & Kohn, N. (2024). Childhood adversity predicts striatal functional connectivity gradient changes after acute stress. Imaging Neuroscience, 2, 1-13.

Abstract

As a primary risk factor for psychiatric vulnerability, childhood adversity (CA) leads to several maladaptive behavioral and brain functional changes, including domains of emotion, motivation and stress regulation. Previous studies on acute stress identified the potential role of a striatum-centered network in revealing the psychopathology outcomes related to CA. To elucidate the interplay between CA, acute stress and striatal functions in psychiatric disorders, more evidence from large-scale brain connectivity studies in diverse psychiatric populations is necessary. In a sample combining 150 psychiatric patients and 26 controls, we utilized 'connectopic gradients' to capture the functional topographic organizations of striatal connectivity during resting-state scans conducted before and after stress induction. Connectivity gradients in rest and under stress were linked to different CA types and their frequency by Spearman correlation. Linear mixed models and moderation models were built to clarify the role of symptom strengths in these correlations. We found one type of CA—emotional neglect negatively predicted the post-stress-induction gradient shape, and stress reactive changes in the anterior-posterior orientation of the first-order striatal gradient. Moderation models revealed the observed correlations were selectively present in individuals with elevated comorbidity. Our results may provide new psychopathology-related biomarkers by tracking stress-induced changes in the general motivation systems. This demonstrates new perspectives in characterizing the striatal network and understanding its alterations in response to adverse childhood experiences.

Keywords: Childhood adversity; Acute stress; Striatum; Connectopic mapping.

Introduction

Childhood adversity (CA) refers to a wide range of negative impactful experiences during childhood (McLaughlin, 2018; McLaughlin, Sheridan, & Lambert, 2014). These experiences can include various forms of abuse, exposure to violence, emotional and physical neglect, as well as long-term poverty (McLaughlin et al., 2019; Moreno-López et al., 2020). CA heightens the risk for psychiatric disorders by altering brain-development trajectories during the highly adaptive periods of childhood (Teicher et al., 2016). One notable psychopathological consequence of CA is its impact on individual's reactivity to acute stress later in life. Typically, after encountering stress, the reactivity of the autonomic nervous system and hypothalamic–pituitary–adrenocortical (HPA) axis contributes to effective coping (Russell & Lightman, 2019). However, individuals with a history CA often exhibit diminished cardiac and cortisol responses to psychosocial stress (Lovallo et al., 2012; Sijtsema et al., 2015). This maladaptive alteration is indicative of an increased likelihood of experiencing more depressive symptoms both currently and in the future (de Rooij et al., 2010; Phillips et al., 2011), and observed in several other psychiatric disorders besides depression, e.g., disordered eating (Ginty et al., 2012), attention-deficit/hyperactivity disorder (ADHD, Pesonen et al., 2011) and substance use dependencies (Ginty et al., 2012). Recently, after integrating evidence from clinical and neuroscience research, Carroll and colleagues proposed that in addition to changes in peripheral physiology, the hypothalamus and brainstem, blunted stress response may be also due to motivational dysregulation (Carroll et al., 2012, 2017). That is, the decreased stress response and related health outcomes usually come together with impairments in motivation-dependent tasks, indicating a broader dysfunction in responding to challenges and mobilizing mental effort (Ginty, 2013). During exposures to stress, hypoactivation of motivation-related brain regions attenuates conscious engagement in appraising the present state and mobilizing resources. It will result in ineffective stress evaluation and strategic coping, thereby limiting the necessary adjustments for further physiological responses. Insufficient cortisol secretion and motivational coping after stress lead to long-term dysphoria, heightening the risks of depressive symptoms, substance abuse and other maladaptive behaviors (al'Absi et al., 2021; Lovallo, 2013), therefore account for parts of the comorbidity related to CA and stress.

The striatum, together with its associated cortical regions (e.g., orbitofrontal cortex, medial prefrontal cortex (mPFC), anterior cingulate cortex) constitute the essential parts of human reward and motivation system. The aforementioned perspective on motivational dysregulation (Carroll et al., 2017) highlights the

potential involvement of the striatum and its cortical connectivity in stress coping behaviors, particularly for elucidating the blunted stress response observed in individuals with a history of CA. Evidence showed that the experience of CA was associated with muted activation of the ventral striatum (Hanson et al., 2015) and striatum related connectivity changes (e.g., striatum- mPFC connectivity (Dennison et al., 2019; Hanson et al., 2018)) during reward processing. Studies in resting-state functional connectivity also identified the CA-related alterations in striatum-mPFC pathway, although the direction of these changes is inconsistent (Increase: Fareri et al., 2017; Decrease: Marshall et al., 2018). There is little research directly examining the relation between CA and striatal networks during stress response. One study found a negative correlation between CA severity and cortico-striatal activities in response to threat stimuli (Yang et al., 2015). Individuals experiencing long-term psychosocial adversity have been shown to exhibit dampened striatal dopaminergic function after stress induction (Bloomfield et al., 2019), indicating the linkage between CA and striatal dysfunctions during stress coping.

These results generally support the motivational account for blunted stress response in people with CA. However, there is a need for more direct evidence on how striatal connectivity varies under the combined impact of acute stress and aversive events experienced early in life. Additionally, most studies have focused on the activity of the striatum or specific connectivity pathways between the striatum and other brain regions. Employing methods that examine whole-brain connectivity can be highly insightful in clarifying the large-scale brain effects of the interaction between stress response and CA (Herzberg & Gunnar, 2020), providing a readout of the living human's motivation system.

An emerging functional connectivity analysis technique, the "connectopic mapping", could serve as an ideal tool to investigate this interaction in-vivo and allow for investigation of whole brain effects of the striatal system. This data-driven method was designed to detect several overlapping connectivity elements (gradients) within a pre-defined region-of-interest (ROI). Each connectivity gradient maps a varying topographic mode of connectivity changes within the ROI in relation to the rest of the brain (Haak et al., 2018). According to animal anatomical studies, projections from cortical regions are overlapping and topographically organized within the striatum (Haber et al., 2000, 2006). Previous research has demonstrated that this organization in the striatum can be effectively captured by connectopic gradients (Marquand et al., 2017). Furthermore, recent studies showed that variations in striatal gradients mapped precisely onto the individual difference in a set of motivation-related tasks (e.g., delay discounting, sustained

attention) and the psychological wellbeing (Marquand et al., 2017). Gradients could predict the comorbidity between psychiatric disorders (Mulders et al., 2022) and Parkinson's disease severity as well (Oldehinkel et al., 2022), which is another disorder associated with reward processing and striatal dysfunction (Cools et al., 2022). Connectivity gradients of the striatum could therefore be an in-vivo readout of the functionality of reward and motivation processing. By estimating gradient maps in resting-state functional connectivity data after stress induction, we can assess the functional state of the motivational system during stress response and coping behaviors, and examine its individual variations related to CA.

In this study, we conducted an analysis of connectopic gradients using data from the 'Measuring Integrated Novel Dimensions in Neurodevelopmental and Stress-related Mental Disorders' (MIND-Set) study (van Eijndhoven et al., 2022), to examine whether striatal connectivity gradients vary depending on CA experience, and how acute stress interacts with this pattern. As the high prevalence of comorbidity and limitations of symptom-based classification have been widely recognized, the idea of incorporating data across distinct diagnostic domains to identify common underpinnings and biological markers is advocated by the Research Domain Criteria (RDoC; Insel et al., 2010) and increasingly becoming a trend in recent research (Buckholtz & Meyer-Lindenberg, 2012; Guineau et al., 2023; Kist et al., 2023). Following this framework, the MIND-Set study comprises a naturalistic psychiatric patient sample and a non-psychiatric control sample, aiming to explore shared mechanisms and risk factors across neurodevelopmental disorders, stress-related disorders, and substance use disorders. Based on this rationale, we examined whether CA could play a role in the shared mechanisms, specifically concerning the striatal motivation system and stress response. Previous research has indicated diverse vulnerable regions underlying different forms of CA, characterized by different profiles of threat and deprivation (McLaughlin, Sheridan, & Lambert, 2014). Therefore, we investigated different CA types and their respective frequency. The literature summarized above has demonstrated that individuals with CA exhibit alterations in their striatal networks both before and after stress exposures. We hypothesized that these alterations would be reflected in differences in the spatial layouts of gradient maps. To be specific: 1.) participants with different types and frequencies of CA were expected to display different gradient organizations at the pre-stress baseline; 2.) after acute stress induction, we expected to observe distinct changes in gradient organization in individuals with different CA histories (in terms of types and frequency). If CA and acute stress, two critical concepts for mental health, are indeed reflected in connectivity gradients, these gradients will demonstrate sensitivity in detecting both individual

characteristics and experimental manipulations. This indicates the future utility as biomarker for diagnosis, monitoring, and prediction of treatment response in mental health disorders.

Methods

Participants

The data used in this study is part of the MIND-Set study, conducted by the Department of Psychiatry of the Radboud University Medical Center and the Donders Institute in Nijmegen, the Netherlands. The MIND-Set study was approved by the Ethical Review Board of the Radboud UMC. All participants signed informed consent before participation. A more detailed description of the MIND-Set study is introduced in prior work (van Eijndhoven et al., 2022; https://scholar.google.nl/citations?user=GBcK84EAAAAJ&hl=nl).

The aim of the present study was to investigate the relations between CA and striatal connectivity, therefore all the participants from the MIND-Set cohort who have experienced CA (measured by NEMESIS questionnaire, details in 2.2 Procedure) and have imaging data available (n = 176; 94 males; age 38.7 ± 14.2 years) were included. In this sample, 150 participants diagnosed with one or more psychiatric disorders (79 males; age 38.9 ± 13.6 years; mood disorder = 131, anxiety disorder = 51, ADHD = 58, autism spectrum disorder (ASD) = 55, addiction = 40), and 26 individuals without a current of past psychiatric disorder (15 males; age 37.6 ± 17.7 years). The diagnostic procedure is described in detail by van Eijndhoven and colleagues (2022). During their participation in the study, 126 participants in this sample were taking one or more medications.

Procedure

In this study, we utilized neuroimaging data from resting-state scans. There are three resting-state scans in total (Figure 3.1). Resting-state scan 1 (8.5 min) was followed by a neutral movie clip (2.3 min; control condition), in turn followed by resting-state scan 2 (pre-stress rs, 8.5 min). Lastly, to induce psychological stress, participants watched a highly aversive movie clip (2.3 min; Hermans et al., 2011; Qin et al., 2009) after which resting-state scan 3 (post-induction rs, 12.6 min) was acquired. Because the main focus of this study is on stress reactivity, performed analyses were based on pre-stress and post-induction rs.

CA was measured by the Netherlands Mental Health Survey and Incidence Study (NEMESIS; Bergman et al., 2020) questionnaire. Participants indicated whether and how frequently they experienced emotional neglect, psychological abuse, physical abuse, and sexual abuse, each of which was categorized into three degrees (0: absent, 1: once or sometimes, 2: regular, often and very often). The overall CA index was computed by summing up the four subscales, ranging from 0-8 (Hovens et al., 2010).

Figure 3.1 Resting-state scan procedure (adapted from van Oort et al., 2020)

Analysis in stress indicators

To examine whether the aversive movie effectively induced participants' stress state, the paired-sample T test ($p < 0.05$, two tailed) was utilized to compare the subjective stress rating and the heart rate (beat per minute, BPM) after watching the neutral movie and the aversive movie. To further examine how CA relates to these stress indicators, we did the spearman correlation analyses ($p < 0.05$) between different types of CA and the stress-induced changes in subjective stress ratings and BPM.

fMRI data analysis

The fMRI acquisition parameters and preprocessing pipeline were reported in previous work (van Eijndhoven et al., 2022; van Oort et al., 2020). In brief, performed by FSL 5.0.11 (FMRIB, Oxford, UK), the preprocessing steps consist of brain extraction, motion correction, bias field correction, high-pass temporal filtering (cut-off of 100 s), spatial smoothing by a 4 mm FWHM Gaussian kernel, boundary-based registration to T1 and nonlinear registration to standard space (MNI152). ICA-based Advanced Removal of Motion Artefacts (ICA-AROMA) was applied to remove motion-related artifacts from the data.

We applied ConGrads to the denoised resting-state data, to find varying topographic modes of connectivity changes within the striatum in relation to all the other regions of the brain (Haak et al., 2018). For our ROIs of left and right striatum,

we produced masks from the Harvard-Oxford atlas using the thresholding of 25% probability (Oldehinkel et al., 2022). ConGrads estimated a similarity matrix based on functional connectivity between each striatal voxel and the rest brain, and utilized a manifold learning algorithm to derive topographical gradient maps from the similarity matrix: similar values in the gradient maps indicate a similar connectivity pattern. Then the trend surface model (TSM) was fitted to statistically represent the spatial organization of gradient maps (Haak et al., 2018; Marquand et al., 2017). We run ConGrads separately for the pre-stress and post-induction rs (each 500 vol), and the individual connectopic maps were obtained for each participant at respective resting-states on both sides of the striatum. All connectopic maps were checked visually. We focused our analysis on the first-order gradient as it has been shown to be associated with a set of goal-directed behaviors, as well as psychological well-being (Marquand et al., 2017). A template derived from previous publications (Oldehinkel et al., 2022) and calculated using data from the Human Connectome Project (HCP) was utilized for the group gradient. To validate correct selection of first-order gradients, participants were excluded if the spatial correlations between their gradients and group level first-order gradients were lower than 0.50. This criterion ensured that only participants whose gradient maps generally aligned with the group template were included in the subsequent analyses.

Linking striatal gradients with CA and acute stress

ConGrads provides trend surface modelling coefficients summarizing the spatial topology of each gradient in the X, Y, and Z axes of the standard MNI152 coordinate space. Trend surface modelling aims to estimate the value of a property (P_i) at any given location within the space based on the coordinates (X_i, Yi, Z_i) of that location through regression functions, and therefore provide a set of coefficients from the regression function to serve as low dimensional representations of the spatial trend (Gelfand et al., 2010). Generally, the similarity in the structure of these coefficients suggests similarities in spatial layouts. In line with prior research applying striatal gradients to the MIND-Set data (Mulders et al., 2022), a trend surface regression model with nine coefficients (3 parameters along 3 axes) was determined to be the best fit, thus it was implemented in the analysis of the acquired first-order gradients. In order to investigate the stress effect on spatial features of the striatal gradient, we subtracted the nine parameters of the gradient at pre-stress resting state from the respective parameters at post-induction resting state, for each participant.

Considering the skewed distribution of the overall CA index and the subscale scores, Spearman correlation coefficients ($p < .05$, FDR corrected) were calculated to identify the relations between CA (overall index and three subscale scores:

emotional neglect, psychological abuse, physical abuse) and the nine coefficients of the first-order gradient (separately for the two resting-states, and the stress induced changes). The subscale of sexual abuse was discarded due to its extremely skewed distribution. The correlation analysis was done by the R package 'bcdstats' (github.com/bcdudek/bcdstats) based on R version 4.2.0.

Dependence with depressive severity and comorbidity

The motivational dysfunction after acute stress may indeed be associated with depressive symptoms and the comorbidity across psychiatric disorders, and disentangling the relationships between CA, depressive severity, and comorbidity has proven challenging (Abercrombie et al., 2018; Vrijsen et al., 2017). Therefore, it's necessary to examine how the observed significant correlations in our study are related to these symptom strength factors. It is possible that the correlations between CA and striatal gradients might be in fact dominated by depressive symptom severity and levels of comorbidity, or they play specific roles (e.g., moderating) in the relation of interest. To explore these possibilities, linear mixed models were built by taking CA and these symptom indicators as factors, using R package 'lmerTest' (Kuznetsova et al., 2017). Here, the depressive severity was measured by Inventory of Depressive Symptomatology–Self Rating (IDS-SR; Rush et al., 2000), and the comorbidity was calculated by summing up the number of psychiatric disorders (including mood disorder, anxiety disorder, ADHD, ASD and addiction) diagnosed for each participant.

Specifically, based on the results from Spearman correlation analysis, we built linear mixed models on the Y cubic parameter of the left striatum (the dependent factor), taking emotional neglect frequency, resting state (pre-stress rs, post-induction rs), depressive severity or comorbidity as fixed factors, and subjects as the random factor. We also ran similar linear mixed models on the stress-induced change of the Y cubic parameter, with emotional neglect frequency, sides of the striatum (left, right), the depressive severity or comorbidity as fixed factors, and subjects as the random factor.

Results

Stress indicators

Compared to watching the neutral movie, the stress induction with aversive movie significant improved participants' subjective stress ratings ($t(170) = 11.136$, $p < 0.001$, Cohen's d = 0.851) and BPM ($t(172) = 3.255$, $p = 0.001$, Cohen's d = 0.247). Furthermore, we found a marginal significantly negative correlation between

emotional neglect frequency and the BPM change (r_s = -0.142, p = 0.062), showing the evidence that CA was related to diminished cardiac responses to stress.

Striatal connectivity gradients in MIND-Set Data

Our results showed similar striatal gradients compared with previous studies (Marquand et al., 2017; Mulders et al., 2022; Oldehinkel et al., 2022), which confirmed the reliability of striatal gradients across different populations and scans. The dominant gradient (zeroth-order) essentially follows the structural boundaries of the caudate, putamen and nucleus accumbens, while the first-order gradient tends to show changes following the coordinate space (e.g., medial–lateral, dorsal–ventral and anterior–posterior. See Figure 3.2). For the first-order gradient, there was a high proportion of participants whose spatial correlation with the HCP group gradient was higher than 0.50 (left striatum pre-stress: 84.09%; right striatum pre-stress: 83.52%; left striatum post-induction: 86.36%; right striatum post-induction: 81.81%).

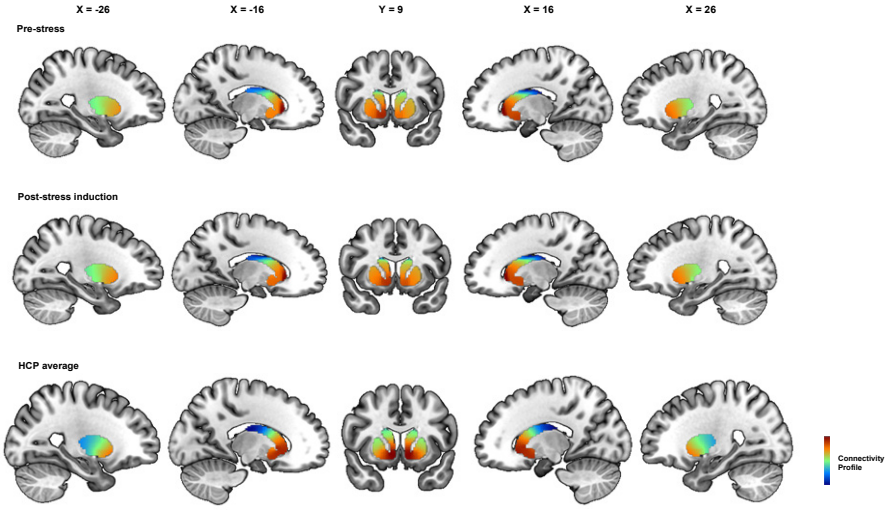

Figure 3.2 The group average of the first-order gradients before and after stress-induction, compared with HCP dataset (Oldehinkel et al., 2022).

Correlation between different types of CA and striatal gradients

The Spearman correlation analyses between CA and the TSM coefficients from the first-order gradient, conducted separately for the pre-stress and post-induction resting state, showed a significant negative correlation only between emotional neglect frequency and the Y cubic parameter (the cubic parameter representing anterior-posterior organizations) of the first-order gradient in the left striatum at post-induction rs (r_s = -0.190, p_{fdr} = 0.042).

For the stress-induced connectivity change, we found significant negative correlations between emotional neglect frequency and the Y cubic parameter change on both sides of the striatum (left: r_s = -0.210, p_{fdr} = 0.033; right: r_s = -0.230, p_{fdr} = 0.014. Figure 3.3). There were no other significant correlations (*p*s > 0.10). The full correlation lists are shown in Table S3.2.

To assess the change in correlations from pre-stress rs to post-induction rs, we utilized the Pearson & Filon 's Z test by the R package 'cocor' (Diedenhofen & Musch, 2015), comparing the correlation between emotional neglect frequency and the Y cubic parameter from the two resting states. The results showed for both sides of the striatum, the correlations between emotional neglect frequency and the Y cubic parameter were significantly different between the two resting-states (left: z = 2.789, p = 0.005; right: z = 2.348, p = 0.019).

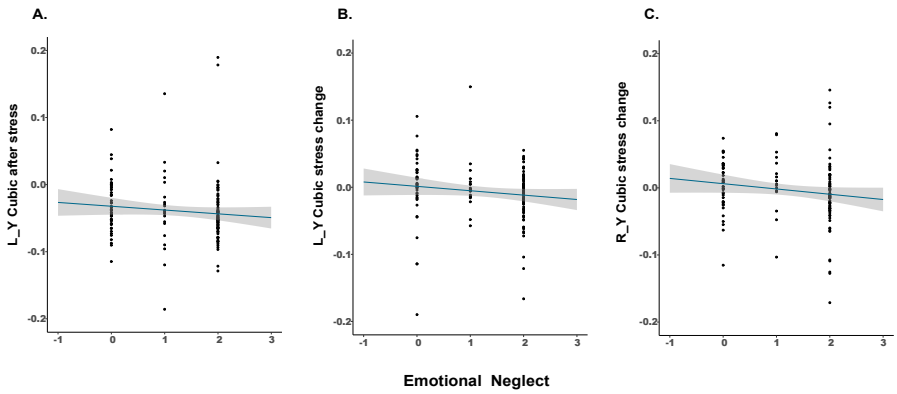

Figure 3.3 Emotional neglect predicts striatal connectivity gradient changes in response to stress, shown by correlations between emotional neglect and Y cubic parameter on the left striatum at post-induction rs (A), Y cubic parameter changes induced by acute stress on the left (B) and right striatum (C). Emotional neglect was assessed using the NEMESIS subscale, and the Y-cubic parameter was derived from the trend-surface regression model, representing spatial trends in the connectivity gradient maps. Stress-related changes were calculated by subtracting the pre-stress resting-state parameters from the corresponding post-induction resting-state parameters. L: Left; R: Right.

We also tested the above correlations controlling for gender, age, and medication use (i.e., with/without medication). The negative correlations between emotional neglect frequency and the Y cubic parameter change on both sides of the striatum remained significant (left: r_s = -0.220, p_{fdr} = 0.021; right: r_s = -0.200, p_{fdr} = 0.038). The correlation between emotional neglect frequency and the Y cubic parameter on the left striatum at post-induction rs was marginally significant (r_s = -0.170, p_{fdr} = 0.088). The full overview of correlations is presented in Table S3.3.

Because the significant correlations we found all included the Y cubic parameter and emotional neglect frequency, we examined whether the correlations with emotional neglect were statistically different from those for the other types of CA, using Pearson & Filon 's Z test. This analysis found that the correlation between emotional neglect frequency and the left Y cubic parameter was significantly different from physical abuse frequency and the respective parameter (z = -1.910, p = 0.028); the correlation between emotional neglect frequency and the right Y cubic parameter change was significantly different from psychological abuse frequency (z = -2,923, p = 0.002) and physical abuse frequency (z = -1.925, p = 0.027; see Table S3.4). Overall, this indicates potentially specific linkage between emotional neglect and the examined gradients.

Moreover, to better interpret the observed correlations, for each hemisphere of the striatum, we ran repeated measures ANOVA for the Y cubic parameter, taking emotional neglect frequency (low, high) and resting state (pre-stress rs, post-induction rs) as independent factors. Here we classified participants scored 0 and 1 as low-frequency group, and participants scored 2 as high-frequency group, to get a relatively balanced group size (n_0 = 59; n_1 = 23; n_2 = 94). The analysis in the right striatum revealed a significant interaction between emotional neglect frequency and resting state (F (1,129) = 4.102, p = 0.045). It was driven by the decrease of Y cubic parameter from pre-stress rs to post-induction rs in high-frequency group (p = 0.049), while the low-frequency group didn't show this change (p = 0.353). Similar results were shown in the left hemisphere as well, but did not reach significance (F (1,134) = 3.172, p = 0.077).

These results indicated the correlations we observed above are related to the stress-induced decrease in high-frequency of emotional neglect group. We next attempted to visualize this effect in the individual striatal gradient maps. We visually inspected all the individual gradients of high-frequency group. Then, for each side of the striatum, we produced the average gradient maps from ten participants of high-frequency group who showed the largest stress-induced decrease in their Y cubic parameter, and compared the average maps at pre-stress and post-induction rs (Figure 3.4). Combining the information from individual and average maps, we made the inference that the first-order gradients of frequently neglected people tend to show a clearer gradual transition from pre-stress rs to post-induction rs, especially in the location of caudates.

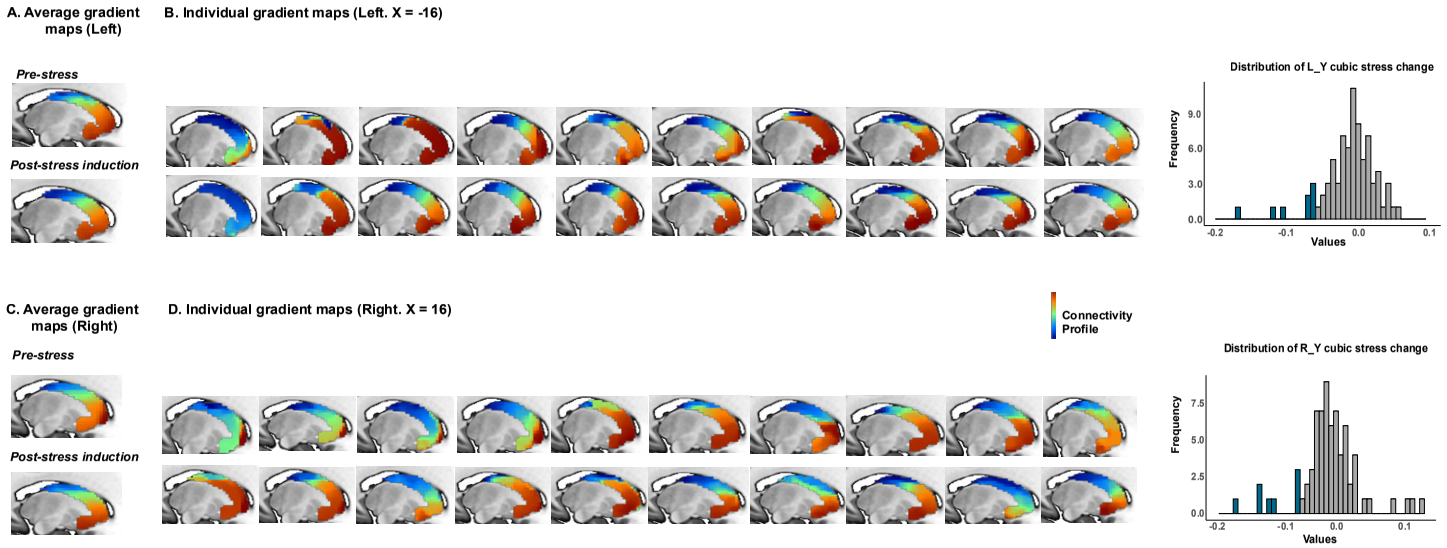

Figure 3.4 The pre-stress and post-induction gradient maps for frequently emotional neglected participants. (A) and (C) depict the average maps derived from 10 participants in the high-frequency group who exhibited the largest decrease in the Y cubic parameter at the left and right striatum (shown as blue bins in the distribution histograms), respectively. (B) and (D) display the individual maps of these participants. In comparison to the pre-stress state, their gradient maps tended to exhibit clearer and more gradual transitions in spatial organizations during the post-induction state. L: Left; R: Right.

The role of psychiatric comorbidity and depressive symptoms

As both stress reactivity and childhood adversity are associated to psychiatric symptoms and depression in particular and we are investigating a clinical sample, we tested the potential role of depressive severity and comorbidity on the correlation between emotional neglect frequency and the Y cubic parameter on the left striatum at the post-induction rs. For this purpose, linear mixed models were built on the Y cubic parameter of the left striatum as the dependent variable, taking emotional neglect frequency, resting state (the repeated measure: pre-stress rs, post-induction rs), depressive severity or comorbidity as fixed factors, and subjects as the random factor. The model with the depressive severity found no significant associations (all *p*s > 0.36), indicating the effect of emotional neglect frequency may prove difficult to disentangle from participants' depressive state (e.g., neither of them could explain the variance in gradients independently). In contrast, the model with comorbidity found a significant interaction between resting state, emotional neglect frequency, and comorbidity (F (1,129.94) = 5.172, p = 0.025). In order to further elucidate the nature of the relations between emotional neglect frequency and the Y cubic parameter in interaction with different comorbidity levels, we tested whether levels of comorbidity moderated the relation between emotional neglect frequency and the Y cubic parameter separately for pre-stress rs and post-induction rs. In these models, the Y cubic parameter was the dependent variable, emotional neglect frequency the independent variable and comorbidity the moderator. These moderation models were tested using PROCESS v2.16 for SPSS (Hayes, 2017), with the bootstrap samples of 5000 and a confidence level of 95%. The model for post-induction resting state found a significant interaction between emotional neglect frequency and comorbidity (F (1,147) = 4.831, p = 0.030). The conditional effect analysis showed that at low and medium levels of comorbidity, the prediction from emotional neglect frequency was not significant (*p*s > 0.24); while for individuals with high comorbidity, emotional neglect frequency negatively predicted the Y cubic parameter (t = -2.212, p = 0.029; Figure 3.5A). It is noteworthy that these results should be inspected with caution as the test for the entire model was not significant (F (3,147) = 2.122, p = 0.100). For the pre-stress-rs model, neither the whole model nor the interaction was significant (*p*s > 0.50).

To test whether this difference in models reflects a significant stress-related change, we also ran similar linear mixed models on the stress-induced change of the Y cubic parameter (the dependent variable). We included emotional neglect frequency, sides of the striatum (the repeated measure: left, right), the depressive severity or comorbidity as fixed factors, and subjects as the random factor. Similarly, the model with the depressive severity found no significant associations (all *p*s > 0.09),

whereas the model with comorbidity found a significant interaction between emotional neglect frequency and comorbidity (F (1,127.67) = 3.985, p = 0.048). The successive moderating effect analysis further elucidated this interaction (F (1,261) = 4.546, p = 0.034): for participants with low levels of comorbidity, the predicting effect of emotional neglect frequency was not significant (p = 0.52); while for individuals with medium and high comorbidity, emotional neglect frequency negatively predicted the Y cubic parameter change (medium: t = -2.637, p = 0.009; high: t = -3.191, p = 0.002. Figure 3.5B). The whole moderating model was also significant (F (3,261) = 3.457, p = 0.017).

The results above show the same pattern after controlling for gender, age, and medication use (see Table S3.8 & S3.9).

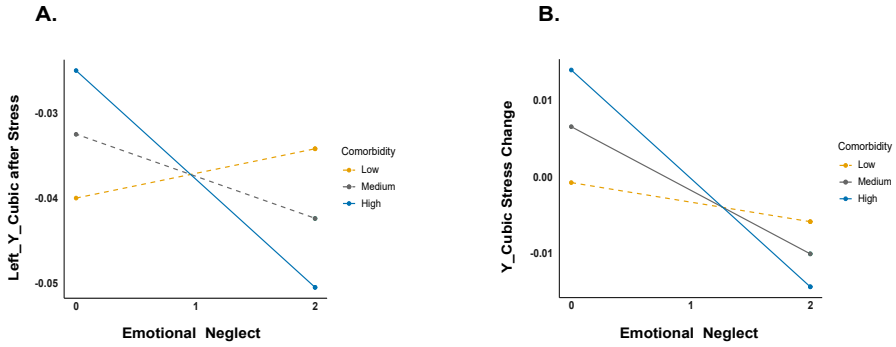

Figure 3.5 The illustration for moderation models. The predictive effects of emotional neglect on the Y cubic parameter of the left striatum at post-stress induction (A) and the stress-induced changes of this parameter (B) vary based on levels of comorbidity. The dashed lines represent insignificant predictions, and solid lines represent significant predictions. Emotional neglect was assessed using the NEMESIS subscale, and comorbidity was indexed by the total number of psychiatric disorders diagnosed for each participant.

Discussion

As far as we know, this study represents the first investigation focusing on striatal connectivity gradients to investigate the inter-individual relations to CA and psychiatric comorbidity, as well as intra-individual modulation of these gradients by acute stress. Through applying connectopic mappings to the psychiatric sample of MIND-Set, we found for the first-order striatal gradient: 1.) participants with different CA histories did not exhibit significantly diverse gradients at the pre-stress baseline, as the connectopic maps could not be predicted by any types of CA; 2.) after the stress-induction, this gradient map became associated with one type

of CA, specifically emotional neglect. Additionally, emotional neglect frequency negatively predicted the stress reactive change in this connectivity mode; 3.) the observed correlations between emotional neglect and striatal gradients only existed in individuals with elevated comorbidity. By highlighting the joint impact of CA and acute stress, our findings contribute to the potential utility of striatal connectivity gradients in understanding and, potentially, diagnosing and treating psychiatric disorders in the future.

Previous studies have reported CA to be associated with a blunted stress response in the HPA axis and cardiac functions (Carpenter et al., 2007; Elzinga et al., 2008; Sijtsema et al., 2015). The recent model proposed this blunted response might be related to the motivation function (Carroll et al., 2012, 2017): people with CA are less motivated to engage in coping with stress, due to their functional changes in striatum and related cortical regions (e.g., mPFC) shaped by CA. Potentially in line with this perspective, we found that emotional neglect was negatively correlated with the stress-induced change of the anterior-posterior organization of the first-order striatal gradients on both sides of the striatum. The first-order striatal gradient has been shown to be associated with goal-directed behaviors (e.g., delay discounting, relational processing, social cognition, sustained attention) and psychological well-being (Marquand et al., 2017), which largely rely on the corticostriatal circuitry, especially the striatum-PFC interaction (Balleine et al., 2007; Barch et al., 2013). Therefore, to some extent, our results provide new evidence for the motivation account of the stress response in CA at the brain connectivity level, as we did observe the motivation-related gradient change under the interaction of CA and acute stress. Moreover, the study by Hanson and colleagues (2018) identified the striatum-PFC connectivity to be a biological link between stress exposure and internalizing depressive symptomatology in adolescents with childhood maltreatment. Taking together, we could infer the corticostriatal connectivity mode, reflected by the first-order striatal gradient, possibly contributing to the neural substrate for high-order cognitive functions (e.g., motivations to cope with stress), is vulnerable to early-life adversity and further linked to psychopathology of mental disorders, e.g., depression, and functional connectivity gradients might provide an individual read-out of the resulting malfunction.

Although our analyses included three types of CA and the overall CA index in an attempt to capture the variance in frequency that encompasses all CA types, we found correlations between the first-order gradient and the frequency of one specific CA—emotional neglect, which also proved different from the respective correlations with other CA types. Emotional neglect describes maltreatment

behaviors failing to meet children's emotion needs and provide enough nurturance and affective support (Stoltenborgh et al., 2013), which lead to a lack of sufficient cognitive and social input for the brain during development. Studies support the notion of separating different types of adversity: while threatening violent behavior (e.g., abuse) affects limbic regions (e.g., hippocampus and amygdala) and their regulations from the cortex, forms of neglect affect cortical areas such as PFC, superior parietal and temporal cortex, which are involved in complex cognitive and social tasks (McLaughlin, Sheridan, & Lambert, 2014; Wu et al., 2023). Additionally, studies among healthy adults have observed structural changes in emotional regulation and motivation regions specifically related to neglect (Everaerd et al., 2015; Tendolkar et al., 2018). Our results identified relations between emotional neglect and the connectivity gradient associated with goal-directed behaviors, which are aligned with the previous viewpoint about neglect, but also link it with the functional coupling of the striatum. It could be inferred that scarce emotional inputs during childhood would limit the knowledge, motivation and ability to process and regulate emotions, especially under the situation of dealing with acute stress. It is noteworthy that our results do not necessarily imply that other types of CA and the overall CA index have no relations with striatal connectivity modes, as here we only examined the first-order gradients and the frequency of each CA type. Future research can explore further whether CA works as an all-or-none manner, and if the level of severity matters.

From the aspect of gradients, our results consistently pointed to the cubic anterior-posterior organization of the first-order gradient: both the stress-induced connectivity change and the post-stress-induction status were related to emotional neglect frequency. The cubic parameter specifically represents the quadratic coefficient for the derivative of cubic functions. It determines the distribution of changing rates along the anterior-posterior direction within the space. These results indicated the spatial changing pattern of connectopic modes along the Y direction was related to CA and stress. Subsequent analyses demonstrated that this association was mainly driven by changes in high frequency of neglect group. Stress induction might "reset" the anterior-posterior organization of the striatal connectivity gradient for these people, as reflected by the spatial changing pattern. In an attempt to visualize and thereby better understand the re-organization, we visually checked all the gradient maps, and produced the average maps with participants showing largest changes in the direction of observed correlations, assuming these extreme cases represent the possible pattern more obviously. By comparing gradient maps for the two resting state scans, we realized that the topographic shape of high-frequency group tended to show a more pronounced

gradual change pattern at post-stress rs, which is more similar to group gradients in the healthy sample (e.g., HCP dataset). This potential pattern can be considered together with the motivation model above: more structured gradients reflect a normal state of motivation network, which might indicate that the motivation system of these individuals functions more normally under elevated stress. Importantly, the results didn't show any difference related to emotional neglect at the pre-stress rs, so we couldn't suppose an impaired baseline striatal connectivity mode for the high-frequency group. What we found only captured the stress-induced change specifically for this group.

CA was shown to be consistently related to depression (Abercrombie et al., 2018; Beck & Bredemeier, 2016) and psychiatric comorbidity (Vrijsen et al., 2017). Our linear mixed models with both depressive severity and emotional neglect frequency as fixed factors found that, when controlling the effect of each other, neither depression nor emotional neglect could explain the significant variance of the anterior-posterior organization parameter and its stress-induced change independently. Due to the relatively high correlation between emotional neglect frequency and depressive symptom levels ($r_s = 0.292$, $p < 0.001$) in our sample, we could not further explore the role of the depressive severity here. Future studies that include a broader and more independent range of variance in the two factors (e.g., individuals with high emotional neglect frequency and low depression, or low emotional neglect frequency and high depression) are necessary. In contrast, comorbidity seems to interact with emotional neglect and influence the striatal gradients: for both post-induction value and stress-induced gradient change, emotional neglect only showcases significant effects in individuals with elevated comorbidity, but not individuals with fewer psychiatric disorders. This finding highlights the psychopathological link between CA, stress and striatal dysfunction. In this sense, the cubic anterior-posterior organization (Y cubic parameter) could be used as a new biomarker for the symptomatology of people with a frequent neglected history, by tracking stress-related brain changes in the general motivation and high-order cognition systems. The targeted diagnostics and treatment could be developed based on the findings.

In addition to these implications, we acknowledge certain limitations in our study. Firstly, to reduce participant drop-out and enhance data collection efficiency in the large database, stress induction via aversive movie watching was administered in the same session as the control task (neutral movie watching). To prevent the carry-over of stress states, stress induction was conducted after the control task, potentially introducing order effects. Future designs separating the two conditions

into different sessions would facilitate a more refined examination of the stress effect. Secondly, the observed correlations fall within the small to medium range of effect size (Cohen, 1988; Funder & Ozer, 2019; Gignac & Szodorai, 2016). It's noteworthy that these correlations were consistently observed across the bilateral striatum, encompassing both the post-stress state and stress-induced changes in the same parameter, indicating a stable predictive pattern. However, a more balanced distribution in CA might be beneficial to validate the results and those analyses might potentially yield a larger effect. Lastly, the Y cubic parameter indeed demonstrates the ability to capture the interacting influence of stress and CA on striatal networks, while additional methods beyond visual inspection could aid in further interpretations, such as how to map differences in TSM parameters with more targeted biological changes.

In conclusion, our study showed that the frequency of emotional neglect predicted alterations in the striatal functional connectopic gradients following acute stress induction, with this association being selectively present in individuals with elevated comorbidity of psychiatric disorders. These findings may contribute to future explorations in the psychopathology of childhood adversity and the utility of functional connectivity gradients for the striatum in clinical applications.

Supplementary Material

Table S3.1 Spearman correlations between childhood adversity and stress-response indicators

		Emotional Neglect	Psychological Abuse	Physical Abuse	Childhood Trauma
Δ Stress rating	r_s	0.103	0.037	-0.102	0.075
	p	0.177	0.627	0.180	0.327
Δ BPM	r_s	-0.142	-0.018	0.023	-0.069
	p	0.062	0.812	0.767	0.366
N = 173					

Childhood trauma and its subcategories were assessed using the NEMESIS; BPM: the heart beat per minute; Δ: the difference between pre-stress and post-induction rs.

Table S3.2 Spearman correlations between CA and the first-order gradient parameters

		Emotional Neglect	Psychological Abuse	Physical Abuse	Childhood Trauma
rs2_Left_X Linear	r_s	0.040	0.020	0.140	0.050
	p_{fdr}	0.778	0.861	0.190	0.771
rs2_Left_Y Linear	r_s	0.030	-0.040	-0.100	-0.010
	p_{fdr}	0.828	0.778	0.396	0.958
rs2_Left_Z Linear	r_s	0.030	-0.030	-0.070	0.000
	p_{fdr}	0.834	0.834	0.648	0.961
rs2_Left_X quadratic	r_s	0.100	0.080	-0.050	0.120
	p_{fdr}	0.388	0.573	0.778	0.273
rs2_Left_Y quadratic	r_s	0.030	0.030	0.010	0.010
	p_{fdr}	0.834	0.828	0.961	0.953
rs2_Left_Z quadratic	r_s	-0.100	-0.040	0.000	-0.110
	p_{fdr}	0.375	0.778	0.961	0.333
rs2_Left_X cubic	r_s	-0.040	-0.020	-0.120	-0.050
	p_{fdr}	0.778	0.861	0.300	0.771
rs2_Left_Y cubic	r_s	0.030	-0.060	0.030	-0.040
	p_{fdr}	0.834	0.657	0.834	0.778
rs2_Left_Z cubic	r_s	0.000	-0.080	0.030	-0.080
	p_{fdr}	0.961	0.533	0.834	0.573
N = 148					
rs3_Left_X Linear	r_s	-0.010	0.050	0.050	0.060
	p_{fdr}	0.981	0.618	0.625	0.595
rs3_Left_Y Linear	r_s	0.110	-0.080	-0.110	0.000
	p_{fdr}	0.282	0.440	0.284	0.986
rs3_Left_Z Linear	r_s	0.020	0.040	0.130	0.130
	p_{fdr}	0.846	0.677	0.219	0.224
rs3_Left_X quadratic	r_s	0.090	0.050	0.130	0.150
	p_{fdr}	0.407	0.643	0.219	0.134
rs3_Left_Y quadratic	r_s	-0.070	0.020	0.030	-0.030
	p_{fdr}	0.481	0.867	0.761	0.815
rs3_Left_Z quadratic	r_s	-0.090	-0.040	-0.070	-0.130
	p_{fdr}	0.398	0.681	0.481	0.223
rs3_Left_X cubic	r_s	0.010	-0.100	-0.070	-0.110
	p_{fdr}	0.981	0.343	0.491	0.317
rs3_Left_Y cubic	r_s	-0.190*	-0.050	0.000	-0.120
	p_{fdr}	0.042	0.618	0.987	0.243
rs3_Left_Z cubic	r_s	0.060	-0.100	-0.130	-0.080
	p_{fdr}	0.583	0.374	0.225	0.440
N = 152					

Table S3.2 Continued

		Emotional Neglect	Psychological Abuse	Physical Abuse	Childhood Trauma
ΔLeft_X Linear	r_s	-0.020	0.000	-0.030	0.020
	p_{fdr}	0.933	0.994	0.886	0.918
ΔLeft_Y Linear	r_s	0.110	0.010	-0.020	0.030
	p_{fdr}	0.376	0.970	0.914	0.886
ΔLeft_Z Linear	r_s	0.070	0.110	0.070	0.150
	p_{fdr}	0.625	0.325	0.634	0.166
ΔLeft_X quadratic	r_s	0.030	-0.020	0.010	0.020
	p_{fdr}	0.911	0.914	0.970	0.914
ΔLeft_Y quadratic	r_s	-0.150	-0.080	0.010	-0.100
	p_{fdr}	0.166	0.600	0.970	0.403
ΔLeft_Z quadratic	r_s	0.030	0.080	-0.060	0.020
	p_{fdr}	0.886	0.532	0.735	0.918
ΔLeft_X cubic	r_s	0.000	-0.010	0.030	-0.050
	p_{fdr}	0.970	0.949	0.895	0.816
ΔLeft_Y cubic	r_s	-0.210*	-0.070	-0.060	-0.130
	p_{fdr}	0.033	0.644	0.729	0.226
ΔLeft_Z cubic	r_s	-0.010	-0.040	-0.050	-0.030
	p_{fdr}	0.970	0.868	0.776	0.895
N = 136					
rs2_Right_X Linear	r_s	-0.010	0.020	-0.030	0.000
	p_{fdr}	0.978	0.913	0.913	0.978
rs2_Right_Y Linear	r_s	-0.050	0.000	-0.070	-0.010
	p_{fdr}	0.747	0.978	0.601	0.978
rs2_Right_Z Linear	r_s	0.030	0.000	0.160	0.020
	p_{fdr}	0.913	0.978	0.102	0.913
rs2_Right_X quadratic	r_s	0.160	0.080	0.070	0.120
	p_{fdr}	0.113	0.535	0.576	0.274
rs2_Right_Y quadratic	r_s	-0.060	0.000	0.080	-0.020
	p_{fdr}	0.621	0.978	0.502	0.913
rs2_Right_Z quadratic	r_s	-0.070	-0.030	-0.120	-0.080
	p_{fdr}	0.571	0.913	0.264	0.540
rs2_Right_X cubic	r_s	0.010	-0.030	0.080	0.000
	p_{fdr}	0.967	0.913	0.520	0.978
rs2_Right_Y cubic	r_s	0.040	-0.010	-0.020	-0.030
	p_{fdr}	0.849	0.972	0.913	0.913
rs2_Right_Z cubic	r_s	-0.120	-0.090	-0.090	-0.100
	p_{fdr}	0.261	0.443	0.436	0.367
N = 147					
rs3_Right_X Linear	r_s	0.030	-0.080	-0.110	-0.030
	p_{fdr}	0.771	0.524	0.348	0.771

Table S3.2 Continued

		Emotional Neglect	Psychological Abuse	Physical Abuse	Childhood Trauma
rs3_Right_Y Linear	r_s	0.070	-0.040	-0.080	0.010
	p_{fdr}	0.535	0.721	0.486	0.933
rs3_Right_Z Linear	r_s	0.040	0.040	0.120	0.000
	p_{fdr}	0.722	0.722	0.284	0.982
rs3_Right_X quadratic	r_s	0.120	0.050	0.080	0.080
	p_{fdr}	0.269	0.686	0.486	0.486
rs3_Right_Y quadratic	r_s	-0.070	0.050	0.040	-0.050
	p_{fdr}	0.535	0.686	0.721	0.686
rs3_Right_Z quadratic	r_s	-0.080	-0.020	-0.060	-0.050
	p_{fdr}	0.534	0.820	0.648	0.709
rs3_Right_X cubic	r_s	0.020	0.070	0.100	0.030
	p_{fdr}	0.832	0.597	0.415	0.798
rs3_Right_Y cubic	r_s	-0.150	0.010	0.040	-0.100
	p_{fdr}	0.153	0.912	0.722	0.399
rs3_Right_Z cubic	r_s	-0.050	-0.060	-0.080	0.000
	p_{fdr}	0.686	0.648	0.486	0.982
N = 144					
ΔRight_X Linear	r_s	0.030	-0.060	-0.060	-0.020
	p_{fdr}	0.849	0.649	0.648	0.898
ΔRight_Y Linear	r_s	0.120	-0.090	0.080	0.010
	p_{fdr}	0.319	0.506	0.561	0.964
ΔRight_Z Linear	r_s	0.000	0.030	-0.080	-0.060
	p_{fdr}	0.984	0.849	0.561	0.648
ΔRight_X quadratic	r_s	-0.060	-0.030	0.000	-0.080
	p_{fdr}	0.660	0.858	0.976	0.561
ΔRight_Y quadratic	r_s	-0.060	0.050	-0.120	-0.080
	p_{fdr}	0.648	0.771	0.283	0.561
ΔRight_Z quadratic	r_s	0.030	-0.010	0.160	0.100
	p_{fdr}	0.862	0.964	0.119	0.455
ΔRight_X cubic	r_s	0.040	0.070	0.030	0.040
	p_{fdr}	0.791	0.589	0.849	0.812
ΔRight_Y cubic	r_s	-0.230*	0.050	-0.020	-0.110
	p_{fdr}	0.014	0.702	0.898	0.351
ΔRight_Z cubic	r_s	0.010	-0.040	-0.010	0.040
	p_{fdr}	0.964	0.791	0.964	0.791
N = 131					

Childhood trauma and its subcategories were assessed using the NEMESIS. A trend surface regression model with nine parameters (linear, quadratic, and cubic parameters along X, Y, and Z axes) was utilized to summarize the spatial topology of gradient maps. rs2: pre-stress rs; rs3: post-induction rs; Δ: the difference between pre-stress and post-induction rs; *p<0.05.

Table S3.3 Spearman correlations between CA and the first-order gradient parameters after controlling age, gender and medication

		Emotional Neglect	Psychological Abuse	Physical Abuse	Childhood Trauma
rs2_Left_X Linear	r_s	0.090	0.010	0.150	0.090
	p_{fdr}	0.440	0.899	0.154	0.440
rs2_Left_Y Linear	r_s	-0.050	-0.010	-0.070	-0.060
	p_{fdr}	0.662	0.898	0.575	0.650
rs2_Left_Z Linear	r_s	0.060	-0.050	-0.050	0.030
	p_{fdr}	0.650	0.670	0.653	0.744
rs2_Left_X quadratic	r_s	0.100	0.070	-0.030	0.120
	p_{fdr}	0.403	0.584	0.773	0.297
rs2_Left_Y quadratic	r_s	0.080	0.040	0.040	0.080
	p_{fdr}	0.495	0.693	0.709	0.541
rs2_Left_Z quadratic	r_s	-0.080	-0.060	-0.050	-0.110
	p_{fdr}	0.495	0.605	0.653	0.352
rs2_Left_X cubic	r_s	-0.100	-0.010	-0.120	-0.100
	p_{fdr}	0.393	0.898	0.297	0.393
rs2_Left_Y cubic	r_s	0.090	-0.050	0.060	0.040
	p_{fdr}	0.469	0.653	0.641	0.709
rs2_Left_Z cubic	r_s	-0.010	-0.050	0.050	-0.070
	p_{fdr}	0.898	0.653	0.663	0.575
N = 148					
rs3_Left_X Linear	r_s	0.030	0.060	0.040	0.080
	p_{fdr}	0.794	0.619	0.734	0.429
rs3_Left_Y Linear	r_s	0.100	-0.080	-0.090	-0.030
	p_{fdr}	0.361	0.429	0.384	0.747
rs3_Left_Z Linear	r_s	0.060	0.050	0.140	0.160
	p_{fdr}	0.569	0.666	0.162	0.095
rs3_Left_X quadratic	r_s	0.050	0.040	0.160	0.130
	p_{fdr}	0.666	0.709	0.089	0.197
rs3_Left_Y quadratic	r_s	-0.080	0.040	0.030	-0.010
	p_{fdr}	0.429	0.709	0.743	0.908
rs3_Left_Z quadratic	r_s	-0.020	-0.040	-0.130	-0.100
	p_{fdr}	0.806	0.709	0.197	0.350
rs3_Left_X cubic	r_s	-0.020	-0.110	-0.070	-0.130
	p_{fdr}	0.821	0.331	0.544	0.197
rs3_Left_Y cubic	r_s	-0.170	-0.050	0.010	-0.090
	p_{fdr}	0.088	0.666	0.908	0.384

Table S3.3 Continued

		Emotional Neglect	Psychological Abuse	Physical Abuse	Childhood Trauma
rs3_Left_Z cubic	r_s	0.040	-0.090	-0.110	-0.090
	p_{fdr}	0.725	0.384	0.319	0.385
N = 152					
ΔLeft_X Linear	r_s	-0.040	0.000	-0.020	0.010
	p_{fdr}	0.800	0.990	0.986	0.990
ΔLeft_Y Linear	r_s	0.130	0.000	-0.010	0.040
	p_{fdr}	0.245	0.990	0.986	0.800
ΔLeft_Z Linear2	r_s	0.060	0.110	0.080	0.140
	p_{fdr}	0.715	0.327	0.602	0.204
ΔLeft_X quadratic	r_s	0.010	-0.040	0.030	0.010
	p_{fdr}	0.990	0.840	0.898	0.990
ΔLeft_Y quadratic	r_s	-0.160	-0.070	0.000	-0.110
	p_{fdr}	0.136	0.620	0.990	0.359
ΔLeft_Z quadratic	r_s	0.030	0.090	-0.060	0.010
	p_{fdr}	0.898	0.510	0.673	0.986
ΔLeft_X cubic	r_s	0.040	-0.010	0.030	-0.010
	p_{fdr}	0.803	0.986	0.898	0.986
ΔLeft_Y cubic	r_s	-0.220*	-0.060	-0.060	-0.150
	p_{fdr}	0.021	0.673	0.707	0.155
ΔLeft_Z cubic	r_s	-0.020	-0.040	-0.050	-0.050
	p_{fdr}	0.933	0.800	0.760	0.800
N = 136					
rs2_Right_X Linear	r_s	-0.040	0.000	-0.020	0.010
	p_{fdr}	0.923	0.895	0.879	0.963
rs2_Right_Y Linear	r_s	0.130	0.000	-0.010	0.040
	p_{fdr}	0.361	0.963	0.776	0.765
rs2_Right_Z Linear	r_s	0.060	0.110	0.080	0.140
	p_{fdr}	0.627	0.963	0.114	0.726
rs2_Right_X quadratic	r_s	0.010	-0.040	0.030	0.010
	p_{fdr}	0.097	0.404	0.355	0.182
rs2_Right_Y quadratic	r_s	-0.160	-0.070	0.000	-0.110
	p_{fdr}	0.895	0.972	0.355	0.895
rs2_Right_Z quadratic	r_s	0.030	0.090	-0.060	0.010
	p_{fdr}	0.353	0.787	0.072	0.223
rs2_Right_X cubic	r_s	0.040	-0.010	0.030	-0.010

Table S3.3 Continued

		Emotional Neglect	Psychological Abuse	Physical Abuse	Childhood Trauma
	p_{fdr}	0.923	0.879	0.545	0.963
rs2_Right_Y cubic	r_s	-0.220	-0.060	-0.060	-0.150
	p_{fdr}	0.396	1.000	0.963	0.895
rs2_Right_Z cubic	r_s	-0.020	-0.040	-0.050	-0.050
	p_{fdr}	0.282	0.563	0.412	0.355
N = 147					
rs3_Right_X Linear	r_s	0.010	-0.060	-0.080	-0.040
	p_{fdr}	0.949	0.638	0.519	0.730
rs3_Right_Y Linear	r_s	0.020	-0.010	-0.070	-0.020
	p_{fdr}	0.865	0.907	0.575	0.865
rs3_Right_Z Linear	r_s	0.080	0.030	0.120	0.030
	p_{fdr}	0.489	0.790	0.291	0.804
rs3_Right_X quadratic	r_s	0.120	0.060	0.130	0.090
	p_{fdr}	0.291	0.638	0.232	0.459
rs3_Right_Y quadratic	r_s	-0.030	0.040	0.020	-0.020
	p_{fdr}	0.790	0.742	0.839	0.843
rs3_Right_Z quadratic	r_s	-0.050	-0.050	-0.110	-0.050
	p_{fdr}	0.675	0.681	0.350	0.703
rs3_Right_X cubic	r_s	0.060	0.060	0.080	0.060
	p_{fdr}	0.646	0.646	0.519	0.648
rs3_Right_Y cubic	r_s	-0.100	-0.030	0.010	-0.090
	p_{fdr}	0.408	0.800	0.906	0.484
rs3_Right_Z cubic	r_s	-0.100	-0.050	-0.090	-0.040
	p_{fdr}	0.368	0.689	0.480	0.742
N = 144					
ΔRight_X Linear	r_s	-0.020	-0.070	-0.050	-0.060
	p_{fdr}	0.842	0.632	0.740	0.688
ΔRight_Y Linear	r_s	0.070	-0.080	0.060	-0.010
	p_{fdr}	0.617	0.616	0.650	0.893
ΔRight_Z Linear	r_s	0.030	0.020	-0.060	-0.040
	p_{fdr}	0.784	0.842	0.650	0.775
ΔRight_X quadratic	r_s	-0.030	-0.040	-0.020	-0.070
	p_{fdr}	0.812	0.784	0.842	0.632
ΔRight_Y quadratic	r_s	-0.050	0.040	-0.160	-0.100
	p_{fdr}	0.697	0.756	0.115	0.446

Table S3.3 Continued

		Emotional Neglect	Psychological Abuse	Physical Abuse	Childhood Trauma
ΔRight_Z quadratic	r_s	0.040	0.010	0.200*	0.130
	p_{fdr}	0.756	0.948	0.046	0.242
ΔRight_X cubic	r_s	0.090	0.070	0.020	0.060
	p_{fdr}	0.543	0.632	0.842	0.657
ΔRight_Y cubic	r_s	-0.200*	0.050	-0.050	-0.110
	p_{fdr}	0.038	0.733	0.737	0.364
ΔRight_Z cubic	r_s	-0.070	-0.020	0.040	0.010
	p_{fdr}	0.632	0.886	0.784	0.893

N = 131

Childhood trauma and its subcategories were assessed using the NEMESIS. A trend surface regression model with nine parameters (linear, quadratic, and cubic parameters along X, Y, and Z axes) was utilized to summarize the spatial topology of gradient maps. rs2: pre-stress rs; rs3: post-induction rs; Δ: the difference between pre-stress and post-induction rs; *p<0.05.

Table S3.4 Comparing the correlations of emotional neglect with other CA types

		rs3_Left_Y cubic	ΔLeft_Y cubic	ΔRight_Y cubic
Psychological Abuse	*z*	-1.575	-1.507	-2.923
	p	0.058	0.066	0.002 **
Physical Abuse	*z*	-1.910	-1.438	-1.925
	p	0.028*	0.075	0.027*

rs3: post-induction rs; Δ: the difference between pre-stress and post-induction rs; *p<0.05, **p<0.01.

Table S3.5 Summary of the linear mixed models

	Dependent variables	Fixed factors	Random factors
Model 1	Left_Y cubic	Resting-state (repeated measure); Emotional Neglect; Depressive Severity.	Subjects
Model 2	Left_Y cubic	Resting-state (repeated measure); Emotional Neglect; Comorbidity	Subjects
Model 3	ΔY cubic	Sides of the striatum (repeated measure); Emotional Neglect; Depressive Severity.	Subjects
Model 4	ΔY cubic	Sides of the striatum (repeated measure); Emotional Neglect; Comorbidity.	Subjects

Left_Y cubic: Y cubic TSM parameter at the left striatum; ΔY cubic: the changes of Y cubic parameter values between the pre-stress rs and post-stress induction rs; Emotional neglect was assessed using the NEMESIS subscale, depressive severity was measured by IDS-SR, and comorbidity was indexed by the total number of psychiatric disorders diagnosed for each participant.

Table S3.6 Linear mixed models with emotional neglect, the depressive severity and comorbidity Type III Analysis of Variance Table with Satterthwaite's method

The model for Y cubic parameter at the left striatum with resting states(rs), emotional neglect and depressive severity						
	Sum Sq	**Mean Sq**	**NumDF**	**DenDF**	**F value**	**Pr(>F)**
rs	0.000	0.000	1	129.530	0.461	0.499
Emotional Neglect	0.001	0.001	1	133.450	0.595	0.442
Depressive Severity	0.000	0.000	1	136.820	0.012	0.915
rs:Emotional Neglect	0.000	0.000	1	121.980	0.364	0.547
rs:Depressive Severity	0.000	0.000	1	125.640	0.410	0.523
Emotional Neglect: Depressive Severity	0.001	0.001	1	132.160	0.820	0.367
rs:Emotional Neglect: Depressive Severity	0.000	0.000	1	120.500	0.022	0.883
The model for Y cubic parameter at the left striatum with rs, emotional neglect and comorbidity						
	Sum Sq	**Mean Sq**	**NumDF**	**DenDF**	**F value**	**Pr(>F)**
rs	0.002	0.002	1	140.890	1.856	0.175
Emotional Neglect	0.001	0.001	1	145.570	0.845	0.360
Comorbidity	0.001	0.001	1	147.850	0.703	0.403
rs:Emotional Neglect	0.002	0.002	1	133.160	1.782	0.184
rs: Comorbidity	0.002	0.002	1	135.010	2.481	0.118
Emotional Neglect: Comorbidity	0.002	0.002	1	142.910	1.626	0.204
rs:Emotional Neglect: Comorbidity	0.005	0.005	1	129.940	5.172	0.025 *
The model for the difference of Y cubic parameter between the two resting states with sides of the striatum (left/right), emotional neglect and depressive severity						
	Sum Sq	**Mean Sq**	**NumDF**	**DenDF**	**F value**	**Pr(>F)**
Side	0.000	0.000	1	110.900	0.269	0.605
Emotional Neglect	0.000	0.000	1	111.940	0.082	0.775
Depressive Severity	0.000	0.000	1	117.120	0.174	0.678
Side: Emotional Neglect	0.005	0.005	1	106.410	2.765	0.099
Side: Depressive Severity	0.000	0.000	1	111.750	0.108	0.743
Emotional Neglect: Depressive Severity	0.001	0.001	1	113.420	0.732	0.394
Side: Emotional Neglect: Depressive Severity	0.005	0.005	1	108.000	2.712	0.102

Table S3.6 Continued

The model for the difference of Y cubic parameter between the two resting states with sides of the striatum (left/right), emotional neglect and comorbidity						
	Sum Sq	**Mean Sq**	**NumDF**	**DenDF**	**F value**	**Pr(>F)**
Side	0.001	0.001	1	121.220	0.613	0.435
Emotional Neglect	0.001	0.001	1	123.090	0.386	0.535
Comorbidity	0.005	0.005	1	129.920	2.806	0.096
Side: Emotional Neglect	0.000	0.000	1	118.020	0.283	0.596
Side: Comorbidity	0.000	0.000	1	125.260	0.095	0.758
Emotional Neglect: Comorbidity	0.007	0.007	1	127.670	3.985	0.048 *
Side: Emotional Neglect: Comorbidity	0.000	0.000	1	122.580	0.083	0.773

*$p<0.05$

Table S3.7 Moderating models with emotional neglect and comorbidity

Model: the interaction between emotional neglect and comorbidity for Y cubic parameter at the left striatum of pre-stress rs							
Model Summary	**R**	**R-sq**	**MSE**	**F**	**df1**	**df2**	**p**
	0.062	0.004	0.002	0.186	3	143	0.906
	coeff	**se**	**t**	**p**	**LLCI**	**ULCI**	
constant	-0.031	0.010	-3.047	0.003**	-0.051	-0.011	
Emotional Neglect	-0.004	0.008	-0.582	0.562	-0.019	0.011	
Comorbidity	-0.002	0.005	-0.318	0.751	-0.012	0.009	
Interaction	0.002	0.003	0.664	0.508	-0.005	0.009	
Test(s) of highest order unconditional interaction(s):							
	R2-chng	**F**	**df1**	**df2**	**p**		
Emotional Neglect * comorbidity	0.003	0.440	1	143	0.508		
Model: the interaction between emotional neglect and comorbidity for Y cubic parameter at the left striatum of post-induction rs							
Model Summary	**R**	**R-sq**	**MSE**	**F**	**df1**	**df2**	**p**
	0.204	0.042	0.002	2.122	3	147	0.100
	coeff	**se**	**t**	**p**	**LLCI**	**ULCI**	
constant	-0.047	0.011	-4.356	0.000**	-0.069	-0.026	
Emotional Neglect	0.011	0.008	1.362	0.175	-0.005	0.026	
Comorbidity	0.008	0.005	1.403	0.163	-0.003	0.018	
Interaction	-0.008	0.004	-2.198	0.030*	-0.015	-0.001	
Test(s) of highest order unconditional interaction(s):							
	R2-chng	**F**	**df1**	**df2**	**p**		
Emotional Neglect * comorbidity	0.032	4.831	1	147	0.030*		
Conditional effects of emotional neglect at values of the moderator (comorbidity):							
Comorbidity	**Effect**	**se**	**t**	**p**	**LLCI**	**ULCI**	
1	0.003	0.005	0.558	0.577	-0.007	0.013	
2	-0.005	0.004	-1.175	0.242	-0.013	0.003	
3	-0.013	0.006	-2.212	0.029*	-0.024	-0.001	
Model: the interaction between emotional neglect and comorbidity for the difference of Y cubic parameter between the two resting states.							
Model Summary	**R**	**R-sq**	**MSE**	**F**	**df1**	**df2**	**p**
	0.196	0.038	0.002	3.457	3	261	0.017*
	coeff	**se**	**t**	**p**	**LLCI**	**ULCI**	
constant	-0.008	0.008	-0.997	0.320	-0.024	0.008	
Emotional Neglect	0.003	0.006	0.553	0.581	-0.008	0.015	
Comorbidity	0.007	0.004	1.794	0.074	-0.001	0.015	
Interaction	-0.006	0.003	-2.132	0.034*	-0.011	0.000	

Table S3.7 Continued

Test(s) of highest order unconditional interaction(s):						
	R2-chng	**F**	**df1**	**df2**	**p**	
Emotional Neglect * comorbidity	0.017	4.546	1	261	0.034*	
Conditional effects of emotional neglect at values of the moderator (comorbidity):						
Comorbidity	**Effect**	**se**	**t**	**p**	**LLCI**	**ULCI**
1	-0.003	0.004	-0.649	0.517	-0.010	0.005
2	-0.008	0.003	-2.637	0.009**	-0.015	-0.002
3	-0.014	0.004	-3.191	0.002**	-0.023	-0.005

*$p<0.05$, **$p<0.01$.

Table S3.8 Linear mixed models with emotional neglect, the depressive severity and comorbidity (controlled by age, gender and medication)
Type III Analysis of Variance Table with Satterthwaite's method

The model for Y cubic parameter at the left striatum with resting states(rs), emotional neglect and depressive severity						
	Sum Sq	**Mean Sq**	**NumDF**	**DenDF**	**F value**	**Pr(>F)**
rs	0.000	0.000	1	128.260	0.385	0.536
Emotional Neglect	0.001	0.001	1	129.860	1.085	0.300
Depressive Severity	0.000	0.000	1	133.600	0.003	0.954
rs:Emotional Neglect	0.000	0.000	1	120.000	0.415	0.521
rs:Depressive Severity	0.000	0.000	1	124.010	0.336	0.564
Emotional Neglect: Depressive Severity	0.001	0.001	1	128.430	1.037	0.311
rs:Emotional Neglect: Depressive Severity	0.000	0.000	1	118.390	0.040	0.841
The model for Y cubic parameter at the left striatum with rs, emotional neglect and comorbidity						
	Sum Sq	**Mean Sq**	**NumDF**	**DenDF**	**F value**	**Pr(>F)**
rs	0.002	0.002	1	140.120	1.598	0.208
Emotional Neglect	0.001	0.001	1	142.730	1.266	0.262
Comorbidity	0.000	0.000	1	145.160	0.003	0.959
rs:Emotional Neglect	0.002	0.002	1	131.820	1.717	0.192
rs: Comorbidity	0.002	0.002	1	133.850	2.220	0.139
Emotional Neglect: Comorbidity	0.001	0.001	1	139.840	1.223	0.271
rs:Emotional Neglect: Comorbidity	0.005	0.005	1	128.400	5.063	0.026*
The model for the difference of Y cubic parameter between the two resting states with sides of the striatum (left/right), emotional neglect and depressive severity						
	Sum Sq	**Mean Sq**	**NumDF**	**DenDF**	**F value**	**Pr(>F)**
Side	0.001	0.001	1	110.410	0.301	0.585
Emotional Neglect	0.000	0.000	1	110.920	0.012	0.914
Depressive Severity	0.000	0.000	1	116.150	0.207	0.650
Side: Emotional Neglect	0.004	0.004	1	105.880	2.611	0.109
Side: Depressive Severity	0.000	0.000	1	111.250	0.121	0.729
Emotional Neglect: Depressive Severity	0.001	0.001	1	112.420	0.478	0.491
Side: Emotional Neglect: Depressive Severity	0.004	0.004	1	107.470	2.578	0.111

Table S3.8 Continued

The model for the difference of Y cubic parameter between the two resting states with sides of the striatum (left/right), emotional neglect and comorbidity						
	Sum Sq	**Mean Sq**	**NumDF**	**DenDF**	**F value**	**Pr(>F)**
Side	0.001	0.001	1	120.590	0.642	0.425
Emotional Neglect	0.001	0.001	1	121.740	0.494	0.484
Comorbidity	0.007	0.007	1	128.650	3.948	0.049*
Side: Emotional Neglect	0.001	0.001	1	117.370	0.317	0.575
Side: Comorbidity	0.000	0.000	1	124.640	0.090	0.764
Emotional Neglect: Comorbidity	0.008	0.008	1	126.360	4.732	0.031*
Side: Emotional Neglect: Comorbidity	0.000	0.000	1	121.960	0.092	0.763

*$p<0.05$

Table S3.9 Moderating models with emotional neglect and comorbidity (controlled by age, gender and medication use)

Model: the interaction between emotional neglect and comorbidity for Y cubic parameter at the left striatum of pre-stress rs							
Model Summary	**R**	**R-sq**	**MSE**	**F**	**df1**	**df2**	**p**
	0.097	0.009	0.002	0.448	3	143	0.719
	coeff	**se**	**t**	**p**	**LLCI**	**ULCI**	
constant	0.009	0.010	0.892	0.374	-0.011	0.028	
Emotional Neglect	-0.003	0.007	-0.366	0.715	-0.017	0.012	
Comorbidity	-0.005	0.005	-1.060	0.291	-0.015	0.005	
Interaction	0.003	0.003	0.830	0.408	-0.004	0.009	
Test(s) of highest order unconditional interaction(s):							
	R2-chng	**F**	**df1**	**df2**	**p**		
Emotional Neglect * comorbidity	0.005	0.689	1	143	0.408		
Model: the interaction between emotional neglect and comorbidity for Y cubic parameter at the left striatum of post-induction rs							
Model Summary	**R**	**R-sq**	**MSE**	**F**	**df1**	**df2**	**p**
	0.221	0.049	0.002	2.518	3	147	0.060
	coeff	**se**	**t**	**p**	**LLCI**	**ULCI**	
constant	-0.006	0.011	-0.543	0.588	-0.026	0.015	
Emotional Neglect	0.011	0.008	1.502	0.135	-0.004	0.026	
Comorbidity	0.003	0.005	0.603	0.548	-0.007	0.013	
Interaction	-0.007	0.003	-2.031	0.044*	-0.014	0.000	
Test(s) of highest order unconditional interaction(s):							
	R2-chng	**F**	**df1**	**df2**	**p**		
Emotional Neglect * comorbidity	0.027	4.125	1	147	0.044*		
Conditional effects of emotional neglect at values of the moderator (comorbidity):							
Comorbidity	**Effect**	**se**	**t**	**p**	**LLCI**	**ULCI**	
1	0.004	0.005	0.886	0.377	-0.006	0.014	
2	-0.003	0.004	-0.626	0.532	-0.011	0.005	
3	-0.010	0.006	-1.709	0.090	-0.020	0.002	

Model: the interaction between emotional neglect and comorbidity for the difference of Y cubic parameter between the two resting states.							
Model Summary	**R**	**R-sq**	**MSE**	**F**	**df1**	**df2**	**p**
	0.205	0.042	0.002	3.827	3	261	0.010*
	coeff	**se**	**t**	**p**	**LLCI**	**ULCI**	
constant	-0.005	0.008	-0.568	0.571	-0.020	0.011	
Emotional Neglect	0.004	0.006	0.639	0.524	-0.008	0.015	
Comorbidity	0.009	0.004	2.099	0.037	0.001	0.017	
Interaction	-0.006	0.003	-2.299	0.022*	-0.012	-0.001	
Test(s) of highest order unconditional interaction(s):							
	R2-chng	**F**	**df1**	**df2**	**p**		
Emotional Neglect * comorbidity	0.019	5.284	1	261	0.022*		
Conditional effects of emotional neglect at values of the moderator (comorbidity):							
Comorbidity	**Effect**	**se**	**t**	**p**	**LLCI**	**ULCI**	
1	-0.002	0.004	-0.634	0.527	-0.010	0.005	
2	-0.009	0.003	-2.763	0.006**	-0.015	-0.003	
3	-0.015	0.004	-3.384	0.001**	-0.024	-0.006	

*$p<0.05$, **$p<0.01$.

Chapter 4.

Characterizing functional connectivity gradients for the hippocampus-amygdala complex in healthy and psychiatric cohorts

This chapter is based on: Liu, X. S., Vrijsen, J. N., Yan, L., Haak, K. V., Collard, R. M., van Eijndhoven, P. F. P., Beckmann, C. F., Fernández, G., Tendolkar, I., & Kohn, N. (Under Review). Characterizing functional connectivity gradients for the hippocampus-amygdala complex in healthy and psychiatric cohorts.

Abstract

The hippocampus and amygdala play essential roles in human cognition and emotion, through their extensive connectivity with other brain regions and close interaction between them. Uncovering the functional organization of the hippocampus–amygdala complex and how it is modulated by neurotransmitters can enhance our understanding of their biological functionality, and provide a basis for further exploration of the clinical relevance. An emerging functional connectivity analysis method, “connectopic mapping”, may offer a novel approach to characterize this functional organization. In this study, we applied "connectopic mapping" to the hippocampus-amygdala complex, testing its utility with resting-state functional magnetic resonance imaging (fMRI) scans of two independent datasets: one comprising healthy individuals (N = 410) and another comprising a psychiatric cohort (N = 367). The spatial organization of derived gradient maps was compared to 18 positron emission tomography (PET) or single photon emission computed tomography (SPECT) scan templates for different neurotransmitter systems. Individual gradient–neurotransmitter similarity indices were correlated with mental health outcomes. Our analyses identified six distinct gradient maps in both datasets. The third-order gradients showed stable similarity with 5-HT1A receptor maps across various resting-state scans. Similarities were also observed between gradient maps and the distribution patterns of neurotransmitters within the dopaminergic system. Individual gradient-to-5-HT1A similarity was positively correlated with depressive severity and anxiety sensitivity, highlighting the psychopathological relevance. These findings demonstrate that across the psychiatric continuum, "connectopic mapping" is a powerful tool for exploring the relationship between functional connectivity and neurotransmitter modulation, showing potential as a comprehensive transdiagnostic biomarker.

Keywords: Hippocampus-amygdala complex; Functional connectivity; Connectopic mapping; Serotonin; Dopamine; Psychopathology

Introduction

The hippocampus and amygdala, as two adjacent medial temporal lobe (MTL) structures, have consistently been investigated as key brain regions in cognitive affective neuroscience (LaBar & Cabeza, 2006; Panksepp et al., 2017). The hippocampus, shaped like a seahorse, is essential for episodic memory. It processes and connects the sensory inputs, enabling our memory for daily events built up with spatial, temporal and other contextual information (Barker & Warburton, 2011; Moscovitch et al., 2016). The anterior segment of hippocampus is closely adjacent to the amygdala — a grey matter complex located in the dorsal sector of MTL. The amygdala is the central region for emotional responses to environmental stimuli, participating in circuits that process heightened arousal and survival-related emotions, such as fear, threat, and reward (Ewbank et al., 2009; Garavan et al., 2001; Hrybouski et al., 2016; Kohn et al., 2011). Effective functioning of these two anatomically adjacent regions is inseparable from their close interactions with each other: processes such as fear learning (Maren et al., 2013), as well as the encoding, retrieval, and consolidation of emotional memories (LaBar & Cabeza, 2006; Phelps, 2004; Richardson et al., 2004) critically depend on hippocampus–amygdala interactions.

As pivotal hubs for cognition and emotion, the hippocampus and amygdala also maintain widespread functional connections with other brain regions. Connections with the medial prefrontal cortex (mPFC), anterior temporal lobe, insula and posterior cortical areas are shown to support episodic encoding and retrieval, aversive learning, as well as stress and emotion regulation (Kohn et al., 2014; Likhtik & Paz, 2015; Poppenk et al., 2013; Roy et al., 2009; van Kesteren et al., 2010; van Marle et al., 2009, 2010). Maladaptive variations in these neural circuits lead to corresponding functional disruptions, which are commonly observed in mood disorders such as depression (Cullen et al., 2014; Mulders et al., 2015), anxiety disorders (Brehl et al., 2020; Shin & Liberzon, 2010) and post-traumatic stress disorder (PTSD; Likhtik & Paz, 2015; Rauch et al., 2006), and may also account for certain comorbidity across these.

Notably, studies demonstrated that functional domains within the hippocampus vary along its long, curved posterior-to-anterior axis, with gradients observed in gene expression, place cell field sizes, and the representation of gist versus detailed information (Poppenk et al., 2013; Strange et al., 2014). Anatomically, dorsoventral (corresponding to anterior-posterior in human) topographical gradients in hippocampal–cortical and subcortical connectivity were revealed in

animal studies (Kishi et al., 2006; Witter, 1993), which may support its functional gradient organization. Building on above findings, it's important to examine if these gradient organization could be replicated in living humans (e.g., using noninvasive imaging techniques such as fMRI) for both healthy and clinical populations, and how it further matches with cognitive performance and psychiatric outcomes. These investigations will help us build a clear overview of hippocampal function and dysfunction.

Similarly, projections between the amygdala and various cortical regions (e.g., mPFC, inferior temporal cortex), as well as subcortical structures (e.g., the striatum), have also been found to exhibit a topographically organized pattern (Haber, 2003; Stefanacci & Amaral, 2000, 2002). As a compact, deep-lying nucleus, however, the amygdala's small size may limit the suitability of investigating this topography in humans using neuroimaging techniques, due to imaging resolution constraints. The hippocampus and amygdala are not only spatially adjacent structures, but both play closely interconnected roles within cognitive and affective functional networks; the amygdala is often regarded as a unit with the hippocampus when examining its functional role or psychiatric aberrance (Rajarethinam et al., 2001; Rutishauser et al., 2006). Considering both practical advantages and biological relevance, we would like to integrate the hippocampus and amygdala into a single complex, and capture the functional connectivity organization of this complex, through a data-driven technique "connectopic mapping". This method is designed to identify multiple overlapping connectivity patterns (gradient maps) within a predefined region of interest (ROI), with each gradient representing a distinct topographic mode of connectivity variation within the ROI relative to the rest of the brain (Haak et al., 2018). A pioneering study focused on the striatum, demonstrating that connectopic gradients replicate the topographical organization of cortical projections to the striatum observed in animal anatomical studies (Marquand et al., 2017). In the current study, with "connectopic mapping", we aimed to provide an overview of functional connectivity for the hippocampus-amygdala complex, by identifying its topographic connectivity gradients, then further explore its psychiatric relevance.

The topographic gradients obtained by "connectopic mapping" are data-derived, and may result from combined influences of multiple biological mechanisms, including anatomical projections and neurotransmitter modulation. As for the hippocampus and amygdala, they are structures functioning under the support of various neurotransmitter systems, which extensively regulate their communication with other regions of functional networks (Garrido Zinn et al., 2016; Vizi & Kiss,

1998). For example, as a fundamental process for long-term memory, hippocampal long-term potentiation depends on N-methyl-D-aspartate (NMDA) glutamatergic receptors and is further regulated by beta-noradrenergic receptors (Izquierdo et al., 1993). The beta-noradrenergic pathway in the amygdala is crucial for both the acquisition and consolidation of fear conditioning (Bush et al., 2010; Krugers et al., 2012). Other neurotransmitter systems, such as serotonin and dopamine, are also extensively distributed, prominently modulating the fear circuitry, emotional processing and learning (Bocchio et al., 2016; Frick et al., 2022). Given the essential role of neurotransmitters in functional networks of the hippocampus-amygdala complex, we hypothesized that topographic gradient modes should, to some extent, reflect the underlying influence of neurotransmitter systems. To test this hypothesis, we compared the spatial topologies of hippocampus-amygdala gradient maps with multiple neurotransmitter maps. The similarity in spatial layouts offers a proxy for estimating the extent of a neurotransmitter's influence and aids in interpreting the biological meanings of these data-driven gradient modes (Nordin et al., 2025; Oldehinkel et al., 2022).

Neurotransmitter modulations in the hippocampus-amygdala complex are closely associated with mental health and the development of various psychiatric disorders. For example, altered function of serotonin receptors and transporters in the hippocampus and amygdala is commonly observed in mood disorders (Albert et al., 2014; Savitz & Drevets, 2013). Such alterations influence individuals' coping mechanisms following stress (Puglisi-Allegra & Andolina, 2015) and interact with childhood trauma to further shape depressive symptomatology (Bartlett et al., 2023). Therefore, it is worthwhile to investigate how individual differences in neurotransmitter modulations of hippocampus-amygdala complex functional connectivity, depicted by gradient maps, relate to mental health outcomes. To achieve this goal, we characterized the gradient-neurotransmitter similarity in spatial topologies for each participant, and tested if this similarity could predict mental health-related factors (e.g., depressive and anxiety symptoms, as well as childhood trauma).

By applying "connectopic mapping" to the hippocampus-amygdala complex, we aim to 1). create an overview of its functional connectivity organization by identifying several topographical gradient modes; 2). assess whether these gradient modes align with specific neurotransmitter functions; and 3). explore if individual differences in the correspondence between neurotransmitter distribution and gradient modes are related to mental health factors. For reproducibility validation, two independent databases were included: the Healthy Brain Study

(HBS) comprising healthy adults (Healthy Brain Study consortium et al., 2021), and 'Measuring Integrated Novel Dimensions in Neurodevelopmental and Stress-related Mental Disorders' (MIND-Set) study including a highly comorbid psychiatric cohort (van Eijndhoven et al., 2022). HBS dataset enables us to characterize hippocampus-amygdala gradient modes in healthy population, and MIND-Set provides the opportunity to explore its translational value for clinical samples.

Methods and Materials

Participants

In this study, two databases were utilized and analyzed independently. One dataset was from the Healthy Brain Study, jointly conducted by Radboud University, Radboud University Medical Center, and the Max Planck Institute for Psycholinguistics in Nijmegen, the Netherlands. The analysis included all participants from the first data release (N = 410; 169 males; mean age = 33.8 ± 2.8 years; see Table S4.1 for characteristic information of the two samples). Participants had no history of psychiatric illness or current diseases affecting the brain, and none were taking brain-targeted medication at the time of participation. The study protocol and more details can be found in Healthy Brain Study Consortium et al (Healthy Brain Study consortium et al., 2021).

Another dataset was from the MIND-Set cohort, collected by the Department of Psychiatry at Radboud University Medical Center and the Donders Institute in Nijmegen, the Netherlands. All participants with available resting-state neuroimaging data were included (N = 367; 202 males; age 37.6 ± 14.0 years). In this sample, 286 participants were psychiatric patients (164 males; age 37.6 ± 13.4 years; see Supplementary for *n* per diagnosis), and 81 individuals did not have a current or past psychiatric disorder (37 males; age 37.67 ± 15.80 years). 242 participants were taking one or more medications during their participation. More details on the sample were introduced in van Eijndhoven et al (2022).

fMRI data acquisition and preprocessing

The HBS study includes three resting-state scans, conducted within one year, each separated by a four-month interval. T2*-weighted resting-state BOLD data were acquired using a multiband-accelerated gradient echo EPI sequence (66 slices; TR = 1000 ms; TE = 34 ms; flip angle = 60°; voxel size = 2.0 × 2.0 × 2.0 mm; FOV = 210 mm), with the duration of 10 minutes. Preprocessing steps comprised motion correction, distortion correction with field maps, and non-linear registration to MNI152 space.

FSL FIX's ICA and Gradient Distortion Correction were used for further denoising and distortion correction (Healthy Brain Study consortium et al., 2021) (https://osf.io/jzwrg/).

In the MIND-Set study, three resting-state scans were conducted as well. Resting-state scans 1 and 2 each lasted 8.5 minutes and were separated by a neutral movie clip. Following resting-state scan 2, an aversive movie clip was shown to induce acute stress. Resting-state scan 3, lasting 12.6 minutes, was then acquired. All resting-state scans used a multi-band 6 protocol with an interleaved slice acquisition sequence to capture T2*-weighted EPI BOLD-fMRI images (66 slices; TR = 1000 ms; TE = 34 ms; flip angle = 60°; voxel size = 2.0 × 2.0 × 2.0 mm; FOV = 210 mm). Preprocessing was performed using FSL version 5.0.11 (FMRIB, Oxford, UK), including brain extraction, motion correction, bias field correction, high-pass temporal filtering (100s cut-off), spatial smoothing with a 4 mm FWHM Gaussian kernel, boundary-based registration to T1-weighted images, and nonlinear registration to standard space (MNI152). Motion-related artifacts were removed using ICA-based Automatic Removal of Motion Artifacts (ICA-AROMA). Further details on fMRI acquisition and preprocessing can be found in previous studies (van Eijndhoven et al., 2022; van Oort et al., 2020).

Characterizing hippocampus-amygdala connectivity gradients

For both datasets, we applied ConGrads (Haak et al., 2018) to the preprocessed resting-state data (three scans per dataset; see Supplementary Methods), using the left and right hippocampus-amygdala complexes as ROIs. The masks were derived from the Harvard-Oxford atlas with a threshold of 20% probability. To better visualize gradient changes along the hippocampal long axis, the functional image data and masks were rotated around the X-axis in MNI152 space by an angle of 37°. ConGrads identified gradient modes of functional connectivity changes based on a similarity matrix computed within the hippocampus-amygdala complex, estimated from the functional connectivity between voxels in the complex and the rest of the brain.

For each resting-state scan of the two datasets, we derived group-average gradient maps by combining functional image data from all available participants as inputs, separately for the left and right hippocampus-amygdala complexes. To enable statistical comparisons across participants, the order of individual gradient maps was adjusted by swapping gradients based on their spatial correlation with group-average maps (i.e., swapping within the participant when the other gradient map showed a higher correlation coefficient with the group average than the original one). After swapping, as a quality control measure, individual maps were excluded if their spatial correlation with the group-average map was below 0.50 (Oldehinkel et al., 2022). We monitored the proportion of participants retained at this threshold

and determined the number of gradient modes based on the point at which a sharp decline in this proportion was observed.

To characterize the spatial organization of these gradient modes, a trend surface model (TSM) was applied to both group-average and individual gradient maps (Haak et al., 2018). Following previous work on hippocampal gradients (Przeździk et al., 2019), a trend surface regression model with nine coefficients (three parameters along X, Y, and Z axes) was chosen.

Mapping gradients with neurotransmitters

To better understand the data-driven gradient maps, we examined their relationships with multiple neurotransmitter systems. We utilized PET or SPECT scans for various neurotransmitters from the publicly available JuSpace toolbox (https://github.com/juryxy/JuSpace). Following prior research exploring striatal connectivity gradients and neurotransmitters (Oldehinkel et al., 2022), a total of 18 neurotransmitter templates were included (see Table S4.2 for a full list).

The same trend surface regression model, with nine coefficients, was applied to these PET/SPECT scans, with the left and right hippocampus-amygdala complexes defined as ROIs. Correlation coefficients were then calculated between the TSM coefficients obtained from these neurotransmitter maps and the TSM coefficients characterizing the group average hippocampus-amygdala gradient maps. To standardize comparisons, the absolute correlation coefficients were transformed using Fisher's r-to-z transformation. To examine the statistical significance of these gradient-neurotransmitter correlations, permutation testing was performed ($N = 10{,}000$, $p < 0.05$, Bonferroni corrected). A null distribution was generated by permuting the PET/SPECT TSM coefficients (separately for each coefficient) and calculating correlations between gradient TSM coefficients and permuted PET/SPECT TSM coefficients (Fisher r-to-z transformed, absolute values). The observed correlations were then compared to this null distribution.

Linking individual gradient-neurotransmitter similarity with behavioral outcomes

Neurotransmitter modulations in the hippocampus-amygdala complex are relevant for psychopathology. Therefore, we also examined whether individual differences in gradient-to-neurotransmitter similarity could be associated with variations in behavioral outcomes for mental health. For neurotransmitters that showed similarity in spatial layouts with the group-average connectivity gradients, we calculated the correlation coefficients between the TSM coefficients of individual gradient maps

per participant and TSM coefficients of PET/SPECT data in the JuSpace toolbox. Subsequently, Spearman correlation analysis was conducted between the Fisher r-to-z transformed absolute correlation coefficients and behavioral outcomes ($p < 0.05$, FDR corrected).

For the behavioral outcomes, we included depression and anxiety symptom levels as psychiatric measures, and childhood trauma as a pathogenic environmental factor. In both datasets, depressive severity were measured using the Inventory of Depressive Symptomatology-Self Report (IDS-SR; Rush et al., 2000), and anxiety sensitivity was assessed with the Anxiety Sensitivity Index (ASI; Rodriguez et al., 2004). In the HBS dataset, childhood trauma was measured using the Childhood Trauma Questionnaire-Short Form (CTQ-SF; Hagborg et al., 2022). Both the total score and subscale scores (emotional neglect, physical neglect, emotional abuse, physical abuse) were included. In MIND-Set, childhood trauma frequency and diversity was measured using the questionnaire from the Netherlands Mental Health Survey and Incidence Study (NEMESIS; Graaf et al., 2010). Both the overall index and subscales (representing the frequency of occurrence of emotional neglect, psychological abuse, and physical abuse before the age of 16 years) were included in the analysis. Additionally, for this psychiatric cohort, we accounted for comorbidity levels by summing the number of diagnosed psychiatric disorder clusters (i.e. Mood Disorder, Anxiety Disorder including PTSD and Obsessive Compulsive Disorder, Attention-Deficit/Hyperactivity Disorder, Autism Spectrum Disorder, and Addiction) for each participant.

Results

The hippocampus-amygdala functional connectivity gradient maps

Across both datasets, we identified six functional connectivity gradient modes in total (as a sharp decline in the proportion of participants retained after quality assurance was observed at the sixth mode; Table S4.3). Figure 4.1 illustrates the hippocampus-amygdala gradient maps for both datasets. Because gradient maps across different resting states were highly similar, we visualized the maps derived from resting-state 1 as a representative example. The dominant (zeroth-order) gradient shows a gradual change along the coordinate space, starting in the amygdala and extending along the hippocampal long axis. The first-order gradient is organized from the middle of the hippocampus towards the anterior and posterior ends of the complex. We observed that the second- and third-order gradients appear in reversed order between the HBS and MIND-set samples,

although their overall spatial patterns remain consistent. In the following results, for the convenience of comparison, we used the order in HBS to name gradient maps.

For quality assurance, we excluded participants whose spatial correlation with the group-average gradient maps was lower than 0.5. Table S4.3 shows the proportion of participants retained based on this threshold. In the HBS dataset, all six connectopic gradient modes had inclusion rates of 50% or higher. In the MIND-Set dataset, while the fourth-order gradient on the right side during resting-state 2 and the fifth-order gradient bilaterally across all three resting states exhibited lower stability, the first four gradient modes consistently showed inclusion rates exceeding 50%. The results indicate the robustness of these data-driven connectopic maps, especially for the first four gradient modes.

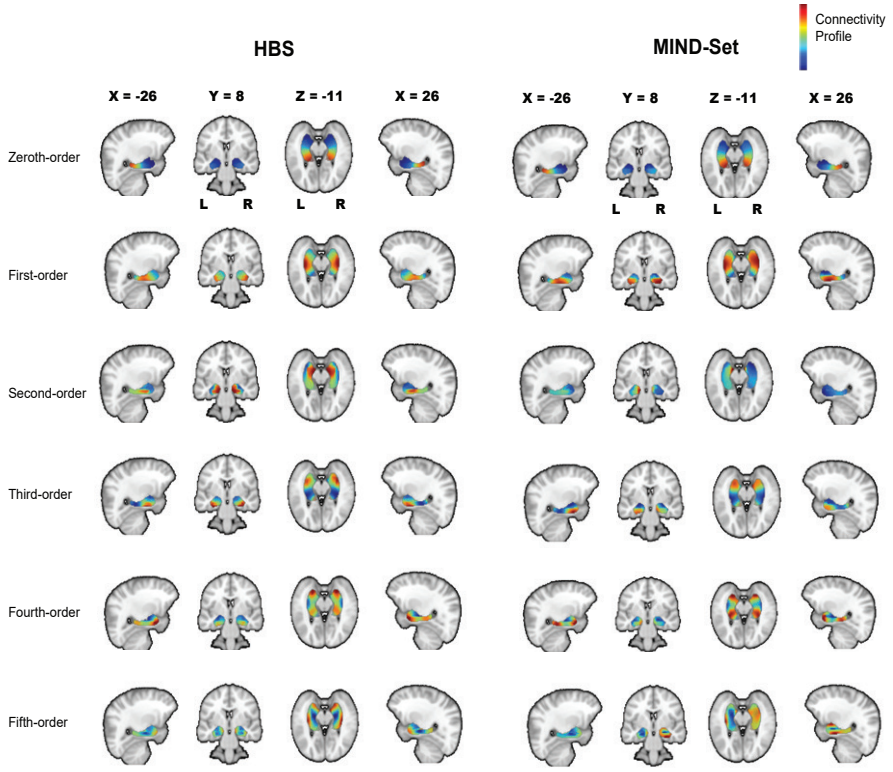

Figure 4.1 Hippocampus-amygdala gradient maps in the HBS and MIND-Set datasets (the second- and third-order gradients in MIND-Set were swapped for the convenience of comparison to HBS). L: Left; R: Right.

Similarity in spatial layouts between gradient and neurotransmitter maps

The correlation analysis with permutation testing identified several significant similarities between hippocampus-amygdala gradient and neurotransmitter maps (see Table 4.1, Figure S4.1; Table S4.4 for the full list), with findings highlighting the serotonin and dopaminergic systems. The most stable similarity is between the third-order gradients and 5-HT1A receptor maps: significant correlations were observed bilaterally across all resting states in both datasets (Figure 4.2A), except for the right side in resting-state 2 of MIND-Set. In HBS, the left-side correlation was not Bonferroni-significant but survived when we applied FDR correction. Additionally, the second-order gradients exhibited similarity with dopamine type 1 (D1) receptor maps on the left side across all resting states in both datasets. In MIND-Set only, the third-order gradients demonstrated similarity to dopamine type 2 (D2) receptor maps on the left side. In HBS only, the fourth-order gradients displayed similarity with dopamine transporter (DAT) maps on the left side (Figure 4.2B).

Table 4.1 Significant correlations between gradient and neurotransmitter layouts

		Left_ Second-order & D1	Left_Third-order &5-HT1A	Right_ Third -order &5-HT1A	Left_ Third -order & D2	Left_ Fourth-order & DAT
HBS	**Resting-State1**	z = 1.948; p < 0.01	z = 1.444; p < 0.05 (FDR)	z = 1.514; p < 0.05	no sig.	z = 1.459; p < 0.05
	Resting-State2	z = 1.799; p < 0.05	z = 1.545; p < 0.05 (FDR)	z = 1.558; p < 0.05	no sig.	z = 1.459; p < 0.05
	Resting-State3	z = 1.813; p < 0.05	z = 1.543; p < 0.05 (FDR)	z = 1.615; p < 0.05	no sig.	z = 1.456; p < 0.05
MIND-Set	**Resting-State1**	z = 1.586; p < 0.05	z = 1.955; p < 0.01	z = 1.838; p < 0.01	z = 1.708; p < 0.05	no sig.
	Resting-State2	z = 1.568; p < 0.05	z = 1.955; p < 0.01	no sig.	z = 1.703; p < 0.05	no sig.
	Resting-State3	z = 1.417; p < 0.05	z = 1.948; p < 0.01	z = 1.507; p < 0.05	z = 1.732; p < 0.05	no sig.

The trend-surface regression model with nine coefficients was applied to group-level gradient maps and the neurotransmitter PET/SPECT scans. Fisher's r-to-z–transformed correlation coefficients were computed between the TSM coefficients representing gradient maps and those representing neurotransmitter maps. The significance was assessed using permutation testing. D1: dopamine type 1; D2: dopamine type 2; DAT: dopamine transporter; 5-HT1A: 5-HT1A receptor.

To determine whether the observed similarities in the MIND-Set sample were specific to psychiatric patients, we further separated the sample into patient and healthy control subgroups. Results showed that both subgroups exhibited the same patterns with those observed in the full sample (Table S4.5).

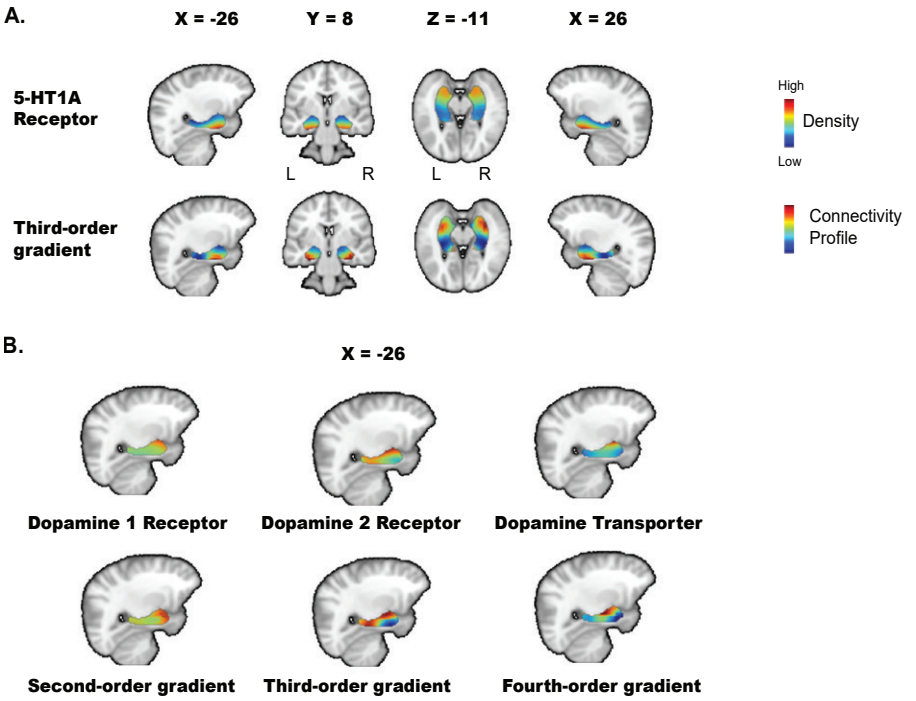

Figure 4.2 Similar spatial layouts between gradients and 5-HT1A receptor maps (A), several neurotransmitters of the dopamine system (B) within the hippocampus-amygdala complex. L: Left; R: Right.

Individual gradient-neurotransmitter similarity predicts mental health outcomes

For neurotransmitter maps that showed significant spatial similarity with group-average gradients (bilateral 5-HT1A receptors; left D2 receptors in MIND-Set; left D1 receptors; and left DAT in HBS), we computed correlation coefficients between the TSM coefficients of JuSpace PET/SPECT images and individual gradient maps for each participant. Taking Fisher r-to-z transformed absolute correlation coefficients, Spearman correlation analysis revealed several significant associations with anxiety sensitivity and depressive severity. For HBS resting-state 1, the similarity between 5-HT1A receptors and the third-order gradients on the left side of the hippocampus-amygdala complex was positively correlated with depressive severity ($r_s = 0.19$, $p_{fdr} = 0.021$), and approaching significance for anxiety sensitivity ($r_s = 0.16$, $p_{fdr} = 0.072$). In the MIND-Set dataset, these correlations were observed for the right side in resting-state 1 (depressive severity: $r_s = 0.13$, $p_{fdr} = 0.057$; anxiety sensitivity: $r_s = 0.15$, $p_{fdr} = 0.038$; Figure 4.3). Given that the two datasets span distinct ranges of anxiety sensitivity and depressive severity (Table S4.1) — with HBS falling into the

relatively lower end and MIND-Set the higher — these replicated correlations may indicate both sensitivity and stability across the symptom spectrum.

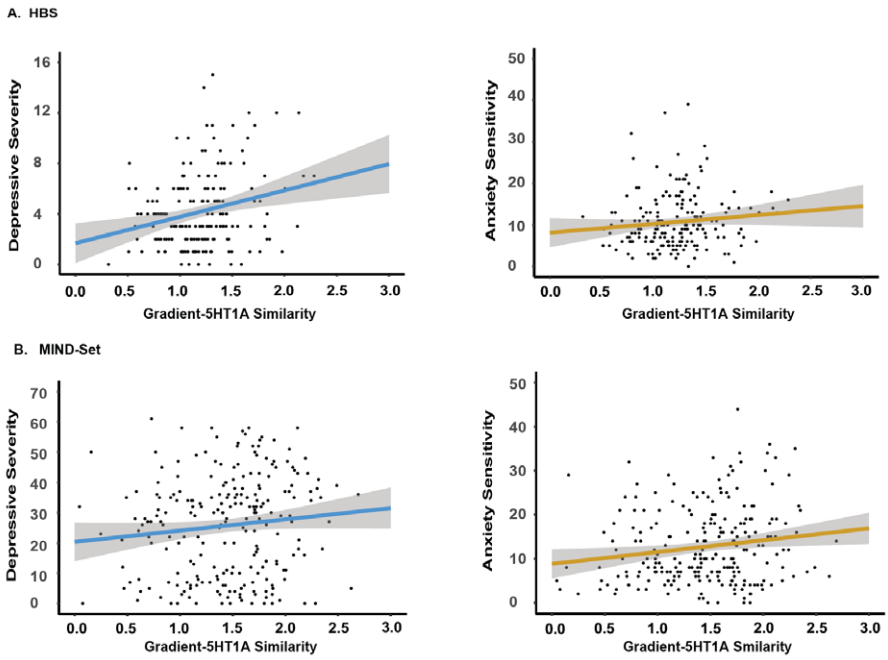

Figure 4.3 The higher level of spatial similarity between the third-order gradients and 5-HT1A receptor maps (Fisher r-to-z transformed absolute correlation coefficients; the horizontal axis) was associated with higher levels of depressive severity and anxiety sensitivity (the vertical axis). In both datasets, depressive severity was measured as the sum score of IDS-SR, and anxiety sensitivity was assessed with the ASI sum score.

As for the dopaminergic system, in MIND-Set resting-state 2, the similarity between D1 receptor and second-order gradient maps showed a positive correlation with anxiety sensitivity (r_s = 0.13, p_{fdr} = 0.046). This association was not significant in the HBS sample (r_s = 0.06, p_{fdr} = 0.50), although Fisher's z test comparing the two correlations (e.g., in MIND-Set and HBS) revealed no significant difference (z = 0.682, p =0.495). In HBS resting-state 3, the similarity between DAT and fourth-order gradient maps was negatively associated with anxiety sensitivity (r_s = -0.18, p_{fdr} = 0.048). No other significant correlations were observed (ps > 0.10). Full lists of correlations are presented in Table S4.6 and S4.7.

We also divided the MIND-Set sample into patient and healthy controls, and ran the correlation analyses separately (Table S4.8). Fisher's z tests revealed no significant differences in the observed correlations above between two subgroups (ps > 0.16).

Discussion

Widespread functional connections between the hippocampus-amygdala complex and other brain regions play important roles in human cognition and emotion, thereby contributing to the most common psychiatric disorders. In this study, with both healthy and psychiatric cohorts, we 1). identified six distinct connectopic gradient modes for the hippocampus-amygdala complex, with the first two exhibiting gradual changes along the hippocampal long axis; 2). revealed that neurotransmitters from the serotonin and dopamine systems displayed spatial similarities with connectopic gradients of the hippocampus-amygdala complex; and 3). found that individual variability in these gradient-neurotransmitter similarities was associated with depressive severity and anxiety sensitivity. Our findings highlight the potential of "connectopic mapping" to bridge functional neuroimaging, biomolecular markers and behavioral measures, offering a novel perspective for understanding brain function and dysfunctions in living human beings.

The first two connectopic gradient maps of the hippocampus–amygdala complex did show gradient changes following the hippocampal long axis in both samples. This demonstrates that "connectopic mapping" can capture the connectivity organization previously identified in animal studies, using fMRI scans of living humans. The spatial organization of our gradient maps also aligns with hippocampal gradients reported in earlier studies (Nordin et al., 2025; Przeździk et al., 2019). The amygdala exhibited connectivity modes similar to those of the anterior hippocampus, partly because of the spatial proximity, also indicating their close functional coupling. While previous research focused on lower-order connectopic gradients, our study extended it by extracting higher-order gradient modes and replicating the findings in both healthy and psychiatric samples.

Various neurotransmitters contribute to regulating the functionality of the hippocampus and amygdala. "connectopic mapping" offers an approach to better understand how neurotransmitters influence hippocampus-amygdala related functional connectivity, by breaking down overall connectivity patterns into specific topographical gradient modes. For each identified gradient, we evaluated its similarity in spatial layouts with various neurotransmitter maps, which serves as an indirect measure of how much influence a particular neurotransmitter has on the functional connectivity.

The most robust gradient-neurotransmitter similarity we found is between the third-order gradients and 5-HT1A receptor maps. 5-HT is a monoamine neurotransmitter

synthesized in both the central nervous system and gastrointestinal cells (Jonnakuty & Gragnoli, 2008). The 5-HT1A receptor is one of the most abundant receptor subtypes in the mammalian brain (Popova & Naumenko, 2013). In the hippocampus and amygdala, most 5-HT1A receptors function as postsynaptic receptors suppressing pyramidal cell firing (Ögren et al., 2008). Our third-order gradient generally captured the organizational patterns of 5-HT1A receptor distribution within the hippocampus-amygdala complex, which may suggest that functional communication between the complex and other brain regions is heavily influenced by serotonin modulation. In addition to previous reports from animal and PET studies (Gener et al., 2019; Jovanovic et al., 2011), our findings provide evidence for the feasibility of receiving serotonin receptor related readouts from resting-state fMRI scans on an individual basis.

The activity of 5-HT1A receptors is implicated in emotion processing and stress coping (Celada et al., 2013; Puglisi-Allegra & Andolina, 2015), with alterations shown in mood disorders. Studies have reported increased hippocampal 5-HT1A receptor binding potential in individuals with depressive episodes and childhood adversity (Bartlett et al., 2023), and elevated 5-HT1A receptor density in people who committed suicide (Underwood et al., 2018). Higher 5-HT1A receptor binding potential was also associated with poor responses to antidepressant treatment (Parsey et al., 2006). In this study, we found that greater similarity between the third-order gradients and 5-HT1A receptor maps was related to more severe depressive symptoms and heightened anxiety sensitivity. This supports previous findings in elevated 5-HT1A receptor involvement and internalizing psychiatric symptoms. These results may suggest that increased involvement of 5-HT1A receptor activity in hippocampus-amygdala related functional connectivity could serve as a potential risk factor underlying mood disorder symptoms. Notably, we observed this relationship in both the healthy sample (with a narrower symptom range) and the clinical sample (with a broader range), suggesting its sensitivity to transdiagnostic symptom variation. Compared to anatomical or PET studies, "connectopic mapping" could be a more efficient and cost-effective approach for depicting this alteration in 5-HT1A receptor functionality.

Beyond the serotonin system, our findings also identified similarities between hippocampus-amygdala gradients and the spatial organization of dopamine-related neurotransmitters: D1 receptors with the second-order gradient, D2 receptors with the third-order gradient, DAT with the fourth-order gradient. D1 and D2 receptors are the most abundant dopamine receptor subtypes (Ayano, 2016). D1 receptors have an excitatory role in signaling pathways, whereas D2 receptors exhibit more

complex effects, generally with inhibitory properties (Beaulieu & Gainetdinov, 2011; Grilli et al., 1988). Together with other dopamine receptors, D1 and D2 receptors coordinate hippocampal plasticity and influence learning and affective behaviors (Edelmann & Lessmann, 2018). DAT regulates dopamine reuptake and maintains homeostasis (Madras et al., 2005). These results highlight the role of dopamine system in hippocampus-amygdala related functional communication. Moreover, we observed that greater gradient-D1 map similarity was associated with higher anxiety sensitivity, while gradient-DAT map similarity showed an inverse relationship. Studies showed the anxiogenic effects of D1 receptor activation; for instance, infusing D1 agonists into the amygdala was proved to induce heightened anxiety behaviors (de la Mora et al., 2010; Guarraci et al., 1999). Reduced DAT availability has been linked to greater anxiety severity in Parkinson's disease patients (Erro et al., 2012). The correlations between D1, DAT and anxiety sensitivity did align with the previous literatures, indicating alterations in the dopamine system may contribute to anxiety symptoms partly through exerting influence on the hippocampus-amygdala related functional connectivity. However, these findings should be interpreted with caution. Although Fisher's z-tests did not reveal significant differences in correlation strengths between the two datasets, these correlations only reached significance in one dataset (D1 in MIND-Set, DAT in HBS). Future studies are needed to determine whether limited replicability reflects meaningful differences between clinical and non-clinical populations or is driven by spurious factors.

Our study has several limitations. First, the neurotransmitter maps used were templates derived from previous studies, rather than data measured directly within HBS and MIND-Set. This may explain the small effect sizes for correlations between individual gradient-neurotransmitter similarities and mental health outcomes. Datasets that include both resting-state fMRI and PET scans could provide a more sensitive approach, while also serving to validate our findings regarding the serotonin and dopamine systems. Second, the relationships between gradient and neurotransmitters remain indirect. Further research is needed to better understand hippocampus-amygdala gradients, particularly how they are influenced by neurochemical modulation, gene expression variability, or changes in mental states. Such investigations will contribute to a deeper interpretation of the gradient–neurotransmitter relationship.

In conclusion, across both healthy and psychiatric cohorts, our study provides an overview of the functional connectivity topography of the hippocampus–amygdala complex. Certain connectopic gradients reflect the influence of serotonin and

dopaminergic system on hippocampus-amygdala related functional connectivity, with individual differences in this influence associated with depression and anxiety symptoms. As an emerging analytical method, "connectopic mapping" demonstrates promise as a biomarker for assessing neurotransmitter related psychiatric symptomatology with resting-state fMRI.

Supplementary Material

Table S4.1 Sample characteristics for HBS and MIND-Set

	Sample size	Age	Gender	Anxiety Sensitivity	Depressive Severity	Comorbidity
HBS	410	33.8 ± 2.8	169 Males	10.9 ± 6.9	4.4 ± 3.3	--
MIND-Set	367	37.6 ± 14.0	202 Males	12.7 ± 9.0	25.5 ± 16.6	1.6 ± 1.2
Difference	--	t = -4.72, p < .001	Chi-suqare = 17.69, p < .001	t = -2.80, p = .005	t = -22.50, p < .001	--

In MIND-Set, 286 participants were psychiatric patients: Mood Disorder = 225, Anxiety Disorder (including Obsessive Compulsive Disorders (OCD) and PTSD) = 80, Attention-Deficit/Hyperactivity Disorder (ADHD) = 110, Autism Spectrum Disorder (ASD) = 91, Addiction = 75. In both datasets, depressive severity was measured as the sum score of IDS-SR, and anxiety sensitivity was assessed with the ASI sum score. Comorbidity in MIND-Set was indexed by the number of diagnosed psychiatric disorder clusters per participant.

Table S4.2 Neurotransmitter templates included from JuSpace

	Template	Reference
5HT 1A receptor	WAY_HC36	(Savli et al., 2012) https://identifiers.org/neurovault.collection:1206
5HT 1B receptor	P943_HC22	(Savli et al., 2012) https://identifiers.org/neurovault.collection:1206
5HT 2A receptor	ALT_HC19	(Savli et al., 2012) https://identifiers.org/neurovault.collection:1206
5HT 4 receptor	sb20_hc59_beliveau	(Beliveau et al., 2017)
5HT transporter	DASB_HC30	(Savli et al., 2012) https://identifiers.org/neurovault.collection:1206
5-HT transporter	MADAM_c11	(Fazio et al., 2016)
Dopamine type 1 receptor	SCH23390_c11	(Kaller et al., 2017)
Dopamine type 2 receptor	RACLOPRIDE_c11	(Alakurtti et al., 2015)
Dopamine transporter	DATSPECT	(Dukart et al., 2018)
F-Dopa	FDOPA_f18	(Gómez et al., 2018)
$GABA_A$ receptor	FLUMAZENIL_c11	(Dukart et al., 2018)
Kappa-opioid receptor	KappaOp_LY2795050_10m_ShokriKojori	(Shokri-Kojori et al., 2022)
Mu-opioid receptor	CARFENTANIL_c11	(Kantonen et al., 2020) https://identifiers.org/neurovault.image:303255
Metabotropic glutamate receptor 5	abp_hc28_dubois	(DuBois et al., 2016)
Cannabinoid receptor 1	FMPEPd2_hc22_laurikainen	(Laurikainen et al., 2019)
Noradrenaline transporter	MRB_c11	(Hesse et al., 2017)
NMDA receptor	ge179_29hc_galovic2021	(Galovic et al., 2021)
Vesicular acetylcholine transporter	feobv_hc4_tuominen	(Hansen et al., 2022)

Table S4.3 The proportions of participants whose spatial correlation with group-average gradients higher than 0.5.

		Resting-State1_ Left	Resting-State1_ Right	Resting-State2_ Left	Resting-State2_ Right	Resting-State3_ Left	Resting-State3_ Right
HBS	**Zeroth-order**	99.727%	99.724%	100.000%	99.656%	100.000%	98.958%
	First-order	99.454%	99.724%	99.308%	98.969%	98.592%	97.917%
	Second-order	96.721%	94.751%	96.540%	92.440%	94.014%	90.972%
	Third-order	93.716%	95.580%	95.502%	93.814%	93.662%	93.403%
	Fourth-order	86.339%	80.939%	86.159%	79.381%	80.986%	77.083%
	Fifth-order	58.470%	55.801%	53.633%	53.608%	53.873%	50.000%
MIND-Set	**Zeroth-order**	98.638%	98.093%	99.454%	98.093%	99.725%	98.630%
	First-order	96.458%	95.913%	95.902%	93.733%	97.802%	95.068%
	Second-order	91.826%	87.738%	89.344%	75.749%	91.758%	82.192%
	Third-order	87.738%	83.651%	86.066%	78.202%	92.308%	82.740%
	Fourth-order	70.845%	75.477%	69.945%	8.719%	75.549%	73.699%
	Fifth-order	22.343%	5.177%	9.016%	6.267%	5.220%	4.658%

Table S4.4 Correlations coefficients (Fisher r-to-z transformed, absolute values) between gradient and neurotransmitter layouts

		HBSResting-State1	HBSResting-State2	HBSResting-State3	MIND-SetResting-State1	MIND-SetResting-State2	MIND-SetResting-State3
Zeroth-order gradient_Left	5HT1A	1.049	1.033	1.041	0.903	0.896	0.901
	5HT1B	0.311	0.318	0.317	0.369	0.374	0.372
	5HT2A	0.057	0.055	0.061	0.018	0.022	0.026
	5HT4	0.877	0.869	0.880	0.799	0.802	0.806
	CB1	0.727	0.727	0.732	0.696	0.699	0.703
	D1	0.211	0.215	0.218	0.243	0.251	0.252
	D2	0.813	0.798	0.804	0.699	0.692	0.694
	DAT	0.100	0.112	0.104	0.179	0.180	0.180
	FDOPA	0.459	0.466	0.468	0.504	0.512	0.514
	GABAa	0.568	0.558	0.567	0.475	0.475	0.478
	KappaOp	0.728	0.733	0.733	0.809	0.817	0.810
	mGluR5	0.622	0.611	0.622	0.532	0.532	0.535
	MU	0.383	0.387	0.387	0.454	0.461	0.455
	NA	0.009	0.013	0.008	0.043	0.040	0.039
	NMDA	0.152	0.157	0.149	0.178	0.173	0.172
	SERT_DAS	0.688	0.695	0.687	0.745	0.742	0.737
	SERT_MADAM	0.506	0.514	0.510	0.588	0.591	0.586
	VACh	0.350	0.339	0.344	0.260	0.255	0.258

Table S4.4 Continued

		HBSResting-State1	HBSResting-State2	HBSResting-State3	MIND-SetResting-State1	MIND-SetResting-State2	MIND-SetResting-State3
Zeroth-order gradient_Right	5HT1A	1.053	1.044	1.040	0.792	0.716	0.760
	5HT1B	0.118	0.120	0.119	0.227	0.255	0.244
	5HT2A	0.050	0.052	0.053	0.098	0.121	0.110
	5HT4	0.619	0.612	0.613	0.476	0.420	0.449
	CB1	0.478	0.475	0.473	0.415	0.382	0.403
	D1	0.037	0.036	0.039	0.088	0.094	0.087
	D2	0.498	0.498	0.494	0.358	0.322	0.342
	DAT	0.000	0.000	0.005	0.134	0.171	0.147
	FDOPA	0.652	0.655	0.653	0.730	0.739	0.736
	GABAa	0.349	0.347	0.341	0.190	0.139	0.172
	KappaOp	1.015	1.025	1.019	1.179	1.224	1.215
	mGluR5	0.511	0.509	0.502	0.343	0.290	0.324
	MU	0.470	0.479	0.473	0.597	0.643	0.628
	NA	0.259	0.252	0.263	0.275	0.273	0.265
	NMDA	0.501	0.505	0.505	0.601	0.641	0.619
	SERT_DAS	0.721	0.730	0.724	0.866	0.917	0.905
	SERT_MADAM	0.908	0.919	0.909	1.050	1.097	1.095
	VACh	0.522	0.519	0.516	0.354	0.307	0.333

Table S4.4 Continued

		HBSResting-State1	HBSResting-State2	HBSResting-State3	MIND-SetResting-State1	MIND-SetResting-State2	MIND-SetResting-State3
First-order gradient_Left	5HT1A	0.617	0.570	0.574	0.038	0.043	0.066
	5HT1B	0.416	0.436	0.427	0.709	0.713	0.737
	5HT2A	0.172	0.218	0.202	0.389	0.381	0.367
	5HT4	0.541	0.483	0.497	0.066	0.070	0.064
	CB1	0.386	0.356	0.357	0.095	0.096	0.098
	D1	0.107	0.084	0.094	0.226	0.240	0.261
	D2	0.613	0.565	0.575	0.040	0.045	0.074
	DAT	0.074	0.029	0.057	0.309	0.306	0.319
	FDOPA	0.199	0.185	0.186	0.281	0.290	0.311
	GABAa	0.426	0.368	0.388	0.123	0.122	0.133
	KappaOp	0.992	1.008	1.002	1.210	1.213	1.234
	mGluR5	0.485	0.423	0.445	0.055	0.054	0.063
	MU	0.740	0.759	0.761	1.291	1.306	1.355
	NA	0.099	0.074	0.093	0.027	0.026	0.014
	NMDA	0.016	0.055	0.028	0.074	0.062	0.050
	SERT_DAS	0.801	0.863	0.825	0.816	0.797	0.783
	SERT_MADAM	0.804	0.860	0.835	1.338	1.326	1.352
	VACh	0.209	0.168	0.181	0.370	0.376	0.404

Table S4.4 Continued

		HBSResting-State1	HBSResting-State2	HBSResting-State3	MIND-SetResting-State1	MIND-SetResting-State2	MIND-SetResting-State3
First-order gradient_Right	5HT1A	0.446	0.381	0.408	0.738	0.875	0.849
	5HT1B	0.338	0.338	0.355	0.716	0.689	0.707
	5HT2A	0.145	0.172	0.154	0.255	0.249	0.245
	5HT4	0.192	0.122	0.160	0.669	0.754	0.730
	CB1	0.199	0.163	0.186	0.282	0.322	0.308
	D1	0.047	0.001	0.044	0.240	0.231	0.236
	D2	0.278	0.257	0.254	0.644	0.715	0.721
	DAT	0.094	0.104	0.079	0.587	0.601	0.601
	FDOPA	0.504	0.457	0.501	0.254	0.193	0.211
	GABAa	0.182	0.167	0.161	0.790	0.850	0.832
	KappaOp	1.371	1.235	1.353	0.447	0.338	0.360
	mGluR5	0.311	0.284	0.285	0.728	0.811	0.787
	MU	1.178	1.191	1.213	0.864	0.743	0.772
	NA	0.059	0.131	0.080	0.115	0.140	0.143
	NMDA	0.441	0.441	0.449	0.352	0.303	0.298
	SERT_DAS	0.940	0.967	0.966	0.565	0.478	0.497
	SERT_MADAM	1.356	1.343	1.378	0.503	0.401	0.425
	VACh	0.256	0.221	0.226	0.829	0.930	0.923

Table S4.4 Continued

		HBSResting-State1	HBSResting-State2	HBSResting-State3	MIND-SetResting-State1	MIND-SetResting-State2	MIND-SetResting-State3
Second-order gradient_Left	5HT1A	0.187	0.330	0.319	0.223	0.265	0.205
	5HT1B	0.446	0.506	0.479	0.389	0.405	0.318
	5HT2A	0.612	0.511	0.545	0.821	0.791	0.876
	5HT4	0.465	0.320	0.335	0.447	0.406	0.451
	CB1	0.403	0.326	0.327	0.380	0.356	0.359
	D1	1.948 **	1.799 *	1.813 *	1.586 *	1.568 *	1.417 *
	D2	0.282	0.441	0.426	0.320	0.367	0.290
	DAT	0.054	0.184	0.142	0.153	0.128	0.227
	FDOPA	1.061	1.053	1.033	0.875	0.872	0.794
	GABAa	0.147	0.002	0.026	0.256	0.219	0.294
	KappaOp	0.404	0.401	0.384	0.293	0.302	0.230
	mGluR5	0.231	0.078	0.105	0.328	0.290	0.362
	MU	0.518	0.546	0.530	0.440	0.462	0.373
	NA	0.174	0.112	0.141	0.455	0.457	0.491
	NMDA	0.806	0.692	0.738	1.211	1.177	1.296
	SERT_DAS	0.378	0.342	0.374	0.537	0.523	0.613
	SERT_MADAM	0.138	0.190	0.162	0.027	0.047	0.045
	VACh	0.368	0.538	0.503	0.303	0.344	0.240

Table S4.4 Continued

		HBSResting-State1	HBSResting-State2	HBSResting-State3	MIND-SetResting-State1	MIND-SetResting-State2	MIND-SetResting-State3
Second-order gradient_Right	5HT1A	0.468	0.462	0.383	1.146	0.917	1.469
	5HT1B	0.388	0.407	0.398	0.145	0.846	0.008
	5HT2A	0.508	0.452	0.504	0.531	0.193	0.357
	5HT4	0.024	0.009	0.079	1.354	0.366	1.205
	CB1	0.011	0.004	0.044	0.815	0.022	0.685
	D1	1.165	1.125	1.196	0.428	0.531	0.218
	D2	0.542	0.543	0.491	0.437	1.579	0.643
	DAT	0.262	0.298	0.253	0.445	0.594	0.510
	FDOPA	0.320	0.333	0.370	0.655	0.278	0.521
	GABAa	0.310	0.348	0.279	0.973	0.485	0.986
	KappaOp	0.161	0.197	0.236	0.812	0.018	0.777
	mGluR5	0.317	0.345	0.270	1.195	0.532	1.245
	MU	0.260	0.291	0.307	0.430	0.314	0.376
	NA	0.031	0.075	0.069	0.097	0.379	0.020
	NMDA	0.356	0.299	0.321	0.217	0.315	0.065
	SERT_DAS	0.315	0.265	0.266	0.180	0.086	0.236
	SERT_MADAM	0.155	0.115	0.094	0.532	0.076	0.551
	VACh	0.489	0.495	0.430	0.629	1.435	0.843

Table S4.4 Continued

		HBSResting-State1	HBSResting-State2	HBSResting-State3	MIND-SetResting-State1	MIND-SetResting-State2	MIND-SetResting-State3
Third-order gradient_Left	5HT1A	1.444* (FDR)	1.545* (FDR)	1.543* (FDR)	1.955 **	1.955 **	1.948 **
	5HT1B	0.064	0.045	0.058	0.039	0.037	0.044
	5HT2A	0.138	0.223	0.217	0.224	0.228	0.217
	5HT4	1.015	1.168	1.161	1.121	1.127	1.107
	CB1	0.691	0.727	0.737	0.646	0.649	0.634
	D1	0.114	0.161	0.159	0.035	0.037	0.028
	D2	1.206	1.290	1.270	1.708 *	1.703 *	1.732 *
	DAT	0.123	0.231	0.213	0.434	0.436	0.439
	FDOPA	0.251	0.268	0.273	0.121	0.123	0.113
	GABAa	0.763	0.914	0.901	1.135	1.143	1.129
	KappaOp	0.376	0.369	0.380	0.301	0.301	0.299
	mGluR5	0.793	0.957	0.942	1.162	1.170	1.156
	MU	0.086	0.092	0.099	0.040	0.040	0.039
	NA	0.093	0.001	0.005	0.137	0.141	0.136
	NMDA	0.078	0.030	0.016	0.082	0.086	0.079
	SERT_DAS	0.386	0.301	0.321	0.275	0.272	0.276
	SERT_MADAM	0.187	0.139	0.156	0.071	0.070	0.069
	VACh	0.621	0.692	0.676	0.917	0.916	0.925

Table S4.4 Continued

		HBSResting-State1	HBSResting-State2	HBSResting-State3	MIND-SetResting-State1	MIND-SetResting-State2	MIND-SetResting-State3
Third-order gradient_Right	5HT1A	1.514 *	1.558 *	1.615 *	1.838 **	1.703	1.507*
	5HT1B	0.043	0.060	0.072	0.247	0.080	0.403
	5HT2A	0.154	0.153	0.123	0.034	0.258	0.112
	5HT4	1.044	1.040	1.012	0.823	1.071	0.607
	CB1	0.571	0.559	0.548	0.416	0.623	0.253
	D1	0.114	0.100	0.061	0.165	0.057	0.367
	D2	0.625	0.657	0.675	1.020	0.784	1.250
	DAT	0.257	0.288	0.289	0.542	0.582	0.574
	FDOPA	0.445	0.435	0.413	0.228	0.409	0.055
	GABAa	0.628	0.652	0.652	0.828	1.063	0.716
	KappaOp	0.670	0.676	0.658	0.539	0.674	0.380
	mGluR5	0.808	0.838	0.839	1.026	1.341	0.861
	MU	0.206	0.216	0.202	0.174	0.305	0.063
	NA	0.334	0.313	0.319	0.156	0.039	0.204
	NMDA	0.147	0.146	0.164	0.188	0.005	0.293
	SERT_DAS	0.273	0.274	0.289	0.279	0.262	0.251
	SERT_MADAM	0.480	0.485	0.490	0.460	0.539	0.358
	VACh	0.797	0.834	0.852	1.213	0.987	1.370

Table S4.4 Continued

		HBSResting-State1	HBSResting-State2	HBSResting-State3	MIND-SetResting-State1	MIND-SetResting-State2	MIND-SetResting-State3
Fourth-order gradient_Left	5HT1A	0.613	0.361	0.314	0.071	0.065	0.091
	5HT1B	0.278	0.271	0.310	0.436	0.428	0.466
	5HT2A	0.609	0.633	0.581	0.300	0.309	0.214
	5HT4	0.598	0.439	0.359	0.113	0.101	0.183
	CB1	0.290	0.179	0.117	0.243	0.233	0.309
	D1	0.018	0.037	0.021	0.270	0.259	0.354
	D2	0.640	0.400	0.363	0.018	0.023	0.012
	DAT	1.459*	1.459 *	1.456 *	0.953	0.962	0.901
	FDOPA	0.118	0.117	0.175	0.452	0.442	0.533
	GABAa	1.191	0.908	0.818	0.286	0.297	0.229
	KappaOp	0.114	0.165	0.209	0.493	0.491	0.508
	mGluR5	1.128	0.875	0.781	0.240	0.251	0.181
	MU	0.169	0.149	0.180	0.352	0.351	0.363
	NA	0.851	0.945	0.929	0.686	0.691	0.633
	NMDA	0.605	0.752	0.698	0.444	0.458	0.361
	SERT_DAS	0.317	0.463	0.472	0.558	0.564	0.499
	SERT_MADAM	0.378	0.430	0.459	0.591	0.591	0.573
	VACh	0.881	0.661	0.651	0.369	0.370	0.366

Table S4.4 Continued

		HBSResting-State1	HBSResting-State2	HBSResting-State3	MIND-SetResting-State1	MIND-SetResting-State2	MIND-SetResting-State3
Fourth-order gradient_Right	5HT1A	0.420	0.281	0.391	0.196	0.274	0.333
	5HT1B	0.322	0.328	0.297	0.384	0.227	0.335
	5HT2A	0.819	0.841	0.886	0.532	0.448	0.485
	5HT4	0.623	0.508	0.630	0.015	0.053	0.096
	CB1	0.384	0.316	0.403	0.072	0.053	0.148
	D1	0.198	0.212	0.242	0.085	0.010	0.098
	D2	0.483	0.389	0.439	0.137	0.075	0.039
	DAT	1.176	1.086	1.111	0.740	0.354	0.622
	FDOPA	0.005	0.051	0.023	0.352	0.332	0.368
	GABAa	1.271	1.055	1.236	0.421	0.303	0.288
	KappaOp	0.095	0.191	0.103	0.549	0.797	0.570
	mGluR5	1.047	0.853	1.012	0.271	0.137	0.146
	MU	0.120	0.172	0.127	0.315	0.563	0.280
	NA	0.719	0.772	0.737	0.745	0.724	0.757
	NMDA	0.781	0.862	0.824	0.802	0.687	0.765
	SERT_DAS	0.532	0.635	0.558	0.874	0.702	0.851
	SERT_MADAM	0.238	0.340	0.256	0.674	0.700	0.689
	VACh	0.585	0.470	0.539	0.139	0.090	0.028

Table S4.4 Continued

		HBSResting-State1	HBSResting-State2	HBSResting-State3	MIND-SetResting-State1	MIND-SetResting-State2	MIND-SetResting-State3
Fifth-order gradient_Left	5HT1A	0.159	0.179	0.151	0.228	0.123	0.606
	5HT1B	0.846	0.771	0.826	0.820	0.507	0.187
	5HT2A	0.422	0.513	0.586	0.116	0.266	0.340
	5HT4	0.370	0.404	0.440	0.254	0.069	0.465
	CB1	0.842	0.840	0.864	0.573	0.053	0.790
	D1	0.298	0.294	0.379	0.025	0.020	0.030
	D2	0.166	0.136	0.159	0.017	0.072	0.262
	DAT	0.415	0.263	0.192	0.250	0.044	0.324
	FDOPA	0.512	0.475	0.525	0.243	0.004	0.237
	GABAa	0.208	0.299	0.349	0.222	0.027	0.343
	KappaOp	0.180	0.139	0.182	0.399	0.386	0.003
	mGluR5	0.166	0.252	0.310	0.186	0.003	0.272
	MU	0.040	0.015	0.082	0.264	0.499	0.295
	NA	0.239	0.375	0.500	0.367	0.321	0.077
	NMDA	0.069	0.174	0.312	0.055	0.260	0.380
	SERT_DAS	0.293	0.209	0.156	0.665	0.308	0.358
	SERT_MADAM	0.407	0.327	0.334	0.696	0.489	0.126
	VACh	0.399	0.320	0.332	0.259	0.258	0.120

Table S4.4 Continued

		HBSResting-State1	HBSResting-State2	HBSResting-State3	MIND-SetResting-State1	MIND-SetResting-State2	MIND-SetResting-State3
Fifth-order gradient_Right	5HT1A	0.107	0.053	0.044	0.577	0.592	0.542
	5HT1B	1.134	0.984	1.079	0.066	0.223	0.032
	5HT2A	0.351	0.442	0.299	0.225	0.291	0.171
	5HT4	0.223	0.403	0.249	0.602	0.333	0.522
	CB1	0.798	0.993	0.832	0.692	0.438	0.691
	D1	0.626	0.681	0.537	0.049	0.170	0.126
	D2	0.868	0.674	0.805	0.156	0.071	0.122
	DAT	0.800	0.674	0.806	0.064	0.477	0.086
	FDOPA	0.679	0.747	0.661	0.075	0.325	0.066
	GABAa	0.047	0.075	0.025	0.453	0.011	0.441
	KappaOp	0.091	0.136	0.088	0.281	0.310	0.283
	mGluR5	0.072	0.060	0.043	0.407	0.103	0.393
	MU	0.004	0.037	0.035	0.755	0.059	0.712
	NA	0.164	0.106	0.120	0.161	0.589	0.086
	NMDA	0.242	0.263	0.206	0.090	0.556	0.052
	SERT_DAS	0.233	0.195	0.271	0.115	0.634	0.029
	SERT_MADAM	0.227	0.226	0.251	0.171	0.485	0.110
	VACh	0.787	0.576	0.718	0.215	0.102	0.172

The trend-surface regression model with nine coefficients was applied to group-level gradient maps and the neurotransmitter PET/SPECT scans. Fisher's r-to-z–transformed correlation coefficients were computed between the TSM coefficients representing gradient maps and those representing neurotransmitter maps. The significance was assessed using permutation testing. *$p<0.05$, **$p<0.01$.

Table S4.5 Correlations coefficients between gradient and neurotransmitter layouts separately for patients and healthy controls in MIND-Set (data is from resting-state 1)

		Patient_Left	Patient_Right	Healthy Control_Left	Healthy Control_Right
Zeroth-order gradient	5HT1A	0.893	0.802	0.974	0.774
	5HT1B	0.373	0.224	0.340	0.236
	5HT2A	0.017	0.094	0.037	0.096
	5HT4	0.794	0.482	0.843	0.468
	CB1	0.695	0.418	0.711	0.411
	D1	0.247	0.088	0.231	0.098
	D2	0.689	0.364	0.759	0.347
	DAT	0.186	0.126	0.134	0.142
	FDOPA	0.509	0.729	0.481	0.740
	GABAa	0.469	0.198	0.524	0.181
	KappaOp	0.814	1.181	0.772	1.198
	mGluR5	0.526	0.352	0.581	0.333
	MU	0.458	0.598	0.423	0.611
	NA	0.045	0.271	0.027	0.272
	NMDA	0.179	0.596	0.158	0.604
	SERT_DAS	0.747	0.862	0.713	0.872
	SERT_MADAM	0.593	1.051	0.548	1.060
	VACh	0.253	0.361	0.306	0.342
First-order gradient	5HT1A	0.074	0.713	0.249	0.694
	5HT1B	0.729	0.691	0.601	0.747
	5HT2A	0.384	0.265	0.288	0.235
	5HT4	0.049	0.664	0.296	0.626
	CB1	0.086	0.294	0.240	0.246
	D1	0.248	0.229	0.199	0.253
	D2	0.079	0.606	0.248	0.637
	DAT	0.332	0.561	0.121	0.570
	FDOPA	0.299	0.251	0.268	0.285
	GABAa	0.149	0.778	0.137	0.735
	KappaOp	1.210	0.469	1.242	0.484
	mGluR5	0.080	0.711	0.202	0.673
	MU	1.327	0.896	1.099	0.914
	NA	0.031	0.108	0.043	0.140
	NMDA	0.067	0.369	0.025	0.341
	SERT_DAS	0.791	0.575	0.843	0.594
	SERT_MADAM	1.351	0.518	1.130	0.545
	VACh	0.410	0.782	0.099	0.809

Table S4.5 Continued

		Patient_Left	Patient_Right	Healthy Control_Left	Healthy Control_Right
Second-order gradient	5HT1A	0.195	0.712	0.283	1.654
	5HT1B	0.362	0.349	0.376	0.063
	5HT2A	0.859	0.745	0.793	0.240
	5HT4	0.470	1.166	0.381	1.058
	CB1	0.386	0.872	0.326	0.605
	D1	1.502 *	0.736	1.467 * (FDR)	0.070
	D2	0.287	0.163	0.376	0.753
	DAT	0.202	0.331	0.155	0.545
	FDOPA	0.839	0.826	0.821	0.426
	GABAa	0.297	0.803	0.213	0.987
	KappaOp	0.275	0.849	0.267	0.715
	mGluR5	0.369	0.934	0.282	1.253
	MU	0.417	0.563	0.434	0.334
	NA	0.493	0.243	0.470	0.002
	NMDA	1.286	0.387	1.211	0.011
	SERT_DAS	0.560	0.139	0.563	0.281
	SERT_MADAM	0.001	0.522	0.015	0.563
	VACh	0.259	0.333	0.334	0.958
Third-order gradient	5HT1A	1.959 **	1.925 **	1.874 **	1.264
	5HT1B	0.040	0.181	0.005	0.587
	5HT2A	0.213	0.083	0.231	0.137
	5HT4	1.104	0.911	1.163	0.537
	CB1	0.638	0.485	0.690	0.140
	D1	0.026	0.092	0.078	0.404
	D2	1.721 *	0.913	1.560* (FDR)	1.457
	DAT	0.427	0.501	0.363	0.562
	FDOPA	0.115	0.295	0.174	0.077
	GABAa	1.117	0.846	1.077	0.600
	KappaOp	0.301	0.590	0.330	0.203
	mGluR5	1.143	1.060	1.110	0.698
	MU	0.039	0.203	0.060	0.123
	NA	0.129	0.152	0.098	0.347
	NMDA	0.071	0.152	0.063	0.315
	SERT_DAS	0.283	0.290	0.292	0.079
	SERT_MADAM	0.075	0.493	0.100	0.142
	VACh	0.916	1.111	0.840	1.494

Table S4.5 Continued

		Patient_Left	Patient_Right	Healthy Control_Left	Healthy Control_Right
Fourth-order gradient	5HT1A	0.051	0.125	0.107	0.257
	5HT1B	0.446	0.403	0.441	0.346
	5HT2A	0.294	0.539	0.363	0.630
	5HT4	0.110	0.060	0.041	0.034
	CB1	0.237	0.052	0.127	0.070
	D1	0.294	0.075	0.260	0.220
	D2	0.036	0.205	0.187	0.064
	DAT	0.954	0.849	1.165	0.641
	FDOPA	0.470	0.326	0.418	0.317
	GABAa	0.296	0.494	0.468	0.349
	KappaOp	0.506	0.469	0.416	0.567
	mGluR5	0.246	0.347	0.417	0.203
	MU	0.373	0.259	0.334	0.342
	NA	0.678	0.770	0.755	0.637
	NMDA	0.421	0.782	0.459	0.897
	SERT_DAS	0.541	0.813	0.487	1.071
	SERT_MADAM	0.596	0.595	0.562	0.792
	VACh	0.388	0.213	0.532	0.075
Fifth-order gradient	5HT1A	0.537	0.505	0.288	0.318
	5HT1B	0.127	0.138	0.818	0.105
	5HT2A	0.354	0.361	0.242	0.494
	5HT4	0.403	0.646	0.342	0.647
	CB1	0.712	0.633	0.765	0.306
	D1	0.051	0.073	0.086	0.567
	D2	0.217	0.163	0.025	0.133
	DAT	0.318	0.004	0.347	0.049
	FDOPA	0.197	0.043	0.346	0.154
	GABAa	0.301	0.448	0.257	0.206
	KappaOp	0.111	0.342	0.368	0.033
	mGluR5	0.225	0.388	0.210	0.212
	MU	0.402	0.843	0.187	0.328
	NA	0.099	0.181	0.306	0.470
	NMDA	0.364	0.192	0.119	0.304
	SERT_DAS	0.257	0.307	0.650	0.541
	SERT_MADAM	0.027	0.330	0.658	0.363
	VACh	0.113	0.230	0.262	0.235

The trend-surface regression model with nine coefficients was applied to group-level gradient maps and the neurotransmitter PET/SPECT scans. Fisher's r-to-z–transformed correlation coefficients were computed between the TSM coefficients representing gradient maps and those representing neurotransmitter maps. The significance was assessed using permutation testing. *p<0.05, **p<0.01.

Table S4.6 Spearman correlations between gradient-neurotransmitter similarity and mental health outcomes in HBS

		Anxiety Sensitivity	Depressive Severity	Childhood Trauma	Emotional Neglect	Physical Neglect	Emotional Abuse	Physical Abuse
5HT1A_ Resting-State 1_Left	r_s	0.160	0.190 *	0.130	0.100	0.120	0.100	0.140
	p	0.072	0.021	0.145	0.245	0.169	0.234	0.125
5HT1A_ Resting-State 1_Right	r_s	-0.130	0.050	0.030	0.010	0.060	0.000	0.070
	p	0.145	0.567	0.774	0.952	0.538	0.988	0.431
N = 179								
5HT1A_ Resting-State 2_Left	r_s	0.080	-0.020	-0.040	-0.060	0.020	0.030	-0.060
	p	0.451	0.855	0.757	0.612	0.836	0.836	0.612
5HT1A_ Resting-State 2_Right	r_s	-0.060	0.020	-0.060	0.010	-0.070	-0.100	0.000
	p	0.601	0.855	0.612	0.934	0.601	0.359	0.958
N = 187								
5HT1A_ Resting-State 3_Left	r_s	0.010	0.140	-0.150	-0.160	-0.070	-0.030	-0.040
	p	0.933	0.112	0.093	0.078	0.471	0.761	0.737
5HT1A_ Resting-State 3_Right	r_s	-0.100	-0.090	-0.070	-0.100	0.030	-0.010	-0.040
	p	0.333	0.374	0.471	0.333	0.756	0.938	0.737
N = 173								
D1_ Resting-State 1_Left	r_s	0.060	0.040	0.030	0.030	0.060	-0.040	0.010
	p	0.573	0.664	0.664	0.664	0.571	0.664	0.847
N = 204								
D1_ Resting-State 2_Left	r_s	0.060	-0.020	-0.070	-0.080	0.000	-0.080	0.010
	p	0.500	0.875	0.409	0.378	0.992	0.378	0.929
N = 200								

Table S4.6 Continued

		Anxiety Sensitivity	Depressive Severity	Childhood Trauma	Emotional Neglect	Physical Neglect	Emotional Abuse	Physical Abuse
D1_ Resting-State 3_Left	r_s	-0.040	0.140	-0.020	-0.030	0.090	-0.050	0.010
	p	0.729	0.103	0.890	0.745	0.329	0.714	0.890
N = 183								
DAT_ Resting-State 1_Left	r_s	0.030	0.010	0.020	-0.020	0.080	0.020	0.080
	p	0.817	0.884	0.817	0.864	0.392	0.817	0.392
N = 180								
DAT_ Resting-State 2_Left	r_s	0.010	-0.030	-0.080	-0.070	0.000	-0.130	-0.020
	p	0.929	0.805	0.388	0.435	0.969	0.135	0.853
N = 181								
DAT_ Resting-State 3_Left	r_s	-0.180 *	0.040	0.030	0.030	0.080	0.030	-0.060
	p	0.048	0.707	0.778	0.778	0.494	0.778	0.613
N = 156								

To simplify, only names of neurotransmitters were listed to indicate the gradient-neurotransmitter similarity. The similarity between 5HT1A and the third-order gradient maps, D1 and the second-order gradient maps, DAT and the fourth-order gradient maps were included to correlate with mental health outcomes. Depressive severity was measured as the sum score of IDS-SR, and anxiety sensitivity was assessed with the ASI sum score. Childhood trauma and its subcategories were measured using the CTQ-SF. *p<0.05.

Table S4.7 Spearman correlations between gradient-neurotransmitter similarity and mental health outcomes in MIND-Set

		Anxiety Sensitivity	Depressive Severity	Comorbidity	Childhood Trauma	Emotional Neglect	Psychological Abuse	Physical Abuse
5HT1A_ Resting-State 1_Left	r_s	-0.050	0.030	0.050	-0.050	-0.050	0.010	-0.090
	p	0.498	0.674	0.510	0.513	0.500	0.913	0.218
5HT1A_ Resting-State 1_Right	r_s	0.150 *	0.130	0.070	-0.080	-0.070	-0.050	-0.060
	p	0.038	0.057	0.400	0.288	0.360	0.510	0.401
N = 237								
5HT1A_ Resting-State 2_Left	r_s	0.060	-0.040	0.010	0.020	0.040	0.030	0.040
	p	0.421	0.555	0.860	0.735	0.555	0.669	0.555
N = 261								
5HT1A_ Resting-State 3_Left	r_s	-0.010	0.020	0.070	0.050	0.070	0.050	-0.030
	p	0.909	0.875	0.400	0.652	0.380	0.652	0.736
5HT1A_ Resting-State 3_Right	r_s	0.090	0.080	-0.010	-0.010	-0.040	0.010	0.020
	p	0.255	0.349	0.896	0.924	0.736	0.909	0.875
N = 236								
D2_ Resting-State 1_Left	r_s	-0.020	0.030	0.030	0.010	0.020	0.050	-0.060
	p	0.821	0.767	0.767	0.876	0.833	0.544	0.371
N = 266								
D2_ Resting-State 2_Left	r_s	-0.010	-0.040	0.040	0.050	0.100	0.050	0.040
	p	0.862	0.513	0.513	0.495	0.149	0.513	0.513
N = 261								
D2_ Resting-State 3_Left	r_s	0.030	0.080	0.070	0.070	0.080	0.070	0.060
	p	0.594	0.238	0.252	0.258	0.242	0.275	0.355
N = 278								

Table S4.7 Continued

		Anxiety Sensitivity	Depressive Severity	Comorbidity	Childhood Trauma	Emotional Neglect	Psychological Abuse	Physical Abuse
D1_ Resting-State 1_Left	r_s	0.000	0.020	-0.040	-0.010	-0.070	0.030	0.020
	p	0.973	0.849	0.557	0.882	0.350	0.785	0.849
N = 279								
D1_ Resting-State 2_Left	r_s	0.130 *	0.090	0.050	0.030	0.040	0.040	0.010
	p	0.046	0.172	0.485	0.701	0.529	0.592	0.922
N = 272								
D1_ Resting-State 3_Left	r_s	0.090	0.070	-0.060	0.080	0.080	0.060	0.020
	p	0.150	0.244	0.334	0.244	0.197	0.340	0.742
N = 278								

The similarity between 5HT1A and the third-order gradient maps, D2 and the third-order gradient maps, D1 and the second-order gradient maps were included to correlate with mental health outcomes. Depressive severity was measured as the sum score of IDS-SR, and anxiety sensitivity was assessed with the ASI sum score. Childhood trauma and its subcategories were assessed using the NEMESIS. Comorbidity was indexed by the number of diagnosed psychiatric disorder clusters per participant. *p<0.05.

Table S4.8 Spearman correlations between gradient-neurotransmitter similarity and mental health outcomes in MIND-Set, separately for patients and healthy controls

		Anxiety Sensitivity	Depressive Severity	Comorbidity	Childhood Trauma	Emotional Neglect	Psychological Abuse	Physical Abuse
5HT1A_ Resting-State 1_Left_patient	r_s	-0.080	-0.010	0.030	-0.090	-0.100	-0.020	-0.130
	p	0.363	0.862	0.803	0.332	0.280	0.803	0.117
5HT1A_ Resting-State 1_Right_patient	r_s	0.180	0.150	0.020	-0.140	-0.120	-0.090	-0.090
	p	0.063	0.083	0.803	0.100	0.183	0.332	0.316
N = 178								
5HT1A_ Resting-State 2_Left_patient	r_s	0.100	-0.060	0.060	0.070	0.060	0.070	0.090
	p	0.195	0.423	0.423	0.367	0.423	0.402	0.284
N = 196								
5HT1A_ Resting-State 3_Left_patient	r_s	-0.050	-0.060	0.020	-0.030	0.020	-0.010	-0.110
	p	0.643	0.586	0.828	0.826	0.826	0.910	0.238
5HT1A_ Resting-State 3_Right_patient	r_s	0.100	0.100	-0.030	-0.030	-0.060	0.000	0.040
	p	0.286	0.260	0.826	0.826	0.608	0.968	0.736
N = 177								
D2_ Resting-State 1_Left_patient	r_s	-0.040	-0.010	0.010	-0.030	-0.050	0.010	-0.100
	p	0.697	0.903	0.903	0.705	0.643	0.903	0.230
N = 197								
D2_ Resting-State 2_Left_patient	r_s	0.000	-0.120	0.060	0.110	0.110	0.100	0.090
	p	0.976	0.136	0.382	0.139	0.139	0.182	0.203
N = 196								
D2_ Resting-State 3_Left_patient	r_s	-0.020	0.020	-0.010	0.020	0.040	0.020	0.000
	p	0.884	0.884	0.915	0.884	0.716	0.884	0.978
N = 207								

Table S4.8 Continued

		Anxiety Sensitivity	Depressive Severity	Comorbidity	Childhood Trauma	Emotional Neglect	Psychological Abuse	Physical Abuse
D1_ Resting-State 1_Left_patient	r_s	0.020	0.070	-0.040	0.010	-0.070	0.060	0.010
	p	0.778	0.404	0.669	0.869	0.367	0.428	0.869
N = 210								
D1_ Resting-State 2_Left_patient	r_s	0.140	0.090	0.010	0.060	0.060	0.080	0.030
	p	0.067	0.254	0.896	0.439	0.439	0.268	0.671
N = 205								
D1_ Resting-State 3_Left_patient	r_s	0.160 *	0.130	-0.110	0.080	0.090	0.080	-0.020
	p	0.027	0.079	0.148	0.288	0.239	0.260	0.807
N = 208								
5HT1A_ Resting-State1_Left_healthy control	r_s	-0.040	0.090	0.000	0.020	0.090	0.060	0.060
	p	0.934	0.891	1.000	0.960	0.891	0.891	0.891
5HT1A_ Resting-State1_Right_healthy control	r_s	-0.030	-0.020	0.050	0.070	0.010	0.050	0.020
	p	0.949	0.960	0.892	0.891	0.961	0.892	0.960
N = 59								
5HT1A_ Resting-State2_Left_healthy control	r_s	-0.020	0.130	-0.050	-0.150	0.030	-0.060	-0.150
	p	0.850	0.720	0.795	0.632	0.842	0.795	0.632
N = 65								
5HT1A_ Resting-State3_Left_healthy control	r_s	-0.030	0.020	0.000	0.270	0.250	0.200	0.220
	p	0.912	0.935	1.000	0.188	0.220	0.310	0.310
5HT1A_ Resting-State3_Right_healthy control	r_s	0.120	0.150	-0.220	0.090	0.060	0.010	-0.050
	p	0.579	0.432	0.310	0.732	0.854	0.963	0.871
N = 59								

Table S4.8 Continued

		Anxiety Sensitivity	Depressive Severity	Comorbidity	Childhood Trauma	Emotional Neglect	Psychological Abuse	Physical Abuse
D2_ Resting-State1_Left_healthy control	r_s	0.070	0.120	0.020	0.110	0.270	0.170	0.080
	p	0.646	0.600	0.886	0.600	0.092	0.383	0.646
N = 68								
D2_ Resting-State2_Left_healthy control	r_s	-0.070	0.120	-0.130	-0.230	0.030	-0.160	-0.200
	p	0.674	0.662	0.662	0.232	0.821	0.565	0.335
N = 65								
D2_ Resting-State3_Left_healthy control	r_s	-0.020	0.010	0.160	0.190	0.150	0.170	0.250
	p	0.917	0.937	0.355	0.322	0.371	0.355	0.124
N = 71								
D1_ Resting-State1_Left_healthy control	r_s	-0.090	0.020	-0.070	-0.080	0.010	-0.090	0.090
	p	0.638	0.929	0.638	0.638	0.963	0.638	0.638
N = 69								
D1_ Resting-State2_Left_healthy control	r_s	-0.050	-0.110	0.000	-0.140	-0.060	-0.180	-0.140
	p	0.734	0.556	1.000	0.478	0.709	0.361	0.478
N = 67								
D1_ Resting-State3_Left_healthy control	r_s	-0.130	-0.040	-0.050	0.090	0.110	-0.020	0.170
	p	0.523	0.784	0.727	0.641	0.589	0.873	0.385
N = 70								

The similarity between 5HT1A and the third-order gradient maps, D2 and the third-order gradient maps, D1 and the second-order gradient maps were included to correlate with mental health outcomes. Depressive severity was measured as the sum score of IDS-SR, and anxiety sensitivity was assessed with the ASI sum score. Childhood trauma and its subcategories were assessed using the NEMESIS. Comorbidity was indexed by the number of diagnosed psychiatric disorder clusters per participant. *p<0.05.

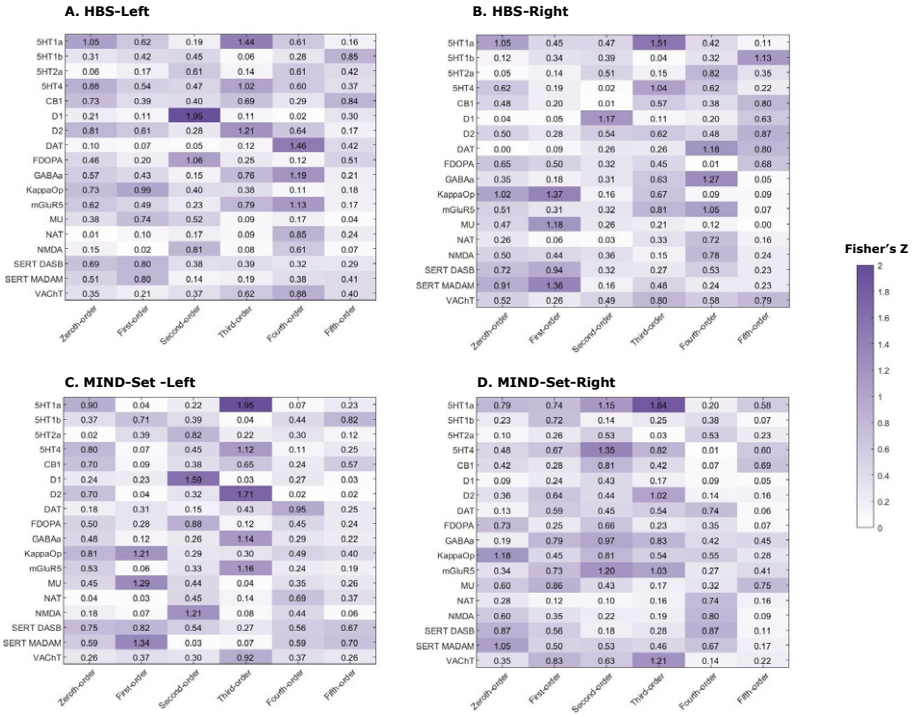

Figure S4.1 Heat maps for correlations coefficients (Fisher r-to-z transformed, absolute values) between gradient and neurotransmitter layouts, taking the resting-state 1 for each dataset as an example.

Chapter 5.
General discussion

Summary of findings

Classical theories in developmental and clinical psychology suggest that childhood experiences play a foundational role in shaping internal working models — the "schemas" that endure across the lifespan. Adverse childhood events, as significant negative experiences that deviate from normative developmental environments, have been proposed to contribute to the formation of maladaptive schemas and influence a range of cognitive and neural processes. In this thesis, we have presented our work aimed at tracing these maladaptive schemas rooted in childhood adversity, from perspectives of both cognitive performance in the emotional memory task and intrinsic large-scale brain functional organization.

In Chapter 2, based on the theoretical framework of Beck's cognitive model, we conducted a multi-session fMRI study to systematically examine the roles and interactions of childhood adversity, levels of depressive symptoms, and external schema activation in relation to negative memory bias and neural activity in the amygdala and hippocampus during emotional memory encoding. In a sample covering diverse but non-collinear levels of childhood adversity and depressive symptoms, we have the following findings: First, negative memory bias was significantly associated with childhood adversity, independent of current depressive symptom levels. Second, external schema activation did not induce more negative memory bias, nor did it modulate the relationship between childhood adversity and memory bias. Third, at the neural level, higher childhood adversity severity was associated with more negatively biased activity in the amygdala and hippocampus during memory encoding.

These findings highlight the enduring impact of childhood adversity on negative memory bias, reflected in both behavioral performance and neural responses. Even individuals with low current depressive symptoms may still exhibit stronger negative memory bias if they have a history of high childhood adversity. This points to a persistent and rigid maladaptive schema formed by childhood adversity, which may be automatically activated in response to emotional stimuli, rather than requiring additional external triggering. While previous research on childhood adversity and negative memory bias has primarily relied on the Self-Referent Encoding Task or autobiographical memory tests, our study extends this relationship using a classical emotional memory encoding and recognition paradigm. This demonstrates that maladaptive schemas shaped by childhood adversity can impact a more general emotional memory process beyond self-referential contexts.

In Chapter 3, we applied "connectopic mapping" to a sample comprising highly comorbid psychiatric patients and healthy controls, to examine how different types and frequencies of childhood adversity interact with acute stress in shaping striatal functional connectivity organization. We found that: First, while participants with different childhood adversity exposures showed no significant variation in striatal connectivity gradients at pre-stress baseline, the gradient organization varied as a function of one specific form of childhood adversity — emotional neglect following stress induction. Second, the stress-induced change in striatal gradient was also associated with emotional neglect. Third, the associations between emotional neglect and striatal connectivity gradients were selectively shown in individuals with high psychiatric comorbidity.

Together, these results provide large-scale functional connectivity evidence for the relationship between childhood adversity, the reward system and stress reactivity. They also support the dimensional model of childhood adversity highlighting the distinction in neural impacts between neglect and abuse. Furthermore, the modulating effect of psychiatric comorbidity underscores the psychopathological relevance of the striatal gradient variations related to childhood adversity and acute stress. In this context, "connectopic mapping" offers a novel approach to tracing the maladaptive schemas potentially embedded in the functional architecture of the reward system.

In Chapter 4, we aimed to characterize the functional connectivity gradients of the hippocampus–amygdala complex and explore the biological and psychological relevance these gradients may reveal. Across both healthy and psychiatric cohorts: First, we identified six distinct connectivity gradient maps within the hippocampus–amygdala complex. Second, we found that certain gradient modes may reflect modulation by the serotonergic and dopaminergic systems. Third, we revealed that individual differences in such neurotransmitter modulation are associated with levels of depressive severity and anxiety sensitivity.

In this study, we did not find the associations with childhood adversity, which may suggest that the functional organization of the hippocampus-amygdala complex and its neurotransmitter modulation could be more directly tied to current affective states than to earlier life experiences. Although the latent maladaptive schemas embedded in the hippocampus and amygdala may not be directly traceable through "connectopic mapping", our findings nonetheless demonstrate the promise of this approach for uncovering associations between large-scale functional connectivity, neurotransmitter modulations, and mental health outcomes.

The maladaptive schema in the emotional memory

Back to Beck's cognitive model

Beck's cognitive model, as a foundational theory of cognitive therapy (Beck & Dozois, 2011; Beck & Haigh, 2014), has a profound impact on clinical practice and suggests the close link between cognitive neuroscience and clinical research. Inspired by this model, in Chapter 2, we comprehensively examined the roles of childhood adversity, depressive symptom levels, and external schema activation in negative memory bias. Our findings align with Beck's model in several aspects. We observed association between childhood adversity and negative memory bias, which may indicate the lasting influence of prior life experiences on the formation of new memories. This finding corresponds to the schema effect on memory widely discussed in cognitive neuroscience (Fernández & Morris, 2018; Gilboa & Marlatte, 2017), and is also in support of the concept of "depressive schemas" proposed in Beck's model. Importantly, we found that this association was independent of individuals' current levels of depressive symptoms or whether external schema activation was experimentally induced, highlighting the robustness and enduring sensitivity of maladaptive schemas shaped by childhood adversity.

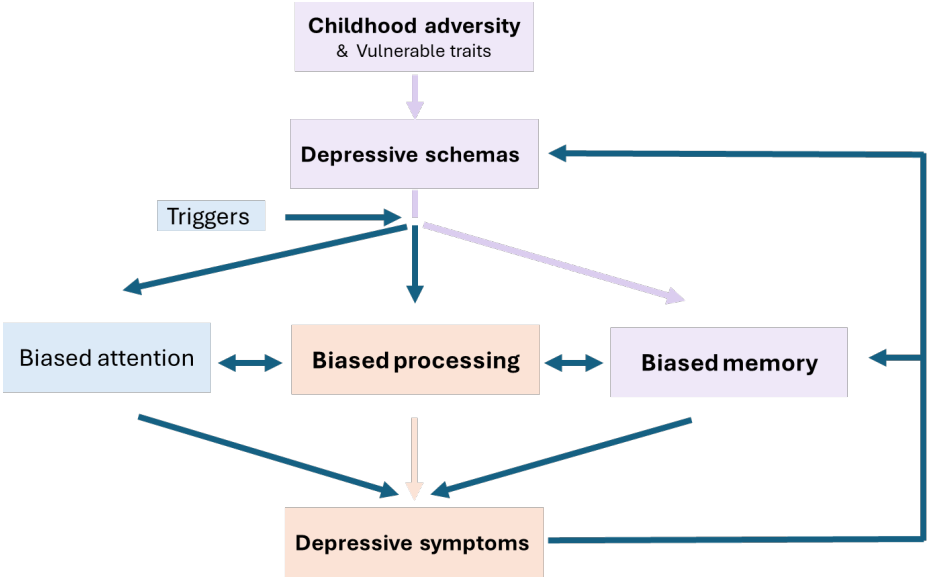

Figure 5.1 Highlighting our results in light of Beck's model: we provide further evidence for the association between childhood adversity and biased memory (the purple components), and between levels of depression symptoms and biased processing (the orange components).

In addition to the pathway linking childhood adversity and biased memory, our results also indicate a strong relationship between depressive symptom levels and biased processing—another cognitive component in Beck's model. By simultaneously assessing childhood adversity and depressive symptoms, our study provides further elaboration to Beck's model. Specifically, it suggests that biased processing may covary more closely with current depressive states, while biased memory may be more dependent on childhood adversity regardless people are currently in depression or not.

The role of the amygdala

The amygdala is a core region for processing emotionally salient stimuli (Anderson & Phelps, 2001; Hariri et al., 2002) and plays a crucial role in the encoding, consolidation, and retrieval of emotional memories (Phelps, 2004; Roozendaal et al., 2009). Functional alterations of the amygdala in memory processing are commonly reported in individuals with depression. Evidence primarily centers on two aspects: First, during memory encoding, patients with depression tend to show hyperactivation of the amygdala in response to negative stimuli, which has been directly linked to the extent of negative memory bias and depressive symptom severity (Hamilton & Gotlib, 2008; Ramel et al., 2007). Second, during memory retrieval — particularly in autobiographical recall — depressed individuals often exhibit reduced amygdala activation for positive content (Dillon & Pizzagalli, 2018; Young et al., 2016), leading to diminished retrieval of specific details and overgeneralized positive memories. Our results in Chapter 2 extend these findings by introducing childhood adversity as another important factor in relation to amygdala function during memory encoding. We observed that individuals with higher levels of childhood adversity, regardless of their current depressive symptom levels, exhibited more negatively biased amygdala responses during memory encoding. This neural pattern parallels the behavioral expression of negative memory bias. Notably, the biased amygdala activity was primarily driven by reduced responses to positive stimuli, resembling the blunted amygdala activity in depression patients during the recall of positive autobiographical memories. Taken together, these findings identified a central role of amygdala in negative memory bias, across different stages of memory processing.

Given the psychopathological relevance of biased amygdala reactivity to negative versus positive stimuli, the amygdala has become an important intervention target. A direct example comes from a line of research by Young et al. (2018), which demonstrated that, in patients with depression, upregulating amygdala activity during positive autobiographical memory recall via real-time fMRI

neurofeedback significantly enhanced the specificity of recalled positive memories. This intervention also led to reductions in symptom severity, including depressive symptoms and anxiety ratings (Young et al., 2014, 2017, 2018). Enhancing amygdala activation during positive memory retrieval may effectively activate broader neural networks involved in positive emotional processing, thereby contributing to symptom improvement (Dillon & Pizzagalli, 2018; Zotev et al., 2016). With regard to negative stimuli, though not specific to memory processes, numerous studies have aimed to downregulate amygdala reactivity to aversive or threatening stimuli using approaches such as neurofeedback (Goldway et al., 2022; Loos et al., 2020), emotion regulation strategies (Firk et al., 2018), or cognitively demanding tasks (de Voogd & Hermans, 2022). Our findings may suggest that these intervention approaches could be meaningfully extended to individuals with childhood adversity exposure, as they also exhibit blunted amygdala responses to positive stimuli and a corresponding negative memory bias. It would be valuable to test whether such amygdala-targeted interventions, e.g., downregulating amygdala responses to negative stimuli and upregulating amygdala responses to positive stimuli, could reduce negative memory bias in this population, and support a healthier cognitive processing style and improved mental health outcomes over time.

Moreover, it is also interesting to consider our findings on serotonergic modulation in Chapter 4. Across the psychopathological continuum, individual differences in the similarity between hippocampus–amygdala connectivity gradients and serotonin 1A receptor distribution were associated with levels of depressive symptoms and anxiety sensitivity. This resting-state association might also extend to task-state contexts: for example, during emotional memory encoding or retrieval, serotonergic modulation may differentially influence amygdala activity depending on individuals' histories of childhood adversity or current depressive states. Further investigations on this possibility may represent a new perspective for understanding the neuromodulator mechanism underlying childhood adversity, depression and memory bias.

The maladaptive schema and memory intervention

The relationship between childhood adversity and negative memory bias involves complex alterations in cognition and brain function, and also reflects the close interplay between memory processing and the internal model of the self (Moscovitch et al., 2023). During early childhood (around the age of five), children undergo substantial development in their sense of self and begin forming a coherent structure of personal experiences (Barry et al., 2006; Conway & Pleydell-Pearce, 2000). At this stage, significant autobiographical memories can constitute the foundational

knowledge base of the self (Conway, 2001; Conway & Pleydell-Pearce, 2000). Adverse experiences are often encoded as emotionally salient autobiographical memories and are further integrated into this still highly plastic self-schema. Once established, the maladaptive self-schema may influence the memory formation of new experiences, for example by fostering a negative memory bias, assimilating new information in ways that maintain and reinforce the existing schema (Barry et al., 2004, 2006). Over time, this creates a rigid, self-perpetuating cycle.

One possible way to break this cycle is by targeting the essential component of it — the self-defining autobiographical memories. Memory-based interventions have already been integrated into existing therapies and have shown clinical benefits (Dalgleish & Hitchcock, 2023). Among them, imagery rescripting is a typical example. The intervention involves encouraging patients to vivid recall the distressing or aversive memories, followed by imagining more positive alternative outcomes, which are then mentally integrated into the original memory trace (Brewin et al., 2009). The efficacy of imagery rescripting has been demonstrated in individuals with depression, anxiety, and PTSD (Brewin et al., 2009; Morina et al., 2017; Sheldon et al., 2024). At the neural level, positive reinterpretation of negative memories has been associated with changes in representational patterns within the hippocampus and ventral striatum (Speer et al., 2021). Our results may indicate that examining the effectiveness of memory-based interventions in populations with a history of childhood adversity could be meaningful. For example, future studies might assess whether imagery rescripting modifies the association between childhood adversity and negative memory bias, as well as its impact on amygdala and hippocampal reactivity to emotional stimuli.

The cognitive bias modification (CBM)-memory training is another promising memory intervention approach. It makes use of retrieval practice as an effective mnemonic enhancer (Roediger & Butler, 2011): participants first learn word pairs of different valences, and then, in the positive modification condition, perform cued-recall practice for positive pairs, in contrast to conditions where neutral or negative pairs are recalled (Vrijsen et al., 2019). After several training sessions, participants under the positive retrieval practice condition have shown a sustained positive recall bias and improved mood during delayed testing (Hertel et al., 2017; Vrijsen et al., 2016). In patients with depression, positive CBM-memory training has been found to reduce their rumination symptoms (Vrijsen et al., 2024). For populations with childhood adversity, the effect of positive CBM-memory training on negative memory bias remains to be tested, as well as its influence on retrieval-related activity in neural targets such as the amygdala and hippocampus. Given the long-

term impact of childhood adversity observed here and the stability of associated memory schemas, such therapy may need to be sustained over extended periods to effectively modify the schemas.

The maladaptive schema in striatal functional connectivity

Besides the maladaptive schema traced in the emotional memory task, in Chapter 3, we also delineate another form of it—embedded in the resting-state functional connectivity organization of the striatum. While no significant variation in striatal functional connectivity gradients was observed across different types or frequencies of childhood adversity at baseline, after acute stress induction, the gradient pattern showed distinct variation associated specifically with the frequency of emotional neglect. This stress induction can be viewed as a form of maladaptive schema activation, which brings to the surface latent individual differences in striatal functional architecture linked to childhood adversity. Previous studies have identified blunted stress reactivity as a typical alteration among individuals with childhood adversity exposure, shown in both the hypothalamic–pituitary–adrenal (HPA) axis and sympathetic nervous system (SNS) (Bunea et al., 2017; Dempster et al., 2021; Sijtsema et al., 2015), which may impair adaptive coping and is often associated with externalizing disorders and impulsive behavior (Lovallo et al., 2012; Raine, 1996). The reduced stress response is dependent on alterations in the HPA axis and SNS, and has also been linked to dysregulation in the brain's reward and motivation systems (Carroll et al., 2012, 2017): childhood adversity may dampen responsivity in these motivation-related regions, leading to reduced engagement in stress appraisal and diminished mobilization of mental effort for coping—ultimately impairing the necessary physiological adjustments to stress.

While this integrative account requires further empirical validation, our findings in Chapter 3 offer direct evidence of how childhood adversity is associated with altered stress responses in the organization of striatal connectivity. Notably, the specific striatal gradient mode associated with childhood adversity corresponds to the one previously implicated in goal-directed behavior (Marquand et al., 2017), highlighting its alignment with the motivational account. Emotional neglect, as a form of adversity involving sensory and hedonic deprivation (Stoltenborgh et al., 2013; Zhou et al., 2025), may leave an imprint on regions related to reward and motivation processing. The striatal gradient mapping could therefore serve as a stable neural read-out of maladaptive schemas rooted in dysfunctions of the reward and motivation system.

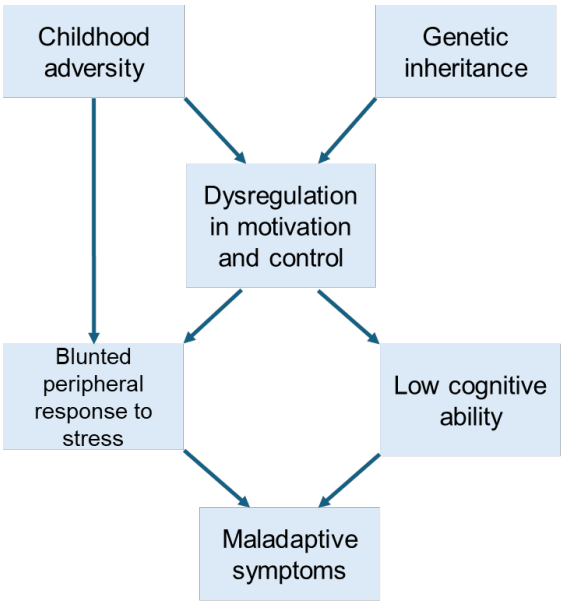

Figure 5.2 A conceptual model illustrating how childhood adversity contributes to dysregulation in the motivational system and blunted stress responses, ultimately leading to maladaptive outcomes. Adapted from Carroll et al., 2017.

Identifying transdiagnostic neural markers through "connectopic mapping"

The biopsychological relevance of connectivity gradient maps

The functional connectivity observed between brain regions reflects the cumulative outcome of multiple modulatory factors. While traditional functional connectivity analyses directly measure and evaluate this aggregate, "connectopic mapping" seeks to decompose it into distinct dimensions. Each dimension captures a gradient changing mode, allowing investigation into the relevance of specific factors to functional connectivity by associating them with these gradient modes. This feature is particularly meaningful in studying brain functional multiplicity. Some gradient modes have been shown to replicate the topographical organization of inter-regional connections observed in animal anatomical studies (Haak et al., 2018; Marquand et al., 2017; Veréb et al., 2023). In our findings, the gradient maps of the striatum and hippocampus–amygdala complex also reflect this anatomical topography.

Another compelling relevance lies in the relationship between gradient maps and neurotransmitter distribution. Over 100 different types of neurotransmitters are

known to extensively modulate brain function and inter-regional communication, and abnormalities in these systems contribute to a wide range of neurological and psychiatric disorders (Purves et al., 2001). Traditional functional connectivity analyses provide limited information in the specific contributions of neurotransmitter systems; in contrast, studies with "connectopic mapping" have shown that certain gradient modes exhibit robust spatial alignment with the distribution of various neurotransmitters. The striatal connectivity gradient has been shown to correspond closely with the distribution of dopamine transporters in the striatum (Oldehinkel et al., 2022), and the hippocampal connectivity gradient aligns with the organization of dopamine type 1 receptors (Nordin et al., 2025). Our findings in Chapter 4 extend previous research by revealing the involvement of the serotonin system. Specifically, we identified a stable alignment between the third-order gradient in the hippocampus–amygdala complex and the spatial distribution of the 5-HT1A receptor, with individual differences in this alignment associated with depressive and anxiety symptomatology. Similarly, a recent study examined cortical connectivity gradients in individuals with mild cognitive impairment, comparing subgroups with and without depressive symptoms (Liu et al., 2025). They found that the spatial differences in connectivity gradients between the two subgroups were associated with the cortical distribution of 5-HT1A receptors, suggesting that alterations in the serotonin system may play a role in the observed functional connectivity changes. Together, these findings show the utility of connectivity gradients in disentangling the influence of specific neurotransmitter systems on functional connectivity, while capturing their psychiatric relevance with high sensitivity. This represents a particularly exciting application, as resting-state fMRI offers a more cost-effective and convenient alternative to molecular imaging techniques. If deviations in neurotransmitter modulation can be reliably captured via "connectopic mapping", this approach could see broad application in future research and clinical translation. For example, the hippocampus–amygdala gradient map with its TSM statistics might serve as a simplified proxy for 5-HT1A receptor activity, enabling researchers and clinicians to conveniently monitor this system through a standard fMRI scan.

Within a Research Domain Criteria Framework

In recent decades, researchers have increasingly recognized the limitations of traditional diagnostic systems in accounting for the substantial heterogeneity and comorbidity observed in clinical populations, which have also posed challenges for translational research (Cuthbert, 2022). In response, an alternative dimensional perspective has emerged. In 2010, the National Institute of Mental Health (NIMH) in the United States introduced the Research Domain Criteria (RDoC) Framework, which called for studies to identify transdiagnostic mechanisms, shared behavioral

and biological markers that underlie psychiatric conditions, as well as targeted treatment approaches (Insel et al., 2010). The framework outlines six core domains fundamental to human functioning and closely linked to the development of mental disorders: negative valence systems, positive valence systems, cognitive systems, social processes, arousal/regulatory systems, and sensorimotor systems. Within each domain, research is encouraged across multiple levels of analysis, from the microscopic (e.g., genes, molecules) to the macroscopic (e.g., circuits, behavior), with neural circuits at the central position (Cuthbert & Kozak, 2013; Insel et al., 2010).

Following this framework, the MIND-Set study was designed to include large samples of individuals with high comorbidity in neurodevelopmental and stress-related psychiatric disorders, aiming to identify both shared and disorder-specific mechanisms and risk factors (van Eijndhoven et al., 2022). Using data from the MIND-Set study, as well as the HBS dataset, our results in Chapters 3 and 4 may contribute to this transdiagnostic objective by revealing neural markers in the functional connectivity of the striatum and the hippocampus–amygdala complex. Chapters 2 and 3 also highlight the transdiagnostic role of childhood adversity in maladaptive cognitive styles and functional changes in reward processing regions. These findings are relevant to the negative valence and positive valence systems as defined in the RDoC framework, and at the same time indicate their close interactions: the negative bias observed in amygdala encoding activity appears to be largely driven by reduced responses to positive stimuli, and the blunted reactivity to a negative stressor may reflect underlying functional changes in the positive (reward) processing system. These observations suggest that the negative and positive valence systems are not isolated, but rather overlapping and dynamically interacting in both neural mechanisms and behavioral outcomes. In clinical contexts, this underscores the importance of attending to both systems concurrently. For example, when assessing the index for anhedonia, the automatic ruminative thinking habits and the loss of reward sensitivity could both be taken into account (Moriarity et al., 2020; Rutherford et al., 2023).

In terms of methodology, the application of "connectopic mapping" demonstrates notable sensitivity to both inter-individual differences and intra-individual manipulations. It effectively captures associations with depressive and anxiety symptomatology across the psychiatric continuum—from healthy individuals to patients with high comorbidity. These characteristics indicate the method's strong potential for identifying transdiagnostic neural markers, aligning with the goals of the RDoC framework. In future research, its applications in diagnosis and treatment monitoring may be further examined.

Future directions

The schema effect in negative memory bias

In Chapter 2, we demonstrated that childhood adversity is associated with a negative bias in memory performance, as well as biased encoding activity in the amygdala and hippocampus, indicating the potential impact of the inherent maladaptive schema shaped by childhood adversity on the emotional memory processing. Based on these findings, an essential next step would be to directly test whether individuals with childhood adversity exhibit the typical brain activity patterns observed in previous schema studies during the processing of emotional memory. First, although we did not observe a significant effect of external schema activation (through negative mood induction) on memory performance, it remains meaningful to examine whether individuals with higher levels of childhood adversity show greater schema instantiation activity under negative mood induction (e.g., while listening to negative music). Schema activation and the online processing of schema-relevant information are typically associated with mPFC activity (Ghosh et al., 2014; Gilboa & Marlatte, 2017). To identify brain regions involved in the interaction between schema activation and childhood adversity during the mood induction, an intersubject synchronization (ISS) approach could be employed (van Kesteren et al., 2010). Second, schema-congruent encoding has been linked to close interplays between the mPFC and medial temporal lobe (Bein & Niv, 2025; Sommer, 2017; Sommer et al., 2022; van Kesteren et al., 2010, 2013). In the context of emotional memory, maladaptive schemas may influence memory encoding through functional coupling among the mPFC, hippocampus (or parahippocampal gyrus), and amygdala. Interplays between these interested regions could be further explored using psychophysiological interaction (PPI) analysis. Third, another characteristic of schema congruent memories is their preferential consolidation (Dudai et al., 2015; Durrant et al., 2015). Spontaneous reactivation during post-encoding rest may play a role in schema-modulated memory enhancement (Hennies et al., 2016; Wu et al., 2022). Thus, it would be valuable to test whether higher childhood adversity is associated with increased reactivation of negative memory engrams in regions such as the mPFC and hippocampus during post-encoding rest, and how this relates to memory bias and psychiatric vulnerability. Finally, after consolidation, schema-congruent information tends to become more abstract and is better integrated into pre-existing schema structures (Audrain & McAndrews, 2022; Sommer et al., 2022). To examine how this representational transformation differs across individuals with varying levels of childhood adversity, a multivariate pattern similarity analysis could be conducted both at the retrieval stage and between the encoding and retrieval phases.

Besides the potential neural mechanisms underlying the schema effect on negative memory bias, it is also worthwhile to consider the nature of the maladaptive schema itself in more depth. Specifically, we may ask whether this schema is more related to the content of personal experiences, emphasizing a pessimistic self-belief shaped by repeated exposure to adverse events—potentially represented in regions such as the mPFC, posterior cingulate cortex (PCC), or a broader network like the DMN (Butterfield et al., 2023; Dixon et al., 2020; Lemogne et al., 2012). Alternatively, it may be more closely linked to the emotional system, reflecting maladaptive emotional knowledge and response patterns acquired from early adverse experiences, possibly embedded within an amygdala-centered circuit (van Tieghem & Tottenham, 2017; McLaughlin et al., 2019). Although our findings in Chapter 2 suggest that the association between childhood adversity and negative memory bias is not confined to self-referential stimuli but extends to general emotional memory processing, it remains possible that both self-referential and emotional elements interact to form a composite schema system rooted in childhood adversity. Such interaction may influence how childhood adversity, depression, and external schema activation differentially relate to memory bias. Also, it can be speculated that a personalized schema-activation approach (e.g., recalling a personal memory that elicits negative affect and rumination) might produce more pronounced effects on subsequent memory processes. Thus, to more clearly characterize these different aspects of maladaptive schema, future research may benefit from experimental paradigms that concurrently manipulate self-referential processing and emotional valence, ideally incorporating more ecologically valid stimuli.

Another interesting point that needs further investigation concerns a specific subgroup of participants in our sample—those who have experienced childhood adversity and exhibit a negative memory bias, but are not currently in a depressive state. It is possible that this subgroup, already demonstrating a maladaptive cognitive processing style, may carry a latent risk of developing depressive disorders. This hypothesis requires verification through longitudinal studies. An alternative possibility is that these individuals are in a well-compensated state underlying resilience. To further understand such resilience, it would be important to conduct systematic and dynamic assessments of other environmental factors, such as recent life events and social support, as well as genetic factors including relevant genotypes (Feder et al., 2009; Gillespie et al., 2009). From a neurobiological perspective, beyond the threat and reward processing systems measured in our study, the efficient functioning of regions involved in cognitive control and executive functions (e.g., the prefrontal cortex) may also serve as a resilience factor, which could be examined using neuropsychological test batteries (Kalisch

et al., 2024). Follow-up research on the cognitive, behavioral, and neural profiles of this subgroup would enhance our understanding of the psychopathological mechanisms related to childhood adversity and memory bias, while informing more targeted clinical prevention and intervention strategies.

In terms of childhood adversity, in the present analysis, we used a composite severity score that combines all types of childhood adversity measured. However, different dimensions of adversity may target distinct neural circuits; for example, deprivation is more likely to impact cortical regions involved in higher-order cognitive and motivational functions, whereas abuse tends to affect limbic areas such as the amygdala and hippocampus (McLaughlin, Sheridan, & Lambert, 2014). Therefore, it is important to further investigate whether these specific dimensions of adversity differentially influence how maladaptive schemas affect emotional memory processing. Moreover, the assessment of childhood adversity in our study was based on self-reported questionnaires, which rely on participants' retrospective evaluations of their childhood experiences for each item. This approach introduces a potential confound: the report of higher levels of childhood adversity may be a result of negative memory biases in itself. Future research may benefit from comparing populations with known "objective" differences in childhood adversity, such as individuals who experienced foster care versus those who grew up with their biological parents, to provide useful complementary evidence.

Transdiagnostic applications of "connectopic mapping"

As summarized above, our findings in Chapters 3 and 4 suggest that "connectopic mapping" holds promise for identifying transdiagnostic neural markers related to childhood adversity and psychiatric symptomatology, particularly in brain regions that play essential roles in stress-related disorders with different accents on positive and negative valence system (e.g., the striatum, amygdala and hippocampus). However, future research could explore its broader applications in the following aspects. First, while sensitively capturing symptom-related alterations may provide implications in mechanisms and diagnosis, the ability to reflect treatment-induced changes can also facilitate the monitoring of therapeutic progress, representing another important application. Therefore, applying "connectopic mapping" in intervention studies would be highly informative for validating this clinical utility. For example, it would be meaningful to examine whether the association between striatal connectivity gradients and childhood adversity changes following the schema therapy, which is aimed at modifying the early maladaptive schema. Similarly, examining the relationship between connectivity gradients and neurotransmitter systems in populations undergoing psychotropic treatments, such

as selective serotonin reuptake inhibitor (SSRI) therapy, could directly assess how these associations change over the course of treatment and relate to clinical efficacy. Longitudinal studies are also critical, as they can provide directional information on how childhood adversity, alterations in connectivity gradients, and psychiatric outcomes interact over time. Second, beyond examining the biological relevance of connectivity gradients from anatomical and neurotransmitter perspectives, gene expression mapping represents another promising aspect. For instance, gene expression domains in the hippocampus are generally organized in a tripartite model along the long-axis (Strange et al., 2014). Exploring the correspondence between this genetic organization and connectivity gradient maps could help establish a gene-environment interacting read-out of hippocampal function. Finally, while connectivity gradient maps depict the functional architecture within regions of interest, the projection maps which reveal how cortical areas participate in these connectivity profiles are also important. Investigating these projection maps, for example through functional decoding, may provide additional insights into the inter-regional functionality and its dysfunctions.

Concluding remarks

In summary, through a multi-session fMRI study, and analysis of resting-state fMRI data from both healthy and psychiatric cohorts, we have traced how maladaptive schemas shaped by childhood adversity manifest in emotional memory processes, and in acute stress-related changes within brain functional connectivity architectures. Our findings provide evidence on how childhood adversity is associated with altered activity in threat-processing regions, including the amygdala and hippocampus, as well as in reward-processing circuits centered on the striatum. Moreover, our results highlight the utility of "connectopic mapping" for identifying transdiagnostic neural markers, offering a basis for future research to explore its broader application in clinical practice.

Appendix

References

A.

Abate, B. B., Sendekie, A. K., Merchaw, A., Abebe, G. K., Azmeraw, M., Alamaw, A. W., Zemariam, A. B., Kitaw, T. A., Kassaw, A., & Wodaynew, T. (2025). Adverse Childhood Experiences Are Associated with Mental Health Problems Later in Life: An Umbrella Review of Systematic Review and Meta-Analysis. Neuropsychobiology, 84(1), 48–63.

Abercrombie, H. C., Frost, C. P., Walsh, E. C., Hoks, R. M., Cornejo, M. D., Sampe, M. C., Gaffey, A. E., Plante, D. T., Ladd, C. O., & Birn, R. M. (2018). Neural signaling of cortisol, childhood emotional abuse, and depression-related memory bias. Biological Psychiatry: Cognitive Neuroscience and Neuroimaging, 3(3), 274–284.

Adler, N. E., Epel, E. S., Castellazzo, G., & Ickovics, J. R. (2000). Relationship of subjective and objective social status with psychological and physiological functioning: Preliminary data in healthy, White women. Health Psychology, 19(6), 586–592.

al'Absi, M., Ginty, A. T., & Lovallo, W. R. (2021). Neurobiological mechanisms of early life adversity, blunted stress reactivity and risk for addiction. Neuropharmacology, 188, 108519.

Alakurtti, K., Johansson, J. J., Joutsa, J., Laine, M., Bäckman, L., Nyberg, L., & Rinne, J. O. (2015). Long-term test–retest reliability of striatal and extrastriatal dopamine D2/3 receptor binding: Study with [11C] raclopride and high-resolution PET. Journal of Cerebral Blood Flow & Metabolism, 35(7), 1199–1205.

Albert, P. R., Vahid-Ansari, F., & Luckhart, C. (2014). Serotonin-prefrontal cortical circuitry in anxiety and depression phenotypes: Pivotal role of pre-and post-synaptic 5-HT1A receptor expression. Frontiers in Behavioral Neuroscience, 8, 199.

Alcaraz, M., Pierce, H., Eggum, N. D., Nuño-Gutiérrez, B. L., & Ghimire, D. (2024). A cross-cultural examination of adverse childhood experiences in low-and middle-income countries and their relation with adolescent educational aspirations. Child Abuse & Neglect, 152, 106756.

Anderson, A. K., & Phelps, E. A. (2001). Lesions of the human amygdala impair enhanced perception of emotionally salient events. Nature, 411(6835), 305–309.

Andersson, J. L., Jenkinson, M., & Smith, S. (2007a). Non-linear optimisation FMRIB technical report TR07JA1. Practice.

Andersson, J. L., Jenkinson, M., & Smith, S. (2007b). Non-linear registration, aka Spatial normalisation FMRIB technical report TR07JA2. FMRIB Analysis Group of the University of Oxford, 2(1).

Arnold, J. F., Fitzgerald, D. A., Fernández, G., Rijpkema, M., Rinck, M., Eling, P. A., Becker, E. S., Speckens, A., & Tendolkar, I. (2011). Rose or black-coloured glasses?: Altered neural processing of positive events during memory formation is a trait marker of depression. Journal of Affective Disorders, 131(1–3), 214–223.

Audrain, S., & McAndrews, M. P. (2022). Schemas provide a scaffold for neocortical integration of new memories over time. Nature Communications, 13(1), 5795.

Ayano, G. (2016). Dopamine: Receptors, functions, synthesis, pathways, locations and mental disorders: Review of literatures. J Ment Disord Treat, 2(120), 2.

B.

Balleine, B. W., Delgado, M. R., & Hikosaka, O. (2007). The role of the dorsal striatum in reward and decision-making. Journal of Neuroscience, 27(31), 8161–8165.

Barch, D. M., Burgess, G. C., Harms, M. P., Petersen, S. E., Schlaggar, B. L., Corbetta, M., Glasser, M. F., Curtiss, S., Dixit, S., & Feldt, C. (2013). Function in the human connectome: Task-fMRI and individual differences in behavior. Neuroimage, 80, 169–189.

Barker, G. R., & Warburton, E. C. (2011). When is the hippocampus involved in recognition memory? Journal of Neuroscience, 31(29), 10721–10731.

Barry, E. S., Naus, M. J., & Rehm, L. P. (2004). Depression and implicit memory: Understanding mood congruent memory bias. Cognitive Therapy and Research, 28, 387–414.

Barry, E. S., Naus, M. J., & Rehm, L. P. (2006). Depression, implicit memory, and self: A revised memory model of emotion. Clinical Psychology Review, 26(6), 719–745.

Bartlett, E. A., Yttredahl, A. A., Boldrini, M., Tyrer, A. E., Hill, K. R., Ananth, M. R., Milak, M. S., Oquendo, M. A., Mann, J. J., & DeLorenzo, C. (2023). In vivo serotonin 1A receptor hippocampal binding potential in depression and reported childhood adversity. European Psychiatry, 66(1), e17.

Basto-Pereira, M., Gouveia-Pereira, M., Pereira, C. R., Barrett, E. L., Lawler, S., Newton, N., Stapinski, L., Prior, K., Costa, M. S. A., & Ximenes, J. M. (2022). The global impact of adverse childhood experiences on criminal behavior: A cross-continental study. Child Abuse & Neglect, 124, 105459.

Beaulieu, J.-M., & Gainetdinov, R. R. (2011). The physiology, signaling, and pharmacology of dopamine receptors. Pharmacological Reviews, 63(1), 182–217.

Beck, A. T. (1967). Depression: Clinical, experimental, and theoretical aspects. Hoeber.

Beck, A. T. (2005). The current state of cognitive therapy: A 40-year retrospective. Archives of General Psychiatry, 62(9), 953–959.

Beck, A. T. (2008). The evolution of the cognitive model of depression and its neurobiological correlates. American Journal of Psychiatry, 165(8), 969–977.

Beck, A. T., & Bredemeier, K. (2016). A unified model of depression: Integrating clinical, cognitive, biological, and evolutionary perspectives. Clinical Psychological Science, 4(4), 596–619.

Beck, A. T., & Dozois, D. J. (2011). Cognitive therapy: Current status and future directions. Annual Review of Medicine, 62(1), 397–409.

Beck, A. T., & Haigh, E. A. (2014). Advances in cognitive theory and therapy: The generic cognitive model. Annual Review of Clinical Psychology, 10(1), 1–24.

Beck, A. T., Steer, R. A., & Brown, G. (1996). Beck depression inventory–II. Psychological Assessment.

Bein, O., & Niv, Y. (2025). Schemas, reinforcement learning and the medial prefrontal cortex. Nature Reviews Neuroscience, 26(3), 141–157.

Beliveau, V., Ganz, M., Feng, L., Ozenne, B., Højgaard, L., Fisher, P. M., Svarer, C., Greve, D. N., & Knudsen, G. M. (2017). A high-resolution in vivo atlas of the human brain's serotonin system. Journal of Neuroscience, 37(1), 120–128.

Bellis, M. A., Hughes, K., Ford, K., Rodriguez, G. R., Sethi, D., & Passmore, J. (2019). Life course health consequences and associated annual costs of adverse childhood experiences across Europe and North America: A systematic review and meta-analysis. The Lancet Public Health, 4(10), e517–e528.

Bergman, M. A., Schene, A. H., Vissers, C. T. W., Vrijsen, J. N., Kan, C. C., & van Oostrom, I. (2020). Systematic review of cognitive biases in autism spectrum disorders: A neuropsychological framework towards an understanding of the high prevalence of co-occurring depression. Research in Autism Spectrum Disorders, 69, 101455.

Berthold-Losleben, M., Papalini, S., Habel, U., Losleben, K., Schneider, F., Amunts, K., & Kohn, N. (2021). A short-term musical training affects implicit emotion regulation only in behaviour but not in brain activity. BMC Neuroscience, 22, 1–11.

Birn, R. M., Patriat, R., Phillips, M. L., Germain, A., & Herringa, R. J. (2014). Childhood maltreatment and combat posttraumatic stress differentially predict fear-related fronto-subcortical connectivity. Depression and Anxiety, 31(10), 880–892.

Bisby, J. A., Horner, A. J., Hørlyck, L. D., & Burgess, N. (2016). Opposing effects of negative emotion on amygdalar and hippocampal memory for items and associations. Social Cognitive and Affective Neuroscience, 11(6), 981–990.

Blair, C., & Raver, C. C. (2012). Child development in the context of adversity: Experiential canalization of brain and behavior. American Psychologist, 67(4), 309.

Bloomfield, M. A., McCutcheon, R. A., Kempton, M., Freeman, T. P., & Howes, O. (2019). The effects of psychosocial stress on dopaminergic function and the acute stress response. Elife, 8, e46797.

Bocchio, M., McHugh, S. B., Bannerman, D. M., Sharp, T., & Capogna, M. (2016). Serotonin, amygdala and fear: Assembling the puzzle. Frontiers in Neural Circuits, 10, 24.

Bolton, J. L., Schulmann, A., Garcia-Curran, M. M., Regev, L., Chen, Y., Kamei, N., Shao, M., Singh-Taylor, A., Jiang, S., & Noam, Y. (2020). Unexpected transcriptional programs contribute to hippocampal memory deficits and neuronal stunting after early-life adversity. Cell Reports, 33(11).

Bowlby, J. (1969). Attachment and loss (Issue 79). Random House.

Brehl, A.-K., Kohn, N., Schene, A. H., & Fernández, G. (2020). A mechanistic model for individualised treatment of anxiety disorders based on predictive neural biomarkers. Psychological Medicine, 50(5), 727–736.

Brewin, C. R., Wheatley, J., Patel, T., Fearon, P., Hackmann, A., Wells, A., Fisher, P., & Myers, S. (2009). Imagery rescripting as a brief stand-alone treatment for depressed patients with intrusive memories. Behaviour Research and Therapy, 47(7), 569–576.

Briggs-Gowan, M. J., Pollak, S. D., Grasso, D., Voss, J., Mian, N. D., Zobel, E., McCarthy, K. J., Wakschlag, L. S., & Pine, D. S. (2015). Attention bias and anxiety in young children exposed to family violence. Journal of Child Psychology and Psychiatry, 56(11), 1194–1201.

Brown, S. M., & Shillington, A. M. (2017). Childhood adversity and the risk of substance use and delinquency: The role of protective adult relationships. Child Abuse & Neglect, 63, 211–221.

Buckholtz, J. W., & Meyer-Lindenberg, A. (2012). Psychopathology and the human connectome: Toward a transdiagnostic model of risk for mental illness. Neuron, 74(6), 990–1004.

Bunea, I. M., Szentágotai-Tătar, A., & Miu, A. C. (2017). Early-life adversity and cortisol response to social stress: A meta-analysis. Translational Psychiatry, 7(12), 1274.

Bush, D. E., Caparosa, E. M., Gekker, A., & LeDoux, J. (2010). Beta-adrenergic receptors in the lateral nucleus of the amygdala contribute to the acquisition but not the consolidation of auditory fear conditioning. Frontiers in Behavioral Neuroscience, 4, 154.

Butterfield, R. D., Grad-Freilich, M., & Silk, J. S. (2023). The role of neural self-referential processes underlying self-concept in adolescent depression: A comprehensive review and proposed neurobehavioral model. Neuroscience & Biobehavioral Reviews, 149, 105183.

C.

Carpenter, L. L., Carvalho, J. P., Tyrka, A. R., Wier, L. M., Mello, A. F., Mello, M. F., Anderson, G. M., Wilkinson, C. W., & Price, L. H. (2007). Decreased adrenocorticotropic hormone and cortisol responses to stress in healthy adults reporting significant childhood maltreatment. Biological Psychiatry, 62(10), 1080–1087.

Carroll, D., Ginty, A. T., Whittaker, A. C., Lovallo, W. R., & De Rooij, S. R. (2017). The behavioural, cognitive, and neural corollaries of blunted cardiovascular and cortisol reactions to acute psychological stress. Neuroscience & Biobehavioral Reviews, 77, 74–86.

Carroll, D., Phillips, A. C., & Lovallo, W. R. (2012). The behavioral and health corollaries of blunted physiological reactions to acute psychological stress: Revising the reactivity hypothesis.

Celada, P., Bortolozzi, A., & Artigas, F. (2013). Serotonin 5-HT1A receptors as targets for agents to treat psychiatric disorders: Rationale and current status of research. CNS Drugs, 27(9), 703–716.

Chen, Y., Aitken, Z., Hammond, D., Thompson, A., Marwaha, S., Davey, C., Berk, M., McGorry, P., Chanen, A., & Nelson, B. (2025). Adverse childhood experiences and their differential relationships with transdiagnostic mental health outcomes in young adults. Psychological Medicine, 55, e147.

Cheng, T. W., Mills, K. L., Miranda Dominguez, O., Zeithamova, D., Perrone, A., Sturgeon, D., Feldstein Ewing, S. W., Fisher, P. A., Pfeifer, J. H., Fair, D. A., & Mackiewicz Seghete, K. L. (2021). Characterizing the impact of adversity, abuse, and neglect on adolescent amygdala resting-state functional connectivity. Developmental Cognitive Neuroscience, 47, 100894.

Cléry-Melin, M.-L., Jollant, F., & Gorwood, P. (2019). Reward systems and cognitions in Major Depressive Disorder. CNS Spectrums, 24(1), 64–77.

Cohen, J. (1988). Statistical Power Analysis for the Behavioral Sciences (2nd ed.). Routledge.

Cohen, N. J., & Squire, L. R. (1980). Preserved learning and retention of pattern-analyzing skill in amnesia: Dissociation of knowing how and knowing that. Science, 210(4466), 207–210.

Comijs, H. C., Beekman, A. T., Smit, F., Bremmer, M., Van Tilburg, T., & Deeg, D. J. (2007). Childhood adversity, recent life events and depression in late life. Journal of Affective Disorders, 103(1–3), 243–246.

Connolly, S. L., & Alloy, L. B. (2018). Negative event recall as a vulnerability for depression: Relationship between momentary stress-reactive rumination and memory for daily life stress. Clinical Psychological Science, 6(1), 32–47.

Conway, M. A. (2001). Sensory–perceptual episodic memory and its context: Autobiographical memory. Philosophical Transactions of the Royal Society of London. Series B: Biological Sciences, 356(1413), 1375–1384.

Conway, M. A., & Pleydell-Pearce, C. W. (2000). The construction of autobiographical memories in the self-memory system. Psychological Review, 107(2), 261.

Cools, R., Tichelaar, J. G., Helmich, R. C., Bloem, B. R., Esselink, R. A., Smulders, K., & Timmer, M. H. (2022). Role of dopamine and clinical heterogeneity in cognitive dysfunction in Parkinson's disease. Progress in Brain Research, 269(1), 309–343.

Cullen, K. R., Westlund, M. K., Klimes-Dougan, B., Mueller, B. A., Houri, A., Eberly, L. E., & Lim, K. O. (2014). Abnormal amygdala resting-state functional connectivity in adolescent depression. JAMA Psychiatry, 71(10), 1138–1147.

Cuthbert, B. N. (2022). Research Domain Criteria (RDoC): Progress and Potential. Current Directions in Psychological Science, 31(2), 107–114.

Cuthbert, B. N., & Kozak, M. J. (2013). Constructing constructs for psychopathology: The NIMH research domain criteria.

D.

Dalgleish, T., & Hitchcock, C. (2023). Transdiagnostic distortions in autobiographical memory recollection. Nature Reviews Psychology, 2(3), 166–182.

Dan-Glauser, E. S., & Scherer, K. R. (2011). The Geneva affective picture database (GAPED): A new 730-picture database focusing on valence and normative significance. Behavior Research Methods, 43, 468–477.

Dannlowski, U., Ohrmann, P., Bauer, J., Kugel, H., Arolt, V., Heindel, W., & Suslow, T. (2007). Amygdala reactivity predicts automatic negative evaluations for facial emotions. Psychiatry Research: Neuroimaging, 154(1), 13–20.

Dannlowski, U., Stuhrmann, A., Beutelmann, V., Zwanzger, P., Lenzen, T., Grotegerd, D., Domschke, K., Hohoff, C., Ohrmann, P., & Bauer, J. (2012). Limbic scars: Long-term consequences of childhood maltreatment revealed by functional and structural magnetic resonance imaging. Biological Psychiatry, 71(4), 286–293.

Dauvermann, M. R., Mothersill, D., Rokita, K. I., King, S., Holleran, L., Kane, R., McKernan, D. P., Kelly, J. P., Morris, D. W., Corvin, A., Hallahan, B., McDonald, C., & Donohoe, G. (2021). Changes in Default-Mode Network Associated With Childhood Trauma in Schizophrenia. Schizophrenia Bulletin, 47(5), 1482–1494.

de la Mora, M. P., Gallegos-Cari, A., Arizmendi-García, Y., Marcellino, D., & Fuxe, K. (2010). Role of dopamine receptor mechanisms in the amygdaloid modulation of fear and anxiety: Structural and functional analysis. Progress in Neurobiology, 90(2), 198–216.

de Rooij, S. R., Schene, A. H., Phillips, D. I., & Roseboom, T. J. (2010). Depression and anxiety: Associations with biological and perceived stress reactivity to a psychological stress protocol in a middle-aged population. Psychoneuroendocrinology, 35(6), 866–877.

de Voogd, L. D., & Hermans, E. J. (2022). Meta-analytic evidence for downregulation of the amygdala during working memory maintenance. Human Brain Mapping, 43(9), 2951–2971.

Dempster, K. S., O'Leary, D. D., MacNeil, A. J., Hodges, G. J., & Wade, T. J. (2021). Linking the hemodynamic consequences of adverse childhood experiences to an altered HPA axis and acute stress response. Brain, Behavior, and Immunity, 93, 254–263.

Dennison, M. J., Rosen, M. L., Sambrook, K. A., Jenness, J. L., Sheridan, M. A., & McLaughlin, K. A. (2019). Differential associations of distinct forms of childhood adversity with neurobehavioral measures of reward processing: A developmental pathway to depression. Child Development, 90(1), e96–e113.

Diedenhofen, B., & Musch, J. (2015). cocor: A comprehensive solution for the statistical comparison of correlations. PloS One, 10(4), e0121945.

Dillon, D. G., Holmes, A. J., Birk, J. L., Brooks, N., Lyons-Ruth, K., & Pizzagalli, D. A. (2009). Childhood adversity is associated with left basal ganglia dysfunction during reward anticipation in adulthood. Biological Psychiatry, 66(3), 206–213.

Dillon, D. G., & Pizzagalli, D. A. (2018). Mechanisms of memory disruption in depression. Trends in Neurosciences, 41(3), 137–149.

Disner, S. G., Beevers, C. G., Haigh, E. A., & Beck, A. T. (2011). Neural mechanisms of the cognitive model of depression. Nature Reviews Neuroscience, 12(8), 467–477.

Dixon, M. L., Moodie, C. A., Goldin, P. R., Farb, N., Heimberg, R. G., & Gross, J. J. (2020). Emotion regulation in social anxiety disorder: Reappraisal and acceptance of negative self-beliefs. Biological Psychiatry: Cognitive Neuroscience and Neuroimaging, 5(1), 119–129.

Dolcos, F., LaBar, K. S., & Cabeza, R. (2004). Interaction between the amygdala and the medial temporal lobe memory system predicts better memory for emotional events. Neuron, 42(5), 855–863.

DuBois, J. M., Rousset, O. G., Rowley, J., Porras-Betancourt, M., Reader, A. J., Labbe, A., Massarweh, G., Soucy, J.-P., Rosa-Neto, P., & Kobayashi, E. (2016). Characterization of age/sex and the regional distribution of mglur5 availability in the healthy human brain measured by high-resolution [11 c] abp688 pet. European Journal of Nuclear Medicine and Molecular Imaging, 43, 152–162.

Dudai, Y., Karni, A., & Born, J. (2015). The Consolidation and Transformation of Memory. Neuron, 88(1), 20–32.

Dukart, J., Holiga, Š., Chatham, C., Hawkins, P., Forsyth, A., McMillan, R., Myers, J., Lingford-Hughes, A. R., Nutt, D. J., & Merlo-Pich, E. (2018). Cerebral blood flow predicts differential neurotransmitter activity. Scientific Reports, 8(1), 4074.

Durrant, S. J., Cairney, S. A., McDermott, C., & Lewis, P. A. (2015). Schema-conformant memories are preferentially consolidated during REM sleep. Neurobiology of Learning and Memory, 122, 41–50.

Duyser, F. A., Eijndhoven, P. F. V., Collard, R. M., Vassena, E., Koekkoek, B., Tendolkar, I., & Vrijsen, J. N. (2025). Measuring Self-Referent Memory Bias as Marker for Depression: Overview, New Insights, and Recommendations. Journal of Psychopathology and Behavioral Assessment, 47(1), 10.

Duyser, F. A., Vrijsen, J. N., van Oort, J., Collard, R. M., Schene, A. H., Tendolkar, I., & van Eijndhoven, P. F. (2022). Amygdala sensitivity for negative information as a neural marker for negative memory bias across psychiatric diagnoses. Psychiatry Research: Neuroimaging, 323, 111481.

Duyser, F., Van Eijndhoven, P., Bergman, M., Collard, R., Schene, A., Tendolkar, I., & Vrijsen, J. (2020). Negative memory bias as a transdiagnostic cognitive marker for depression symptom severity. Journal of Affective Disorders, 274, 1165–1172.

E.

Edelmann, E., & Lessmann, V. (2018). Dopaminergic innervation and modulation of hippocampal networks. Cell and Tissue Research, 373, 711–727.

Elzinga, B. M., Roelofs, K., Tollenaar, M. S., Bakvis, P., van Pelt, J., & Spinhoven, P. (2008). Diminished cortisol responses to psychosocial stress associated with lifetime adverse events: A study among healthy young subjects. Psychoneuroendocrinology, 33(2), 227–237.

Erro, R., Pappatà, S., Amboni, M., Vicidomini, C., Longo, K., Santangelo, G., Picillo, M., Vitale, C., Moccia, M., & Giordano, F. (2012). Anxiety is associated with striatal dopamine transporter availability in newly diagnosed untreated Parkinson's disease patients. Parkinsonism & Related Disorders, 18(9), 1034–1038.

Evans, G. W., Li, D., & Whipple, S. S. (2013). Cumulative risk and child development. Psychological Bulletin, 139(6), 1342.

Everaerd, D., Klumpers, F., van Wingen, G., Tendolkar, I., & Fernández, G. (2015). Association between neuroticism and amygdala responsivity emerges under stressful conditions. Neuroimage, 112, 218–224.

Ewbank, M. P., Barnard, P. J., Croucher, C. J., Ramponi, C., & Calder, A. J. (2009). The amygdala response to images with impact. Social Cognitive and Affective Neuroscience, 4(2), 127–133.

F.

Fani, N., Bradley-Davino, B., Ressler, K. J., & McClure-Tone, E. B. (2011). Attention bias in adult survivors of childhood maltreatment with and without posttraumatic stress disorder. Cognitive Therapy and Research, 35, 57–67.

Fareri, D. S., Gabard-Durnam, L., Goff, B., Flannery, J., Gee, D. G., Lumian, D. S., Caldera, C., & Tottenham, N. (2017). Altered ventral striatal–medial prefrontal cortex resting-state connectivity mediates adolescent social problems after early institutional care. Development and Psychopathology, 29(5), 1865–1876.

Fazio, P., Schain, M., Varnäs, K., Halldin, C., Farde, L., & Varrone, A. (2016). Mapping the distribution of serotonin transporter in the human brainstem with high-resolution PET: validation using postmortem autoradiography data. Neuroimage, 133, 313–320.

Feder, A., Nestler, E. J., & Charney, D. S. (2009). Psychobiology and molecular genetics of resilience. Nature Reviews Neuroscience, 10(6), 446–457.

Fernández, G., & Morris, R. G. (2018). Memory, novelty and prior knowledge. Trends in Neurosciences, 41(10), 654–659.

Fisher, H. L., Jones, P. B., Fearon, P., Craig, T. K., Dazzan, P., Morgan, K., Hutchinson, G., Doody, G. A., McGuffin, P., & Leff, J. (2010). The varying impact of type, timing and frequency of exposure to childhood adversity on its association with adult psychotic disorder. Psychological Medicine, 40(12), 1967–1978.

Frick, A., Björkstrand, J., Lubberink, M., Eriksson, A., Fredrikson, M., & Åhs, F. (2022). Dopamine and fear memory formation in the human amygdala. Molecular Psychiatry, 27(3), 1704–1711.

Frühholz, S., Godde, B., Lewicki, P., Herzmann, C., & Herrmann, M. (2011). Face recognition under ambiguous visual stimulation: fMRI correlates of "encoding styles." Human Brain Mapping, 32(10), 1750–1761.

Funder, D. C., & Ozer, D. J. (2019). Evaluating effect size in psychological research: Sense and nonsense. Advances in Methods and Practices in Psychological Science, 2(2), 156–168.

G.

Gaddy, M. A., & Ingram, R. E. (2014). A meta-analytic review of mood-congruent implicit memory in depressed mood. Clinical Psychology Review, 34(5), 402–416.

Gálber, M., Anett Nagy, S., Orsi, G., Perlaki, G., Simon, M., & Czéh, B. (2024). Depressed patients with childhood maltreatment display altered intra- and inter-network resting state functional connectivity. NeuroImage: Clinical, 43, 103632.

Galovic, M., Erlandsson, K., Fryer, T. D., Hong, Y. T., Manavaki, R., Sari, H., Chetcuti, S., Thomas, B. A., Fisher, M., & Sephton, S. (2021). Validation of a combined image derived input function and venous sampling approach for the quantification of [18F] GE-179 PET binding in the brain. Neuroimage, 237, 118194.

Garavan, H., Pendergrass, J. C., Ross, T. J., Stein, E. A., & Risinger, R. C. (2001). Amygdala response to both positively and negatively valenced stimuli. Neuroreport, 12(12), 2779–2783.

Garrido Zinn, C., Clairis, N., Silva Cavalcante, L. E., Furini, C. R. G., de Carvalho Myskiw, J., & Izquierdo, I. (2016). Major neurotransmitter systems in dorsal hippocampus and basolateral amygdala control social recognition memory. Proceedings of the National Academy of Sciences, 113(33), E4914–E4919.

Gelfand, A. E., Diggle, P., Guttorp, P., & Fuentes, M. (2010). Handbook of spatial statistics. CRC press.

Gener, T., Campo, A. T., Alemany-González, M., Nebot, P., Delgado-Sallent, C., Chanovas, J., & Puig, M. V. (2019). Serotonin 5-HT1A, 5-HT2A and dopamine D2 receptors strongly influence prefronto-hippocampal neural networks in alert mice: Contribution to the actions of risperidone. Neuropharmacology, 158, 107743.

Gerritsen, L., Rijpkema, M., Van Oostrom, I., Buitelaar, J., Franke, B., Fernández, G., & Tendolkar, I. (2012). Amygdala to hippocampal volume ratio is associated with negative memory bias in healthy subjects. Psychological Medicine, 42(2), 335–343.

Gethin, J. A., Lythe, K. E., Workman, C. I., Mayes, A., Moll, J., & Zahn, R. (2017). Early life stress explains reduced positive memory biases in remitted depression. European Psychiatry, 45, 59–64.

Ghosh, V. E., & Gilboa, A. (2014). What is a memory schema? A historical perspective on current neuroscience literature. Neuropsychologia, 53, 104–114. https://doi.org/10.1016/j.neuropsychologia.2013.11.010

Ghosh, V. E., Moscovitch, M., Colella, B. M., & Gilboa, A. (2014). Schema representation in patients with ventromedial PFC lesions. Journal of Neuroscience, 34(36), 12057–12070.

Gignac, G. E., & Szodorai, E. T. (2016). Effect size guidelines for individual differences researchers. Personality and Individual Differences, 102, 74–78.

Gilboa, A., & Marlatte, H. (2017). Neurobiology of schemas and schema-mediated memory. Trends in Cognitive Sciences, 21(8), 618–631.

Gilboa, A., & Moscovitch, M. (2017). Ventromedial prefrontal cortex generates pre-stimulus theta coherence desynchronization: A schema instantiation hypothesis. Cortex, 87, 16–30.

Gillespie, C. F., Phifer, J., Bradley, B., & Ressler, K. J. (2009). Risk and resilience: Genetic and environmental influences on development of the stress response. Depression and Anxiety, 26(11), 984–992.

Ginty, A. T. (2013). Blunted responses to stress and reward: Reflections on biological disengagement? International Journal of Psychophysiology, 90(1), 90–94.

Ginty, A. T., Phillips, A. C., Higgs, S., Heaney, J. L., & Carroll, D. (2012). Disordered eating behaviour is associated with blunted cortisol and cardiovascular reactions to acute psychological stress. Psychoneuroendocrinology, 37(5), 715–724.

Goldway, N., Jalon, I., Keynan, J. N., Hellrung, L., Horstmann, A., Paret, C., & Hendler, T. (2022). Feasibility and utility of amygdala neurofeedback. Neuroscience & Biobehavioral Reviews, 138, 104694.

Gómez, F. J. G., Huertas, I., Ramírez, J. A. L., & Solís, D. G. (2018). Elaboración de una plantilla de SPM para la normalización de imágenes de PET con 18F-DOPA. Imagen Diagnóstica, 9(01), 23–25.

Gotlib, I. H., & Joormann, J. (2010). Cognition and depression: Current status and future directions. Annual Review of Clinical Psychology, 6(1), 285–312.

Gotlib, I. H., Kasch, K. L., Traill, S., Joormann, J., Arnow, B. A., & Johnson, S. L. (2004). Coherence and specificity of information-processing biases in depression and social phobia. Journal of Abnormal Psychology, 113(3), 386.

Gotlib, I. H., & Krasnoperova, E. (1998). Biased information processing as a vulnerability factor for depression. Behavior Therapy, 29(4), 603–617.

Gotlib, I. H., Krasnoperova, E., Yue, D. N., & Joormann, J. (2004). Attentional biases for negative interpersonal stimuli in clinical depression. Journal of Abnormal Psychology, 113(1), 127.

Graaf, R., Have, M. L., & van Dorsselaer, S. (2010). De psychische gezondheid van de Nederlandse bevolking: NEMESIS-2: Opzet en eerste resultaten. Trimbos-instituut [host].

Grant, M. M., Cannistraci, C., Hollon, S. D., Gore, J., & Shelton, R. (2011). Childhood trauma history differentiates amygdala response to sad faces within MDD. Journal of Psychiatric Research, 45(7), 886–895.

Grilli, M., Nisoli, E., Memo, M., Missale, C., & Spano, P. (1988). Pharmacological characterization of D1 and D2 dopamine receptors in rat limbocortical areas. II. Dorsal hippocampus. Neuroscience Letters, 87(3), 253–258.

Groenewold, N. A., Opmeer, E. M., de Jonge, P., Aleman, A., & Costafreda, S. G. (2013). Emotional valence modulates brain functional abnormalities in depression: Evidence from a meta-analysis of fMRI studies. Neuroscience & Biobehavioral Reviews, 37(2), 152–163.

Guarraci, F. A., Frohardt, R. J., & Kapp, B. S. (1999). Amygdaloid D1 dopamine receptor involvement in Pavlovian fear conditioning. Brain Research, 827(1–2), 28–40.

Guineau, M. G., Ikani, N., Rinck, M., Collard, R., Van Eijndhoven, P., Tendolkar, I., Schene, A., Becker, E., & Vrijsen, J. (2023). Anhedonia as a transdiagnostic symptom across psychological disorders: A network approach. Psychological Medicine, 53(9), 3908–3919.

Günther, V., Dannlowski, U., Kersting, A., & Suslow, T. (2015). Associations between childhood maltreatment and emotion processing biases in major depression: Results from a dot-probe task. BMC Psychiatry, 15, 1–9.

Guo, D., & Yang, J. (2020). Interplay of the long axis of the hippocampus and ventromedial prefrontal cortex in schema-related memory retrieval. Hippocampus, 30(3), 263–277.

Gur, R. E., Moore, T. M., Rosen, A. F., Barzilay, R., Roalf, D. R., Calkins, M. E., Ruparel, K., Scott, J. C., Almasy, L., & Satterthwaite, T. D. (2019). Burden of environmental adversity associated with psychopathology, maturation, and brain behavior parameters in youths. JAMA Psychiatry, 76(9), 966–975.

H.

Haak, K. V., Marquand, A. F., & Beckmann, C. F. (2018). Connectopic mapping with resting-state fMRI. NeuroImage, 170, 83–94.

Haber, S. N. (2003). The primate basal ganglia: Parallel and integrative networks. Journal of Chemical Neuroanatomy, 26(4), 317–330.

Haber, S. N., Fudge, J. L., & McFarland, N. R. (2000). Striatonigrostriatal pathways in primates form an ascending spiral from the shell to the dorsolateral striatum. Journal of Neuroscience, 20(6), 2369–2382.

Haber, S. N., Kim, K.-S., Mailly, P., & Calzavara, R. (2006). Reward-related cortical inputs define a large striatal region in primates that interface with associative cortical connections, providing a substrate for incentive-based learning. Journal of Neuroscience, 26(32), 8368–8376.

Hagborg, J. M., Kalin, T., & Gerdner, A. (2022). The Childhood Trauma Questionnaire—Short Form (CTQ-SF) used with adolescents–methodological report from clinical and community samples. Journal of Child & Adolescent Trauma, 15(4), 1199–1213.

Hamilton, J. P., & Gotlib, I. H. (2008). Neural substrates of increased memory sensitivity for negative stimuli in major depression. Biological Psychiatry, 63(12), 1155–1162.

Hammen, C., & Zupan, B. A. (1984). Self-schemas, depression, and the processing of personal information in children. Journal of Experimental Child Psychology, 37(3), 598–608.

Hansen, J. Y., Shafiei, G., Markello, R. D., Smart, K., Cox, S. M., Nørgaard, M., Beliveau, V., Wu, Y., Gallezot, J.-D., & Aumont, É. (2022). Mapping neurotransmitter systems to the structural and functional organization of the human neocortex. Nature Neuroscience, 25(11), 1569–1581.

Hanson, J. L., Albert, W. D., Skinner, A. T., Shen, S. H., Dodge, K. A., & Lansford, J. E. (2019). Resting state coupling between the amygdala and ventromedial prefrontal cortex is related to household income in childhood and indexes future psychological vulnerability to stress. Development and Psychopathology, 31(3), 1053–1066.

Hanson, J. L., Hariri, A. R., & Williamson, D. E. (2015). Blunted ventral striatum development in adolescence reflects emotional neglect and predicts depressive symptoms. Biological Psychiatry, 78(9), 598–605.

Hanson, J. L., Knodt, A. R., Brigidi, B. D., & Hariri, A. R. (2018). Heightened connectivity between the ventral striatum and medial prefrontal cortex as a biomarker for stress-related psychopathology: Understanding interactive effects of early and more recent stress. Psychological Medicine, 48(11), 1835–1843.

Hariri, A. R., Tessitore, A., Mattay, V. S., Fera, F., & Weinberger, D. R. (2002). The amygdala response to emotional stimuli: A comparison of faces and scenes. Neuroimage, 17(1), 317–323.

Healthy Brain Study consortium, Aarts, E., Akkerman, A., Altgassen, M., Bartels, R., Beckers, D., Bevelander, K., Bijleveld, E., Blaney Davidson, E., & Boleij, A. (2021). Protocol of the Healthy Brain Study: An accessible resource for understanding the human brain and how it dynamically and individually operates in its bio-social context. Plos One, 16(12), e0260952.

Heller, A. S., Johnstone, T., Shackman, A. J., Light, S. N., Peterson, M. J., Kolden, G. G., Kalin, N. H., & Davidson, R. J. (2009). Reduced capacity to sustain positive emotion in major depression reflects diminished maintenance of fronto-striatal brain activation. Proceedings of the National Academy of Sciences, 106(52), 22445–22450.

Hennies, N., Ralph, M. A. L., Kempkes, M., Cousins, J. N., & Lewis, P. A. (2016). Sleep spindle density predicts the effect of prior knowledge on memory consolidation. Journal of Neuroscience, 36(13), 3799–3810.

Hermans, E. J., Van Marle, H. J., Ossewaarde, L., Henckens, M. J., Qin, S., Van Kesteren, M. T., Schoots, V. C., Cousijn, H., Rijpkema, M., Oostenveld, R., & Fernández, G. (2011). Stress-related noradrenergic activity prompts large-scale neural network reconfiguration. Science, 334(6059), 1151–1153.

Herringa, R. J., Birn, R. M., Ruttle, P. L., Burghy, C. A., Stodola, D. E., Davidson, R. J., & Essex, M. J. (2013). Childhood maltreatment is associated with altered fear circuitry and increased internalizing symptoms by late adolescence. Proceedings of the National Academy of Sciences, 110(47), 19119–19124.

Hertel, P., Mor, N., Ferrari, C., Hunt, O., & Agrawal, N. (2014). Looking on the dark side: Rumination and cognitive-bias modification. Clinical Psychological Science, 2(6), 714–726.

Hertel, P. T., Maydon, A., Cottle, J., & Vrijsen, J. N. (2017). Cognitive bias modification: Retrieval practice to simulate and oppose ruminative memory biases. Clinical Psychological Science, 5(1), 122–130.

Herzberg, M. P., & Gunnar, M. R. (2020). Early life stress and brain function: Activity and connectivity associated with processing emotion and reward. NeuroImage, 209, 116493.

Hesse, S., Becker, G.-A., Rullmann, M., Bresch, A., Luthardt, J., Hankir, M. K., Zientek, F., Reißig, G., Patt, M., & Arelin, K. (2017). Central noradrenaline transporter availability in highly obese, non-depressed individuals. European Journal of Nuclear Medicine and Molecular Imaging, 44, 1056–1064.

Hovens, J. G., Wiersma, J. E., Giltay, E. J., Van Oppen, P., Spinhoven, P., Penninx, B. W., & Zitman, F. G. (2010). Childhood life events and childhood trauma in adult patients with depressive, anxiety and comorbid disorders vs. Controls. Acta Psychiatrica Scandinavica, 122(1), 66–74.

Hrybouski, S., Aghamohammadi-Sereshki, A., Madan, C. R., Shafer, A. T., Baron, C. A., Seres, P., Beaulieu, C., Olsen, F., & Malykhin, N. V. (2016). Amygdala subnuclei response and connectivity during emotional processing. Neuroimage, 133, 98–110.

Humphreys, K. L., & Zeanah, C. H. (2015). Deviations from the expectable environment in early childhood and emerging psychopathology. Neuropsychopharmacology, 40(1), 154–170.

I.

Insel, T., Cuthbert, B., Garvey, M., Heinssen, R., Pine, D. S., Quinn, K., Sanislow, C., & Wang, P. (2010). Research domain criteria (RDoC): Toward a new classification framework for research on mental disorders. American Journal of Psychiatry, 167(7), 748–751.

Izquierdo, I., Medina, J. H., Bianchin, M., Walz, R., Zanatta, M. S., Da Silva, R. C., Silva, M. B. E., Ruschel, A. C., & Paczko, N. (1993). Memory processing by the limbic system: Role of specific neurotransmitter systems. Behavioural Brain Research, 58(1–2), 91–98.

J.

Jenkinson, M., Bannister, P., Brady, M., & Smith, S. (2002). Improved optimization for the robust and accurate linear registration and motion correction of brain images. Neuroimage, 17(2), 825–841.

Jenkinson, M., Beckmann, C. F., Behrens, T. E., Woolrich, M. W., & Smith, S. M. (2012). Fsl. Neuroimage, 62(2), 782–790.

Jonnakuty, C., & Gragnoli, C. (2008). What do we know about serotonin? Journal of Cellular Physiology, 217(2), 301–306.

Jovanovic, H., Perski, A., Berglund, H., & Savic, I. (2011). Chronic stress is linked to 5-HT1A receptor changes and functional disintegration of the limbic networks. Neuroimage, 55(3), 1178–1188.

K.

Kalisch, R., Russo, S. J., & Müller, M. B. (2024). Neurobiology and systems biology of stress resilience. Physiological Reviews, 104(3), 1205–1263.

Kaller, S., Rullmann, M., Patt, M., Becker, G.-A., Luthardt, J., Girbardt, J., Meyer, P. M., Werner, P., Barthel, H., & Bresch, A. (2017). Test–retest measurements of dopamine d 1-type receptors using simultaneous pet/mri imaging. European Journal of Nuclear Medicine and Molecular Imaging, 44, 1025–1032.

Kantonen, T., Karjalainen, T., Isojärvi, J., Nuutila, P., Tuisku, J., Rinne, J., Hietala, J., Kaasinen, V., Kalliokoski, K., & Scheinin, H. (2020). Interindividual variability and lateralization of μ-opioid receptors in the human brain. Neuroimage, 217, 116922.

Kark, S. M., & Kensinger, E. A. (2019). Post-encoding amygdala-visuosensory coupling is associated with negative memory bias in healthy young adults. Journal of Neuroscience, 39(16), 3130–3143.

Kellough, J. L., Beevers, C. G., Ellis, A. J., & Wells, T. T. (2008). Time course of selective attention in clinically depressed young adults: An eye tracking study. Behaviour Research and Therapy, 46(11), 1238–1243.

Kensinger, E. A. (2007). Negative emotion enhances memory accuracy: Behavioral and neuroimaging evidence. Current Directions in Psychological Science, 16(4), 213–218.

Kensinger, E. A., Addis, D. R., & Atapattu, R. K. (2011). Amygdala activity at encoding corresponds with memory vividness and with memory for select episodic details. Neuropsychologia, 49(4), 663–673.

Kishi, T., Tsumori, T., Yokota, S., & Yasui, Y. (2006). Topographical projection from the hippocampal formation to the amygdala: A combined anterograde and retrograde tracing study in the rat. Journal of Comparative Neurology, 496(3), 349–368.

Kist, J., Vrijsen, J., Mulders, P., van Eijndhoven, P., Tendolkar, I., & Collard, R. (2023). Transdiagnostic psychiatry: Symptom profiles and their direct and indirect relationship with well-being. Journal of Psychiatric Research, 161, 218–227.

Klengel, T., & Binder, E. B. (2015). Epigenetics of stress-related psychiatric disorders and gene× environment interactions. Neuron, 86(6), 1343–1357.

Ko, S. Y., Rong, Y., Ramsaran, A. I., Chen, X., Rashid, A. J., Mocle, A. J., Dhaliwal, J., Awasthi, A., Guskjolen, A., Josselyn, S. A., & Frankland, P. W. (2025). Systems consolidation reorganizes hippocampal engram circuitry. Nature, 1–9.

Kohn, N., Eickhoff, S. B., Scheller, M., Laird, A. R., Fox, P. T., & Habel, U. (2014). Neural network of cognitive emotion regulation—An ALE meta-analysis and MACM analysis. Neuroimage, 87, 345–355.

Kohn, N., Kellermann, T., Gur, R. C., Schneider, F., & Habel, U. (2011). Gender differences in the neural correlates of humor processing: Implications for different processing modes. Neuropsychologia, 49(5), 888–897.

Korkeila, J., Vahtera, J., Nabi, H., Kivimäki, M., Korkeila, K., Sumanen, M., Koskenvuo, K., & Koskenvuo, M. (2010). Childhood adversities, adulthood life events and depression. Journal of Affective Disorders, 127(1–3), 130–138.

Krenz, V., Sommer, T., Alink, A., Roozendaal, B., & Schwabe, L. (2021). Noradrenergic arousal after encoding reverses the course of systems consolidation in humans. Nature Communications, 12(1), 6054.

Krugers, H. J., Karst, H., & Joels, M. (2012). Interactions between noradrenaline and corticosteroids in the brain: From electrical activity to cognitive performance. Frontiers in Cellular Neuroscience, 6, 15.

Kube, T., Schwarting, R., Rozenkrantz, L., Glombiewski, J. A., & Rief, W. (2020). Distorted cognitive processes in major depression: A predictive processing perspective. Biological Psychiatry, 87(5), 388–398.

Kuo, J. R., Edge, I. G., Ramel, W., Edge, M. D., Drabant, E. M., Dayton, W. M., & Gross, J. J. (2012). Trait rumination is associated with enhanced recollection of negative words. Cognitive Therapy and Research, 36, 722–730.

Kuznetsova, A., Brockhoff, P. B., & Christensen, R. H. (2017). lmerTest package: Tests in linear mixed effects models. Journal of Statistical Software, 82, 1–26.

L.

LaBar, K. S., & Cabeza, R. (2006). Cognitive neuroscience of emotional memory. Nature Reviews Neuroscience, 7(1), 54–64.

Lambert, H. K., Peverill, M., Sambrook, K. A., Rosen, M. L., Sheridan, M. A., & McLaughlin, K. A. (2019). Altered development of hippocampus-dependent associative learning following early-life adversity. Developmental Cognitive Neuroscience, 38, 100666.

Lambert, H. K., Sheridan, M. A., Sambrook, K. A., Rosen, M. L., Askren, M. K., & McLaughlin, K. A. (2017). Hippocampal contribution to context encoding across development is disrupted following early-life adversity. Journal of Neuroscience, 37(7), 1925–1934.

Lang, P. J., Bradley, M. M., & Cuthbert, B. N. (1997). International affective picture system (IAPS): Technical manual and affective ratings. NIMH Center for the Study of Emotion and Attention, 1(39–58), 3.

Laurikainen, H., Tuominen, L., Tikka, M., Merisaari, H., Armio, R.-L., Sormunen, E., Borgan, F., Veronese, M., Howes, O., & Haaparanta-Solin, M. (2019). Sex difference in brain CB1 receptor availability in man. Neuroimage, 184, 834–842.

Lemogne, C., Delaveau, P., Freton, M., Guionnet, S., & Fossati, P. (2012). Medial prefrontal cortex and the self in major depression. Journal of Affective Disorders, 136(1–2), e1–e11.

Leppänen, J. M. (2006). Emotional information processing in mood disorders: A review of behavioral and neuroimaging findings. Current Opinion in Psychiatry, 19(1), 34–39.

Letkiewicz, A. M., Silton, R. L., Mimnaugh, K. J., Miller, G. A., Heller, W., Fisher, J., & Sass, S. M. (2020). Childhood abuse history and attention bias in adults. Psychophysiology, 57(10), e13627.

Likhtik, E., & Paz, R. (2015). Amygdala–prefrontal interactions in (mal) adaptive learning. Trends in Neurosciences, 38(3), 158–166.

Liu, X., Chen, X., Cheng, J., Wei, F., Hou, H., Li, J., Liu, K., Guo, Z., Yan, Z., & Wu, A. (2025). Functional connectivity gradients and neurotransmitter maps among patients with mild cognitive impairment and depression symptoms. Journal of Psychiatry and Neuroscience, 50(1), E11–E20.

Loos, E., Schicktanz, N., Fastenrath, M., Coynel, D., Milnik, A., Fehlmann, B., Egli, T., Ehrler, M., Papassotiropoulos, A., & de Quervain, D. J.-F. (2020). Reducing Amygdala Activity and Phobic Fear through Cognitive Top–Down Regulation. Journal of Cognitive Neuroscience, 32(6), 1117–1129.

Lovallo, W. R. (2013). Early life adversity reduces stress reactivity and enhances impulsive behavior: Implications for health behaviors. International Journal of Psychophysiology, 90(1), 8–16.

Lovallo, W. R., Farag, N. H., Sorocco, K. H., Cohoon, A. J., & Vincent, A. S. (2012). Lifetime Adversity Leads to Blunted Stress Axis Reactivity: Studies from the Oklahoma Family Health Patterns Project. Biological Psychiatry, 71(4), 344–349.

Luo, Q., Chen, J., Li, Y., Wu, Z., Lin, X., Yao, J., Yu, H., Wu, H., & Peng, H. (2022). Aberrant brain connectivity is associated with childhood maltreatment in individuals with major depressive disorder. Brain Imaging and Behavior, 16(5), 2021–2036.

Luo, Q., Zou, Y., Nie, H., Wu, H., Du, Y., Chen, J., Li, Y., & Peng, H. (2023). Effects of childhood neglect on regional brain activity and corresponding functional connectivity in major depressive disorder and healthy people: Risk factor or resilience? Journal of Affective Disorders, 340, 792–801.

M.

Madras, B. K., Miller, G. M., & Fischman, A. J. (2005). The dopamine transporter and attention-deficit/hyperactivity disorder. Biological Psychiatry, 57(11), 1397–1409.

Mahalanobis, P. C. (1930). On tests and measures of group divergence. J. Asiat. Soc. Bengal, 26, 541–588.

Maren, S., Phan, K. L., & Liberzon, I. (2013). The contextual brain: Implications for fear conditioning, extinction and psychopathology. Nature Reviews Neuroscience, 14(6), 417–428.

Marquand, A. F., Haak, K. V., & Beckmann, C. F. (2017). Functional corticostriatal connection topographies predict goal-directed behaviour in humans. Nature Human Behaviour, 1(8), 0146.

Marshall, N. A., Marusak, H. A., Sala-Hamrick, K. J., Crespo, L. M., Rabinak, C. A., & Thomason, M. E. (2018). Socioeconomic disadvantage and altered corticostriatal circuitry in urban youth. Human Brain Mapping, 39(5), 1982–1994.

Marusak, H. A., Etkin, A., & Thomason, M. E. (2015). Disrupted insula-based neural circuit organization and conflict interference in trauma-exposed youth. NeuroImage: Clinical, 8, 516–525.

Matheson, S., Shepherd, A. M., Pinchbeck, R., Laurens, K., & Carr, V. J. (2013). Childhood adversity in schizophrenia: A systematic meta-analysis. Psychological Medicine, 43(2), 225–238.

Mathews, A., & MacLeod, C. (2005). Cognitive vulnerability to emotional disorders. Annu. Rev. Clin. Psychol., 1(1), 167–195.

Matt, G. E., Vázquez, C., & Campbell, W. K. (1992). Mood-congruent recall of affectively toned stimuli: A meta-analytic review. Clinical Psychology Review, 12(2), 227–255.

McCrory, E. J., De Brito, S. A., Sebastian, C. L., Mechelli, A., Bird, G., Kelly, P. A., & Viding, E. (2011). Heightened neural reactivity to threat in child victims of family violence. Current Biology, 21(23), R947–R948.

McKay, M. T., Kilmartin, L., Meagher, A., Cannon, M., Healy, C., & Clarke, M. C. (2022). A revised and extended systematic review and meta-analysis of the relationship between childhood adversity and adult psychiatric disorder. Journal of Psychiatric Research, 156, 268–283.

McLaughlin, K. A. (2018). Future directions in childhood adversity and youth psychopathology. In Future work in clinical child and adolescent psychology (pp. 345–366). Routledge.

McLaughlin, K. A., Colich, N. L., Rodman, A. M., & Weissman, D. G. (2020). Mechanisms linking childhood trauma exposure and psychopathology: A transdiagnostic model of risk and resilience. BMC Medicine, 18, 1–11.

McLaughlin, K. A., Green, J. G., Gruber, M. J., Sampson, N. A., Zaslavsky, A. M., & Kessler, R. C. (2010). Childhood adversities and adult psychopathology in the National Comorbidity Survey Replication (NCS-R) III: associations with functional impairment related to DSM-IV disorders. Psychological Medicine, 40(5), 847–859.

McLaughlin, K. A., Peverill, M., Gold, A. L., Alves, S., & Sheridan, M. A. (2015). Child Maltreatment and Neural Systems Underlying Emotion Regulation. Journal of the American Academy of Child & Adolescent Psychiatry, 54(9), 753–762.

McLaughlin, K. A., & Sheridan, M. A. (2016). Beyond cumulative risk: A dimensional approach to childhood adversity. Current Directions in Psychological Science, 25(4), 239–245.

McLaughlin, K. A., Sheridan, M. A., & Lambert, H. K. (2014). Childhood adversity and neural development: Deprivation and threat as distinct dimensions of early experience. Neuroscience & Biobehavioral Reviews, 47, 578–591.

McLaughlin, K. A., Sheridan, M. A., Winter, W., Fox, N. A., Zeanah, C. H., & Nelson, C. A. (2014). Widespread Reductions in Cortical Thickness Following Severe Early-Life Deprivation: A Neurodevelopmental Pathway to Attention-Deficit/Hyperactivity Disorder. Biological Psychiatry, 76(8), 629–638.

McLaughlin, K. A., Weissman, D., & Bitrán, D. (2019). Childhood adversity and neural development: A systematic review. Annual Review of Developmental Psychology, 1(1), 277–312.

Monteleone, A. M., Monteleone, P., Esposito, F., Prinster, A., Ruzzi, V., Canna, A., Aiello, M., Di Salle, F., & Maj, M. (2019). The effects of childhood maltreatment on brain structure in adults with eating disorders. The World Journal of Biological Psychiatry.

Moreno-López, L., Ioannidis, K., Askelund, A. D., Smith, A. J., Schueler, K., & Van Harmelen, A.-L. (2020). The resilient emotional brain: A scoping review of the medial prefrontal cortex and limbic structure and function in resilient adults with a history of childhood maltreatment. Biological Psychiatry: Cognitive Neuroscience and Neuroimaging, 5(4), 392–402.

Moriarity, D. P., Ng, T., Titone, M. K., Chat, I. K.-Y., Nusslock, R., Miller, G. E., & Alloy, L. B. (2020). Reward responsiveness and ruminative styles interact to predict inflammation and mood symptomatology. Behavior Therapy, 51(5), 829–842.

Morina, N., Lancee, J., & Arntz, A. (2017). Imagery rescripting as a clinical intervention for aversive memories: A meta-analysis. Journal of Behavior Therapy and Experimental Psychiatry, 55, 6–15.

Moscovitch, D. A., Moscovitch, M., & Sheldon, S. (2023). Neurocognitive Model of Schema-Congruent and -Incongruent Learning in Clinical Disorders: Application to Social Anxiety and Beyond. Perspectives on Psychological Science, 18(6), 1412–1435.

Moscovitch, M., Cabeza, R., Winocur, G., & Nadel, L. (2016). Episodic memory and beyond: The hippocampus and neocortex in transformation. Annual Review of Psychology, 67(1), 105–134.

Mulders, P. C., van Eijndhoven, P. F., Schene, A. H., Beckmann, C. F., & Tendolkar, I. (2015). Resting-state functional connectivity in major depressive disorder: A review. Neuroscience & Biobehavioral Reviews, 56, 330–344.

Mulders, P. C., van Eijndhoven, P. F., van Oort, J., Oldehinkel, M., Duyser, F. A., Kist, J. D., Collard, R. M., Vrijsen, J. N., Haak, K. V., & Beckmann, C. F. (2022). Striatal connectopic maps link to functional domains across psychiatric disorders. Translational Psychiatry, 12(1), 513.

N.

Nelson, C. A., Sullivan, E. F., & Valdes, V. (2025). Early adversity alters brain architecture and increases susceptibility to mental health disorders. Nature Reviews Neuroscience, 1–15.

Ng, T. H., Alloy, L. B., & Smith, D. V. (2019). Meta-analysis of reward processing in major depressive disorder reveals distinct abnormalities within the reward circuit. Translational Psychiatry, 9(1), 293.

Nolen-Hoeksema, S., Wisco, B. E., & Lyubomirsky, S. (2008). Rethinking rumination. Perspectives on Psychological Science, 3(5), 400–424.

Nordin, K., Pedersen, R., Falahati, F., Johansson, J., Grill, F., Andersson, M., Korkki, S. M., Bäckman, L., Zalesky, A., & Rieckmann, A. (2025). Two long-axis dimensions of hippocampal-cortical integration support memory function across the adult lifespan. eLife, 13, RP97658.

Norman, R. E., Byambaa, M., De, R., Butchart, A., Scott, J., & Vos, T. (2012). The long-term health consequences of child physical abuse, emotional abuse, and neglect: A systematic review and meta-analysis. PLoS Medicine, 9(11), e1001349.

O.

Ögren, S. O., Eriksson, T. M., Elvander-Tottie, E., D'Addario, C., Ekström, J. C., Svenningsson, P., Meister, B., Kehr, J., & Stiedl, O. (2008). The role of 5-HT1A receptors in learning and memory. Behavioural Brain Research, 195(1), 54–77.

Oldehinkel, M., Llera, A., Faber, M., Huertas, I., Buitelaar, J. K., Bloem, B. R., Marquand, A. F., Helmich, R. C., Haak, K. V., & Beckmann, C. F. (2022). Mapping dopaminergic projections in the human brain with resting-state fMRI. Elife, 11, e71846.

Oltean, L.-E., Șoflău, R., Miu, A. C., & Szentágotai-Tătar, A. (2023). Childhood adversity and impaired reward processing: A meta-analysis. Child Abuse & Neglect, 142, 105596.

P.

Panksepp, J., Lane, R. D., Solms, M., & Smith, R. (2017). Reconciling cognitive and affective neuroscience perspectives on the brain basis of emotional experience. Neuroscience & Biobehavioral Reviews, 76, 187–215.

Parsey, R. V., Olvet, D. M., Oquendo, M. A., Huang, Y., Ogden, R. T., & Mann, J. J. (2006). Higher 5-HT1A receptor binding potential during a major depressive episode predicts poor treatment response: Preliminary data from a naturalistic study. Neuropsychopharmacology, 31(8), 1745–1749.

Pesonen, A.-K., Kajantie, E., Jones, A., Pyhälä, R., Lahti, J., Heinonen, K., Eriksson, J. G., Strandberg, T. E., & Räikkönen, K. (2011). Symptoms of attention deficit hyperactivity disorder in children are associated with cortisol responses to psychosocial stress but not with daily cortisol levels. Journal of Psychiatric Research, 45(11), 1471–1476.

Phelps, E. A. (2004). Human emotion and memory: Interactions of the amygdala and hippocampal complex. Current Opinion in Neurobiology, 14(2), 198–202.

Phillips, A. C., Hunt, K., Der, G., & Carroll, D. (2011). Blunted cardiac reactions to acute psychological stress predict symptoms of depression five years later: Evidence from a large community study. Psychophysiology, 48(1), 142–148.

Piaget, J. (1953). The origin of intelligence in the child / (M. Cook, Ed.). Routledge & Kegan Paul,.

Pine, D. S., Mogg, K., Bradley, B. P., Montgomery, L., Monk, C. S., McClure, E., Guyer, A. E., Ernst, M., Charney, D. S., & Kaufman, J. (2005). Attention bias to threat in maltreated children: Implications for vulnerability to stress-related psychopathology. American Journal of Psychiatry, 162(2), 291–296.

Popova, N. K., & Naumenko, V. S. (2013). 5-HT1A receptor as a key player in the brain 5-HT system. Reviews in the Neurosciences, 24(2), 191–204.

Poppenk, J., Evensmoen, H. R., Moscovitch, M., & Nadel, L. (2013). Long-axis specialization of the human hippocampus. Trends in Cognitive Sciences, 17(5), 230–240.

Pronier, É., Morici, J. F., & Girardeau, G. (2023). The role of the hippocampus in the consolidation of emotional memories during sleep. Trends in Neurosciences, 46(11), 912–925.

Pruim, R. H., Mennes, M., van Rooij, D., Llera, A., Buitelaar, J. K., & Beckmann, C. F. (2015). ICA-AROMA: A robust ICA-based strategy for removing motion artifacts from fMRI data. Neuroimage, 112, 267–277.

Przeździk, I., Faber, M., Fernández, G., Beckmann, C. F., & Haak, K. V. (2019). The functional organisation of the hippocampus along its long axis is gradual and predicts recollection. Cortex, 119, 324–335.

Puglisi-Allegra, S., & Andolina, D. (2015). Serotonin and stress coping. Behavioural Brain Research, 277, 58–67.

Purves, D., Augustine, G. J., Fitzpatrick, D., Katz, L. C., LaMantia, A.-S., McNamara, J. O., & Williams, S. M. (2001). Neurotransmitters. In Neuroscience. 2nd edition. Sinauer Associates.

Q.

Qasim, S. E., Mohan, U. R., Stein, J. M., & Jacobs, J. (2023). Neuronal activity in the human amygdala and hippocampus enhances emotional memory encoding. Nature Human Behaviour, 7(5), 754–764.

Qin, P., & Northoff, G. (2011). How is our self related to midline regions and the default-mode network? NeuroImage, 57(3), 1221–1233.

Qin, S., Hermans, E. J., Van Marle, H. J., Luo, J., & Fernández, G. (2009). Acute psychological stress reduces working memory-related activity in the dorsolateral prefrontal cortex. Biological Psychiatry, 66(1), 25–32.

R.

R Core Team. (2024). R: A language and environment for statistical computing (Version 4.3.3) [Computer software]. R Foundation for Statistical Computing. https://www.R project.org/

Raine, A. (1996). Autonomic nervous system factors underlying disinhibited, antisocial, and violent behavior. Biosocial perspectives and treatment implications. Annals of the New York Academy of Sciences, 794, 46–59.

Rajarethinam, R., DeQuardo, J. R., Miedler, J., Arndt, S., Kirbat, R., Brunberg, J. A., & Tandon, R. (2001). Hippocampus and amygdala in schizophrenia: Assessment of the relationship of neuroanatomy to psychopathology. Psychiatry Research: Neuroimaging, 108(2), 79–87.

Ralph, M. A. L., Jefferies, E., Patterson, K., & Rogers, T. T. (2017). The neural and computational bases of semantic cognition. Nature Reviews Neuroscience, 18(1), 42–55.

Ramel, W., Goldin, P. R., Eyler, L. T., Brown, G. G., Gotlib, I. H., & McQuaid, J. R. (2007). Amygdala reactivity and mood-congruent memory in individuals at risk for depressive relapse. Biological Psychiatry, 61(2), 231–239.

Rauch, S. L., Shin, L. M., & Phelps, E. A. (2006). Neurocircuitry models of posttraumatic stress disorder and extinction: Human neuroimaging research—Past, present, and future. Biological Psychiatry, 60(4), 376–382.

Raymond, C., Marin, M.-F., Majeur, D., & Lupien, S. (2018). Early child adversity and psychopathology in adulthood: HPA axis and cognitive dysregulations as potential mechanisms. Progress in Neuro-Psychopharmacology and Biological Psychiatry, 85, 152–160.

Richardson, M. P., Strange, B. A., & Dolan, R. J. (2004). Encoding of emotional memories depends on amygdala and hippocampus and their interactions. Nature Neuroscience, 7(3), 278–285.

Riem, M. M., Alink, L. R., Out, D., Van Ijzendoorn, M. H., & Bakermans-Kranenburg, M. J. (2015). Beating the brain about abuse: Empirical and meta-analytic studies of the association between maltreatment and hippocampal volume across childhood and adolescence. Development and Psychopathology, 27(2), 507–520.

Rizvi, S. J., Pizzagalli, D. A., Sproule, B. A., & Kennedy, S. H. (2016). Assessing anhedonia in depression: Potentials and pitfalls. Neuroscience & Biobehavioral Reviews, 65, 21–35.

Rodriguez, B. F., Bruce, S. E., Pagano, M. E., Spencer, M. A., & Keller, M. B. (2004). Factor structure and stability of the Anxiety Sensitivity Index in a longitudinal study of anxiety disorder patients. Behaviour Research and Therapy, 42(1), 79–91.

Roediger, H. L., & Butler, A. C. (2011). The critical role of retrieval practice in long-term retention. Trends in Cognitive Sciences, 15(1), 20–27.

Roozendaal, B., McEwen, B. S., & Chattarji, S. (2009). Stress, memory and the amygdala. Nature Reviews Neuroscience, 10(6), 423–433.

Roy, A. K., Shehzad, Z., Margulies, D. S., Kelly, A. C., Uddin, L. Q., Gotimer, K., Biswal, B. B., Castellanos, F. X., & Milham, M. P. (2009). Functional connectivity of the human amygdala using resting state fMRI. Neuroimage, 45(2), 614–626.

RStudio Team. (2024). RStudio: Integrated Development Environment for R (Version 2024.4.2.764) [Computer software]. https://posit.co/downloads/

Ruiz-Caballero, J. A., & Gonzilez, P. (1994). Implicit and explicit memory bias in depressed and non depressed subjects. Cognition & Emotion, 8(6), 555–569.

Rumelhart, D. E., & Ortony, A. (2017). The representation of knowledge in memory 1. In Schooling and the acquisition of knowledge (pp. 99–135). Routledge.

Rush, A. J., Carmody, T., & Reimitz, P. (2000). The Inventory of Depressive Symptomatology (IDS): Clinician (IDS-C) and self-report (IDS-SR) ratings of depressive symptoms. International Journal of Methods in Psychiatric Research, 9(2), 45–59.

Russell, G., & Lightman, S. (2019). The human stress response. Nature Reviews Endocrinology, 15(9), 525–534.

Rutherford, A. V., McDougle, S. D., & Joormann, J. (2023). "Don't [ruminate], be happy": A cognitive perspective linking depression and anhedonia. Clinical Psychology Review, 101, 102255.

Rutishauser, U., Mamelak, A. N., & Schuman, E. M. (2006). Single-trial learning of novel stimuli by individual neurons of the human hippocampus-amygdala complex. Neuron, 49(6), 805–813.

S.

Sætren, S. S., Bjørnestad, J. R., Ottesen, A. A., Fisher, H. L., Olsen, D. A., Hølland, K., & Hegelstad, W. ten V. (2024). Unraveling the concept of childhood adversity in psychosis research: A systematic review. Schizophrenia Bulletin, 50(5), 1055–1066.

Sahle, B. W., Reavley, N. J., Li, W., Morgan, A. J., Yap, M. B. H., Reupert, A., & Jorm, A. F. (2021). The association between adverse childhood experiences and common mental disorders and suicidality: An umbrella review of systematic reviews and meta-analyses. European Child & Adolescent Psychiatry, 1–11.

Sarason, I. G., Pierce, G. R., & Sarason, B. R. (2014). Cognitive interference: Theories, methods, and findings. Routledge.

Savitz, J. B., & Drevets, W. C. (2013). Neuroreceptor imaging in depression. Neurobiology of Disease, 52, 49–65.

Savli, M., Bauer, A., Mitterhauser, M., Ding, Y.-S., Hahn, A., Kroll, T., Neumeister, A., Haeusler, D., Ungersboeck, J., & Henry, S. (2012). Normative database of the serotonergic system in healthy subjects using multi-tracer PET. Neuroimage, 63(1), 447–459.

Saxbe, D., Khoddam, H., Piero, L. D., Stoycos, S. A., Gimbel, S. I., Margolin, G., & Kaplan, J. T. (2018). Community violence exposure in early adolescence: Longitudinal associations with hippocampal and amygdala volume and resting state connectivity. Developmental Science, 21(6), e12686.

Schaefer, H. S., Putnam, K. M., Benca, R. M., & Davidson, R. J. (2006). Event-related functional magnetic resonance imaging measures of neural activity to positive social stimuli in pre-and post-treatment depression. Biological Psychiatry, 60(9), 974–986.

Sheldon, S., Atack, L., Ngo, N., Moscovitch, M., & Moscovitch, D. A. (2024). Targeting schema change in social anxiety via autobiographical memory reconstruction. Cognition and Emotion, 1–9.

Sheline, Y. I., Barch, D. M., Price, J. L., Rundle, M. M., Vaishnavi, S. N., Snyder, A. Z., Mintun, M. A., Wang, S., Coalson, R. S., & Raichle, M. E. (2009). The default mode network and self-referential processes in depression. Proceedings of the National Academy of Sciences, 106(6), 1942–1947.

Sheridan, M. A., Peverill, M., Finn, A. S., & McLaughlin, K. A. (2017). Dimensions of childhood adversity have distinct associations with neural systems underlying executive functioning. Development and Psychopathology, 29(5), 1777–1794.

Shestyuk, A. Y., Deldin, P. J., Brand, J. E., & Deveney, C. M. (2005). Reduced sustained brain activity during processing of positive emotional stimuli in major depression. Biological Psychiatry, 57(10), 1089–1096.

Shin, L. M., & Liberzon, I. (2010). The neurocircuitry of fear, stress, and anxiety disorders. Neuropsychopharmacology, 35(1), 169–191.

Shokri-Kojori, E., Naganawa, M., Ramchandani, V. A., Wong, D. F., Wang, G., & Volkow, N. D. (2022). Brain opioid segments and striatal patterns of dopamine release induced by naloxone and morphine. Human Brain Mapping, 43(4), 1419–1430.

Siegle, G. J., Steinhauer, S. R., Thase, M. E., Stenger, V. A., & Carter, C. S. (2002). Can't shake that feeling: Event-related fMRI assessment of sustained amygdala activity in response to emotional information in depressed individuals. Biological Psychiatry, 51(9), 693–707.

Sijtsema, J. J., Van Roon, A. M., Groot, P. F. C., & Riese, H. (2015). Early life adversities and adolescent antisocial behavior: The role of cardiac autonomic nervous system reactivity in the TRAILS study. Biological Psychology, 110, 24–33.

Sloan, D. M., Strauss, M. E., & Wisner, K. L. (2001). Diminished response to pleasant stimuli by depressed women. Journal of Abnormal Psychology, 110(3), 488.

Smith, K. E., & Pollak, S. D. (2021). Rethinking concepts and categories for understanding the neurodevelopmental effects of childhood adversity. Perspectives on Psychological Science, 16(1), 67–93.

Smith, S. M. (2002). Fast robust automated brain extraction. Human Brain Mapping, 17(3), 143–155.

Snaith, R. P. (2003). The hospital anxiety and depression scale. Health and Quality of Life Outcomes, 1, 1–4.

Sommer, T. (2017). The emergence of knowledge and how it supports the memory for novel related information. Cerebral Cortex, 27(3), 1906–1921.

Sommer, T., Hennies, N., Lewis, P. A., & Alink, A. (2022). The Assimilation of Novel Information into Schemata and Its Efficient Consolidation. Journal of Neuroscience, 42(30), 5916–5929.

SooHoo, J. F., Davis, C. N., Han, A., Jinwala, Z., Gelernter, J., Feinn, R., & Kranzler, H. R. (2025). Associations of Childhood Adversity and Polygenic Scores with Substance Use Initiation and Disorder Severity. Psychological Medicine, 55, e132.

Speer, M. E., Ibrahim, S., Schiller, D., & Delgado, M. R. (2021). Finding positive meaning in memories of negative events adaptively updates memory. Nature Communications, 12(1), 6601.

Squire, L. R. (1987). Memory and brain. Oxford University Press.

Sripada, R. K., Swain, J. E., Evans, G. W., Welsh, R. C., & Liberzon, I. (2014). Childhood Poverty and Stress Reactivity Are Associated with Aberrant Functional Connectivity in Default Mode Network. Neuropsychopharmacology, 39(9), 2244–2251.

Stefanacci, L., & Amaral, D. G. (2000). Topographic organization of cortical inputs to the lateral nucleus of the macaque monkey amygdala: A retrograde tracing study. Journal of Comparative Neurology, 421(1), 52–79.

Stefanacci, L., & Amaral, D. G. (2002). Some observations on cortical inputs to the macaque monkey amygdala: An anterograde tracing study. Journal of Comparative Neurology, 451(4), 301–323.

Stoltenborgh, M., Bakermans-Kranenburg, M. J., & Van Ijzendoorn, M. H. (2013). The neglect of child neglect: A meta-analytic review of the prevalence of neglect. Social Psychiatry and Psychiatric Epidemiology, 48(3), 345–355.

Strange, B. A., Witter, M. P., Lein, E. S., & Moser, E. I. (2014). Functional organization of the hippocampal longitudinal axis. Nature Reviews Neuroscience, 15(10), 655–669.

Surguladze, S. A., Young, A. W., Senior, C., Brébion, G., Travis, M. J., & Phillips, M. L. (2004). Recognition accuracy and response bias to happy and sad facial expressions in patients with major depression. Neuropsychology, 18(2), 212.

T.

Teicher, M. H., Andersen, S. L., Polcari, A., Anderson, C. M., Navalta, C. P., & Kim, D. M. (2003). The neurobiological consequences of early stress and childhood maltreatment. Neuroscience & Biobehavioral Reviews, 27(1–2), 33–44.

Teicher, M. H., Anderson, C. M., Ohashi, K., Khan, A., McGreenery, C. E., Bolger, E. A., Rohan, M. L., & Vitaliano, G. D. (2018). Differential effects of childhood neglect and abuse during sensitive exposure periods on male and female hippocampus. NeuroImage, 169, 443–452.

Teicher, M. H., & Parigger, A. (2015). The 'Maltreatment and Abuse Chronology of Exposure'(MACE) scale for the retrospective assessment of abuse and neglect during development. PLoS One, 10(2), e0117423.

Teicher, M. H., Samson, J. A., Anderson, C. M., & Ohashi, K. (2016). The effects of childhood maltreatment on brain structure, function and connectivity. Nature Reviews Neuroscience, 17(10), 652–666.

Tendolkar, I., Mårtensson, J., Kühn, S., Klumpers, F., & Fernández, G. (2018). Physical neglect during childhood alters white matter connectivity in healthy young males. Human Brain Mapping, 39(3), 1283–1290.

Thivierge, J.-P., & Marcus, G. F. (2007). The topographic brain: From neural connectivity to cognition. Trends in Neurosciences, 30(6), 251–259.

Thomason, M. E., Marusak, H. A., Tocco, M. A., Vila, A. M., McGarragle, O., & Rosenberg, D. R. (2015). Altered amygdala connectivity in urban youth exposed to trauma. Social Cognitive and Affective Neuroscience, 10(11), 1460–1468.

Tompary, A., & Davachi, L. (2017). Consolidation promotes the emergence of representational overlap in the hippocampus and medial prefrontal cortex. Neuron, 96(1), 228–241.

Tooley, U. A., Bassett, D. S., & Mackey, A. P. (2021). Environmental influences on the pace of brain development. Nature Reviews Neuroscience, 22(6), 372–384.

Tse, D., Langston, R. F., Kakeyama, M., Bethus, I., Spooner, P. A., Wood, E. R., Witter, M. P., & Morris, R. G. (2007). Schemas and memory consolidation. Science, 316(5821), 76–82.

Tsuang, M. T., Bar, J. L., Stone, W. S., & Faraone, S. V. (2004). Gene-environment interactions in mental disorders. World Psychiatry, 3(2), 73.

Tulving, E., & Markowitsch, H. J. (1998). Episodic and declarative memory: Role of the hippocampus. Hippocampus, 8(3), 198–204.

Tunnard, C., Rane, L. J., Wooderson, S. C., Markopoulou, K., Poon, L., Fekadu, A., Juruena, M., & Cleare, A. J. (2014). The impact of childhood adversity on suicidality and clinical course in treatment-resistant depression. Journal of Affective Disorders, 152, 122–130.

U.

Underwood, M. D., Kassir, S. A., Bakalian, M. J., Galfalvy, H., Dwork, A. J., Mann, J. J., & Arango, V. (2018). Serotonin receptors and suicide, major depression, alcohol use disorder and reported early life adversity. Translational Psychiatry, 8(1), 279.

UNICEF. (2024). Nearly 400 million young children worldwide regularly experience violent discipline at home – UNICEF. https://www.unicef.org/press-releases/nearly-400-million-young-children-worldwide-regularly-experience-violent-discipline

V.

van Buuren, M., Kroes, M. C., Wagner, I. C., Genzel, L., Morris, R. G., & Fernández, G. (2014). Initial investigation of the effects of an experimentally learned schema on spatial associative memory in humans. Journal of Neuroscience, 34(50), 16662–16670.

van der Werff, S. J., Pannekoek, J. N., Veer, I. M., Van Tol, M.-J., Aleman, A., Veltman, D. J., Zitman, F. G., Rombouts, S. A., Elzinga, B. M., & van der Wee, N. J. (2013). Resting-state functional connectivity in adults with childhood emotional maltreatment. Psychological Medicine, 43(9), 1825–1836.

van Eijndhoven, P., Collard, R., Vrijsen, J., Geurts, D. E., Vasquez, A. A., Schellekens, A., van den Munckhof, E., Brolsma, S., Duyser, F., & Bergman, A. (2022). Measuring Integrated Novel Dimensions in Neurodevelopmental and Stress-Related Mental Disorders (MIND-SET): Protocol for a cross-sectional comorbidity study from a Research Domain Criteria perspective. JMIRx Med, 3(1), e31269.

van Eijndhoven, P., van Wingen, G., Fernández, G., Rijpkema, M., Verkes, R. J., Buitelaar, J., & Tendolkar, I. (2011). Amygdala responsivity related to memory of emotionally neutral stimuli constitutes a trait factor for depression. Neuroimage, 54(2), 1677–1684.

van Kesteren, M. T., Beul, S. F., Takashima, A., Henson, R. N., Ruiter, D. J., & Fernández, G. (2013). Differential roles for medial prefrontal and medial temporal cortices in schema-dependent encoding: From congruent to incongruent. Neuropsychologia, 51(12), 2352–2359.

van Kesteren, M. T., Fernández, G., Norris, D. G., & Hermans, E. J. (2010). Persistent schema-dependent hippocampal-neocortical connectivity during memory encoding and postencoding rest in humans. Proceedings of the National Academy of Sciences, 107(16), 7550–7555.

van Kesteren, M. T., Ruiter, D. J., Fernández, G., & Henson, R. N. (2012). How schema and novelty augment memory formation. Trends in Neurosciences, 35(4), 211–219.

van Marle, H. J., Hermans, E. J., Qin, S., & Fernández, G. (2009). From specificity to sensitivity: How acute stress affects amygdala processing of biologically salient stimuli. Biological Psychiatry, 66(7), 649–655.

van Marle, H. J., Hermans, E. J., Qin, S., & Fernández, G. (2010). Enhanced resting-state connectivity of amygdala in the immediate aftermath of acute psychological stress. Neuroimage, 53(1), 348–354.

van Oort, J., Kohn, N., Vrijsen, J., Collard, R., Duyser, F., Brolsma, S., Fernandez, G., Schene, A., Tendolkar, I., & van Eijndhoven, P. (2020). Absence of default mode downregulation in response to a mild psychological stressor marks stress-vulnerability across diverse psychiatric disorders. NeuroImage: Clinical, 25, 102176.

Van Tieghem, M. R., & Tottenham, N. (2017). Neurobiological programming of early life stress: Functional development of amygdala-prefrontal circuitry and vulnerability for stress-related psychopathology. Behavioral Neurobiology of PTSD, 117–136.

Veréb, D., Mijalkov, M., Canal-Garcia, A., Chang, Y.-W., Gomez-Ruiz, E., Gerboles, B. Z., Kivipelto, M., Svenningsson, P., Zetterberg, H., Volpe, G., Betts, M., Jacobs, H. I., & Pereira, J. B. (2023). Age-related differences in the functional topography of the locus coeruleus and their implications for cognitive and affective functions. eLife, 12, RP87188.

Verheul, E., Jacobs, B., Meijer, C., Hildebrandt, M., & de Ruiter, J. (2016). Polymorphic encryption and pseudonymisation for personalised healthcare. Cryptology ePrint Archive.

Vizi, E. S., & Kiss, J. P. (1998). Neurochemistry and pharmacology of the major hippocampal transmitter systems: Synaptic and nonsynaptic interactions. Hippocampus, 8(6), 566–607.

Vrijsen, J. N., Dainer-Best, J., Witcraft, S. M., Papini, S., Hertel, P., Beevers, C. G., Becker, E. S., & Smits, J. A. (2019). Effect of cognitive bias modification-memory on depressive symptoms and autobiographical memory bias: Two independent studies in high-ruminating and dysphoric samples. Cognition and Emotion, 33(2), 288–304.

Vrijsen, J. N., Hertel, P. T., & Becker, E. S. (2016). Practicing Emotionally Biased Retrieval Affects Mood and Establishes Biased Recall a Week Later. Cognitive Therapy and Research, 40(6), 764–773.

Vrijsen, J. N., Tendolkar, I., Arias-Vásquez, A., Franke, B., Schene, A. H., Fernández, G., & van Oostrom, I. (2015). Interaction of the 5-HTTLPR and childhood trauma influences memory bias in healthy individuals. Journal of Affective Disorders, 186, 83–89.

Vrijsen, J. N., van Amen, C. T., Koekkoek, B., van Oostrom, I., Schene, A. H., & Tendolkar, I. (2017). Childhood trauma and negative memory bias as shared risk factors for psychopathology and comorbidity in a naturalistic psychiatric patient sample. Brain and Behavior, 7(6), e00693.

Vrijsen, J. N., Van Oostrom, I., Arias-Vásquez, A., Franke, B., Becker, E., & Speckens, A. (2014). Association between genes, stressful childhood events and processing bias in depression vulnerable individuals. Genes, Brain and Behavior, 13(5), 508–516.

Vrijsen, J. N., Windbergs, H., Becker, E. S., Scherbaum, N., Müller, B. W., & Tendolkar, I. (2024). A Randomized Controlled Pilot Study Exploring the Additive Clinical Effect of Cognitive Bias Modification-Memory in Depressed Inpatients. Cognitive Therapy and Research, 48(2), 212–224.

W.

Wagner, I. C., van Buuren, M., Kroes, M. C., Gutteling, T. P., van der Linden, M., Morris, R. G., & Fernández, G. (2015). Schematic memory components converge within angular gyrus during retrieval. eLife, 4, e09668.

Watson, D., Clark, L. A., & Tellegen, A. (1988). Development and validation of brief measures of positive and negative affect: The PANAS scales. Journal of Personality and Social Psychology, 54(6), 1063–1070.

Webb, C. E., Turney, I. C., & Dennis, N. A. (2016). What's the gist? The influence of schemas on the neural correlates underlying true and false memories. Neuropsychologia, 93, 61–75.

Wei, S.-Y., Tsai, T.-H., Tsai, T.-Y., Chen, P. S., Tseng, H.-H., Yang, Y. K., Zhai, T., Yang, Y., & Wang, T.-Y. (2024). The Association between Default-mode Network Functional Connectivity and Childhood Trauma on the Symptom Load in Male Adults with Methamphetamine Use Disorder. Clinical Psychopharmacology and Neuroscience, 22(1), 105–117.

Wessa, M., Kanske, P., Neumeister, P., Bode, K., Heissler, J., & Schönfelder, S. (2010). EmoPics: Subjektive und psychophysiologische Evaluation neuen Bildmaterials für die klinisch-bio-psychologische Forschung. Zeitschrift Für Klinische Psychologie Und Psychotherapie, 39(Suppl. 1/11), 77.

WHO. (2024). Child maltreatment. https://www.who.int/news-room/fact-sheets/detail/child-maltreatment

Williams, J. M., & Broadbent, K. (1986). Autobiographical memory in suicide attempters. Journal of Abnormal Psychology, 95(2), 144.

Witter, M. P. (1993). Organization of the entorhinal-hippocampal system: A review of current anatomical data. HIPPOCAMPUS-NEW YORK-CHURCHILL LIVINGSTONE-, 3, 33–33.

Woolrich, M. W., Ripley, B. D., Brady, M., & Smith, S. M. (2001). Temporal autocorrelation in univariate linear modeling of FMRI data. Neuroimage, 14(6), 1370–1386.

Woolway, G. E., Smart, S. E., Lynham, A. J., Lloyd, J. L., Owen, M. J., Jones, I. R., Walters, J. T., & Legge, S. E. (2022). Schizophrenia polygenic risk and experiences of childhood adversity: A systematic review and meta-analysis. Schizophrenia Bulletin, 48(5), 967–980.

Wu, J., Liu, Y., Zhang, L., Wang, N., Kohn, N., & Duan, H. (2023). Integrating the pattern of negative emotion processing and acute stress response with childhood stress among healthy young adults. Stress, 26(1), 2195503.

Wu, X., Viñals, X., Ben-Yakov, A., Staresina, B. P., & Fuentemilla, L. (2022). Post-encoding reactivation is related to learning of episodes in humans. Journal of Cognitive Neuroscience, 35(1), 74–89.

Y.

Yang, H., Spence, J. S., Briggs, R. W., Rao, U., North, C., Devous Sr, M. D., Xiao, H., & Adinoff, B. (2015). Interaction between early life stress and alcohol dependence on neural stress reactivity. Addiction Biology, 20(3), 523–533.

Yoon, K. L., Joormann, J., & Gotlib, I. H. (2009). Judging the intensity of facial expressions of emotion: Depression-related biases in the processing of positive affect. Journal of Abnormal Psychology, 118(1), 223.

Young, J. E. (1999). Cognitive therapy for personality disorders: A schema-focused approach. Professional Resource Press/Professional Resource Exchange.

Young, J. E., Klosko, J. S., & Weishaar, M. E. (2006). Schema therapy: A practitioner's guide. guilford press.

Young, K. D., Siegle, G. J., Bodurka, J., & Drevets, W. C. (2016). Amygdala activity during autobiographical memory recall in depressed and vulnerable individuals: Association with symptom severity and autobiographical overgenerality. American Journal of Psychiatry, 173(1), 78–89.

Young, K. D., Siegle, G. J., Misaki, M., Zotev, V., Phillips, R., Drevets, W. C., & Bodurka, J. (2018). Altered task-based and resting-state amygdala functional connectivity following real-time fMRI amygdala neurofeedback training in major depressive disorder. NeuroImage: Clinical, 17, 691–703.

Young, K. D., Siegle, G. J., Zotev, V., Phillips, R., Misaki, M., Yuan, H., Drevets, W. C., & Bodurka, J. (2017). Randomized Clinical Trial of Real-Time fMRI Amygdala Neurofeedback for Major Depressive Disorder: Effects on Symptoms and Autobiographical Memory Recall. American Journal of Psychiatry, 174(8), 748–755.

Young, K. D., Zotev, V., Phillips, R., Misaki, M., Drevets, W. C., & Bodurka, J. (2018). Amygdala real-time functional magnetic resonance imaging neurofeedback for major depressive disorder: A review. Psychiatry and Clinical Neurosciences, 72(7), 466–481.

Young, K. D., Zotev, V., Phillips, R., Misaki, M., Yuan, H., Drevets, W. C., & Bodurka, J. (2014). Real-Time fMRI Neurofeedback Training of Amygdala Activity in Patients with Major Depressive Disorder. PLOS ONE, 9(2), e88785.

Z.

Zhang, R., Xiao, X., Dong, D., Xu, T., Hu, Y., Zhou, F., Zhai, T., Qi, Y., Yang, Y., & He, Q. (2025). Abnormal ventromedial-to-dorsolateral hierarchical topography of striatal circuits in cocaine use disorder and its modulations by brain stimulation. Neuropsychopharmacology, 1–10.

Zhou, H.-Y., Zhou, L., Zheng, T., Ma, L., Fan, M.-X., Liu, L., Zhao, X., & Yan, C. (2025). Unraveling the link between childhood maltreatment and depression: Insights from the role of ventral striatum and middle cingulate cortex in hedonic experience and emotion regulation. Development and Psychopathology, 37(1), 292–302.

Zhu, J., Anderson, C. M., Ohashi, K., Khan, A., & Teicher, M. H. (2023). Potential sensitive period effects of maltreatment on amygdala, hippocampal and cortical response to threat. Molecular Psychiatry, 28(12), 5128–5139.

Zotev, V., Yuan, H., Misaki, M., Phillips, R., Young, K. D., Feldner, M. T., & Bodurka, J. (2016). Correlation between amygdala BOLD activity and frontal EEG asymmetry during real-time fMRI neurofeedback training in patients with depression. NeuroImage: Clinical, 11, 224–238.

Zwiers, M. P., Moia, S., & Oostenveld, R. (2022). BIDScoin: A user-friendly application to convert source data to Brain Imaging Data Structure. Frontiers in Neuroinformatics, 15, 770608.

Summary of thesis

Childhood adversity increases the risk of developing psychiatric disorders through its lifelong impacts on the brain and behavior. Beck's cognitive model of depression, an influential theoretical framework in clinical practice, proposes that childhood adversity can contribute to the formation of a negative internal working model—a schema system that, when activated by stressful life events, triggers negatively biased cognition. Building the constructs of Beck's model, in this thesis, we have traced how maladaptive schemas shaped by childhood adversity are represented in the brain and behavior, through a task-state fMRI study on emotional memory and analyses of resting-state functional brain organization across the psychopathological continuum.

First, we conducted a multi-session fMRI study in a sample encompassing a wide range of childhood adversity and levels of depressive symptom, to investigate the roles and interactions of childhood adversity, depressive symptom levels, and external depressive schema activation in relation to one key domain of biased cognition—negative memory bias. We found that individuals with higher childhood adversity severity exhibited stronger negative memory bias, independent of depressive symptom levels or external schema activation condition. At the neural level, higher childhood adversity severity was also associated with more negatively biased encoding activity in the amygdala and hippocampus, paralleling the behavioral bias. These findings highlight the role of childhood adversity in negative memory bias, suggesting how the inherent maladaptive schema potentially influences emotional memory processing (**Chapter 2**).

Second, we applied an emerging resting-state fMRI analysis approach— "connectopic mapping" —to a combined sample of psychiatric patients and healthy controls, investigating how childhood adversity and acute stress interact in shaping the topographic organization of striatal resting-state functional connectivity. We found that one form of childhood adversity, the emotional neglect, was related to both post-stress states and stress-induced changes in striatal connectivity gradient maps. This effect was selectively observed in individuals with high psychiatric comorbidity. These results demonstrate "connectopic mapping" as a sensitive tool for capturing both inter-individual differences and intra-individual manipulations, and illustrate how maladaptive schemas shaped by childhood adversity are embedded in the functional organization of reward- processing regions (**Chapter 3**).

Third, we applied "connectopic mapping" to the hippocampus-amygdala complex, to characterize the functional organization of these important threat-processing

regions. In both healthy and psychiatric cohorts, we identified six distinct connectopic gradient maps for the hippocampus–amygdala complex, some of which exhibited spatial similarity to the distribution of neurotransmitters in the serotonergic and dopaminergic systems. Although no significant associations with childhood adversity were found, individual variation in gradient–neurotransmitter similarity was associated with depression and anxiety symptoms across the psychiatric continuum. This work suggests the potential of "connectopic mapping" to serve as a transdiagnostic marker linking functional neuroimaging, neurotransmitter systems, and mental health indicators (**Chapter 4**).

In conclusion, through the series of studies in this thesis, we have traced how maladaptive schemas shaped by childhood adversity are embedded in emotional memory processes and in acute stress–induced changes in brain functional connectivity. Collectively, we present new evidence linking childhood adversity to functional alterations in threat-processing regions (e.g., the amygdala and hippocampus) and reward-processing regions (e.g., the striatum). These findings may contribute to a transdiagnostic perspective on the psychopathological mechanisms of childhood adversity, and inspire future investigations into broader clinical utility of resting-state neural markers.

Samenvatting

Jeugdtrauma vergroot het risico op het ontwikkelen van psychiatrische stoornissen door de levenslange invloed op het brein en het gedrag. Het cognitieve model van Beck over depressie, een invloedrijk theoretisch kader in de klinische praktijk, stelt dat jeugdtrauma kan bijdragen aan de vorming van een negatief intern werkmodel—een schemasysteem dat, wanneer geactiveerd door stressvolle levensgebeurtenissen, leidt tot negatief gekleurde cognitieve processen. Voortbouwend op de concepten van Becks model, hebben we in dit proefschrift onderzocht hoe door jeugdtrauma gevormde maladaptieve schema's in het brein en gedrag worden gerepresenteerd, door middel van een taakgebonden fMRI-studie naar emotioneel geheugen en analyses van de rusttoestand-organisatie van de hersenfunctie over het gehele psychopathologische spectrum.

Ten eerste voerden we een meersessie-fMRI-studie uit in een steekproef die een brede variatie in jeugdtrauma en niveaus van depressieve symptomen omvatte, om de rollen en interacties van jeugdtrauma, de ernst van depressieve symptomen en externe activatie van depressieve schema's te onderzoeken in relatie tot één belangrijk domein van vertekend cognitief functioneren—de negatieve geheugensbias. We vonden dat personen met een hogere ernst van jeugdtrauma een sterkere negatieve geheugensbias vertoonden, onafhankelijk van de ernst van depressieve symptomen of de conditie van externe schema-activatie. Op hersenniveau werd een hogere ernst van jeugdtrauma ook geassocieerd met sterker negatief gekleurde coderingsactiviteit in de amygdala en hippocampus, parallel aan de gedragsmatige bias. Deze bevindingen benadrukken de rol van jeugdtrauma in negatieve geheugensbias en suggereren hoe het inherente maladaptieve schema mogelijk de verwerking van emotioneel geheugen beïnvloedt (**Hoofdstuk 2**).

Ten tweede pasten we een opkomende analysemethode voor rusttoestand-fMRI toe—connectopic mapping—op een gecombineerde steekproef van psychiatrische patiënten en gezonde controles, om te onderzoeken hoe jeugdtrauma en acute stress interacteren bij het vormgeven van de topografische organisatie van de striatale rusttoestand-functionele connectiviteit. We ontdekten dat één vorm van jeugdtrauma, namelijk emotionele verwaarlozing, verband hield met zowel post-stresstoestanden als met door stress geïnduceerde veranderingen in de connectiviteitsgradiëntkaarten van het striatum. Dit effect werd uitsluitend waargenomen bij personen met een hoge psychiatrische comorbiditeit. Deze resultaten tonen connectopic mapping aan als een gevoelig instrument om zowel interindividuele verschillen als intra-individuele veranderingen vast te leggen, en illustreren hoe door jeugdtrauma

gevormde maladaptieve schema's zijn ingebed in de functionele organisatie van beloningsverwerkende hersengebieden (**Hoofdstuk 3**).

Ten derde pasten we connectopic mapping toe op het hippocampus–amygdala-complex, om de functionele organisatie van deze belangrijke hersengebieden voor dreigingsverwerking in kaart te brengen. In zowel gezonde als psychiatrische cohorten identificeerden we zes verschillende connectiviteitsgradiëntkaarten voor het hippocampus–amygdala-complex, waarvan sommige een ruimtelijke gelijkenis vertoonden met de verdeling van neurotransmitters in de serotonerge en dopaminerge systemen. Hoewel er geen significante verbanden met jeugdtrauma werden gevonden, bleek individuele variatie in de gelijkenis tussen gradiënt en neurotransmitter samen te hangen met depressie- en angstsymptomen over het gehele psychiatrische spectrum. Dit werk suggereert het potentieel van connectopic mapping als een transdiagnostische marker die functionele neuroimaging, neurotransmittersystemen en mentale gezondheidsindicatoren met elkaar verbindt (**Hoofdstuk 4**).

Concluderend hebben we in deze reeks studies binnen dit proefschrift onderzocht hoe door jeugdtrauma gevormde maladaptieve schema's zijn ingebed in emotionele geheugenprocessen en in door acute stress geïnduceerde veranderingen in de functionele connectiviteit van de hersenen. Gezamenlijk presenteren wij nieuw bewijs dat jeugdtrauma in verband brengt met functionele veranderingen in hersengebieden die betrokken zijn bij dreigingsverwerking (bijv. de amygdala en hippocampus) en beloningsverwerking (bijv. het striatum). Deze bevindingen kunnen bijdragen aan een transdiagnostisch perspectief op de psychopathologische mechanismen van jeugdtrauma en toekomstige onderzoeken inspireren naar een bredere klinische toepasbaarheid van rusttoestand-neurale markers.

Research data management

Research presented in this thesis followed the applicable laws and ethical guidelines. Research data management was conducted according to the FAIR principles. The paragraphs below specify in detail how this was achieved.

Ethics and privacy

This thesis is based on the results of human studies, which were conducted in accordance with the principles of the Declaration of Helsinki.

In Chapter 2, local data acquisition was approved by the regional ethics committee (METC Oost-Nederland; NL81194.091.22). This study was funded by the Donders Centre for Cognitive Neuroimaging (DCCN). All participants received a clear explanation of the study information. Informed consent (IC) was obtained from participants to collect and process their data for this research project. Consent was also obtained for sharing and reuse of the (pseudonymized) data for future research. The privacy of the participants in these studies was warranted by the use of pseudonymization. Participant identification code list (Key-file) is kept in a strict confidential way and stored separately from other data in a password-protected file.

Chapters 3 and 4 have made use of data from the MIND-Set study (Van Eijndhoven et al., 2021), which was approved by the local medical research ethics committee (METC Oost-Nederland; NL55618.091.15) and funded by the Radboud University Medical Center. The pseudonymization is used to protect privacy. The pseudonymisation key is stored on a secured network drive and separately from the research data.

Chapter 4 has also utilized data from the HBS study (Healthy Brain Study consortium et al., 2021). This research was approved by the Institutional Review Board of Radboud University Medical Center (reference number: 2018–4894), and funded by the Reinier Post Foundation and Radboud University, Nijmegen, the Netherlands. A Polymorphic Encryption and Pseudonymization (PEP) infrastructure was developed to protect the privacy of participants (Verheul et al., 2016).

Data collection and storage

For Chapter 2, data was collected in the behavioral and MRI testing rooms of DCCN. The case report form (CRF) and questionnaires were administrated through a secure data management platform – Castor EDC. All research data has been stored at the central project archive of DCCN, and a Data Acquisition Collection

(DAC; DOI:10.34973/q2yp-0487) in the Radboud Data Repository (RDR). The data is accessible to all members involved in the project. The IC forms are archived in the central archive of the Centre for 10 years after termination of the studies.

Data from the MIND-Set study (Chapters 3 and 4) was collected at Radboud University Medical Center and DCCN. The dataset for this study was stored and analyzed in workspace (mindset-xl) the Azure DRE (DRE Portal (mydre.org)). For data obtained at DCCN, a DAC with closed access in RDR (di.dccn.DAC_3013061.01_195) is also used. In accordance with the IC form, data will be stored for 15 years.

Data from the HBS study (Chapter 4) was collected at the Radboud campus, Nijmegen. The data used for this study was stored at the central project archive of DCCN, and analyzed in the DCCN High-Performance Computing (HPC) cluster. The HBS dataset is stored with closed access at a DAC (di.dccn.DAC_3013081.01_497) in the RDR. In accordance with the IC form, data will be stored for 15 years from 2029 onward.

Data sharing

The manuscript of Chapter 2 is still in preparation. The data used in this unpublished chapter are archived in a DAC (DOI:10.34973/q2yp-0487) and Research Documentation Collection (RDC; DOI:10.34973/4r04-6r43) of the RDR. Upon publication of the chapter, the data will be published via the RDR with restricted access.

Chapter 3 and 4 are based on existing data, which were obtained from the MIND-Set study (DOI: 10.34973/t6m1-x414). Questions about these data can be addressed to mindsetonderzoek@radboudumc.nl. To access the HBS study data, see healthybrainstudy.nl/en/home. The processed data and analysis scripts are archived in RDCs within the RDR (DOI:10.34973/at8k-4346; DOI:10.34973/96e4-bk09).

Curriculum vitae

Xiangshen was born in November 1996 in Shandong Province, China. She obtained her bachelor's degree in Computer Science and Technology from Beijing Foreign Studies University, where she also discovered her growing fascination with the human mind. This interest led her to pursue a master's degree in Psychology at Peking University in 2018. During her master's training, she studied how acute stress and stress-induced cortisol secretion influence memory.

Xiangshen's PhD research continued to focus on human memory, specifically applying neuroscience methodologies to understand psychiatric phenomena. Under the guidance of an interdisciplinary supervisory team, she combined neuroimaging, eye-tracking, and physiological measures to investigate the mechanisms underlying negative memory bias in individuals with childhood adversity and depressive symptoms. Additionally, she utilized datasets from both healthy and clinical cohorts to characterize the impact of childhood adversity on brain functional architecture.

She enjoys studying mechanisms, and at the same time, she hopes to bring tangible positive changes to the vulnerable population. After completing her PhD, Xiangshen will join the lab led by Prof. Raffael Kalisch as a postdoctoral fellow, where she will explore potential interventions for the overwhelming negative memory.

Outside of the lab, Xiangshen also became unexpectedly productive in the field of planting. During her PhD, she grew a Kentia palm into a towering tree and successfully harvested lemons and an orange of her own. Her hiking journey has also never ceased—the deep silence of the mountains and forests is where she feels at home.

Academic portfolio

Academic courses

- Cognitive Control and Decision Making, 2024
- Effective Writing Strategies, 2023
- Computational Psychiatry Summer School, Zurich, 2023
- Neurobiology of (Mal)adaptation, 2023
- Language Development for Academic Writing, 2022
- Academic English Conversation and Pronunciation, 2022
- Internship Supervision Training Course, 2021

Conference presentations

- Annual Meeting for Cognitive Neuroscience Society 2025 (Boston) – poster presentation
- Annual Meeting for Association for Cognitive Bias Modification 2024 (London) – poster presentation
- Annual Meeting for the Organization for Human Brain Mapping 2024 (Seoul) – poster presentation
- Dutch Society for Brain and Cognition Winter Conference 2023 (Egmond aan Zee) – poster presentation

Ad-Hoc reviewer

- Translational Psychiatry

Extra-curricular certification

- Certified user 3T MRI-scanner (Donders Center for cognitive neuroimaging) (2023)

Teaching & mentoring experience

- Co-supervisor of master internship: Jil Fröhling, Angeliki Sideri, Karolina Figa, Mareike Pfaffernoschke
- Mentor: Introduction to medical neuroscience (2024)

Acknowledgments

As I began to write this acknowledgment, I realized it is a typical autobiographical memory recall. These memories unfold in my mind like a slowly unrolling scroll. It is you, those who entered my life during the four years, who have painted it with the most vivid colors.

Guillén, I first knew you from the literature, and joining your lab was, in many ways, a dream come true. I cannot thank you enough for the opportunity; this was the start of my adventure in the Netherlands and meant a lot to me. Over these four years, I have benefited immensely from your inspiring perspectives on the big picture as well as your guidance on scientific rigor in the details. I also want to thank you for your steady support at every important moment and for your advice on my future career. These opened my horizons, gave me strength, and made my PhD journey smoother. I will always be proud to be one of your PhD students, and I hope that one day you will be proud of me too (in some way).

Indira, chatting with you always brings me energy and great encouragement. I am often impressed by how you balance clinical work, research, and administrative tasks at the same time. Your strong theoretical foundation greatly inspired my experimental design and data analysis. My background in psychiatry was relatively weak, and your presence gave me a sense of safety and strong support throughout the project. I also want to thank you for giving me the opportunity to analyze the MIND-Set data, which made my research training more complete and rich.

Nils, I think I have said this many times: you are the best daily supervisor ever. Every step of my progress and every new skill I learned could not have happened without your help, and you were always the first to know. I felt safe telling you my troubles, pressure, and whatever I had in mind. I have bothered you too much with stupid questions, while you always dealt with them with the greatest patience. Thinking from your perspective, I know how difficult this must have been. I will never forget the moment you showed up at the last scan of my project, with celebration gifts. The academic world can be tough, Nijmegen was cold, but you gave us warmth. This is a memory I will always treasure.

Janna, you have many qualities I want to learn from. Your sharp thinking, rigorous style, abundant energy, and excellent time management have set a direct example for me. Your expertise and rich experience in memory bias and mood induction were essential for the smooth progress of my research. Whenever I needed help,

your response was always incredibly timely, positive, and considerate. This helped solve my problems efficiently and pushed the project forward. At the same time, you cared about my future development and how I felt; these gave me a lot of courage and strength.

Together, the four of you form my exceptionally "luxurious" supervisory team that always work together seamlessly. Beyond each of you individually, I also want to thank you as a team. It was this team that, together with me, drove everything in my PhD journey. I feel so lucky to have all of you and all your support from different aspects.

I also feel so lucky to be part of the **Memory & Emotion Group**. This is a group full of joy and friendship. **Wei** and **Yan-nan**, thank you for your help even before I arrived in Nijmegen; your detailed introductions made me well-prepared. **Yan-nan**, thank you for helping me initially set up the experimental equipment; I still remember you staying so late that evening to solve problems with me. **Hongxia**, you are both a mentor and a friend. Your warm help allowed me to adapt to life in Nijmegen quickly, and your valuable inputs contributed a lot to my project. I will always miss the lovely dinners in your yard during summer evenings, especially Freek's wonderful lasagna. I would also like to thank **James**, **Clara**, **Céline**, **Silvia**, **Lisa W**, **Javier**, **Jeshua** and **all the former and present students**, for forming such a joyful and harmonious group and making me part of it. The **FitMind Group** has been another place where I felt a sense of belonging. Thanks for all the support throughout my project. The excellent presentations and discussions have greatly enriched my understanding of clinical practice and of many fascinating behavioral paradigms.

I want to give special thanks to the interns who accompanied me in completing my PhD project; they are all very talented and outstanding students. **Mareike**, we were both fresh to Nijmegen and doing research there at the time. Thanks for accompanying me through all the initial setups, familiarizing with the administrative system, and completing the pilot with me. I still remember the scene where we climbed onto my roof eating cookies and got scolded by the neighbor. **Karolina**, thank you for being with me through the most difficult early scanning stage, accompanying me with all my panic and growth. You are so smart and diligent, and I know you will have a fruitful PhD journey. **Angeliki**, you brought us a lot of joy and fun; thank you for your help in finding participants and recommending the great piercing store. **Jil**, you were the intern who stayed with me the longest during my PhD. With the company of a friend like you, the long scan and intake sessions became much more enjoyable. I often feel that in many ways you are more mature

than I am, and our discussions on the project gave me a lot of inspiration. I believe you will find your passion and make something of it.

My thanks also go to all the PIs and collaborators who have helped me. **Karin**, your support spanned my entire PhD journey — whether as my external advisor, the chair of my manuscript committee, or helping me with my next step. All of this was very important for my development. **Raffael**, thank you for being willing to host my postdoc research and for all the time and effort you put into my fellowship application. I look forward to exploring the world of dopamine and memory updating with you. To **Andre**, **Udo**, and **all other members of my doctoral committee**, thank you for your helpful feedback on my thesis and for taking the time to attend my defense. I also want to thank **Koen**, **Marianne**, and **Peter** for their guidance on the gradient methods, as well as all **the staff** involved in data collection and management for **MIND-Set** and **HBS**.

My research during the PhD would not have been possible without the help of the administrative staff at the DCCN and Radboud UMC. **Paul**, **Marek**, **Mike**, **Miranda**, **Ellen**, **Erna**, **Nino**, **Tildie**, **Mirjam**, **Marliese**, **Geeralien**, **Wendy**, thank you for your work that ensured everything ran smoothly. Thank you to all my participants for being willing to complete these long testing sessions; your efforts provided me with precious data. At the same time, I also want to thank my recruitment team (**Lisa L** and **Inge W**); your work greatly accelerated the progress of my project.

Thanks to my friends and peers. **琳琳**，我特别开心也感到特别幸运有你在组里，与我分享一切喜怒哀乐。你经历着我所经历着的，这让一切陪伴都那么亲切和自然而然。同样陪着我的还有你做的好吃的，我一定会在许多午夜梦回怀念你的炒鸡、卤味、丸子、肉饼、栗子奶茶、抹茶红豆麻薯……希望以后还能找机会去你家蹭饭。**鑫源**，你应该是全天下最能理解做实验艰辛的人吧，每次听完你犀利的吐槽都能通体舒畅。希望你可以早日找到一个温暖的城市，过上无忧无虑的生活。**娆**，你是我见过最有活力的人之一了，每次和你约会都能精神几天。希望生活对你好一点，让你永远做一个活力满满的人，有机会继续给我充电。**Nikos**, thank you for sharing your experience in project management and showing me around the MRI lab; this was incredibly helpful when I was just starting. You are so warm and reliable, and I wish you all the best in the future.

深深的感激写给我的家人。爸爸妈妈，感谢你们总是坚定支持我的选择，做我最坚强的后盾，把牵挂藏在心里，允许我轻装前行。奶奶，感谢你几乎忘记了所有事情，但还记得叮嘱我好好吃饭。小郭，感谢你一直一直在我身边，包括写下这句话的此刻。我知道你所有的付出，希望我的未来你会一直都在。

亲爱的爷爷，感谢你等我回去。我有太多的话想跟你说，太多好玩的事情想要告诉你。希望你可以多来我的梦里。

At the end of this autobiographical memory, I thank the version of myself who was full of desire and vitality. She traveled across mountains and oceans to bring me all the way here.

Donders Graduate School

For a successful research Institute, it is vital to train the next generation of scientists. To achieve this goal, the Donders Institute for Brain, Cognition and Behaviour established the Donders Graduate School in 2009. The mission of the Donders Graduate School is to guide our graduates to become skilled academics who are equipped for a wide range of professions. To achieve this, we do our utmost to ensure that our PhD candidates receive support and supervision of the highest quality.

Since 2009, the Donders Graduate School has grown into a vibrant community of highly talented national and international PhD candidates, with over 500 PhD candidates enrolled. Their backgrounds cover a wide range of disciplines, from physics to psychology, medicine to psycholinguistics, and biology to artificial intelligence. Similarly, their interdisciplinary research covers genetic, molecular, and cellular processes at one end and computational, system-level neuroscience with cognitive and behavioural analysis at the other end. We ask all PhD candidates within the Donders Graduate School to publish their PhD thesis in de Donders Thesis Series. This series currently includes over 600 PhD theses from our PhD graduates and thereby provides a comprehensive overview of the diverse types of research performed at the Donders Institute. A complete overview of the Donders Thesis Series can be found on our website: https://www.ru.nl/donders/donders-series

The Donders Graduate School tracks the careers of our PhD graduates carefully. In general, the PhD graduates end up at high-quality positions in different sectors, for a complete overview see https://www.ru.nl/donders/destination-our-former-phd. A large proportion of our PhD alumni continue in academia (>50%). Most of them first work as a postdoc before growing into more senior research positions. They work at top institutes worldwide, such as University of Oxford, University of Cambridge, Stanford University, Princeton University, UCL London, MPI Leipzig, Karolinska Institute, UC Berkeley, EPFL Lausanne, and many others. In addition, a large group of PhD graduates continue in clinical positions, sometimes combining it with academic research. Clinical positions can be divided into medical doctors, for instance, in genetics, geriatrics, psychiatry, or neurology, and in psychologists, for instance as healthcare psychologist, clinical neuropsychologist, or clinical psychologist. Furthermore, there are PhD graduates who continue to work as researchers outside academia, for instance at non-profit or government organizations, or in pharmaceutical companies. There are also PhD graduates who work in education, such as teachers in high school, or as lecturers in higher education. Others continue in a wide range of positions, such as policy advisors,

project managers, consultants, data scientists, web- or software developers, business owners, regulatory affairs specialists, engineers, managers, or IT architects. As such, the career paths of Donders PhD graduates span a broad range of sectors and professions, but the common factor is that they almost all have become successful professionals.

For more information on the Donders Graduate School, as well as past and upcoming defences please visit: http://www.ru.nl/donders/graduate-school/phd/

9 789465 152219 >

DONDERS INSTITUTE

Radboud University

Radboudumc